GROUNDWATER FLOW AND TRANSPORT MODEL OF THE RED RIVER/INTERLAKE AREA IN SOUTHERN MANITOBA

by

Paula Lynn Kennedy

A Thesis

Submitted to the Faculty of Graduate Studies

In Partial Fulfillment of the Requirements for the Degree of

Doctor of Philosophy

Department of Civil and Geological Engineering

University of Manitoba

Winnipeg, Manitoba

2002

THE UNIVERSITY OF MANITOBA

FACULTY OF GRADUATE STUDIES

*****

COPYRIGHT PERMISSION PAGE

GROUNDWATER FLOW AND TRANSPORT MODEL OF THE RED RIVER/INTERLAKE AREA IN SOUTHERN MANITOBA

BY

PAULA LYNN KENNEDY

A Thesis/Practicum submitted to the Faculty of Graduate Studies of The University of Manitoba in partial fulfillment of the requirements of the degree of

Doctor of Philosophy

DEDICATION

I would like to dedicate this thesis and its completion to my parents. To my Mom for being a sounding board who has helped me through all of my education from kindergarten through to my Ph.D. To my Dad, who did not make it through to the completion of my thesis, but who I know is here in spirit still encouraging me just as he did in life. I would not have made it here without you both.

ACKNOWLEDGEMENTS

To complete the research conducted for my Ph.D. thesis, many people helped in both professional and personal capacity.

First and foremost, I would like to acknowledge the supervision and guidance provided by my supervisor Dr. Allan Woodbury at the University of Manitoba. Other people who provided help in this research, either through help in gathering data, with the numerical model or advice on the research include Bob Betcher, Frank Render and John Little of the Water Branch of Manitoba, Harvey Thorleifson and Alfonso Rivera of the Geological Survey of Canada, René Therrien of Laval University, Rob McLaren of University of Waterloo, Gaywood Matile and Greg Keller of Industry, Trade and Mines of Manitoba and Rebecca McMillan and Paul Laznicka of University of Manitoba. I would like to thank all of the aforementioned people for their help during the completion of this thesis.

On a more personal side, I would like to acknowledge the support of fellow students James Blatz (now professor at University of Manitoba) and Nelson Ferreira. On a daily basis, you have both provided moral and personal support.

Lastly, I would like to thank Craig Osborne for his love, understanding and patience while I completed this thesis. Even though at times it may have been difficult, you have always been there for me.

Thank you all.

ABSTRACT

A regional flow and solute transport model was constructed for two bedrock aquifers in Southern Manitoba. The "Carbonate Aquifer" is located in the fractured, more permeable region of the outcropping carbonate rocks and is used for rural domestic, industrial, irrigation and agricultural purposes. The "Sandstone Aquifer" is located within the interbedded sandstones and shales of the Winnipeg Formation and is utilized for rural domestic purposes.

Transmissivity measurements were obtained for both aquifers from pump and specific capacity tests. It was determined that the transmissivity in m^2/s followed a natural log normal distribution for both aquifers with a mean of –7.2 and –8.0 for the Carbonate and Sandstone Aquifers, respectively. The variograms were calculated using an estimator developed by Li and Lake (1994). Fractal nature was not evident in the variogram of either aquifer. Bayesian Updating was used to generate heterogeneous hydraulic conductivity fields. For the Carbonate Aquifer this field was successfully used to assign hydraulic conductivity, however due to lack of measurements the hydraulic conductivity for the Sandstone Aquifer was assigned through zonation.

The resulting flow model had a RMS error of 7.49 m. The plot of computed versus observed equivalent freshwater heads showed significant correlation. Linear regression was conducted and the slope and intercept compared against the desired values of 1.0 and

0.0, respectively, using the t-test. For the transport model, the RMS error was 2.9 g/L, however the plot of computed versus observed concentrations had a slope significantly different than one.

The model was used to evaluate several water resources engineering applications. The model runs examining sustainability showed that 1 g/L contour moved slightly northeast in the Carbonate Aquifer and only had slight movement in the Sandstone Aquifer.

TABLE OF CONTENTS

LIST OF TABLES

LIST OF FIGURES

LIST OF SYMBOLS AND ABBREVIATIONS

a	Range of semi-variogram [L]
AIC	Akaike Information Criterion
A_L	Longitudinal dispersivity as a results of heterogeneous hydraulic conductivity
b	Saturated thickness of aquifer [L]
b(m)	Joint boxcar probability distribution function
BC	Boundary condition
BU	Bayesian Updating
C	Ion concentration [M/L^3]
C(0)	Covariance at 0 lag distance
$C(h_d)$	Covariance at separation distance, h_d
C_0	Nugget effect
$\mathbf{C_d}$	Covariance matrix of data
$\mathbf{C_m}$	Covariance matrix of model parameters
C_{max}	Maximum concentration [M/L^3]
Cov	Covariance
$\mathbf{C_q}$	Covariance of posterior probability distribution
C_r	Relative concentration []
d	Dimension
d	Data vector containing measurements [Nx1]
D	Hydrodynamic dispersion [L^2/T]
d*	Data vector of size [Nx1]
D_d	Diffusion coefficient [L^2/T]
DEM	Digital elevation model
$D_{i,l}$	Data in moving window $\Delta_{i,l}$
DOF	Degrees of freedom
E	Expected value
E[Y(x)]	Expected value of Y(x)
$f_j(x)$	Function at x
$\bar{f}_j$	Expected value of q(x)
G	Data kernel, matrix of size [Nxm]
g	Gravitational constant [L/T^2]
GIS	Geographical Information System
GMS	Groundwater Modeling System
GSC	Geological Survey of Canada
GWDrill	Database of all water wells drilled in Manitoba
h	Total head [L]
H_A	Alternate hypothesis
h_c	Capillary head [L]
h_d	Separation distance [L]
h_f	Equivalent freshwater head [L]

H_0	Null hypothesis
$H(\hat{q}, p)$	Relative entropy of $\hat{q}(x)$ relative to a prior estimate p(x)
I	Identity matrix
I	Information
IC	Initial condition
ITM	Department of Industry, Trade and Mines of Manitoba
k	Intrinsic permeability [L^2]
K	Saturated hydraulic conductivity [L/T]
k_{AIC}	Number of parameters in model
K_d	Equilibrium distribution coefficient
k_{rw}	Relative permeability []
L	Length parameter [L]
L_{AIC}	Negative log likelihood function in Akaike Information Criterion calculation
LB	Lower bound
m	Model parameter vector [mx1]
M	Number of equal probability areas
m	Number of interpolated points
<m>	Vector of conditional expected values
m_d	Number of data in moving window $\Delta_{i,l}$
m_f	Fitting parameter for saturation – relative permeability relationship
MRE	Minimum relative entropy
MSD	Manitoba Stratigraphic Database
MWB	Manitoba Water Branch
n	Porosity []
N	Total number of data
$N(h_d)$	Number of data pairs at separation distance, h_d
n_f	Fitting parameter for saturation – relative permeability relationship
n_1	Number of points in 2D models
n_2	Number of points in 3D model
O	Observed value
p	"New" prior estimate in MRE
P	Pressure [$M/T^2 \cdot L$] ≡ [F/L^2]
p(m)	Expected value of **p**
p(**u**)	Prior probability of hyperparameter set **u**
p(x)	Prior estimate of multivariate pdf q(x)
p[**d***|**m**,I]	Likelihood function
p[**m**|**d***,I]	Posterior conditional probability
p[**m** $\mid I$]	Prior pdf used in Bayes' Theorem
pdf	Probability distribution function
Q	Flow rate [L^3/T]
q	Darcy flux [L/T]
q(x)	Multivariate probability distribution of x
$\hat{q}(x)$	Estimate of q(x) by MRE method
R	Retardation factor []
RMS	Root mean square

r_w	Radius of well [L]
s	Drawdown [L]
s	Vector of prior unconditional mean
S	Storativity []
S_e	Effective saturation []
s_m	Numerical value of mean
s_p	Pooled variance
S_r	Residual water saturation []
S_s	Specific storage
S_w	Water saturation []
s_1^2	Variance from 2D transport models
s_2^2	Variance from 3D transport model
t	Time [T]
T	Transmissivity [L^2/T]
T	Transpose of matrix
TDS	Total dissolved solids [M/L^3]
TIN	Triangulated Irregular Network
u	Vector of hyperparameters in Bayesian Updating
UB	Upper bound
UTM	Universal Transverse Mercator
v_L	Linear groundwater velocity [L/T]
w	Sources and sinks
WCSB	Western Canada Sedimentary Basin
x	A possible state
x	Spatial coordinate [L]
x_i	Spatial coordinate
Y	Variable under interest
$Y(\mathbf{x})$	Random function of **x**
$y(\mathbf{x}_i)$	Measured y values at $\mathbf{x}_i$ used in kriging interpolation
y_i	Data values
$\hat{y}_0(x_0)$	Estimated y_0 value at x_0 using kriging
y_1	Sample mean of absolute value of residuals from 2D models
y_2	Sample mean of absolute value of residuals from 3D model
z	Elevation head [L]
Z	Normal score value
z_i	Standard normal percentile
α	Aquifer compressibility [$L \cdot T^2/M$] ≡ [1/F]
α_f	Fitting parameter for saturation – relative permeability relationship
α_L	Longitudinal dispersivity [L]
α_{LP}	Pore-scale longitudinal dispersivity [L]
α_T	Transverse dispersivity [L]
α_{TP}	Pore-scale transverse dispersivity [L]
α_v	Vertical dispersivity [L]
β_n	Lagrange multiplier in MRE
β_w	Water compressibility [$L \cdot T^2/M$]
χ^2	Chi square calculated from data

χ_{crit}^2	Critical χ^2 value at specified confidence interval and degrees of freedom
δ_{ij}	Kronecker delta function
$\Delta_{i,l}$	Moving window of size l centered on i
γ	Semi-variance
$\hat{\gamma}_c(h_d)$	Estimated Classical Semi-variance at lag distance h_d []
γ_F	Flow factor
$\gamma_N(h_d)$	New semi-variance estimator presented by Li and Lake (1994)
$\hat{\gamma}_N(h_d)$	Estimated moving window semi-variance []
γ_r	Constant used in equation of state
$\boldsymbol{\eta}$	Normal vector
λ	First-order decay constant
λ_e	Integral scale [L]
λ_i	Interpolation weights in kriging
λ_j	Lagrange multiplier in MRE
μ	Mean
μ_f	Fluid viscosity [M/L·T]
μ_L	Lagrange multiplier in MRE
μ_Y	Expected value of ensemble
μ_1	Mean of absolute residuals for 2D transport models
μ_2	Mean of absolute residuals for 3D transport model
$\boldsymbol{\nu}$	Vector of uncertainties used in Bayesian Updating Interpolation
ν_k	Lagrange multiplier in kriging
θ	Volumetric water content []
θ_s	Saturated volumetric water content []
ρ	Fluid density [M/L^3]
ρ_0	Reference (freshwater) density [M/L^3]
ρ_b	Bulk density [M/L^3]
ρ_{max}	Maximum density [M/L^3]
ρ_r	Relative density []
σ	Standard deviation
σ^2	Variance of data
σ_d^2	Uncertainty in form of variance of data
σ_Y^2	Sill of semi-variogram
σ_1^2	Variance of 2D models
σ_2^2	Variance of 3D model
τ	Tortuosity
ψ	Pressure head [L]

CHAPTER 1

INTRODUCTION

Water was been termed the 'resource of the new millennium' and maintaining clean, viable resources has been brought to the forefront within the past several decades. After the water tainted with E.Coli bacteria in Walkerton, Ontario in 2000 killed six and caused illness in 2,300 others and the threat of contaminated water in Saskatchewan, clean water has become an immediate concern. Groundwater comprises 97% of the world's freshwater (Sampat, 2000). As demand for water is continuously increasing and surface water resources are becoming threatened or over-taxed, groundwater use as a resource will invariably grow. Whereas river water takes an average 20 days to renew, groundwater takes on average 1,400 years (Sampat, 2000). The time for an aquifer to renew depends on a number of factors, such as recharge to the system, natural and man-made discharges and the hydrogeological properties. When groundwater is pumped, it is potentially being removed from the system for many years (Sampat, 2000), depending on the nature of the aquifers. Therefore, proper groundwater management is becoming an issue at the forefront of water resources today. To manage these systems properly requires in-depth knowledge of complicated hydrogeological areas. A report *Our Common Future* (WCED, 1987) defined sustainable development as "development which meets the needs of the present without compromising the ability of future generations to meet their own needs". Overexploitation has negative consequences, such as increasing water cost, environmental changes (e.g. salinity problems), reduction of existing water

sources, water salinization and deterioration of quality (Villarroya and Aldwell, 1998). These issues are important to Manitobans, as southern Manitoba contains many aquifers, with two regional-scale bedrock aquifers that are heavily developed. The "Carbonate Aquifer" is a paleokarst aquifer that occurs in the upper 15 to 30 m of the outcropping Paleozoic carbonate formations, where the rocks are highly fractured and very permeable (Render, 1970). In southeastern and central Manitoba, the Carbonate Aquifer provides water for municipal, industrial, rural residential, and agricultural uses (Betcher et al., 1995). The total quantity of water pumped from the Carbonate Aquifer has varied from less than 0.0525 m^3/s to 0.525 m^3/s (10^6 to 10^7 gallons/day) (Render, 1970). The second "Sandstone Aquifer" is contained within the sandstone of the Winnipeg Formation, which directly overlies the Precambrian basement. The Winnipeg Formation ranges from a thickness of about 30 to 60 m in the south and to about 5 m in the north (Betcher et al., 1995). The Sandstone Aquifer provides a source of domestic water to the southeast region of the province and along the western shore of Lake Winnipeg (Betcher et al., 1995).

The Carbonate Aquifer contains saline (TDS > 50 g/L) waters in the southwest and south-central Manitoba. The water quality is better towards the east and is associated with a physiographic depression (Betcher et al., 1995). A transition zone between fresh and salt water runs north-south approximately along the Red River (see Figure 1.1). The transition zone is thought to be at equilibrium within this aquifer (Betcher et al., 1995). The Sandstone Aquifer contains saline, brine and brackish waters throughout south-central and southwestern regions. These waters extend into the western Interlake region

and go as far east as the outcrop zone, which is located south of Lake Winnipeg and east of the city of Winnipeg (Betcher et al., 1995). The freshwater is therefore contained in the southeastern areas, the eastern zone of the Interlake region and the northernmost portions (Betcher et al., 1995). A transition zone between fresh and salt water is located east of that in the Carbonate Aquifer. The transition zone is thought to move eastward at a rate of approximately 1 m/yr (Betcher et al., 1995).

The Carbonate and Sandstone Aquifers are investigated within this thesis to establish sustainability of the overall system and examine movement of the salt water/fresh water interface. A three-dimensional finite element model was constructed to evaluate both flow and transport. The study region is shown in Figure 1.1 and is essentially the south-eastern part of the province. The model consists of the region south to the U.S.A.-Manitoba border, east to the Manitoba-Ontario border, north into the Interlake region and west to the Manitoba Escarpment. The western boundary was chosen so that it was within the saltwater portion to obtain reasonable boundary conditions. The model consists of the two aquifers and surrounding confining units. The hydraulic conductivity values are heterogeneous and other hydrogeological properties are considered homogeneous within each unit. The model also accounted for variable density flow as a result of the presence of salt water within the system. The final model is then used to generate predictions in order to observe effects of different scenarios on the system. The runs conducted for this thesis included: current sustainability; future sustainability; effects of a pumping centre close to the salt water/fresh water interface; effect of a drought; effect of a flood; and natural movement of the salt water/fresh water interface.

This thesis is divided into eight additional chapters. Chapter 2 contains a literature review with all background information required for the remainder of the thesis. Chapter 3 covers the generation of a hydrostratigraphic model and the sources of geology that were used to construct the model. The fourth chapter illustrates the compilation of data required in the generation of the model. Chapter 5 contains the geostatistical analysis that was conducted on the transmissivity data, which was then used in Chapter 6 to generate heterogeneous fields for each unit using Bayesian Updating. Chapter 7 provides a detailed overview of the model construction and comparison with field results. Chapter 8 presents and discusses the results of the different runs that were examined using the model. Chapter 9 is the last chapter in the thesis and is where conclusions and summation remarks are given.

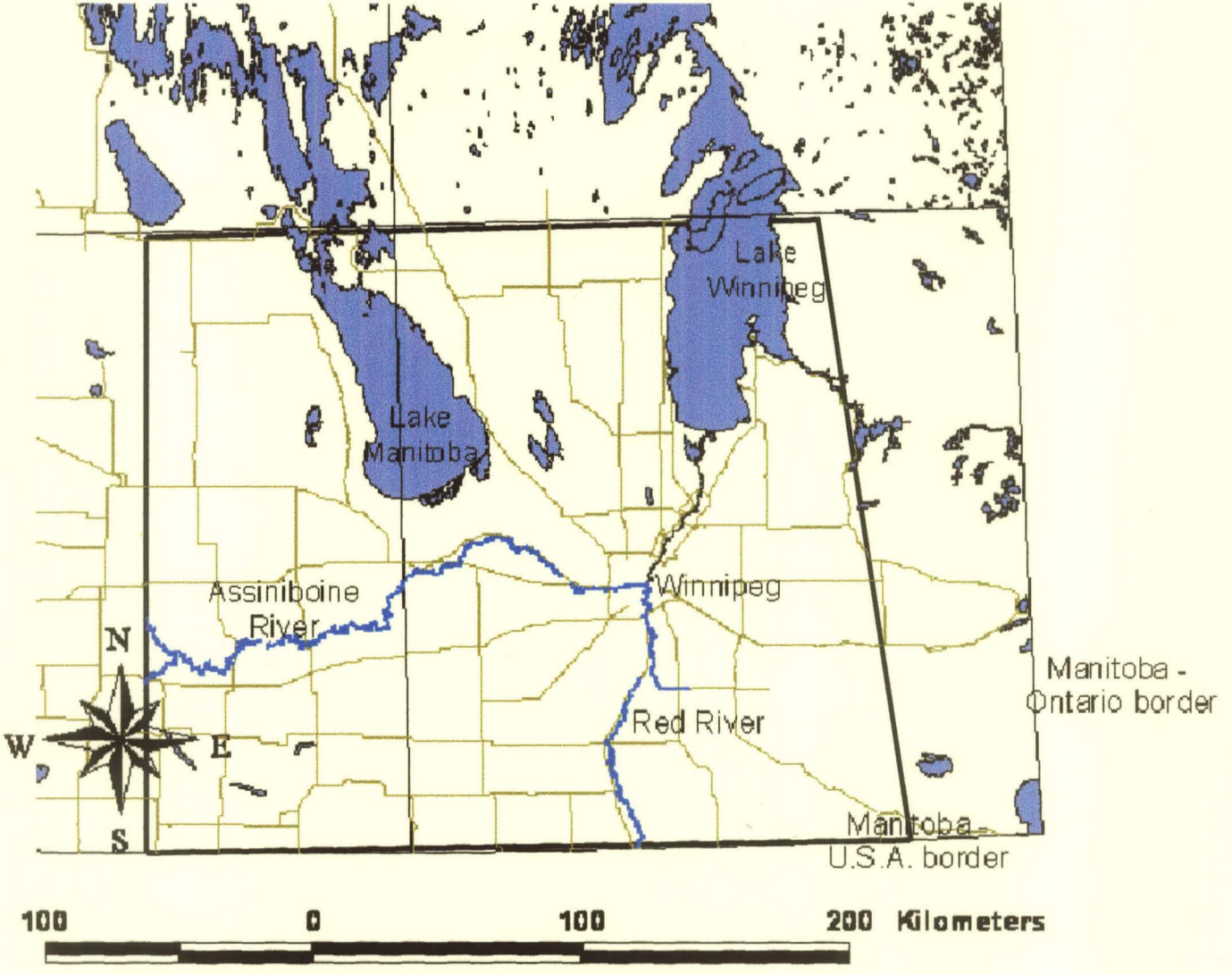

Figure 1.1 – Map showing scope of study area.

CHAPTER 2

LITERATURE REVIEW

2.1 Introduction

The aim of this chapter is to provide background information and hypotheses that will be addressed in the remainder of the thesis. Section 2.2 describes the geology that is present throughout the study area in Southern Manitoba. Section 2.3 provides an overview of the Sandstone and Carbonate Aquifers that will be modeled in this research. Section 2.4 gives an overview of the modeling methodology that was followed in the construction of the flow and transport model. Section 2.5 describes the hydrogeological properties that are required and the theory behind estimation of properties that were not measured. Section 2.6 presents the equations used to develop the mathematical and numerical models. Sections 2.7 and 2.8 describe theory on geostatistics and interpolation techniques that were used to assess the data and assign properties to the finite element mesh.

2.2 Geology of Southern Manitoba

A stratigraphic column of the geologic formations that are present in southern Manitoba are shown in Table 2.1. Precambrian rocks form the basement throughout the entire study area. In the eastern and northern parts of the province, these Precambrian rocks outcrop and form the uppermost bedrock. Towards the Southwest portion of the

province, the Precambrian rocks are overlain by a succession of Paleozoic rocks (See Figure 2.1) (Betcher et al., 1995; Bezys and McCabe, 1996).

Table 2.1 – Stratigraphic column of geological formations located in Southern Manitoba (from Betcher et al., 1995).

ERA	PERIOD	FORMATION (GROUP)	MEMBER	BASIC LITHOLOGY	THICKNESS METRES	HYDROSTRATIGRAPHIC UNITS AQUIFERS AND AQUITARDS
CENOZOIC	Quat. Recent			Soil, alluvial deposits, sand dunes, bogs		OVERBURDEN UNIT
	Pleistocene			Glacial deposits	0—260	
	Tertiary Eocene to Pliocene	Not reported in Manitoba				UPPER CLASTIC UNIT
	Paleocene	Turtle Mountain		Shale, sandstone, lignite	—145+	sandstone aquifer
MESOZOIC	Cretaceous	Boissevain		Sand and sandstone, greenish grey, kaolinitic shale	30—45	
		Pierre Shale	Coulter Odanah	Bentonitic clayey silt Hard grey siliceous shale	20—55 —245+	shale aquifer
			Millwood	Greenish bentonitic shale	15—150	
			Pembina	Non-calc. shale, bentonite beds	2—12	
		Niobrara		Calcareous speckled shale	2—32	shale aquitard
		Morden Shale		Carbonaceous shale, septarian concretions	15—60	
		Favel		Calc. speckled shale, limestone bands	18—40	
		Ashville / Ashville sand		Non-calc. silty shale; 0-27m sand	37—113	
		Swan River		Sand, sandstone, shale, clay, lignite	0—120	
	Jurassic	Waskada		Varicoloured shale	0—50	sandstone aquifers
		Melita		Varicoloured shale, calc. shale, limestone	100—145	
		Reston		Argillaceous limestone and shale	0—50	
		Amaranth	Upper evaporite	Anhydrite, gypsum, shale, dolostone	0—50	
			Lower red beds	Dolomitic shale to siltstone, anhydritic	0—42	
	Triassic					
PALEOZOIC	Permian Pennsylvanian	Not reported in Manitoba except Permian? Lake St. Martin cryptoexplosion structure				evaporite aquitard
	Mississippian	Charles		Dolostone and anhydrite	—37	CARBONATE - EVAPORITE UNIT
		Mission Canyon		Limestone, dolostone, anhydrite; oil production	80—100	
		Lodgepole	Whitewater Lake Virden Scallion Routledge	Limestone, argillaceous and cherty; shale, oil production	145—175	carbonate aquifer
		Bakken		Black shale and siltstone	3—15	
	Devonian	Qu'Appelle Group	Three Forks	Red dolomitic shale	11—55	shale aquitard
		Saskatchewan Group	Birdbear	Fossiliferous limestone and dolostone	12—43	
			Duperow	Shaly limestone, dolostone, anhydrite; cyclical	120—195	
		Manitoba Group	Souris River First Red	Limestone, evaporite, shale; cyclical	65—95	carbonate aquifer
			Dawson Bay Second Red	Limestone, anhydrite, basal red shale	42—67	
		Elk Point Group	Prairie Evaporite	Halite, with potash, anyhdrite, dolostone	0—130	
			Winnipegosis	Dolostone, reef and inter-reef	9—107	evaporite aquitard
			Elm Point	High-calcium limestone	0—14+	
			Ashern	Dolostone and shale, brick red	2—18	
	Silurian	Interlake Group		Dolostone	53—115	
		Stonewall		Dolostone	9—21	
	Ordovician	Stony Mountain	Gunton Penitentiary Gunn	Dolostone, upper part shaly Argillaceous dolostone Fossiliferous calc. shale; red, grey, green	30—50	carbonate aquifer
		Red River	Fort Garry Selkirk Cat Head Dog Head	Dolostone, minor limestone Dolomitic limestone, mottled Dolostone, cherty Dolomitic limestone, mottled	53—150	sandstone aquifer
		Winnipeg		Quartzose sand, sandstone; shale	0—67	BASAL CLASTIC UNIT
	Cambrian	Deadwood		Glauconitic sandstone	?	
PRECAMBRIAN						PRECAMBRIAN

The basal units overlying the Precambrian rocks are the Deadwood and Winnipeg Formations. The Deadwood Formation is only present in the extreme southwest corner of the province and is outside of the study region. The Winnipeg Formation consists of interbedded shales and sandstones (Betcher et al., 1995). The thickness changes irregularly from its maximum of about 60 m in the south to zero at its northern limit (Bezys and McCabe, 1996). McCabe (1978) divided the Formation into two subsections, which he labeled the Lower Winnipeg and Upper Winnipeg. At the base of the Lower Winnipeg, there is a single blanket-type sand deposit that is present throughout (McCabe, 1978). The distribution of sandstone and shale in both subsections is very irregular, making it difficult to separate the unit into one sandstone layer and one shale layer. For these reasons McCabe (1978) divided the Lower and Upper Winnipeg into facies (see Figure 2.2). The sand distribution is not the same for both divisions but the regional pattern is similar. A thick shale facies with only small amounts of sandstone is present in the south. A transition facies is present towards the north, where at least two sandstone contacts are observed. Continuing northward into the sand facies, the entire unit thins and the sand content increases until the unit is composed entirely of sand. One anomalous feature that is present in the Upper Winnipeg is the presence in the south of an extensive sand body called the Carman Sand (see Figure 2.2b) (McCabe, 1978). Persistent shale at the top of the Winnipeg Formation is present throughout the study area providing a hydraulic boundary with overlying units (Betcher et al., 1995).

The Red River Formation consists of dolostone and limestone rocks. This unit has been subdivided into four smaller members: the Fort Garry; Selkirk; Cat Head; and Dog Head members (McCabe, 1971). The Ordovician through Devonian aged rocks, including the Stony Mountain, Stonewall, Interlake Group, Elk Point Group, Manitoba Group and Saskatchewan Group Formations are also all composed primarily of limestone or dolostone rocks (Bezys and McCabe, 1996). The Qu'Appelle Formation of the Devonian Period and Bakken Formation of the Mississippian Period consist of different types of shale (McCabe, 1971). The remaining Mississippian Period rocks are composed of limestone or dolostone rocks and subcrop to the west (McCabe, 1971). The Jurassic Period rocks are divided into four formations, the Waskada, Melita, Reston and Amaranth. These formations consist primarily of shale with some limestone, dolostone and gypsum (McCabe, 1971). The remaining rocks are from the Cretaceous period and Cenozoic Era and are primarily composed of shales with some minor exceptions. For example the Swan River Formation also contains sand and sandstone (McCabe, 1971). These rocks are only present in the extreme west of the study region and are considered one unit.

A bedrock map is presented in Figure 2.3 showing the outcrop zones of the Precambrian, Winnipeg Formation, Red River Formation, Stonewall and Stony Mountain Formations, Interlake Group Formation, Elk Point Group Formation, Manitoba Group Formation and the Jurassic Period rocks. Generally, the outcrop zones are such that younger rocks outcrop to the west. However, the Jurassic Period rocks outcrop in an anomalous manner with a tongue overlying the other formations towards the South.

2.3 Hydrogeology of Southern Manitoba

2.3.1 Carbonate Aquifer

The Carbonate Aquifer is a primary source of groundwater in Southern Manitoba. It is used for industrial, rural residential, agricultural and irrigation purposes (Betcher et al., 1995). The aquifer is located within the fractured, more permeable outcrop region of the carbonate rocks of the Red River, Stony Mountain, Stonewall, Interlake Group, Elk Point Group, Manitoba Group and Saskatchewan Group Formations (Betcher et al., 1995; McCabe et al., 1993). Potential causes of the fracturing are thought to be due to pre-Pleistocene weathering of the carbonate rocks or due to stresses caused by Pleistocene glaciation (McCabe et al., 1993). The zone of permeability is variable through the outcrop zone and is thought to be located in the upper 15 and 30 m (Render, 1970).

In the Carbonate Aquifer, there is salt water to the west and fresh water to the east. There is a north-south trending transition zone, which approximately follows the Red River (see Figure 1.1). Betcher et al. (1995) postulate that the transition zone is at natural equilibrium and is not moving.

2.3.2 Sandstone Aquifer

The Sandstone Aquifer is located within the Winnipeg Formation. The Sandstone Aquifer is not as heavily developed as the Carbonate Aquifer and is primarily used for domestic purposes in southeastern Manitoba and along the western shore of Lake Winnipeg (Betcher et al., 1995). As previously stated, a shale layer is present over the

entire unit within the study area. This shale layer provides a hydraulic boundary between the Sandstone and Carbonate Aquifers.

In the Sandstone Aquifer there is also the presence of salt water to the west and fresh water to the east. There is a north-south trending transition that is located to the east of that in the Carbonate Aquifer. It is thought that this transition zone is moving eastwards further into freshwater zone at about 1 m/year (Betcher et al., 1995).

2.4 Modeling Methodology

This section describes the method that was followed to develop the three-dimensional flow and transport model. Anderson and Woessner (1992) have suggested a protocol that was followed in this research (see Figure 2.4). The first step was to establish a purpose, which in this case was to examine the long-term sustainability of the Carbonate and Sandstone Aquifers and the movement of the salt water/fresh water transition zones. Sustainability of groundwater systems for this thesis signified conditions in which the level of water was not lowered significantly and water quality does not deteriorate. Quality may deteriorate if development is such that the salt water/fresh water interface moves towards the fresh water region. The desired model results are total head (h) to monitor water levels and ion concentration (C) to investigate movement of saltwater/freshwater transition zone.

The second step is the construction of the conceptual model. In this phase the real system is conceptualized into an equivalent system that is capable of being modeled. It should

be simplified enough to avoid excessive computational problems, yet complicated enough to capture the essential features that affect flow and transport. This phase also includes the collection and assimilation of all required data from field measurements and observations. The geology is simplified into hydrostratigraphic units, which are "bodies of rock with considerable lateral extent that compose a geologic framework for a reasonably distinct hydrologic system" (Maxey, 1964). An aquifer unit represents one that has a greater transmissivity than surrounding units and can transmit a quantity of water that is economically useable, usually a well yield greater than $2x10^{-5}$ m^3/s (Maxey, 1964). An aquiclude or confining unit is defined as those units of low permeability that bound the aquifer (Maxey, 1964). If an appreciable amount of water moves through the confining bed, then it is called an aquitard (Maxey, 1964).

The next few steps involve the choice of mathematical and numerical models. The mathematical model includes the governing equations for flow and transport and the required constitutive relationships. The numerical model is the choice of numerical method, for example finite element or finite difference approach, and the choice of code that will be used. The chosen code must be "verified", ensuring that the governing equations of the numerical model have been implemented correctly. The model results are compared against an analytical solution and is verified if the match is good. The analytical solutions that are used for comparison are generally simplified problems, but the goal of the numerical model is to solve complicated problems. Konikow and Bredehoeft (1992) point out that even though the numerical code matches an analytical

solution perfectly, there is no assurance that the model will continue to correctly solve the equations for more complicated problems.

Once a numerical model has been chosen and verified, simulations can proceed. This includes construction of a finite element mesh for the hydrostratigraphic units defined in the conceptual model. Hydrogeological properties, or ranges of each property, are assigned based on the collected data (measurements). Boundary conditions for both flow and transport must be assigned to all boundaries of the model. Three types of boundary conditions are available. Type I or Dirichlet boundary conditions are specified dependent variable boundaries (Anderson and Woessner, 1992). For flow this would be specified head (h) and for solute transport this would be specified concentration (C). An example of where this type of boundary condition would be used would be for a lake where the water level and therefore hydraulic head is known. Type II or Neuman boundary conditions are specified first derivatives of the dependent variable ($\partial h / \partial x_i$ for flow and $\partial C / \partial x_i$ for solute transport) (Anderson and Woessner, 1995). This type of boundary condition may be used to represent a no flow boundary such as a groundwater divide or impermeable boundary, or if the magnitude of the flux is known at some point. Type III or Cauchy boundary conditions are a mixture of the first two types (Anderson and Woessner, 1995). An example of where this type of boundary condition would be used is for seepage faces where the flux rate is dependent on the value of the head.

The determination of the combination of hydrogeological properties and boundary conditions that provide model results matching field observations will be termed the

"calibration" phase. Konikow and Bredehoeft (1992) state that even when a good fit is obtained between model results and observations, the model is not necessarily valid. In other words, the model has been shown to simulate one scenario, but may not predict future changes correctly. Prior to calibrating the model, calibration criteria must be specified, that once met, the model is said to be calibrated. Examples of calibration criteria are accepted intervals around observations and error across the region.

Once the model is calibrated, it may be difficult to ascertain whether the correct combination of model parameters has been found. This is related to solution and geologic uniqueness, which is difficult to establish (Woodbury, 1987). Therefore, model "validation" or "history match" is conducted, in which the "calibrated" model is checked against a second set of data (current observation in this research) collected hopefully under different "stress" conditions. Stress conditions in this thesis signify pumping wells or other development schemes that are placed on the groundwater system. If the calibrated model results of this new simulation match this second (independent) dataset, then the model is deemed validated. If not, the calibration phase must be revisited until validation is successful. As Konikow and Bredehoeft (1992) pointed out, even though the term validation is used for this phase, it does not necessarily indicate that the model is "valid". The validation phase, however, gives more confidence in the final model. A rule of thumb, is that the final model can be used to make future predictions within a period of time that was used for history matching.

The final step of the protocol is the postaudit. This step is done at some point in the future to determine whether the predicted model results are accurately simulating what is occurring within the field. Due to practically constraints, this portion of the protocol will not be conducted for this research.

2.5 Hydrogeological Properties

Hydrogeological properties are required for each hydrostratigraphic unit in the numerical model. Transmissivity (T) is defined as the ability of an aquifer to transmit water through its entire thickness. Storativity (S) is defined as the volume of water released from storage per unit surface area of aquifer due to a unit decline in hydraulic head (Freeze and Cherry, 1979). Both transmissivity and storativity can be determined through pump tests, slug tests or drill stem tests (Domenico and Schwartz, 1990). A pump test involves removing water from the aquifer at a constant flow rate and monitoring the changes in water level within the aquifer at one or more observation well and can be analyzed by several methods, including Theis and Cooper-Jacob methods (see Domenico and Schwartz, 1990). These methods include different assumptions such as the aquifer is of infinite areal extent, that the pumping well fully penetrates the aquifer, that water is released instantaneously due to a decline in head, and that the soil medium is homogeneous and isotropic (Domenico and Schwartz, 1990). Due to the variability and complexity of geological systems, these assumptions may not be satisfied. The numerous assumptions involved in analyzing pump tests may cause the values of transmissivity to be in error by up to an order of magnitude (Freeze and Cherry, 1979).

The aforementioned types of analyses of pump tests require the presence of at least one observation well other than the pumping well. Due to economics, it is quite common for practitioners to pump water from one well and monitor the changes in water level within this same well. In the vicinity of the well, the flow may be turbulent and adds to nonlinearities in the drawdown around the well. When calculating transmissivity, this invalidates assumptions in the analysis and increases inaccuracy. This test type will be referred to as a "single-well drawdown test" for the remainder of this thesis. A pump test with at least one observation well other than the pumping well will be referred to as a "multiple-well drawdown test". Transmissivity can also be estimated from specific capacity, which is defined as the flow (Q) per unit drawdown (s). This estimation method assumes that the pumping well is 100% efficient, in other words that there is no well loss (Domenico and Schwartz, 1990). The transmissivity can be estimated by solving the following equation:

$$\frac{Q}{s} = \frac{4\pi T}{\ln \frac{4Tt}{r_w^2 S} - 0.5772} \qquad \textbf{(2.1)}$$

Where r_w is the radius of the well and t is the time of the test. As the well loss is assumed to be zero in this approximation (well loss is unavoidable) the resulting transmissivity value is underestimated (Domenico and Schwartz, 1990).

Transmissivity values in the Carbonate Aquifer are reported to range from about zero in a select few wells to over 0.139 m^2/s in other areas (Betcher et al., 1995). For the Sandstone Aquifer, transmissivity values in the eastern Interlake and southeastern area of

Manitoba were reported to range between 5.2 x 10^{-5} m^2/s to 3.6 x 10^{-2} m^2/s (Betcher, 1986).

Storativity can also be estimated using the first principle equation:

$$S = \rho g b(\alpha + n\beta_w) \qquad (2.2)$$

Where ρ is the density of the fluid, g is the gravitational constant, b is the saturated thickness of the medium, n is the porosity of the soil medium, α is the compressibility of the aquifer medium and β_w is the compressibility of water. The gravitational constant is 9.81 m/s^2 and compressibility of water at 25°C is equal to 4.8x10^{-10} Pa^{-1} (Domenico and Schwartz, 1990). Compressibility of fissured rock ranges between 6.9x10^{-10} and 3.3x10^{-10} Pa^{-1} and that of sound rock is less than 3.3x10^{-10} Pa^{-1} (Domenico and Schwartz, 1990). The water density varies due to changes in ion concentrations across the region. The resulting uncertain factors are ρ, α, b and n as these vary spatially over the study region. For the Carbonate Aquifer, Render (1970) reported that the storativity ranges between 1x10^{-6} and 1x10^{-3}.

To model the solute transport equation, estimates or measurements of dispersion are required. The hydrodynamic dispersion tensor, **D**, is a function of longitudinal and transverse dispersivity (Bear, 1972).

$$\theta_s S_w \mathbf{D} = (\alpha_L - \alpha_T)\frac{\mathbf{q}_i \mathbf{q}_j}{|\mathbf{q}|} + \alpha_T |\mathbf{q}| \delta_{ij} + \theta_s S_w \tau D_d \delta_{ij} \qquad (2.3)$$

Where α_L and α_T are longitudinal and transverse dispersivities, $|\mathbf{q}|$ is the magnitude of the Darcy flux **q**, δ_{ij} is the kronecker delta function, τ is the tortuosity, S_w is the water

saturation, θ_s is the saturated volumetric water content ($\equiv$ n) and D_d is the diffusion coefficient.

A method of determining the dispersivities for equation 2.3 is required. Gelhar and Axness (1983) presented a method of estimating both the longitudinal and transverse dispersivity. Longitudinal asymptotic macrodispersivity, α_L, is a function of asymptotic longitudinal dispersivity (result of heterogeneous hydraulic conductivity) A_L, pore-scale dispersivity, α_{LP}, and finally due to bulk diffusion. The equation to determine the longitudinal dispersivity is:

$$\alpha_L = A_L + \alpha_{LP} + \frac{D_d}{v_L} \qquad \textbf{(2.4)}$$

Where:

$$A_L = \frac{\sigma^2 \cdot \lambda_e}{\gamma_F^2}$$

Where σ^2 is the variance of parameter Y (Y=lnK), λ_e is the integral scale from an assumed exponential covariance model (as will be presented later in this chapter), γ_F is a flow factor (assumed equal to 1.0) and v_L is the linear groundwater velocity. Equation 2.4 assumes that flow is unidirectional. A similar equation can be used to calculate the transverse dispersivity.

$$\alpha_T = \alpha_{TP} + \frac{D_d}{v_L} \qquad \textbf{(2.5)}$$

Where α_{TP} is the pore-scale transverse dispersivity. This equation assumes that the heterogeneous nature of the hydraulic conductivity does not affect the transverse dispersivity. The transverse dispersivity can also be estimated as one to two orders of

magnitude lower than α_L (Gelhar et al., 1992). In three-dimensions, the vertical dispersivity is also required and can be assumed another order of magnitude lower than α_t (Gelhar et al., 1992).

Neuman (1990) and Gelhar et al. (1992) investigated dispersivity as a function of scale. Scale being the distance that the plume has traveled from the source of initial contamination. Both studies investigated data from many research projects and showed that dispersivity increased with increasing scale. The data from Gelhar et al. (1992) were used to plot longitudinal and transverse dispersivity as a function of scale (see Figure 2.5). Neuman (1990) investigated both unconditioned (based on a Fickian interpretation) and conditioned (based on calibration of a numerical model) values of dispersivity. It was found that conditioned dispersivity values were lower than unconditioned values at all scales. Neuman (1990) stated that the lower conditioned dispersivity values were a reflection of increased information on the heterogeneous nature of the hydraulic conductivity.

2.6 Mathematical/Numerical Model

2.6.1 Governing Equations and Numerical Solution

In order to create a model of the flow and solute transport, a mathematical and numerical model was required. The chosen numerical model for this research was the finite element code, FRAC3DVS, which is three-dimensional, allows for saturated and unsaturated flow, heterogeneous hydraulic conductivity and transport in a variable density field. The development and verification of this code is presented in Therrien and Sudicky (1996). A

summary of the governing equations and methods used to develop FRAC3DVS is presented in this section. For the purposes of this research, FRAC3DVS was modified by Therrien to account for variable density flow and transport using the methodology presented by Frind (1982).

For flow, it was assumed that the fluid is incompressible, isothermal conditions are present and that the air phase is infinitely mobile. The governing equation for three-dimensional transient flow as presented by Bear (1972) is:

$$\frac{\partial}{\partial \mathbf{x}}(\rho \cdot \mathbf{q}) \pm w = -\frac{S_s}{g}\frac{\partial P}{\partial t} \qquad (2.6)$$

Where P is the pressure, **x** is the spatial coordinate, w represents the sources and sinks in the system and S_s is the specific storage (=S/b). The flux can be determined from the Darcy equation (Bear, 1972).

$$\mathbf{q} = -\frac{k_{rw} \cdot \mathbf{k}}{\mu_f}\left(\frac{\partial P}{\partial \mathbf{x}} + \rho g \boldsymbol{\eta}\right) \qquad (2.7)$$

Where k_{rw} is the relative permeability, **k** is the intrinsic permeability tensor, μ_f is the dynamic viscosity and $\boldsymbol{\eta}$ is a vector if equal to 1 indicates the vertical direction and 0 represents the horizontal direction. The hydraulic head is the sum of pressure head (ψ) and elevation head (z).

$$h = \psi + z = \frac{P}{\rho g} + z \qquad (2.8)$$

As density changes within the system due to concentration variations, the equivalent freshwater head, h_f, can be expressed as:

$$h_f = \frac{P}{\rho_o \cdot g} + z \tag{2.9}$$

Where ρ_0 is the reference density (freshwater = 1000 kg/m^3). The Darcy flux can then be expressed in terms of head as follows.

$$\mathbf{q} = -k_{rw} \cdot \mathbf{K}\left(\frac{\partial h_f}{\partial \mathbf{x}} + \rho_r \boldsymbol{\eta}\right) \tag{2.10}$$

Where:

$$\mathbf{K} = \frac{\mathbf{k}\rho_0 g}{\mu_f} \tag{2.11}$$

and

$$\rho_r = \frac{\rho}{\rho_0} - 1 \tag{2.12}$$

The tensor **K** is the saturated hydraulic conductivity and ρ_r is the relative density.

An equation of state representing the relationship between fluid density and concentration was required. In this case, the following linear relationship between relative concentration and density was used, which was satisfactory for isothermal conditions and dilute solutions.

$$\rho = \rho_0(1 + \gamma_r C_r) \tag{2.13}$$

Where

$$C_r = \frac{C}{C_{\max}} \tag{2.14}$$

and

$$\gamma_r = \frac{\rho_{\max}}{\rho} - 1 \tag{2.15}$$

Equation 2.13 states that at a relative concentration (C_r) equal to 0, the density will be equal to the freshwater density and if the relative concentration equals 1, then the density will equal maximum density. Equations 2.12 and 2.13 can be combined, to give the following equation.

$$\rho_r = \gamma_r C_r \tag{2.16}$$

Equation 2.16 can be substituted back into equation 2.10 to give an equation for flux that is dependent on relative concentration rather than density.

$$\mathbf{q} = -k_{rw} \cdot \mathbf{K}\left(\frac{\partial h_f}{\partial \mathbf{x}} + \gamma_r \cdot C_r \boldsymbol{\eta}\right) \tag{2.17}$$

The original groundwater flow equation (equation 2.6) can also be re-written in terms of freshwater head and relative concentration.

$$\frac{\partial}{\partial \mathbf{x}}\left[k_{rw} \cdot \mathbf{K}\left(\frac{\partial h_f}{\partial \mathbf{x}} + \gamma C_r \boldsymbol{\eta}\right)\right] \pm w = S_s \frac{\partial h_f}{\partial t} \tag{2.18}$$

The level of saturation and relative permeability is dependent on head and FRAC3DVS used the relationships developed by van Genuchten (1980) and Mualem (1976).

$$S_e = \frac{S_w - S_r}{1 - S_r} = \left[\frac{1}{1 + (\alpha_f \cdot h_c)^{n_f}}\right]^{m_f} \tag{2.19}$$

$$k_{rw} = S_e^{1/2}\left[1 - \left(1 - S_e^{1/m_f}\right)^{m_f}\right]^2 \tag{2.20}$$

Where α_f, n_f and m_f are fitting parameters, S_e is the effective saturation (scales saturation between 0 and 1), S_r is the residual water saturation and h_c is the capillary head. From these relationships, the saturation can be determined at any capillary head and the relative permeability can be determined for any saturation.

The solute transport equation in three-dimensional transport is as follows (Bear, 1972).

$$\theta_s S_w R \frac{\partial C_r}{\partial t} + \mathbf{q} \frac{\partial C_r}{\partial \mathbf{x}} - \frac{\partial}{\partial \mathbf{x}} \left(\theta_s S_w \mathbf{D} \frac{\partial C_r}{\partial \mathbf{x}} \right) + \theta_s S_w R \lambda C_r = 0 \qquad \textbf{(2.21)}$$

Where R is a retardation factor and λ is the first-order decay constant. This equation assumes that the fluid is incompressible. The retardation factor is given by (Freeze and Cherry, 1979).

$$R = 1 + \frac{\rho_b}{\theta_s S_w} K_d \qquad \textbf{(2.22)}$$

Where ρ_b is the bulk density of the aquifer medium and K_d is the equilibrium distribution coefficient.

The flow and transport equations in FRAC3DVS were solved using a Galerkin finite-element approach (e.g. Huyakorn and Pinder, 1983). The equations were coupled through the relative concentration and velocity to account for changes in density. For each time step, the concentration from the previous time step was initially assumed. The heads at each node were then solved using the assumed concentrations. The velocities for each element were calculated and the distribution of concentrations was calculated. The heads were then re-calculated with the new concentrations and this iterative procedure was repeated. FRAC3DVS used the Picard iteration for this coupling. The large system of equations was solved using a pre-conditioned ORTHOMIN solver. This solver had been shown to be both efficient and robust (Behie and Forsyth, 1984). The time derivative was solved using a variable time-stepping procedure similar to that outlined by Forsyth and Sammon (1986) and Kropinski (1990). This method allowed for

increasing time steps when no drastic changes in head or concentration were occurring. Unfortunately, the code does not solve a steady state problem directly.

2.7 Geostatistics

2.7.1 Ergodicity, Stationarity and the Intrinsic Assumption

To completely assign parameters in a deterministic manner would require extensive testing which is generally not economically or technically feasible. Therefore, recent transport theories take the viewpoint that hydrogeological parameters can be represented as random processes. For example, assume $Y(\mathbf{x}) = \log(T(\mathbf{x}))$ and a stochastic process signifies every possible record with spatial coordinates $\mathbf{x}$. The collection of all of these records is an ensemble (see Figure 2.6) with an expected value, $E[Y] = \mu_Y$. In hydrogeology, we only have one "realization" of the stochastic process, as it is deterministic. Therefore, it is not possible to calculate the ensemble average. Therefore, in hydrogeological applications we have to assume the ergodic hypothesis, which is that the spatial average of the single realization is equal to the ensemble average (Gelhar, 1993).

A second assumption of stationarity is often also made. A stationary process is one that states that all moments are invariant under shifts of origin of data. In other words, a variable is stationary if the mean, variance, etc. calculated at one point in the realization is the same as that calculated at another. What is generally assumed is a second-order stationary process, having the following properties (Gelhar, 1993).

$$\begin{aligned} E[Y(x)] &= \mu \\ Cov(x) &= Cov(x_1 - x_2) \end{aligned} \tag{2.23}$$

where $x = x_1 - x_2$ for any x_1 and x_2, E[Y(x)] is the expected value of Y(x) and Cov and μ are covariance and constant mean.

Another common assumption is the 'intrinsic hypothesis', which refers to the variogram (as will be discussed later in this chapter). If the semi-variance is only a function of separation distance, s_d, and not on the location, **x**, then the process satisfies the intrinsic hypothesis (Gelhar, 1993).

2.7.2 Distribution Type

In the Bayesian Updating method that will be discussed later in this chapter, it is assumed that the data (or transform of the data) follows a Gaussian distribution. In the literature, it has been reported that the transmissivity (or equivalently hydraulic conductivity) (Freeze and Cherry, 1979) and storativity (Hoeksema and Kitanidis, 1985) generally follow a natural log-normal distribution. Therefore, methods of testing whether a dataset or transform of dataset follow a normal distribution are required. Two different methods are presented here: the Chi Square Test and the Normal Scores Plot test.

The Chi Square Test assumes a null hypothesis that there is no difference between the dataset and the proposed (normal) distribution (Scheaffer and McClave, 1995). Critical chi square, χ_{crit}^2, values are obtained from tables for particular significance levels and degrees of freedom (DOF) (for example see Scheaffer and McClave, 1995). Chi square, χ^2, values are calculated from the dataset and compared against χ_{crit}^2.

$$\chi^2 = \sum_{i=1}^{N} \frac{(O-E)^2}{E} \tag{2.24}$$

where O and E represent the observed and expected values, respectively and N is the total number of data. If $\chi^2 < \chi_{crit}^2$ then the null hypothesis is not rejected and it can be assumed that the dataset follows the tested distribution at the chosen significance level.

The Normal Scores Plot test is a graphical method and is based on the fact that if the data, Y, is normally distributed with mean, μ, and standard deviation, σ, then the normal score, Z, is defined as (Scheaffer and McClave, 1995):

$$Z = \frac{Y-\mu}{\sigma} \tag{2.25}$$

With the assumption of Y being normal, Z will follow the standard normal distribution. To check a dataset by this method, the first step is to arrange the data, y_i, in ascending order. Percentiles can be calculated for each y_i and the corresponding standard normal percentile (z_i) can be determined. A plot of y_i versus z_i should be approximately a straight line if the dataset does indeed follow a normal distribution. Also, the intercept of the line should be close to the mean of the data and the slope of the line should be approximately the same as the standard deviation of the data.

2.7.3 Variogram

A variogram is a plot of the semi-variance (γ) versus separation distance (h_d). The semi-variance is related to how the function is co-related spatially. It is expected that at small separation distances, the semi-variance will be low due to similarity of values. As separation distance increases the semi-variance will increase due to larger variability.

An ideal semi-variance estimator should be both robust (not significantly affected by lack of conformance with underlying assumptions) and resistant (not severely affected by small changes in data). Matheron (1962) developed the "classical semi-variance estimator", which is the arithmetic mean of the squared differences between data values.

$$\hat{\gamma}_c(h_d) = \frac{1}{2N(h_d)} \sum_{i=1}^{N(h_d)} [Y(x_i) - Y(x_i + h_d)]^2 \qquad (2.26)$$

where $\hat{\gamma}_C(h_d)$ is the estimated semi-variance as a function of lag distance, h_d, calculated from the Classical Estimator, $N(h_d)$ is the number of data pairs separated by h_d, Y is the variable under interest and x_i are the spatial coordinates. The Classical Estimator has been found to have stability problems especially at larger lag distances and is mainly caused by the decreasing number of data pairs in the semi-variance calculation with increasing lag distance (Woodbury and Sudicky, 1991). The precision is also affected by the total number of data values (N), the degree of autocorrelation, the variance of the data (σ^2), the underlying probability distribution function (pdf) and the presence of outliers (Li and Lake, 1994).

Li and Lake (1994) proposed a new semi-variance estimator in order to overcome the instability problems of the Classical Estimator. They defined a new semi-variance $\gamma_N(h_d)$ by taking a d-1th moment of the original semi-variance definition, resulting in the following equation.

$$\gamma_N(h_d) = \frac{1}{\int_0^l \xi^{d-1} d\xi} \int_0^l \xi^{d-1} \gamma(\xi) d\xi \qquad (2.27)$$

This new definition could be described as a weighted average with $\xi^{d-1} \Big/ \int_0^h \xi^{d-1} d\xi$ as the weights with d as the dimension (Li and Lake, 1994). Li and Lake (1994) derived an estimator of this new semi-variance definition, which will be referred to in this thesis as the Moving Window Estimator.

$$\hat{\gamma}_N(h_d) = \frac{1}{N}\sum_{i=1}^{n}\left\{\frac{1}{2m_d}\sum_{j\in D_{i,hd}}\left[Y(x_i)-Y(x_j)\right]^2\right\} \qquad \textbf{(2.28)}$$

Where $\hat{\gamma}_N(h_d)$ is the estimate of the Moving Window semi-variance, N is the total number of data in the entire database, $D_{i,hd}$ is the index set of data in a moving window, $\Delta_{i,l}$ (size h_d centered on i), excluding x_i, and m_d is the number of data in $D_{i,hd}$. Figure 2.7 shows two examples of windows that can be used in this method. The square window is for an isotropic estimate and the strip window is for an anisotropic estimate. The Moving Window Estimator uses data points within the moving window and averages the results over the entire dataset. The advantages of this estimator is that equation 2.28 relies on the total number of data in the set, N, not only on the number of data at distance h_d, $N(h_d)$. As all points are used in calculation at every lag distance the Moving Window Estimator is more resistant to outliers and more robust than the Classical Estimator (Li and Lake, 1994).

The variogram contains semi-variance values at all lag distances available in the database. However, problems arise when a semi-variance value is required at a lag distance not contained within the database. Therefore, a function describing the semi-variance at all lag distances was required. There are several standard equations that can

be used to model the semi-variance (e.g. Kitanidis 1996). The sill (σ_Y^2) is the semi-variance at which the variogram levels off, the range (a) is the distance at which the semi-variance is 0.95 of the sill (see Figure 2.8) (Kitanidis, 1996). If there is an observed discontinuity at the origin, this is termed the nugget effect (C_0). This nugget effect is caused by variations in data at scales less than smallest measured lag distance (Journel and Huijbregts, 1978). If the measurements were such that at the smallest lag distance there is zero variability then there will be no observed nugget effect (i.e. C_0=0). Three models that account for presence of a sill are the spherical model, exponential model and the Gaussian model (see Figure 2.9) (Kitanidis, 1996). The covariance function, ($C(h_d)$), can be calculated from semi-variance using the equation $C(h_d)=C(0) - \gamma(h_d)$, where C(0) is the covariance at zero lag distance, which is equal to σ_Y^2.

The equations of semi-variance and covariance at lag distance, h_d, for the spherical model, are:

$$\gamma(h_d) = C_0[1-\delta(h_d)] + (\sigma_Y^2 - C_0)\cdot\begin{cases}\frac{3}{2}\frac{h_d}{a} - \frac{1}{2}\frac{h_d^3}{a^3} & 0 \le h_d \le a \\ 1 & h_d > a\end{cases}$$

$$C(h_d) = C_0\cdot\delta(h_d) + \sigma_Y^2 - C_0 + (C_0 - \sigma_Y^2)\cdot\begin{cases}\frac{3}{2}\frac{h_d}{a} - \frac{1}{2}\frac{h_d^3}{a^3} & 0 \le h_d \le a \\ 1 & h_d > a\end{cases} \quad \textbf{(2.29)}$$

The equations for the Gaussian model are:

$$\gamma(h_d) = C_0 \cdot [1 - \delta(h_d)] + (\sigma_Y^2 - C_0) \cdot \left(1 - \exp\left(-\frac{h_d^{\,2}}{L^2}\right)\right)$$
$$C(h_d) = C_0 \delta(h_d) + \sigma_Y^2 - C_0 + (C_0 - \sigma_Y^2) \cdot \left(1 - \exp\left(-\frac{h_d^2}{L^2}\right)\right) \quad \textbf{(2.30)}$$

Where L is the length parameter and the range (a) is approximately 7·L/4 for this model.

The equations for the exponential model are:

$$\gamma(h_d) = \sigma_Y^2 - (\sigma_Y^2 - C_0) \cdot \exp\left(-\frac{h_d}{\lambda_e}\right)$$
$$C(h_d) = C_0 \delta(h_d) + (\sigma_Y^2 - C_0) \cdot \exp\left(-\frac{h_d}{\lambda_e}\right) \quad \textbf{(2.31)}$$

Where λ_e is the integral scale and is equal to approximately a/3 for the exponential model. The exponential model tends to be most widely accepted in hydrogeological applications (e.g. Sudicky, 1986; Gelhar, 1993; Woodbury and Sudicky, 1991; Hoeksema and Kitanidis, 1985).

Another concept presented in the literature is that of fractal dimension (e.g. Fetter, 1993). This is the idea that the pattern of semi-variance is repeated at different scales, a property known as self-similarity. Therefore, the variations in semi-variance at one scale (e.g. pore scale) may be observed at another (e.g. geologic formation scale) (Fetter, 1993).

In some cases, variograms will not be well represented by any of the aforementioned models and may be a result of a nested structure. A nested structure is the superposition of two or more variograms, each expressing variability due to different scales (Journel and Huijbregts, 1978). Figure 2.10 shows an example of a nested structure with three

different models. The first model is a pure nugget effect (γ_0), which is represented by a straight horizontal line. The second model is a spherical model (γ_1) with a sill of 0.8 and a range of 100. The third model is also a spherical model (γ_2) with a sill of 1.4 and a range of 150. The final nested model is the sum of these three individual models.

$$\gamma(h_d) = C_0 + (\sigma_1^2 - C_0)\cdot\begin{Bmatrix} \frac{3}{2}\frac{h_d}{a_1} - \frac{1}{2}\left(\frac{h_d}{a_1}\right)^3, & h_d < a_1 \\ 1, & h_d \geq a_1 \end{Bmatrix} + (\sigma_2^2 - \sigma_1^2)\cdot\begin{Bmatrix} \frac{3}{2}\frac{h_d}{a_2} - \frac{1}{2}\left(\frac{h_d}{a_2}\right)^3, & h_d < a_2 \\ 1, & h_d \geq a_2 \end{Bmatrix} \quad \textbf{(2.32)}$$

$$C(h_d) = \sigma_2^2 - C_0 + (C_0 - \sigma_1^2)\cdot\begin{Bmatrix} \frac{3}{2}\frac{h_d}{a_1} - \frac{1}{2}\left(\frac{h_d}{a_1}\right)^3, & h_d < a_1 \\ 1, & h_d \geq a_1 \end{Bmatrix} + (\sigma_1^2 - \sigma_2^2)\cdot\begin{Bmatrix} \frac{3}{2}\frac{h_d}{a_2} - \frac{1}{2}\left(\frac{h_d}{a_2}\right)^3, & h_d < a_2 \\ 1, & h_d \geq a_2 \end{Bmatrix} + C_0\delta(h_d)$$

The variogram is said to be anisotropic if the semi-variance relationship is not the same in every spatial direction. Variograms in different directions can be constructed and modeled using any of the aforementioned models. Within a variogram that exhibits a nested structure, the individual models that compose the model may demonstrate their own anisotropy (Journel and Huijbregts, 1978). This means that one of the individual models may be isotropic while another may exhibit anisotropy.

2.7.3.1 Akaike Information Criterion

In order to determine the best variogram model, a testing criterion is required. The Akaike Information Criterion (AIC), considers both the fit of the model to the variogram and the number of parameters required in the model (Hoeksema and Kitanidis, 1985). The AIC is calculated from the following equation.

$$AIC = 2 \cdot (L_{AIC} + k_{AIC}) \tag{2.33}$$

where k_{AIC} is the number of parameters used in a model and L_{AIC} is the negative log likelihood function defined as (Hoeksema and Kitanidis, 1985):

$$L_{AIC} = 0.5 \cdot \left| N \ln(2\pi) + N \ln(\sigma^2) + \chi^2 \right| \tag{2.34}$$

The model of the variogram that results in the minimum value of AIC is the optimal fit between number of parameters and goodness of fit to the experimental variogram.

2.8 Interpolation Techniques

In order to generate heterogeneous fields from a limited amount of data, an interpolation method is required. A problem of this nature can be stated such that given N measurements of y at locations x_1, x_2,..., x_n, estimate the values of y at the m other desired x_i locations. The forward model can be represented by:

$$\underset{N\times 1}{\mathbf{d}} = \underset{N\times m}{\mathbf{G}}\ \underset{m\times 1}{\mathbf{m}} \tag{2.35}$$

where **d** is a data vector [N x 1] containing measurements of y, **m** is a vector [m x 1] with model parameters (the interpolated values) and **G** is a data kernel [N x m], which transfers between data space and model space. If the number of measurements (N) is greater than the number of interpolated points (m), then the problem is stated to be well posed and can be solved directly. If N << m, then the problem is underdetermined and a linear interpolation method can be used to solve the problem. This section describes two interpolation methods, kriging and Bayesian Updating.

2.8.1 Kriging

Kriging is a 'best linear unbiased estimation' (BLUE) method and is a non-parametric; i.e. minimum variance model (Kitanidis, 1997). This method uses a linear combination of the measurements of y (x_1 to x_N), to estimate the value, $\hat{y}_o(x_0)$, at an unmeasured location, $\mathbf{x}_0$.

$$\hat{y}_0(\mathbf{x}_0) = \sum_{i=1}^{N} \lambda_i y(\mathbf{x}_i) \qquad (2.36)$$

Where λ_i are the interpolations weights and are determined through the kriging method. The estimation error that exists between $\hat{y}_o(x_0)$ and the actual value of $y_0(\mathbf{x}_0)$ can be determined using the following equation.

$$\hat{y}_0(\mathbf{x}_0) - y(\mathbf{x}_0) = \sum_{i=1}^{N} \lambda_i y(\mathbf{x}_i) - y(\mathbf{x}_0) \qquad (2.37)$$

On average, the estimation error must be zero.

$$E[\hat{y}_0(\mathbf{x}_0) - y(\mathbf{x}_0)] = \sum_{i=1}^{N} \lambda_i s_m - s_m = \left(\sum_{i=1}^{N} \lambda_i - 1 \right) s_m = 0 \qquad (2.38)$$

Where s_m is the numerical value of the mean, which is unknown. The above equation is solved such that every possible mean can be satisfied, maintaining the unbiasedness. This results in a constraint equation, which is not a function of s_m, but only of the interpolation weights.

$$\sum_{i=1}^{N} \lambda_i = 1 \qquad (2.39)$$

To determine the interpolation weights, the mean square estimation error is set to a minimum, resulting in the following objective function.

$$E\left[\left(\hat{y}_0(\mathbf{x}_0)-y(\mathbf{x}_0)\right)^2\right]=-\sum_{i=1}^{N}\sum_{j=1}^{N}\left(\lambda_i\lambda_j\gamma\left(\left\|\mathbf{x}_i-\mathbf{x}_j\right\|\right)\right)+ \qquad \textbf{(2.40)}$$

$$2\sum_{i=1}^{N}\lambda_i\gamma\left(\left\|\mathbf{x}_i-\mathbf{x}_0\right\|\right)$$

The above formulation reduces the problem to a constrained optimization problem. It is desired to determine the interpolation weights, $\lambda_1,\lambda_2,\ldots,\lambda_N$, that minimize the objective function while satisfying the constraint equation. This is a problem that can be solved using Lagrange multipliers, which is a standard optimization method. A linear kriging system of N+1 equations with N+1 unknowns is established.

$$-\sum_{j=1}^{N}\lambda_i\gamma\left(\left\|\mathbf{x}_i-\mathbf{x}_j\right\|\right)+\nu_k=-\gamma\left(\left\|\mathbf{x}_i-\mathbf{x}_0\right\|\right) \qquad \textbf{(2.41)}$$

Subject to:

$$\sum_{j=1}^{N}\lambda_j=1$$

where ν_k is Lagrange multiplier.

The advantage of this method is that it is possible to interpolate to an infinite number of points from a limited dataset of measurements. Generally kriging incorporates hard data, meaning exact measurements. In newer types of kriging this condition can be relaxed. In traditional kriging, soft data in form of uncertain data, upper and lower bounds and probability distribution functions are not incorporated. A disadvantage of this method is that the variogram structure needs to be well specified to get meaningful results as the correlation is used to determine the interpolations weights. If the variogram has a lot of scatter and a variogram model is approximated, this model directly affects the quality of

interpolations. Obtaining a well specified variogram may not be possible to obtain if the original dataset is not large enough.

2.8.2 Bayesian Updating

Bayesian Updating is based on Bayes' Theorem, which quantifies how a prior pdf changes on the basis of measurements (e.g. Press, 1989). The Bayesian Updating theory is presented in several texts and journals (Bryson and Ho, 1969; Sivia, 1996; Woodbury, 1989; and Ulrych et al., 2001). Bayes' theorem is as follows:

$$p[\mathbf{m}|\mathbf{d}^*, I] = \frac{p[\mathbf{d}^*|\mathbf{m}, I] \cdot p[\mathbf{m}|I]}{\int p[\mathbf{d}^*|\mathbf{m}, I] \cdot p[\mathbf{m}|I]\, d\mathbf{m}} \qquad (2.42)$$

Where I refers to the information available to an observer. This is a very powerful equation in that it relates a likelihood function ($p[\mathbf{d}^*|\mathbf{m}, I]$) and a prior pdf ($p[\mathbf{m}|I]$), which can be determined or estimated, to a posterior conditional probability ($p[\mathbf{m}|\mathbf{d}^*, I]$), which is the pdf of interest (Sivia, 1996).

If it is assumed that the forward model is linear equation 2.35 becomes:

$$\mathbf{d}^* = \mathbf{G}\mathbf{m} + \nu \qquad (2.43)$$

where $\mathbf{G}$ is a kernel that transforms from data to model space and consists of 1's and 0's and ν is a vector of noise values (Woodbury and Ulrych, 2000). One could invert this system directly, but some method of determining the best solution from an infinite number of possible solutions is required. The Bayesian Updating approach is to choose the model that is closest to some pre-conceived notion (Woodbury and Ulrych, 2000).

Assume the following statistics for model **m**.

$$E[\mathbf{m}] = \mathbf{s}$$
$$E[(\mathbf{m}-\mathbf{s})(\mathbf{m}-\mathbf{s})^T] = \mathbf{C}_m \quad (2.44)$$

where **s** is the prior unconditional mean, $\mathbf{C}_m$ is the covariance matrix representing the correlation structure of the model parameters and T represents the transpose.

Assume the following statistics for the noise in the data, **v**.

$$E(\nu) = 0$$
$$E(\nu\nu^T) = \mathbf{C}_d \quad (2.45)$$

Where $\mathbf{C}_d$ is the covariance matrix for the data and typically consists of σ_d^2 (the uncertainty in form of the variance of data) on the diagonal.

Assume that the measurement errors and prior distribution follow a normal distribution.

$$p[\mathbf{d}^*|\mathbf{m},I] = \left((2\pi)^n|\mathbf{C}_d|\right)^{-1/2}\exp\left[-\frac{1}{2}(\mathbf{d}^*-\mathbf{Gm})^T C_d^{-1}(\mathbf{d}^*-\mathbf{Gm})\right] \quad (2.46)$$

$$p[\mathbf{m}|I] = \left((2\pi)^m|\mathbf{C}_m|\right)^{-1/2}\exp\left[-\frac{1}{2}(\mathbf{m}-\mathbf{s})^T\mathbf{C}_m^{-1}(\mathbf{m}-\mathbf{s})\right] \quad (2.47)$$

Tarantola (1987) showed the important result that the product of two Gaussian pdfs is also a Gaussian pdf. Therefore, substituting equations 2.46 and 2.47 into Bayes' Theorem, equation 2.42, gives:

$$p[\mathbf{m}|\mathbf{d}^*,I] = \left((2\pi)^m|\mathbf{C}_q|\right)^{-1/2}\exp\left[-\frac{1}{2}(\mathbf{m}-\langle\mathbf{m}\rangle)^T\mathbf{C}_q^{-1}(\mathbf{m}-\langle\mathbf{m}\rangle)\right] \quad (2.48)$$

Where $\mathbf{C}_q$ is covariance of the posterior pdf and <**m**> is the vector of conditional expected values.

Tarantola (1987) derived the first two unconditional moments of this equation.

$$\langle \mathbf{m} \rangle = \mathbf{s} + \mathbf{C}_m \mathbf{G}^T \left(\mathbf{G} \mathbf{C}_m \mathbf{G}^T + \mathbf{C}_d \right)^{-1} (\mathbf{d}^* - \mathbf{G}\mathbf{s}) \qquad (2.49)$$

$$\mathbf{C}_q = \mathbf{C}_m - \mathbf{C}_m \mathbf{G}^T \left(\mathbf{G} \mathbf{C}_m \mathbf{G}^T + \mathbf{C}_d \right)^{-1} \mathbf{G} \mathbf{C}_m \qquad (2.50)$$

In the formulation of the Bayesian Updating method, knowledge of the correlation structure ($\mathbf{C}_m$) is required. This information may not be known and some assumptions may be necessary. In this formulation, it will be assumed for now that the correlation structure ($\mathbf{C}_m$) is exponential (equation 2.31).

To interpolate using the Bayesian Updating methodology, the parameters of $\mathbf{C}_m$ (λ_e, σ_Y^2, and C_0), **s** and σ_d are required. If any of these parameters are not known, then they are called "hyperparameters" and are marginalized out of the solution. Looking at the expected value of <**m**>.

$$\langle \mathbf{m} \rangle = \int p(\mathbf{m} | \mathbf{d}^*, I) \mathbf{m} \, d\mathbf{m} \qquad (2.51)$$

Consider the set of hyperparameters, $\mathbf{u} = (\lambda_e, C_0, \mathbf{s}, \sigma_d)$.

$$\langle \mathbf{m} \rangle = \int_m \int_u p(\mathbf{m} | \mathbf{d}^*, I, \mathbf{u}) p(\mathbf{u}) \mathbf{m} \, d\mathbf{u} \, d\mathbf{m} \qquad (2.52)$$

$$= \int_u p(\mathbf{u}) \left[\int_m p(\mathbf{m} | \mathbf{d}^*, I, \mathbf{u}) \mathbf{m} \, d\mathbf{m} \right] d\mathbf{u}$$

Where p(**u**) is the prior probability for hyperparameter set **u**. The term in the square bracket is equal to equation 2.49 and therefore becomes:

$$\langle \mathbf{m} \rangle = \int_u \left[\mathbf{s} + \mathbf{C}_m \mathbf{G}^T \left(\mathbf{G} \mathbf{C}_m \mathbf{G}^T + \sigma_d^2 \mathbf{I} \right)^{-1} \left(\mathbf{d}^* - \mathbf{G}\mathbf{s} \right) \right] p(\mathbf{u}) d\mathbf{u} \quad (2.53)$$

Analogously, the following equation for $\mathbf{C}_q$ can be obtained.

$$\mathbf{C}_q = \int_u \left[\mathbf{C}_m - \mathbf{C}_m \mathbf{G}^T \left(\mathbf{G} \mathbf{C}_m \mathbf{G}^T + \sigma_c^2 \mathbf{I} \right)^{-1} \mathbf{G} \mathbf{C}_m \right] p(\mathbf{u}) d\mathbf{u} \quad (2.54)$$

The integrals in equation 2.53 and 2.54 can be solved using a numerical integration technique such as Monte Carlo Sampling or Latin Hypercube Sampling.

2.8.2.1 Prior Probabilities for Hyperparameters

A prior probability, p(**u**) is required for each hyperparameter and is assigned based on the information available for each parameter. In this section, several different methods for determining prior probabilities will be illustrated.

2.8.2.1.1 Scaling Parameter with no Knowledge

For a scaling parameter, in which no knowledge is available it is desired to choose a prior that will not inject a bias towards this unknown information. Suppose we have a scaling parameter, such as the standard deviation σ, and have no other knowledge except that it varies between zero and infinity (Woodbury and Ulrych, 2000). If a uniform prior is chosen, then difficulties arise in carrying out the required transformations. In these cases, it is generally considered to be a reasonable choice to use the following equation (Sivia, 1996).

$$p(\sigma) \propto \frac{1}{\sigma} \quad (2.55)$$

This is known as Jeffrey's prior and does not exhibit the same problems with transformations as the uniform pdf. However, it is not normalized such that the sum of possible probabilities will sum to 1. For use within the Bayesian Reasoning, the posterior pdf can be normalized (Sivia, 1996).

2.8.2.1.2 Specified Upper and Lower Bounds and Mean

For this type of information, a method called minimum relative entropy (MRE) can be used. The roots of this method lie in probability theory and was originally developed by Shore (1981). Assume that we have a system of possible states, with **x** being one state. Also, assume that the multivariate pdf of **x**, q(**x**), exists but is not known (Woodbury and Ulrych, 1998). The pdf is normalized:

$$\int q(\mathbf{x})d\mathbf{x} = 1 \qquad (2.56)$$

Other information is also available in terms of expected value constraints.

$$\int q(\mathbf{x}) f_j(\mathbf{x})d\mathbf{x} = \bar{f}_j \qquad (2.57)$$

where $f_j(\mathbf{x})$ and $\bar{f}_j$ are known (for example, from data) (Woodbury and Ulrych, 1993). The problem at hand is to determine an estimate of q(**x**), which will be labeled $\hat{q}(\mathbf{x})$, based on the provided information. The solution is to minimize the relative entropy of $\hat{q}(\mathbf{x})$ relative to a prior estimate, p(**x**), H($\hat{q}$,p), subject to the constraint equations 2.56 and 2.57. The equation for relative entropy is as follows:

$$H(\hat{q}, p) = \int \hat{q}(\mathbf{x}) \ln\left[\frac{\hat{q}(\mathbf{x})}{p(\mathbf{x})}\right] d\mathbf{x} \qquad (2.58)$$

Woodbury and Ulrych (1993) present the formulation of this method and show that the posterior estimate $\hat{q}(\mathbf{x})$ has the following form.

$$\hat{q}(\mathbf{x}) = p(\mathbf{x})\exp\left[-1-\mu_L - \sum_{j=1}^{M}\lambda_j f_j(\mathbf{x})\right] \qquad (2.59)$$

Where μ_L and λ_j are Lagrange multipliers that must be determined.

The MRE method can be used to estimate appropriate prior pdfs that can be used in assigning prior probabilities for hyperparameters in which lower and upper bounds are known. The development of this theory is covered in Woodbury and Ulrych (1993), Woodbury and Ulrych (1996) and Woodbury and Ulrych (1998), but will be summarized here. A few assumptions are required, the first being that it is assumed that the model has a finite number of parameters. Each of the model parameters can be assumed to be represented by a random variable, in which the expected value of the pdf is the "true" model value. MRE can be used to generate a "prior" pdf for use in Bayesian Updating methodology (actually the posterior pdf in MRE) given a prior pdf and subject to the constraints. In most hydrogeological applications, it can be safely assumed that databases are such that reasonable lower (LB) and upper (UB) bounds of each parameter can be ascertained. This implies that the base level of knowledge is a joint boxcar pdf.

$$\begin{aligned} b(\mathbf{m}) &= \frac{1}{UB-LB} \qquad LB \le \mathbf{m} \le UB \\ b(\mathbf{m}) &= 0 \qquad\quad \text{otherwise} \end{aligned} \qquad (2.60)$$

The relative entropy in this case can be defined analogous to equation 2.58.

$$H(p,b) = \int_M p(\mathbf{m})\ln\left[\frac{p(\mathbf{m})}{b(\mathbf{m})}\right]d\mathbf{m} \qquad (2.61)$$

Suppose that new information, such as new measurements or postulation, becomes available in terms of a "new" prior estimate, denoted here as **s**. It is assumed that **s** is the

expected value of p(**m**) such that it has minimum relative entropy relative to a prior boxcar pdf subject to constraint p_n. If LB is equal to 0, then this results in the following pdf:

$$p(\mathbf{m}) = \prod_{n=0}^{N} \frac{-\beta_n}{\exp(-\beta_n \cdot UB) - 1} \exp(-\beta_n m_n) \qquad (2.62)$$

where β_n are Lagrange multipliers, which are determined from the bounds. The properties of this pdf are that it is independent, as no unknown information has been injected into the posterior pdf, and the distribution is not symmetric.

The MRE method can be carried further to not only generate prior pdfs for other interpolation methods, but can be used itself to solve inverse problems. MRE has been used to reconstruct source release history of a contaminant release (Woodbury and Ulrych, 1996; Woodbury et al., 1998) and to determine past ground surface temperatures from borehole temperatures (Kennedy et al., 2000).

2.8.2.1.3 Specified Mean and Variance

For a specific variable in which the mean, s_m, and variance, σ^2, are known, the maximum entropy principle can be applied (Woodbury and Ulrych, 2000). The result is that the prior distribution is Gaussian (Bretthorst, 1988; Kapur, 1989).

$$p(x|\sigma, s_m, I) = \frac{1}{\sqrt{2\pi\sigma^2}} \exp\left(-\frac{(x - s_m)^2}{2\sigma^2}\right) \qquad (2.63)$$

2.9 Sampling Methods

In order to solve the integrals in the Bayesian Updating method Equations 2.53 and 2.54, a numerical integration routine is required. A method such as Monte Carlo with random sampling or with Latin Hypercube sampling may be used.

The Monte Carlo method consists of using a random number generator to provide a random value of the pdf, p(**u**) in this case. The value of $\langle \mathbf{m} \rangle$ and $\mathbf{C}_q$ are evaluated from equations 2.53 and 2.54 using this random value of p(**u**). A new value of p(**u**) is generated and $\langle \mathbf{m} \rangle$ and $\mathbf{C}_q$ are once again evaluated. This iterative process is repeated until a satisfactory number of $\langle \mathbf{m} \rangle$ and $\mathbf{C}_q$ have been generated, to achieve the desired precision. As the posterior pdf of Bayesian Updating is Gaussian, the final value of $\langle \mathbf{m} \rangle$ and $\mathbf{C}_q$ are the averages of the values generated from the Monte Carlo iterations.

The Latin Hypercube method is a type of the Monte Carlo method with a different sampling philosophy (McKay et al., 1979). The distributions of each parameter in **u** are divided into M equal probability areas. As an example, suppose there are two random variables x and y with Gaussian distributions with different means and standard deviations (Figure 2.11). Both distributions have been divided into six equal probability areas. One random value is obtained from within each interval, i.e. for x $(x_1,\ldots,x_6)$ and for y $(y_1,\ldots,y_6)$. This sampling methodology ensures that every portion of each pdf are sampled. The components of each are matched at random, for example $\{(x_1, y_2), (x_2, y_6), (x_3, y_1), (x_4, y_4), (x_5, y_3), (x_6, y_5)\}$as shown in the bottom of Figure 2.11. These combinations are then used to calculate the parameter of interest.

McKay et al. (1978) compared Monte Carlo and Latin Hypercube Sampling Methods. They found in all cases that the Latin Hypercube Sampling Method provided more precise results with the same number of realizations.

2.10 Summary

This chapter provided background information that will be required for the remainder of this thesis. In subsequent chapters, the reader will be referred back to sections in this chapter where the theory is required.

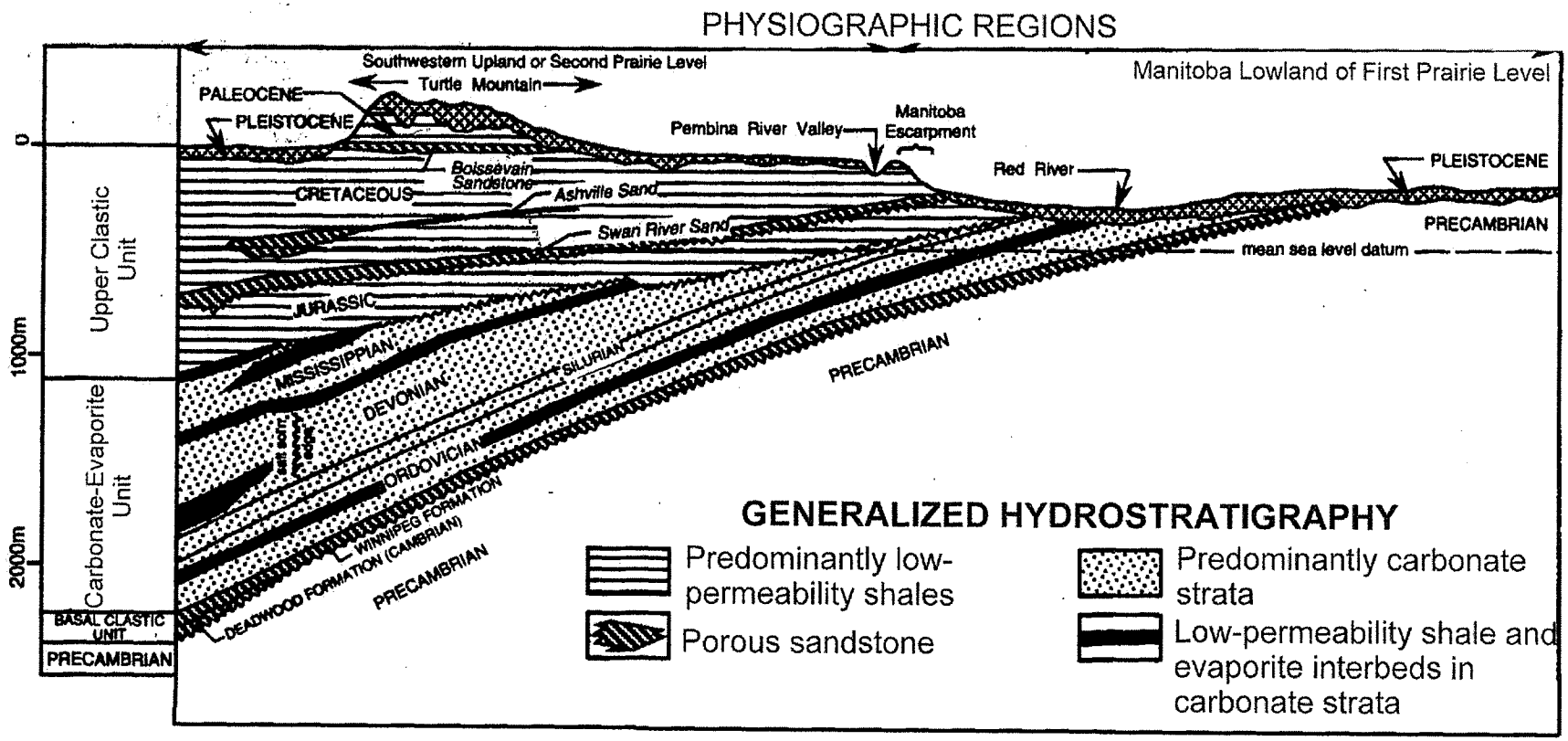

Figure 2.1 – Geologic cross-section along Manitoba-U.S.A. border. Vertical exaggeration approximately 50:1 (taken from Betcher et al., 1995).

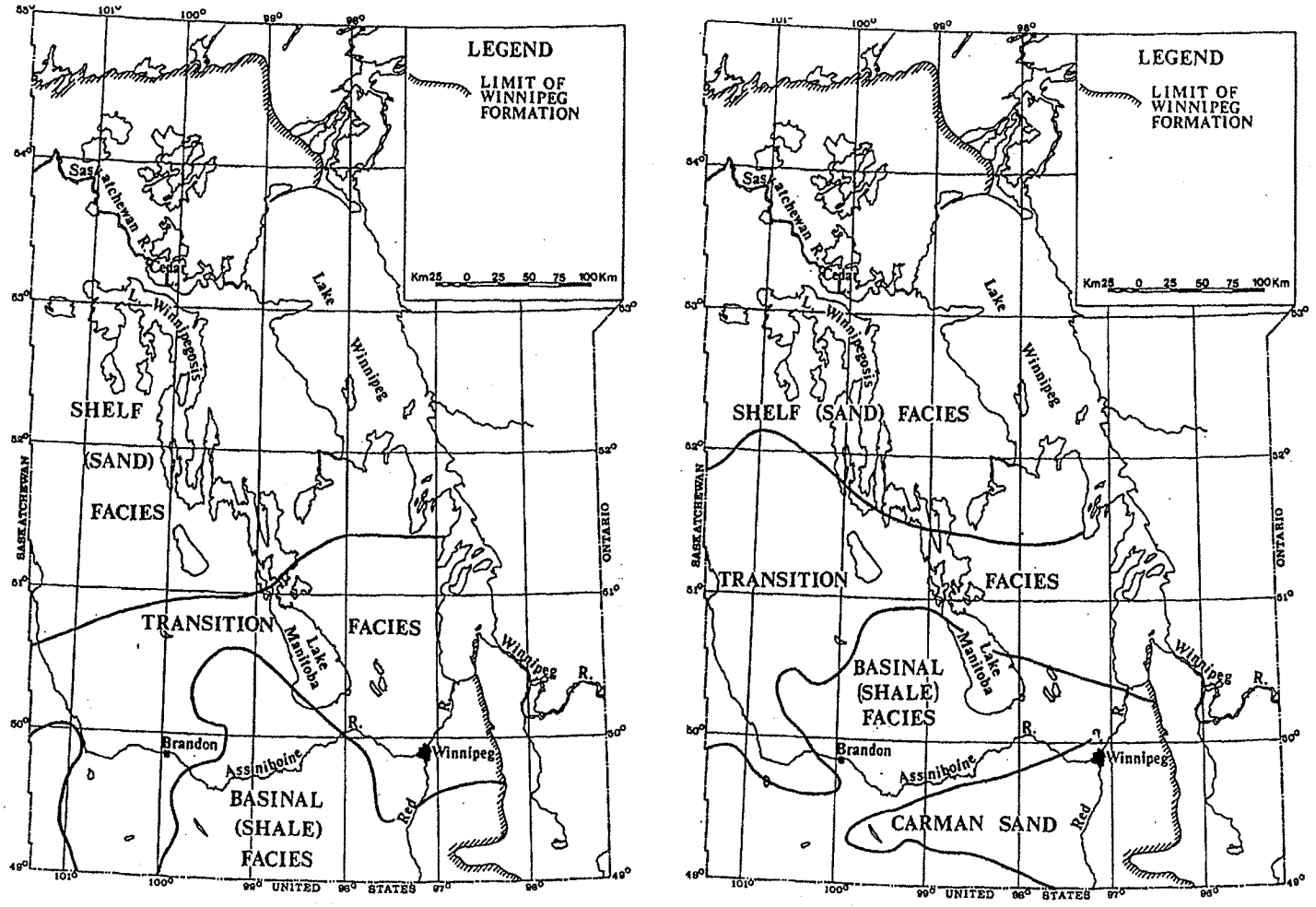

(A) **(B)**

Figure 2.2 – Depositional facies of the (A) Lower Winnipeg Formation and (B) Upper Winnipeg Formation (taken from McCabe, 1978).

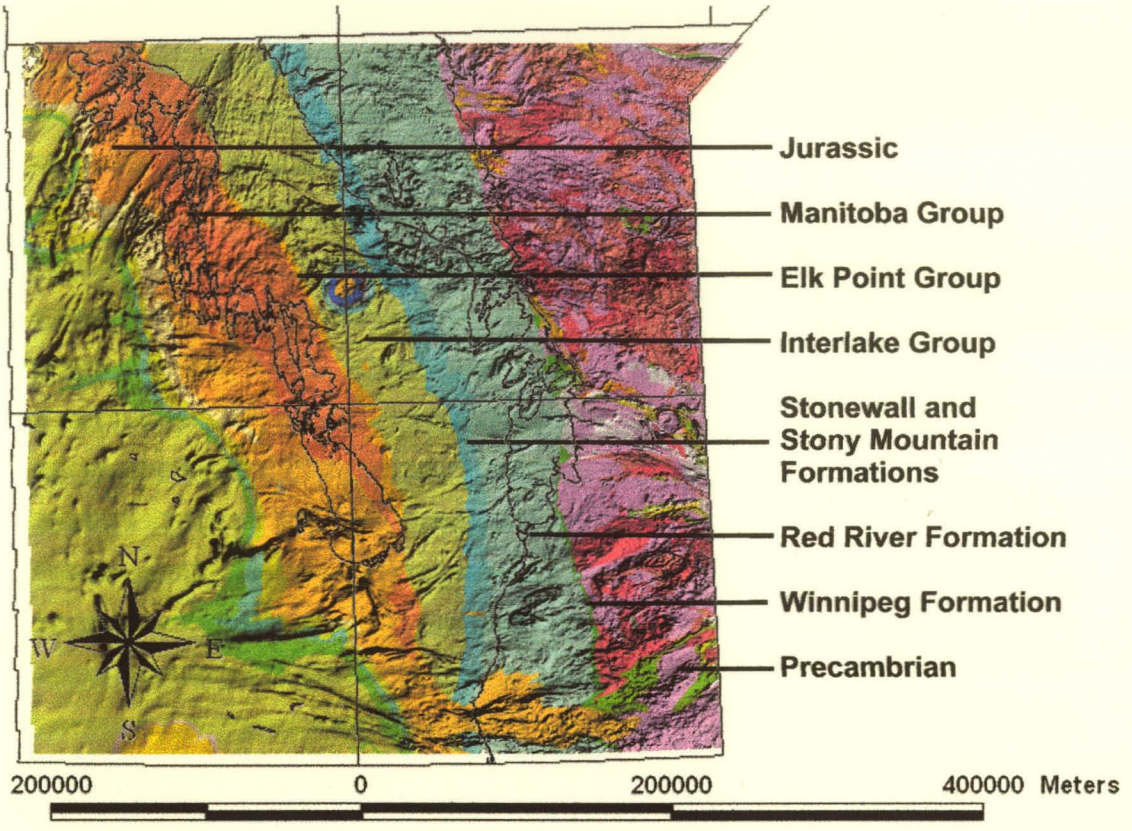

Figure 2.3 – Bedrock geology map of Southern Manitoba (adapted from Viljoen et al., 1999).

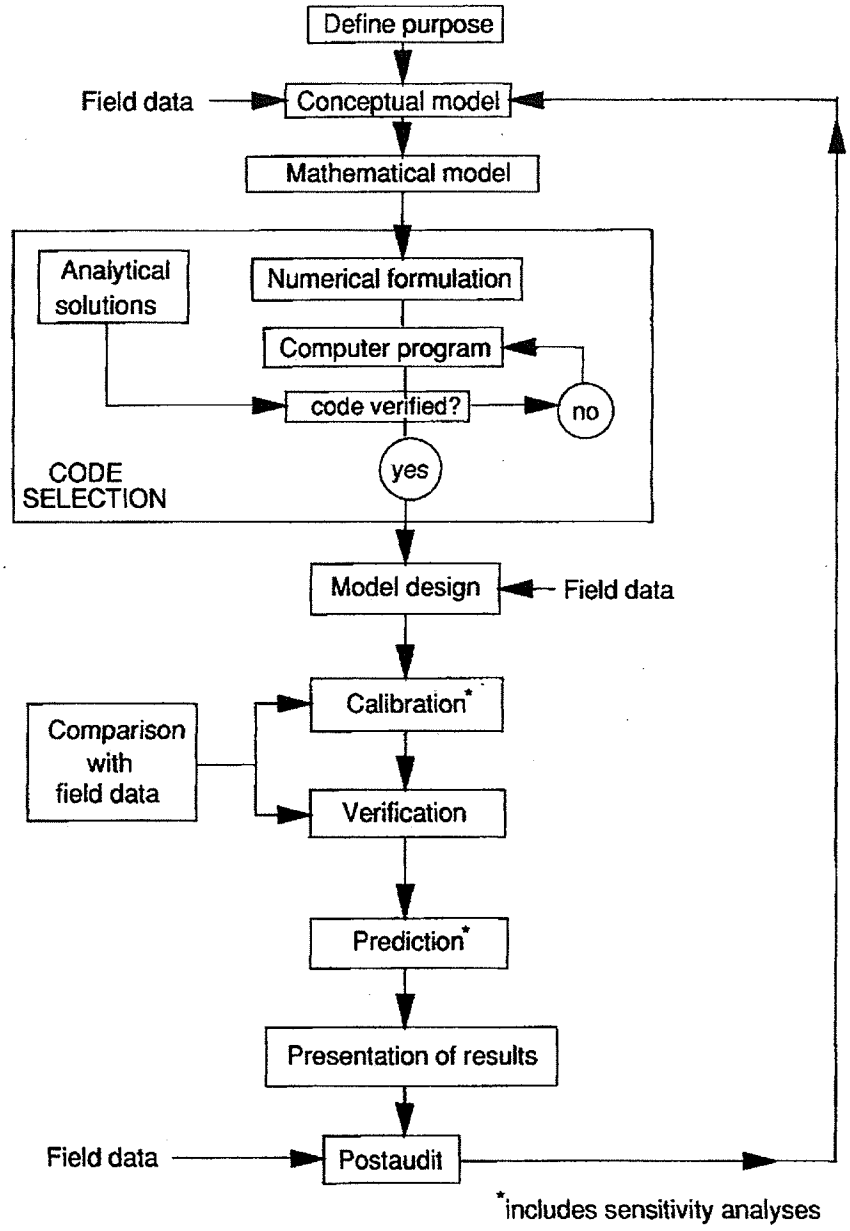

Figure 2.4 – Steps in a protocol for model application (taken from Anderson and Woessner, 1995).

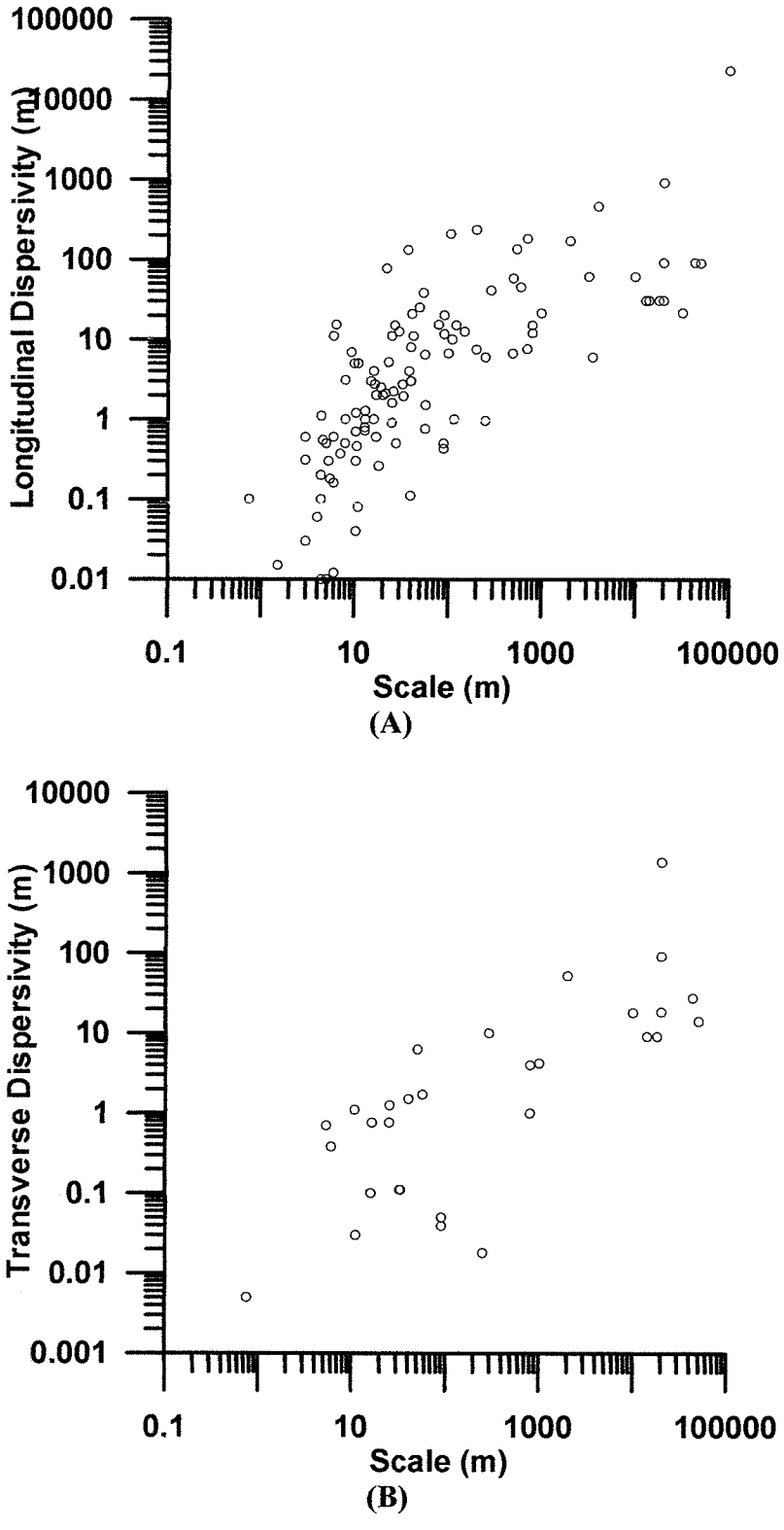

Figure 2.5 – (A) Longitudinal and (B) transverse dispersivity as a function of scale from Gelhar et al. (1992).

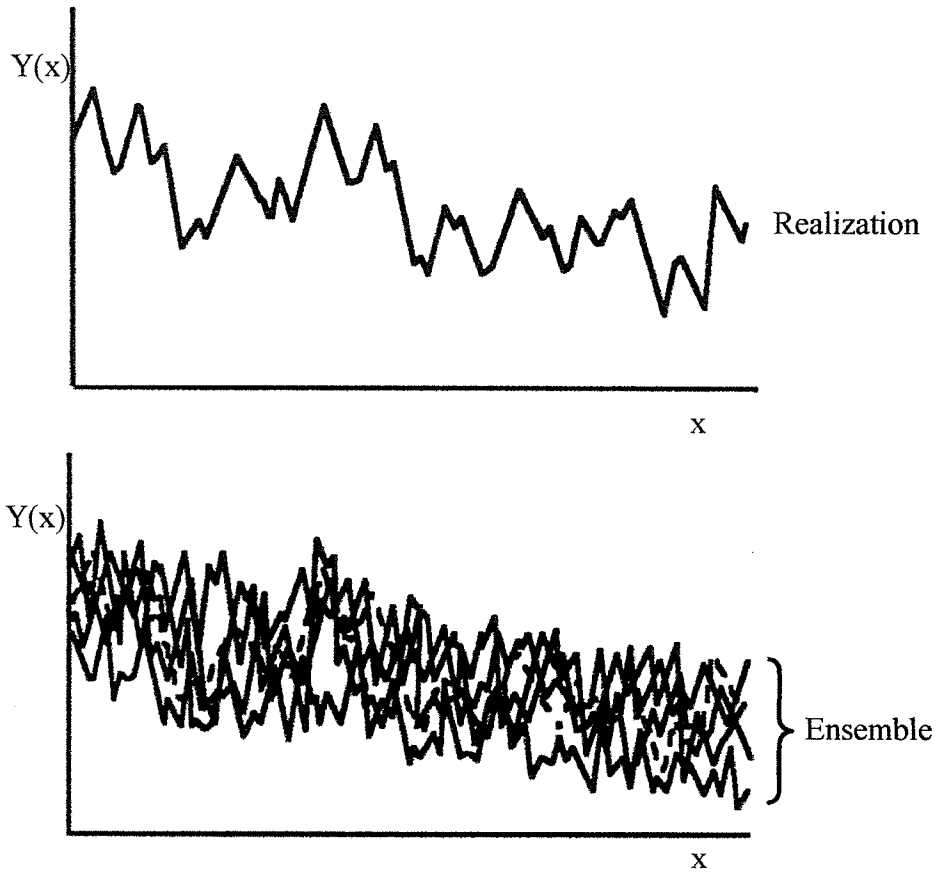

Figure 2.6 – A realization of a stochastic process and the ensemble from which it belongs. (Taken from Gelhar, 1993)

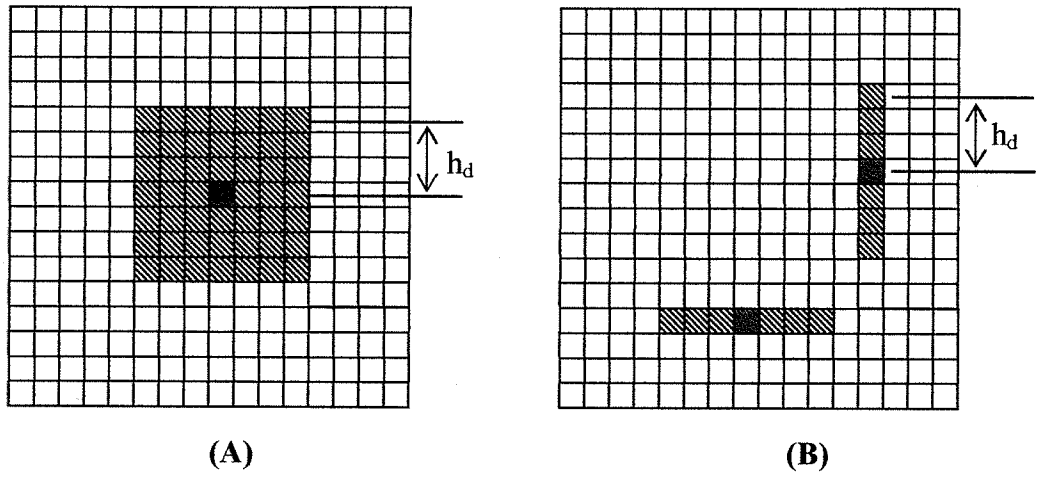

Figure 2.7 – Two-dimensional moving window for (A) isotropic and (B) anisotropic Moving Window Estimator for lag distance of size h_d.

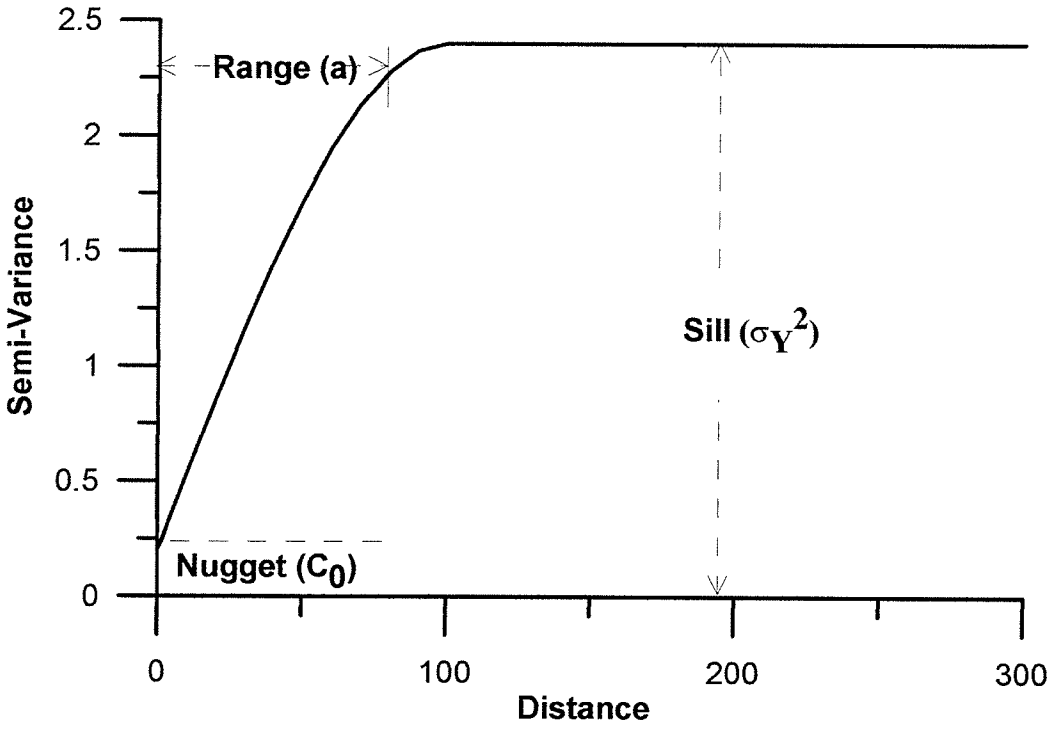

Figure 2.8 – Generic variogram model showing definition of sill, range and nugget effect.

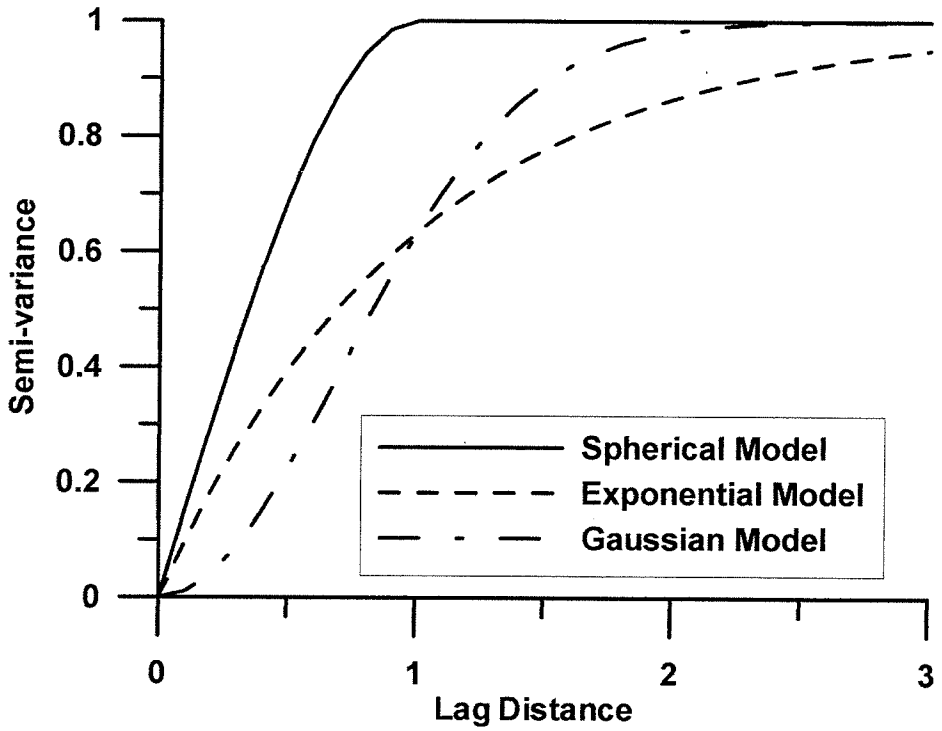

Figure 2.9 – Variogram models with sills (sill normalized to 1.0).

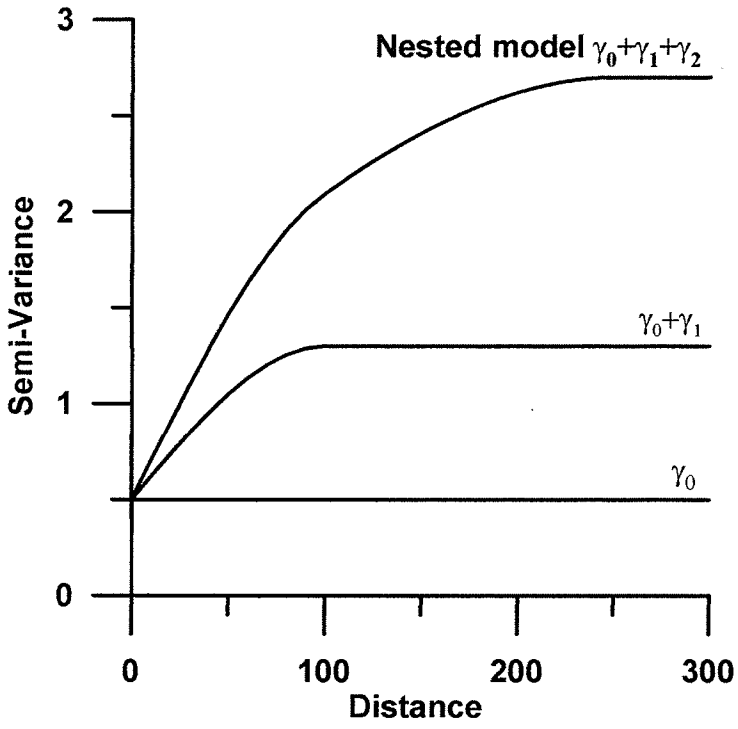

Figure 2.10 – Example variogram showing a nested structure with a nugget effect (γ_0), a spherical model, γ_1 (range = 100, sill = 0.8) and a second spherical model, γ_2 (range = 150, sill = 1.4).

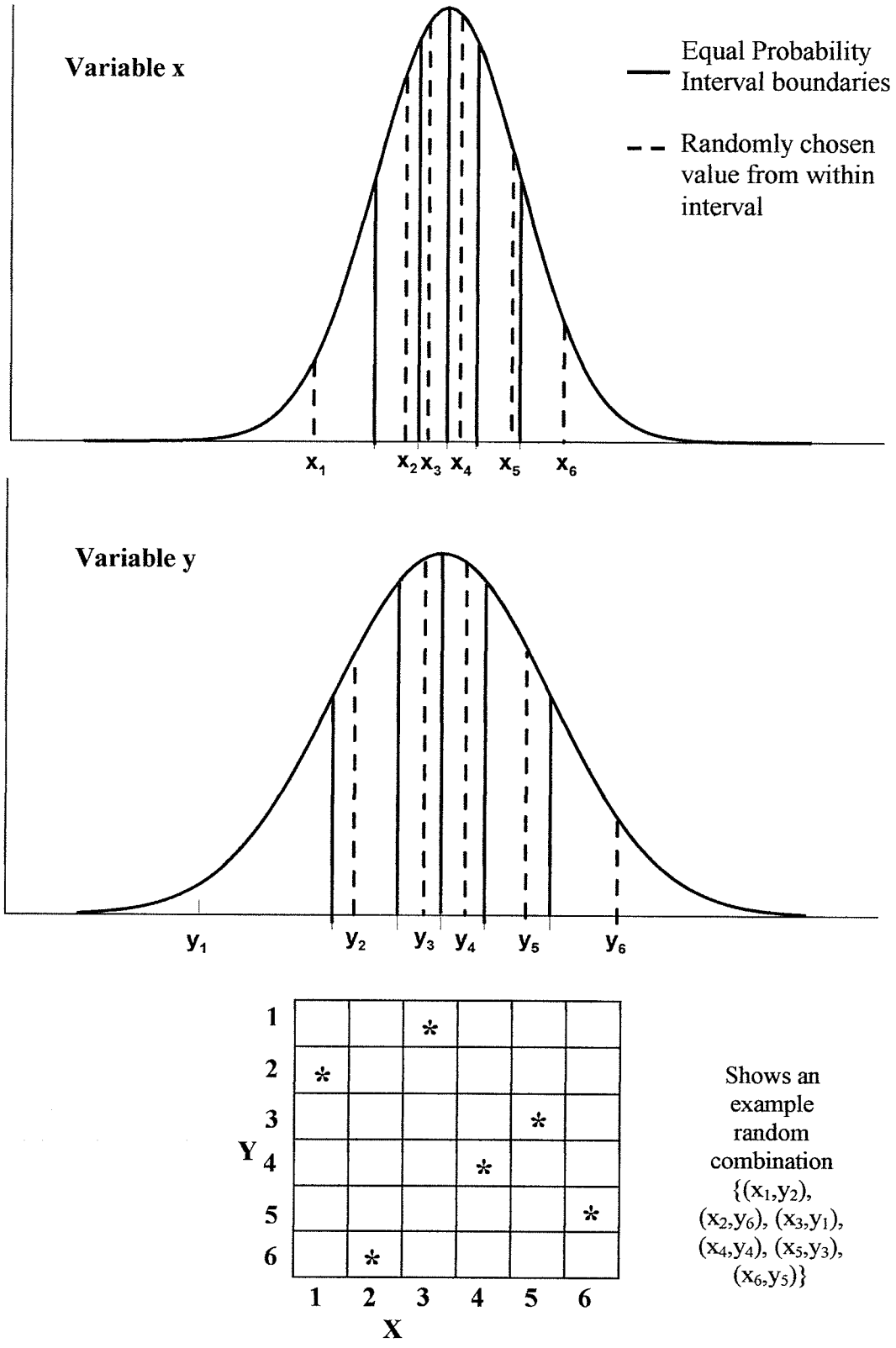

Figure 2.11 – Schematic showing methodology of Latin Hypercube Sampling for two normally distributed variables that are stratified into six equal probability sections.

CHAPTER 3

HYDROSTRATIGRAPHIC MODEL

This chapter describes the development of the hydrostratigraphic model from the lithological units that were described in Chapter 2, Sections 2.2 and 2.3.

3.1 Lithological to Hydrostratigraphic Units

The geological formations described in Section 2.2 were reinterpreted as hydrostratigraphic units (see Figure 3.1 and Table 3.1). Adjacent units with similar hydrogeological properties were combined. The Precambrian rocks were maintained as one unit as the hydrogeological properties could be considered similar.

The Winnipeg Formation consists of interbedded shales and sandstones, with a persistent shale layer confining the unit and providing a hydraulic boundary with overlying layers. This formation was divided into two separate units: one aquifer unit to represent the interbedded shales and sandstones; and a second confining unit representing the shale layer at the top. As the thickness of the overlying shale layer was not known, it was assumed to be 1.5 m (Betcher, personal communication 1999).

The Red River Formation was divided into the Upper Red River Formation (Fort Garry Member) and the Lower Red River Formation (Selkirk, Cat Head and Dog Head Members). The reason for the separation was to account for a zone of enhanced

permeability present in the Fort Garry Member. By separating the units, the hydrogeological properties could be varied between units if required.

Table 3.1 – Geological formations that compose each hydrostratigraphic unit.

Hydrostratigraphic unit	**Geological Formation**
Manitoba Escarpment	Turtle Mountain Boissevain Pierre Shale Niobrara Morden Shale Favel Ashville
Jurassic	Waskada Melita Reston Amaranth Bakken Qu'Appelle Group
Carbonate	Saskatchewan Group Manitoba Group Elk Point Group Interlake Group Stonewall Stony Mountain
Upper Red River	Red River Formation – Fort Garry Member
Lower Red River	Red River Formation – Selkirk Member Cat Head Member Dog Head Member
Carbonate Aquifer	Upper 15 m of Carbonate, Upper Red River and Lower Red River Formations in outcrop region
Winnipeg Shale	Upper 1.5 m of Winnipeg Formation across entire extent
Sandstone Aquifer	Winnipeg (minus the portion included in Winnipeg Shale)
PRECAMBRIAN	PRECAMBRIAN

The carbonate rocks of the Stony Mountain, Stonewall, Interlake Group, Elk Point Group, Manitoba Group and Saskatchewan Group Formations were combined into one single unit, called "carbonates", as they are all composed of rocks with similar hydrogeological properties. The subcropping of these carbonate rocks, and those from

the Red River Formation were combined into one unit representing the Carbonate Aquifer. As there was little or no information regarding the spatially varying thickness of the aquifer, it was decided to assume that the upper 15 m of these carbonate rocks form the Carbonate Aquifer (Render, 1970).

The Qu'Appelle Group, Bakken Formations and Jurassic period rocks were combined into one unit. Each of these units is composed primarily of shale and there was a lack of data to separate these units. The remaining rocks of the Manitoba Escarpment were combined into one unit as they were on the border or outside the study area and there was a lack of available data logged in these upper portions.

The overburden units were separated into clay, till, and sand and gravel units. Only the major sand and gravel bodies, such as those in the Sandilands (southeast of Winnipeg) and Birds Hill (northeast of Winnipeg) were considered. Any small sand lenses completely imbedded in the clay or till, would not have a significant effect on the regional flow.

3.2 Model Construction

The hydrostratigraphic model was constructed using the software package Groundwater Modeling System (GMS). For the bedrock units, two different methodologies were taken. In the early stages of research, borehole logs from two sources were available and were used to construct the initial model. These were the Western Canada Sedimentary Basin (WCSB) Atlas and the Manitoba Stratigraphic Database (MSD) (Bezys and

Conley, 1998). The WCSB was developed by the Geological Survey of Canada (GSC) and contained 350 well logs. The MSD contained approximately 1200 logs obtained primarily from mineral and oil exploration purposes by the Department of Industry, Trade and Mines of the Province of Manitoba (ITM). The bulk of the well logs from these two databases were located in the western part of the province.

The borehole log information was entered into GMS, and a Triangulated Irregular Network (TIN) surface was created for the top of each hydrostratigraphic unit. A solid model was constructed from the TINs. However, as most of the well logs were located in the western part of the province, the location of the outcropping units in the eastern zones were erroneous when compared to published bedrock geology. Therefore, fictitious wells were constructed in the outcrop zones. These "helper" wells were created using depth to bedrock and bedrock geology maps contained within the Water Availability Map Series published by Manitoba Water Branch (MWB). The addition of these contact points greatly improved the model in the outcrop regions. The resulting three-dimensional hydrostratigraphic model is displayed in Figure 3.2. A cross-section along the same line as that presented in Figure 2.1 is presented in Figure 3.3. A plan view of the bedrock model is presented in Figure 3.4.

In the later stages of the research, geologists at ITM developed a three-dimensional bedrock model. Most of the necessary surfaces were available, except for the Lower Red River Formation and the top and bottom of the Carbonate Aquifer. These surfaces were

at a resolution of 100 m, which was significantly higher than that provided by the borehole logs.

The construction of the final model was completed from a combination of the two sources of data. The surfaces used in construction of the final model are presented in Table 3.2. Structure maps of the resulting surfaces are presented in Figures 3.5 – 3.9.

Table 3.2 – Source of data for each hydrostratigraphic unit in final model.

Hydrostratigraphic Unit	Source
Bedrock	ITM (RockGrid)
Jurassic	ITM (Jurassic_Top)
Carbonates	ITM (Mississippian_CharlesGrid)
Carbonate Aquifer	Initial model – borehole logs
Upper Red River	ITM (Ordovician_RedRiverGrid)
Lower Red River	Initial model – borehole logs
Winnipeg Shale	ITM (Ordovician_WinnipegGrid)
Sandstone Aquifer	ITM (Ordovician_WinnipegGrid-1.5m)
Precambrian	ITM (PrecambrianGrid)

The surficial model consists of the thicknesses of clays, tills and sands and gravels. A figure showing the surficial units overlying the bedrock units is shown in Figure 3.10. ITM, in conjunction with the GSC, developed a three-dimensional surficial model. Their methodology consisted of using all wells within GWDrill, a water-well database maintained by MWB. Any driller constructing a water-well within Manitoba, must fill out a well log that is subsequently added to the GWDrill database. Due to the variability in recording styles amongst drillers, the resulting database consisted of well logs that are of variable quality. The GSC and ITM vetted the database prior to construction of their surficial model. The 80,000 wells were examined, completely erroneous wells were

rejected and the remaining logs were given consistent terminology. East West transects of these well logs were plotted using a software package called Borehole Mapper. The transect distances were 5 km wide in the North-South direction. ITM connected the surficial deposits manually according to geological judgement and experience. Each resulting East-West transect was read into Borehole Mapper digitally by recording the surfaces of each contact at every 5 km. The result was a 5 km X 5 km grid of contact points. From these contact points, surfaces of the top of each deposit were created and a 3D model was constructed. The model was extremely detailed, comprising many small features (e.g. sand lenses) that were not required for this research. ITM prepared a surficial model with the required detail for this research. An East-West cross-section approximately through the city of Winnipeg is shown in Figure 3.11. In this area, clays generally overly tills which overly the bedrock units. A large sand body is also shown towards the east, which is in the Sandilands region. A plan view of the final surficial model is shown in Figure 3.12. In the region of the City of Winnipeg, a large clay body forms the uppermost unit. In the Interlake region, the tills form the uppermost unit.

3.3 Summary

This chapter presented the assumptions that were used in the construction of the hydrostratigraphic model. The sources that were used to collect the elevations of each geological unit were presented. The hydrostratigraphic model will be used in the design of the computer model.

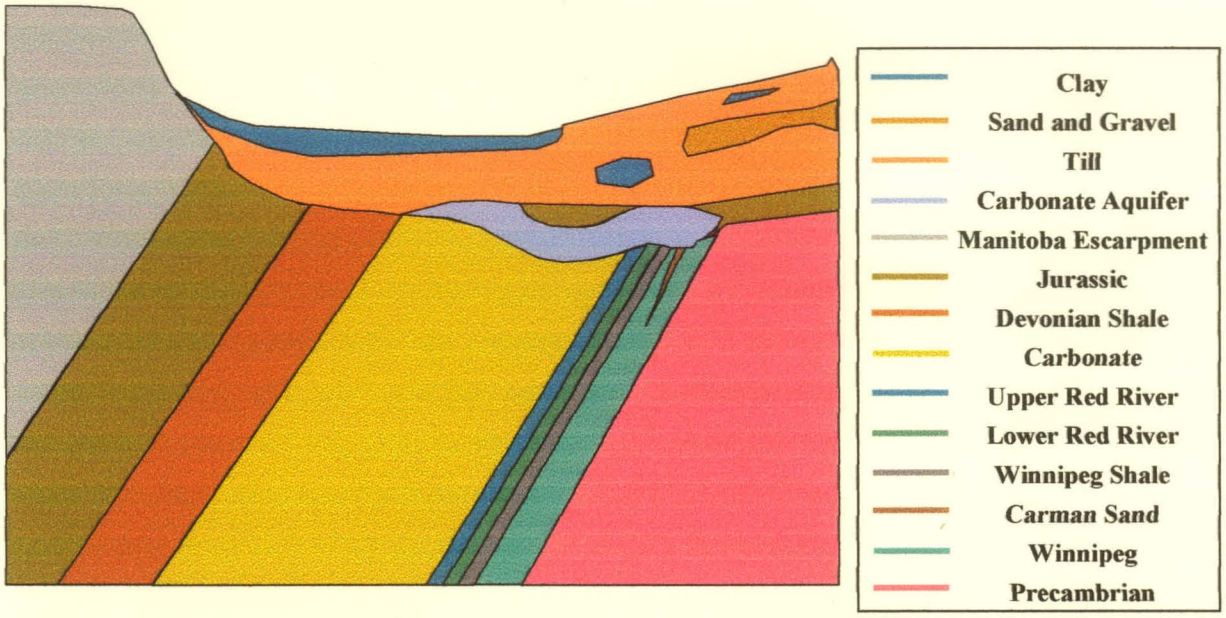

Figure 3.1 – Hydrostratigraphic model assumed for groundwater flow and transport model.

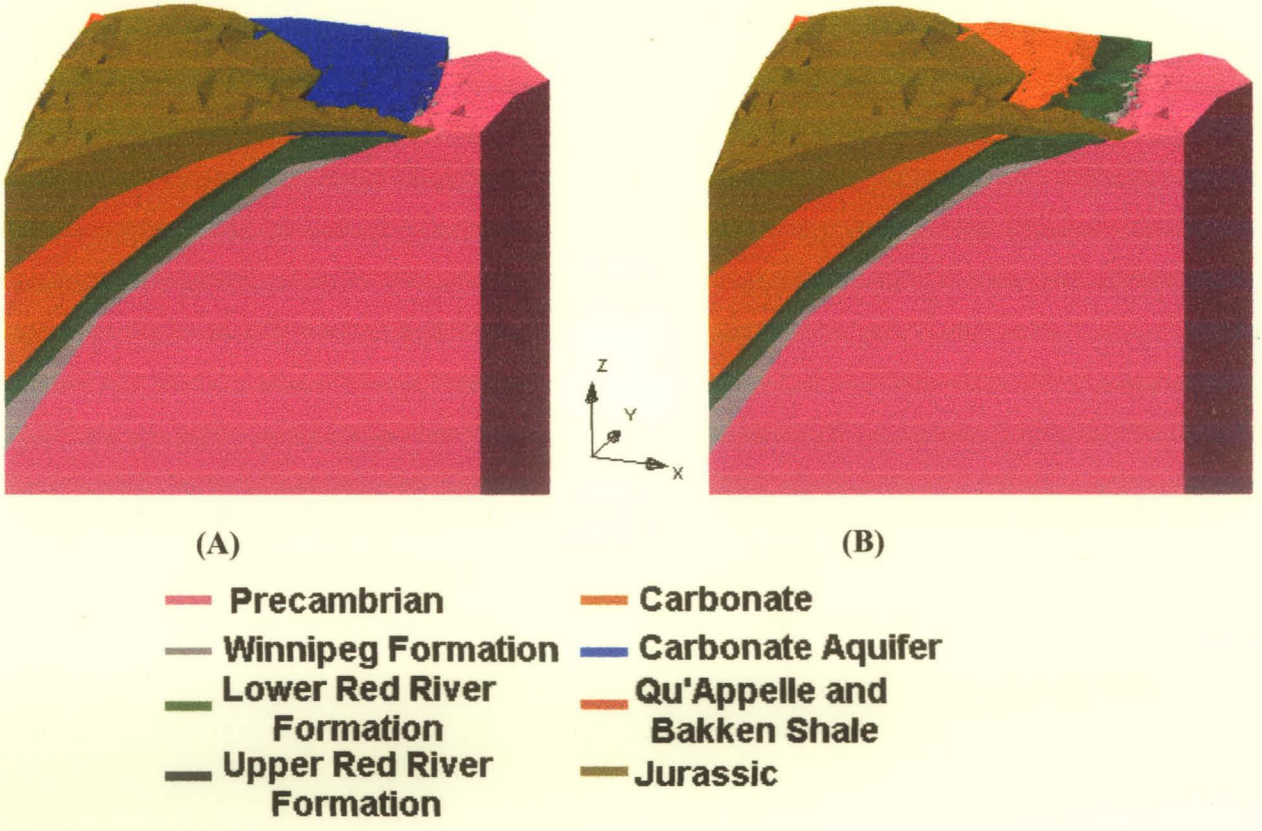

Figure 3.2 – Bedrock model (A) with Carbonate Aquifer and (B) with Carbonate Aquifer removed.

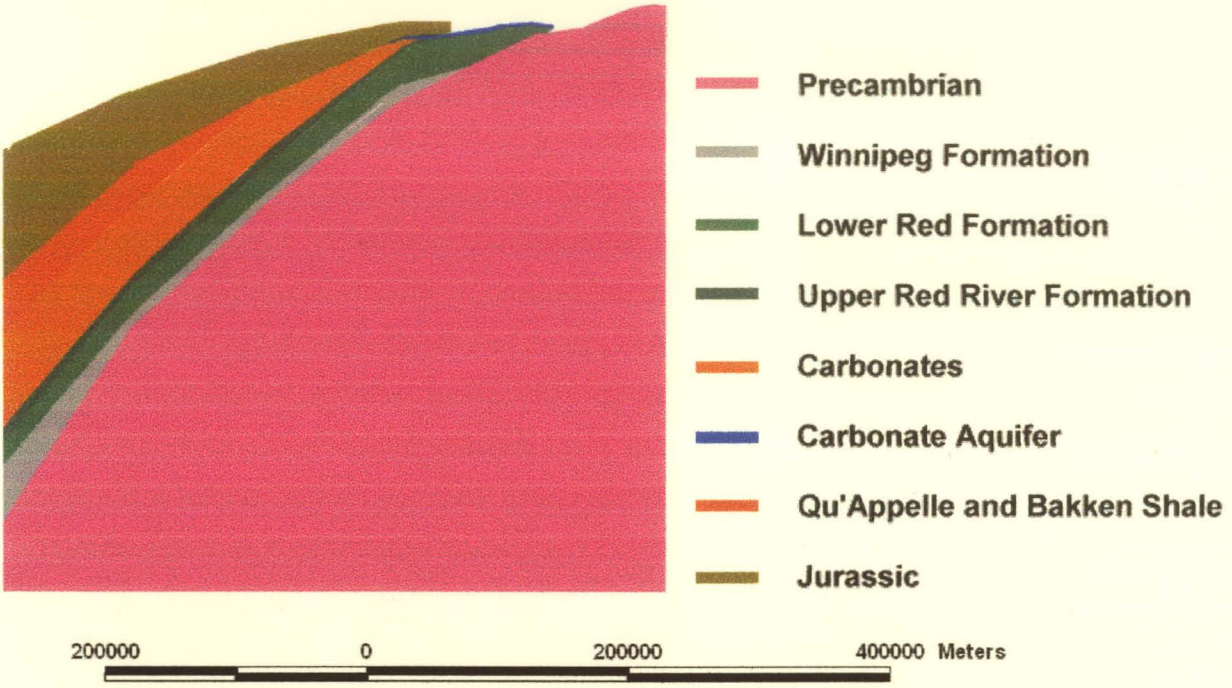

Figure 3.3 – Cross-section along same line as in Figure 2.1, generated from hydrostratigraphic model constructed for this research (vertical exaggeration 150x).

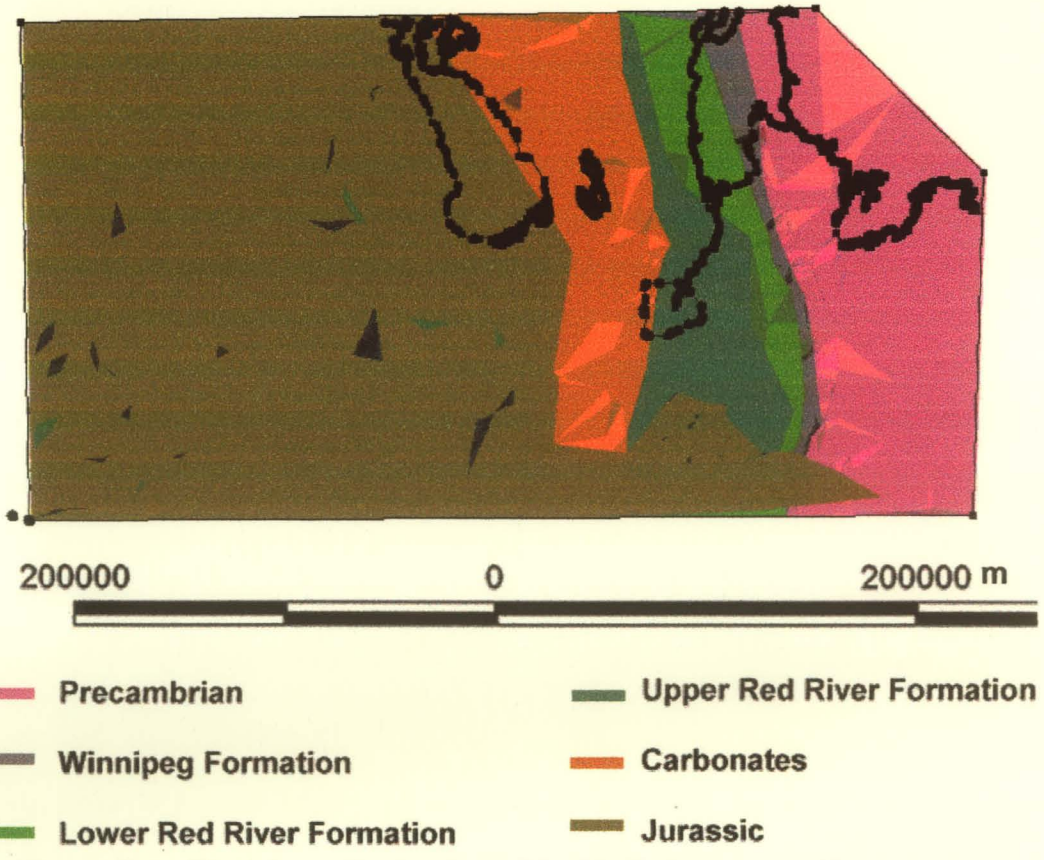

Figure 3.4 – Plan view of bedrock model with Carbonate Aquifer removed.

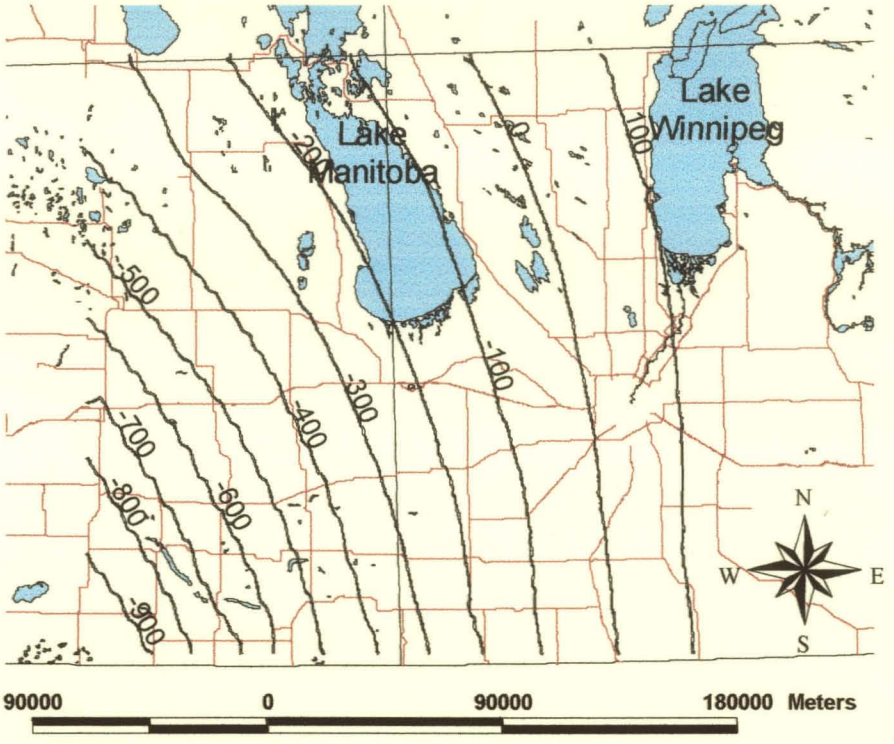

Figure 3.5 – Precambrian structure in meters.

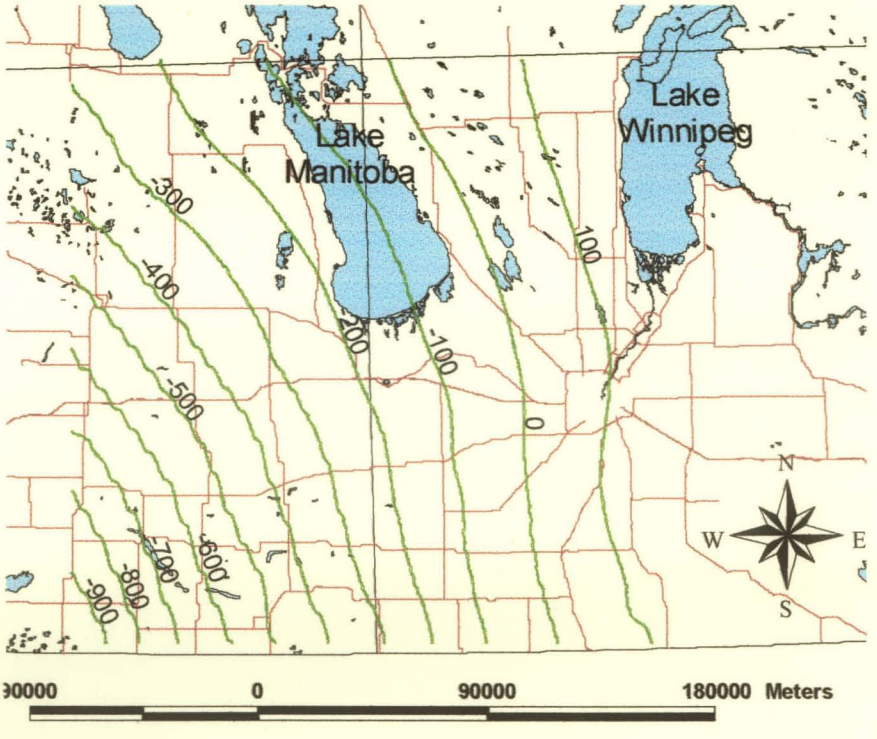

Figure 3.6 – Winnipeg formation structure in meters.

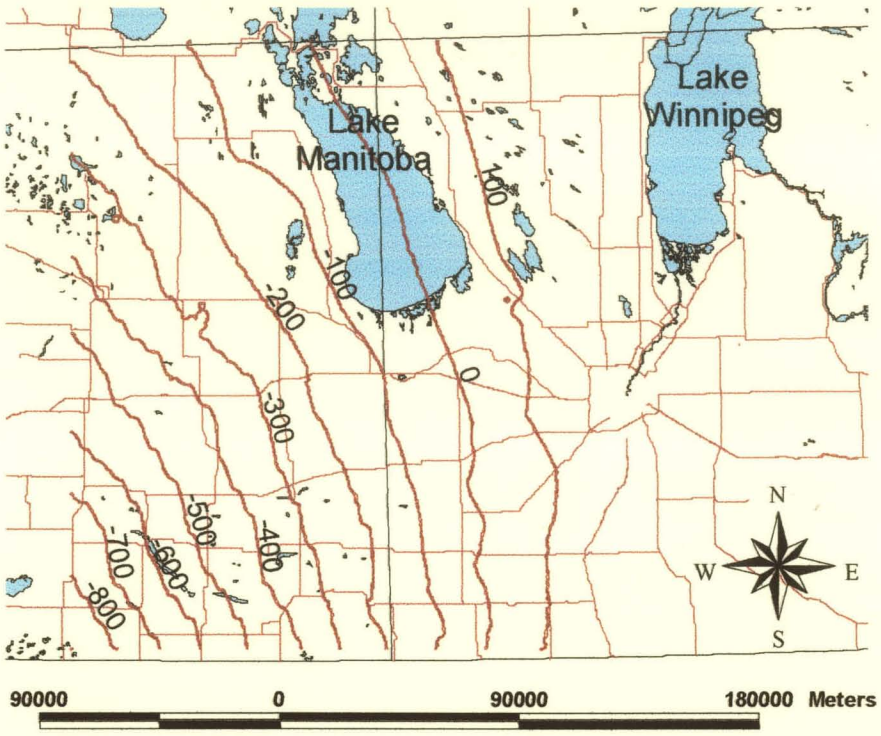

Figure 3.7 – Lower Red River Formation structure map in meters.

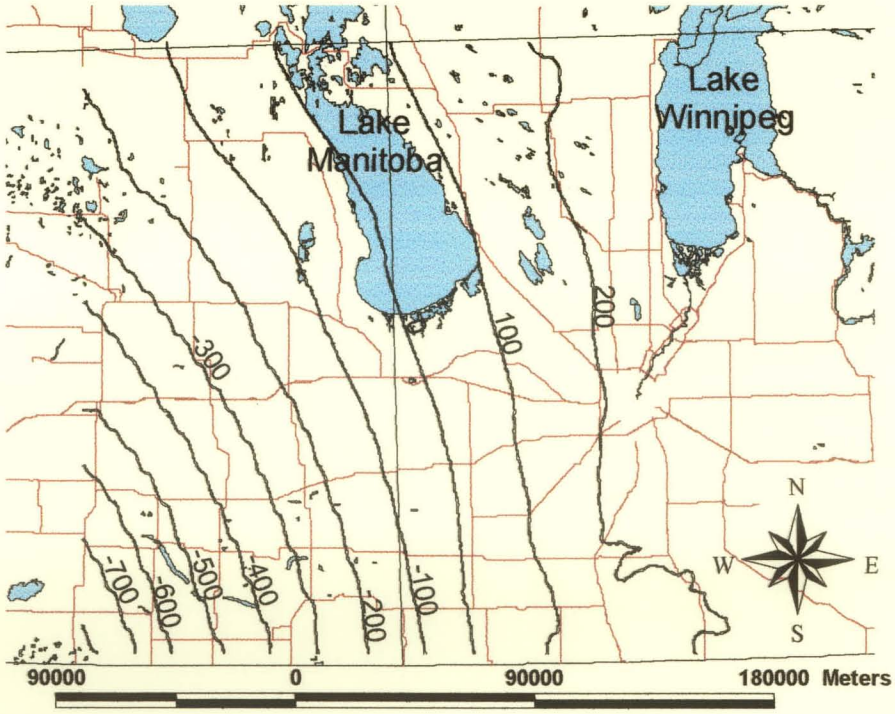

Figure 3.8 – Upper Red River Formation structure map in meters.

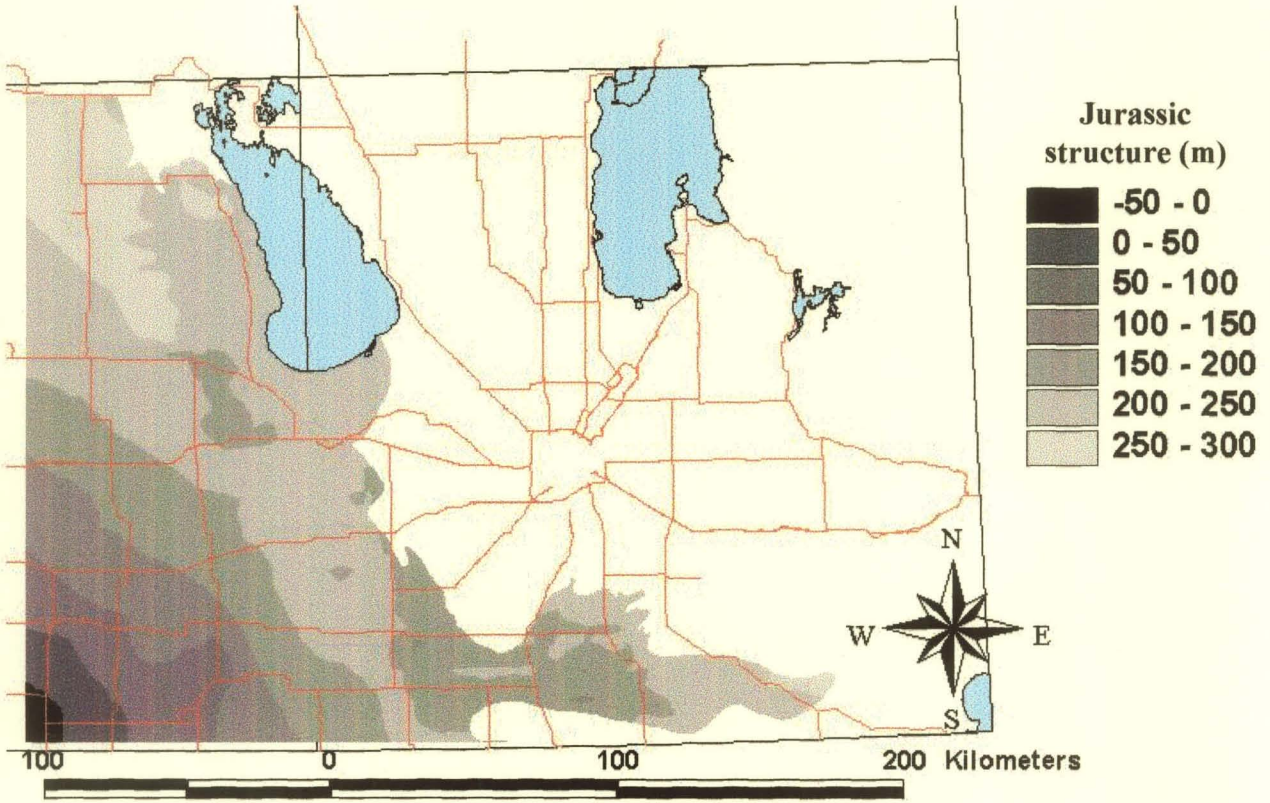

Figure 3.9 – Jurassic Period structure map in meters.

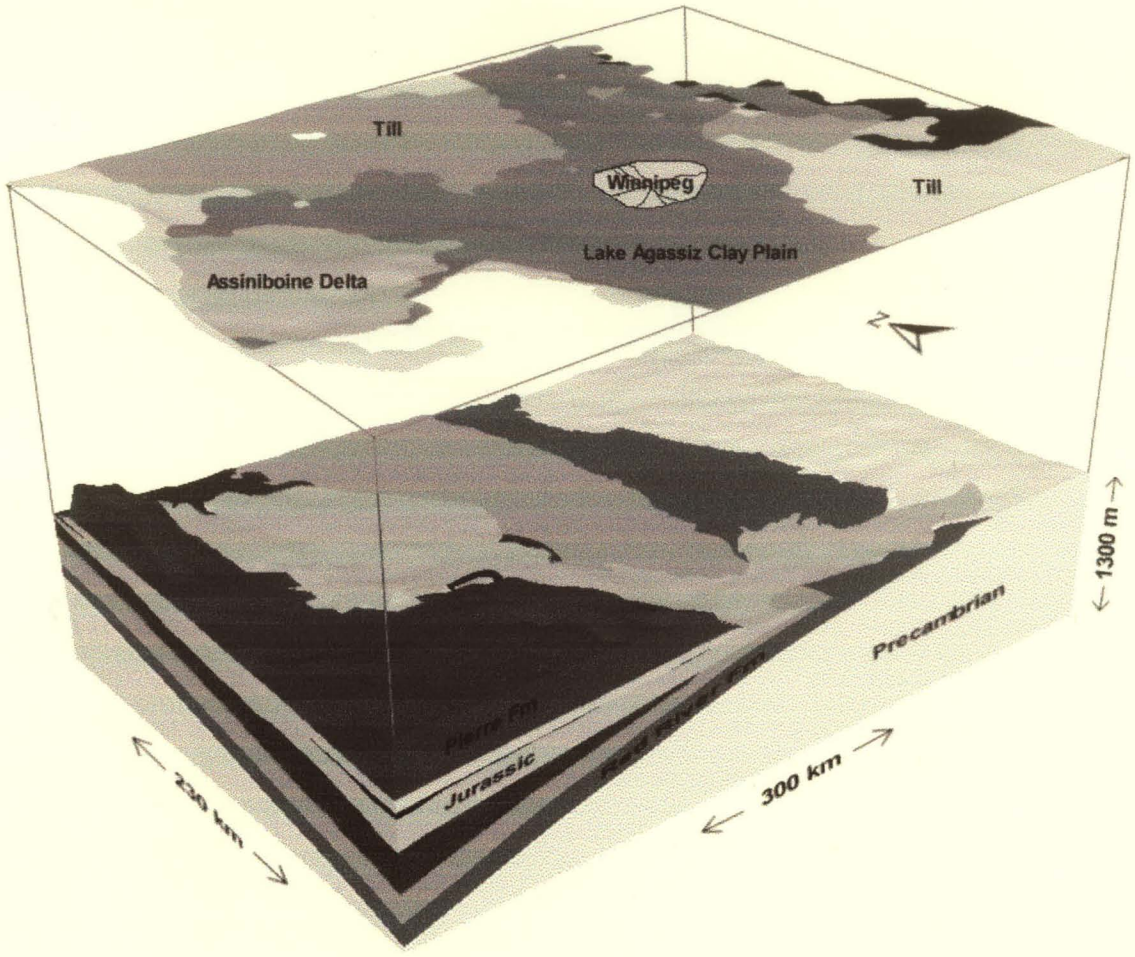

Figure 3.10 – Surficial units overlying bedrock units (constructed by ITM).

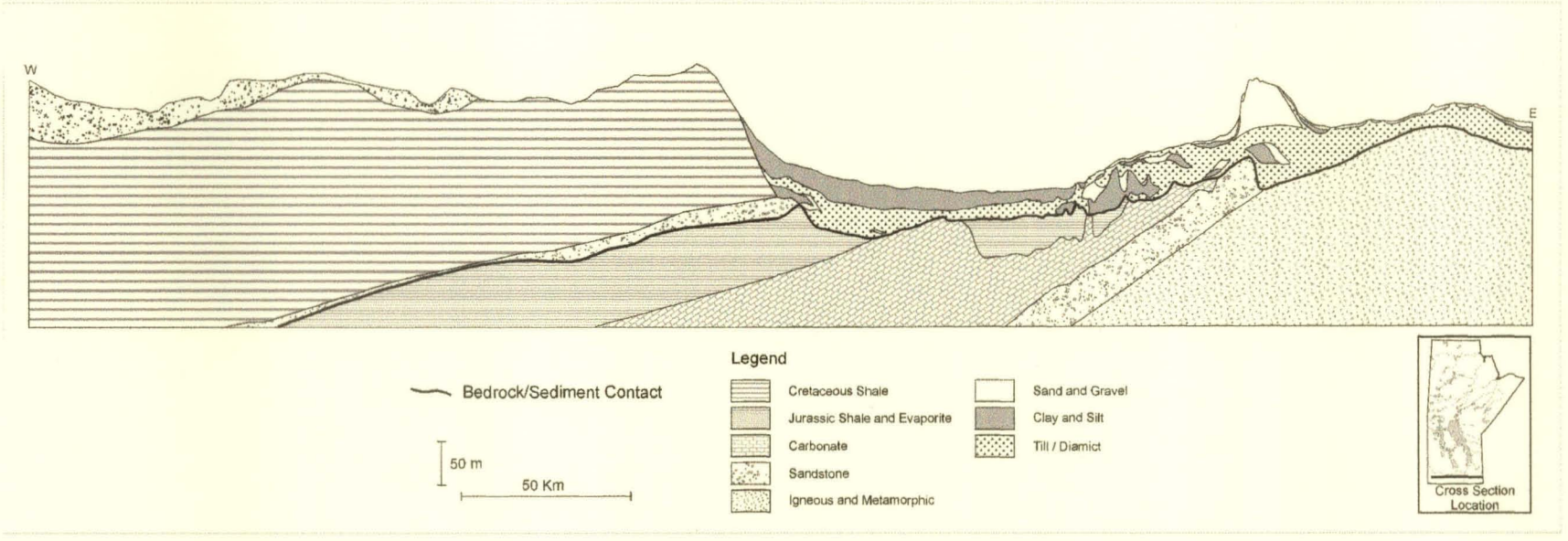

Figure 3.11 –East-west cross-section of bedrock and surficial units (constructed by ITM).

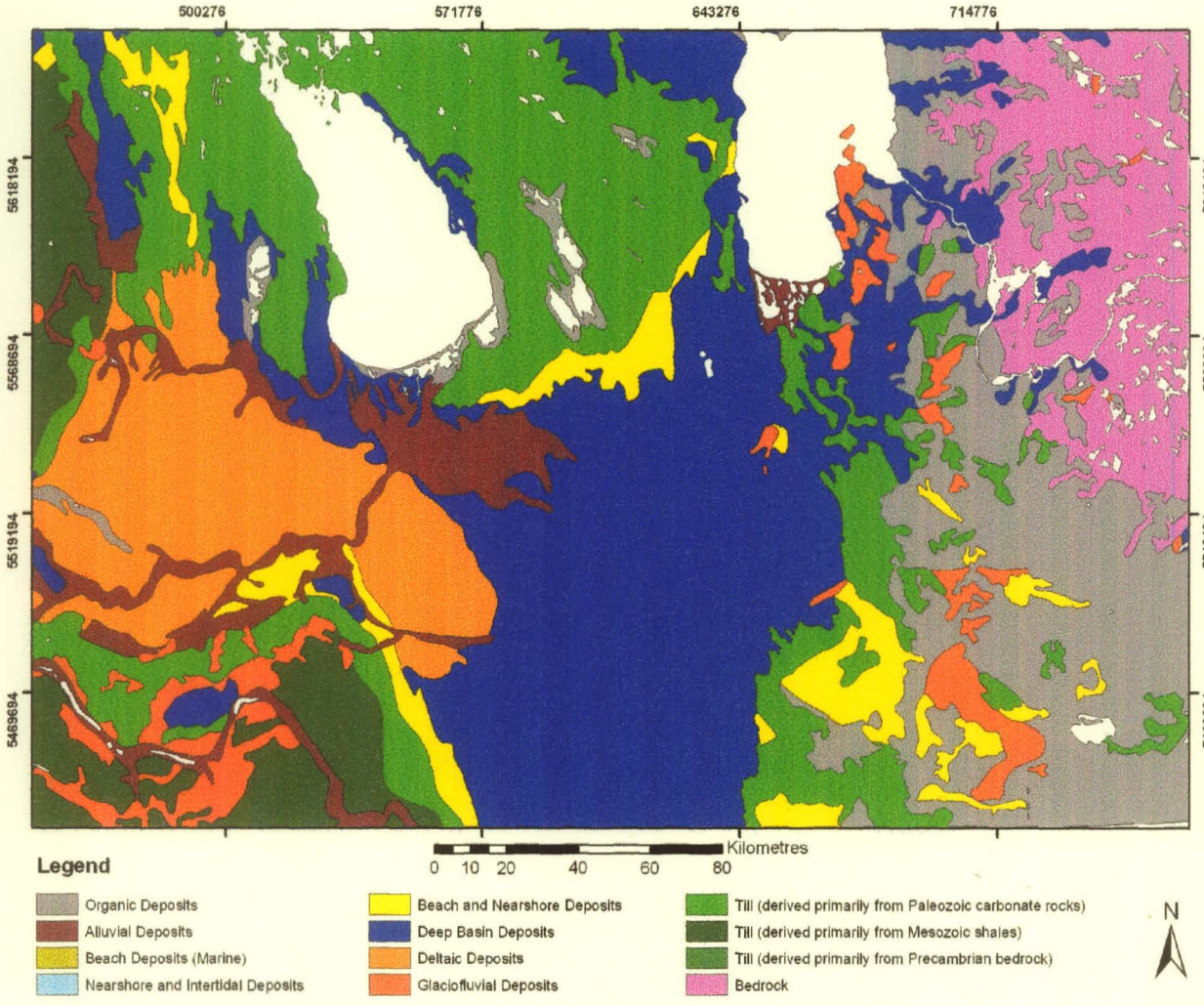

Figure 3.12 – Plan view of surficial model constructed by ITM.

CHAPTER 4

HYDROGEOLOGICAL DATA COLLECTION

4.1 Introduction

In order to solve the flow and solute transport equation, various and numerous types of information are required. Hydrogeological properties of the aquifers and other units were needed to characterize flow and transport. Water levels within the aquifers over time were needed for calibration and validation of the model. Geochemistry was required to determine density changes and solute movement. Recharge and discharge rates were necessary to determine inflows and outflows. A database of these parameters was developed in Microsoft Access and incorporated into a Geographical Information System (GIS) package Arc/View™.

The province of Manitoba is divided into a grid system of section-township-range, by which most wells are located (see Figure 4.1). The township determines how far north and the range determines the east-west location relative to the meridian. A Township and Range is a square that is 9.66 km x 9.66 km (6 miles x 6 miles). Each square is subdivided into 36 sections, which are 1.6 km x 1.6 km (1 mile x 1 mile). These sections are further subdivided into 4 quarter sections. However, an x-y coordinate system called the Universal Transverse Mercator (UTM) coordinate system (Zone 14) was used so that data could be digitized in GIS. The UTM coordinates were determined using digital orthophotos. In most cases, the location of the well was at best in the closest quarter

section. If a building was visible on the quarter section from the digital orthophotos, then the well was assumed to be next to the building. However, in many cases, no building or multiple buildings were present. In these cases, the UTM coordinates were taken at the center of the quarter section. This meant that the UTM coordinates could be in error by up to 200 m in the both the north and east directions. However, if the closest section or parish described the well location, then the error could be more. Ground surface elevation was determined from two digital elevation models (DEM). The first DEM consisted of ground surface elevation on a 120 m grid, which were determined using stereoscopy. Both the orthophotos and this DEM were obtained from Linnet Geomatics in Winnipeg, Manitoba. The second DEM was that developed by ITM (Matile and Keller, 1999). The grid resolution of this DEM was 100 m with a vertical accuracy of $\pm$ 3 m. This accuracy, however, is only good if the UTM coordinates were exact.

4.2 Hydrogeological Properties

4.2.1 Transmissivity

Values of transmissivity have been collected from pump tests for both the Carbonate and Sandstone Aquifers. The type of pump test used to measure transmissivity at each point was important in order to estimate the uncertainty associated with each value. This uncertainty was important for subsequent interpolation of the transmissivity field using Bayesian Updating.

The first source of data was a previously discussed database GWDrill. Within GWDrill there were a number of wells with a reported transmissivity. However, the exact field

test and analysis methods used to determine this transmissivity were not noted in the database. It was assumed that the most likely method was a single-well drawdown test (Betcher et al., 1995).

Consulting firms also carry out pump tests for major hydrogeological projects. The results of these pump tests are included in the final consultant's report. Transmissivities were collected from a number of these reports and in general, multiple-well drawdown tests were conducted, hence providing high quality results (Manitoba Natural Resources, 1986; UMA Engineering Inc., 1987, 1991a, 1991b, 1993, 1997; and Wardrop Engineering Inc., 1995).

At MWB, files are maintained for all users requiring a license to pump water. For any user desiring to pump above 25,000 L/day, a permit must be obtained (The Water Rights Act, 1988). Before a permit is granted, MWB sometimes requires that a pump test be conducted to ensure that adequate water is available in the aquifer. The pump tests contained within these files were obtained for the Carbonate and Sandstone Aquifers.

After collecting the transmissivity from the three sources listed above, it was observed that there was insufficient data for the needs of this particular project. To improve the situation, it was decided to estimate transmissivity from specific capacity data. Values of specific capacity were obtained from GWDrill and the transmissivity was estimated using equation 2.1.

The ultimate goal was to obtain the hydraulic conductivity, which is equal to the transmissivity divided by the saturated thickness (b). Some hydraulic conductivity values for clays and tills were obtained from consultants' reports and an M.Sc. thesis by Pach (1994). The saturated thickness was determined from the hydrostratigraphic model.

Table 4.1 presents the transmissivity that was collected for each stratigraphic unit. The data is divided into source and test type. Figures 4.2 and 4.3 show maps of locations of the transmissivity measurements for the Carbonate and Sandstone Aquifers, respectively. There were relatively few measurements towards the west in both aquifers, due to increased salinity. Transmissivity measurements for Precambrian, shale, sand and gravel, silt, clay and till are presented in Figures 4.4 to 4.9.

4.2.2 Storativity

The number of storativity points obtained through data collection was very limited. For the Carbonate Aquifer, there were two wells in which several values of storativities from different analyses were reported. For the Sandstone Aquifer, no values of storativity were found. Therefore, upper and lower bounds were obtained from first principles (Chapter 2, Equation 2.2) and from values reported in the literature. For the former case, several parameters were required. As stated previously, the uncertain factors were b, n, α and ρ (Section 2.5). The thickness of the Carbonate Aquifer ranges between 0 and 30 m and that of the Sandstone Aquifer ranges between 0 and 60 m (Betcher et al., 1995). The porosity of sandstone varies between 10 and 20% and that of limestone varies between 1 and 10% (Bear, 1972). The water density in the study region as will be shown later in

this chapter was found to vary between 986 and 1150 kg/m^3. Table 4.2 presents the possible ranges of storativity estimated from first principles and values reported in Render (1970). For the Carbonate Aquifer, storativity ranging between 10^{-5} and 10^{-4} was obtained. This falls within the range reported by Render (1970) of 10^{-6} to 10^{-3}. In the modeling, a possible range of storativity between 10^{-6} and 10^{-3} was assumed. The Sandstone Aquifer was calculated to have a storativity with a range between 10^{-4} and 10^{-5}. For modeling purposes, a slightly larger range of 10^{-6} to 10^{-3} was assumed to ensure that the entire possible range was covered.

Table 4.1 – Number of measured transmissivity data obtained from each source and type of test used.

Source/Test Type	**Hydrogeological Unit**								
	Carbonate	*Lower Carbonate*	*Sandstone*	*Shale*	*Sand and Gravel*	*Till*	*Silt*	*Clay*	*Granite*
GWDrill									
Total	**2258**	--	**76**	**592**	**1846**	**20**	**5**	**33**	**39**
Multiple-well drawdown	--	--	--	--	--	--	--	--	--
Single-well drawdown	43	--	28	--	--	--	--	--	--
From specific capacity	2215	--	48	592	1846	20	5	33	39
Consultants' Reports/Thesis									
Total	**275**	**6**	--	--	--	**7**	--	**66**	--
Multiple-well drawdown	198	4	--	--	--	--	--	--	--
Single-well drawdown	33	2	--	--	--	--	--	--	--
From specific capacity	--	--	--	--	--	--	--	--	--
Unknown	44	--	--	--	--	--	--	--	--
Water Licensing Files									
Total	**154**	--	**2**	--	--	--	--	--	--
Multiple-well drawdown	27	--	--	--	--	--	--	--	--
Single-well drawdown	35	--	--	--	--	--	--	--	--
From specific capacity	46	--	2	--	--	--	--	--	--
Unknown	46	--	--	--	--	--	--	--	--
TOTAL	**2708**	**6**	**78**	**592**	**1846**	**27**	**5**	**99**	**429**

Table 4.2 – Storativity estimated from first principles for the Carbonate and Sandstone Aquifers and reported by Render (1970).

			Carbonate Aquifer				**Sandstone Aquifer**	
			α=6.9x10^{-10} Pa^{-1}		**α=3.3x10^{-10} Pa^{-1}**		**α=3.3x10^{-10} Pa^{-1}**	
			Density = 986 kg/m^3					
			Porosity					
			0.01	*0.1*	*0.01*	*0.1*	*0.1*	*0.2*
From First Principles	**Saturated Thickness (m)**	*5*	3.36x10^{-5}	3.55x10^{-5}	1.62x10^{-5}	1.81x10^{-5}	1.81x10^{-5}	2.02x10^{-5}
		15	1.01x10^{-4}	1.06x10^{-4}	4.85x10^{-5}	5.43x10^{-5}	5.43x10^{-5}	6.06x10^{-5}
		30	2.02x10^{-4}	2.13x10^{-4}	9.70x10^{-5}	1.09x10^{-4}	1.09x10^{-4}	1.21x10^{-4}
			Density = 1150 kg/m^3					
			Porosity					
			0.01	*0.1*	*0.01*	*0.1*	*0.1*	*0.2*
	Saturated Thickness (m)	*5*	3.92x10^{-5}	4.14x10^{-5}	1.89x10^{-5}	2.11x10^{-5}	2.11x10^{-5}	2.36x10^{-5}
		15	1.18x10^{-5}	1.24x10^{-4}	5.66x10^{-5}	6.33x10^{-5}	6.33x10^{-5}	7.07x10^{-5}
		30	2.35x10^{-4}	2.48x10^{-4}	1.13x10^{-5}	1.27x10^{-4}	1.27x10^{-4}	1.41x10^{-4}
	Minimum		1.62 x 10^{-5}				1.81 x 10^{-5}	
	Maximum		2.48 x 10^{-4}				1.41 x 10^{-4}	
Reported by Render (1970)			1x10^{-6} to 1x10^{-3}				--	

4.3 Water Levels

For model calibration, the model was compared against water levels from relatively undeveloped times. Historically, MWB did not start monitoring water levels on a regular basis until the 1960's. As very few observation wells existed at that time, and the groundwater systems were fairly developed, another source of historical data was required. For the Carbonate Aquifer, this was taken as the water levels for wells constructed prior to 1920 as reported in GWDrill. It was assumed that the dataset represented the system at steady state. Figure 4.10 shows the location of historical water level measurements and piezeometric surfaces in the Carbonate Aquifer. Taking the

water level measurements provides values of hydraulic head. However, the model calculates equivalent freshwater head and therefore could not be compared directly. The measured hydraulic heads were put in terms of equivalent freshwater head using equation 2.9. The density was determined from the chemistry dataset, which will be presented in Section 4.4. The effects of density on the head values were quite small (< 0.12 m) as the bulk of the head measurements are from relatively freshwater zones. The pumping rates within the city of Winnipeg varied over this time due to changes in the city water supply in 1918 from groundwater sources to being brought in from Shoal Lake, Ontario. Therefore, prior to 1918, there was significant groundwater withdrawal within the city and after 1918 a significant decline occurred. As the majority of the wells collected for this historical database were outside of the City of Winnipeg, these observed water levels were not likely affected by this change in pumping. The resulting database has a total of 152 observed water levels for the Carbonate Aquifer. The resulting piezeometric surface from these water elevations was not instantaneous, meaning that the measurements were not taken at the same time. As water levels can vary by several meters due to seasonal and temporal variations, the piezeometric surface was less than ideal. However, this is the best source of historical data available and was used in the calibration phase. The regional direction of flow in the Carbonate Aquifer is presented in Figure 4.11. For the Sandstone Aquifer, no wells were reported in GWDrill for wells constructed prior to 1920. A figure of the Sandstone Aquifer flow regime was found in Betcher (1986), from more recent water level observations (see Figure 4.12).

To validate the model as described in Section 2.4, the calibrated model needs to be run under a different scenario in which a dataset is available. This second dataset was collected from current conditions from MWBs system of observation wells. MWB had 141 wells in the Carbonate Aquifer and 6 wells in the Sandstone Aquifer, in which water levels were recorded on a daily basis. Therefore, this database could be used to generate instantaneous piezeometric surfaces for validation purposes. The locations of these observation wells are presented in Figures 4.13 and 4.14 for the Carbonate and Sandstone Aquifers, respectively.

4.4 Geochemical Data

In order to model the solute transport, geochemical data was required. One reason was that the changes in ion concentrations cause variations in density, which in turn affects flow. The chloride ion concentration was used as a surrogate for all species in brine. The chloride ion concentration is conservative, meaning it would not react with other ions or the soil medium. Therefore, the chloride ion should move with the bulk flow and retardation factor (equation 2.22) would be equal to 1.

For the Carbonate Aquifer, the required geochemical data was collected from an open file report by Grasby et al. (1999). The location of the sample points and chloride ion concentration is presented in Figure 4.15. The Sandstone Aquifer chemistry data was compiled at the University of Texas. The location of the data points is presented in Figure 4.16. The bulk of the Sandstone Aquifer samples were obtained from fresh water regions and therefore, the dataset was not representative of what was occurring in the

salt-water region to the west. No information of chloride ion concentration was available in the western (saltwater) region of the aquifer. To improve this situation, a map showing total dissolved solids (TDS) concentrations is presented in Figure 4.17 (Betcher et al., 1995). This TDS map does not provide information of chloride ion concentration but helps provide brine location.

4.5 Sources and Sinks (Recharge and Discharge Zones)

Water is supplied to the aquifer through recharge zones. The primary recharge zones of the Carbonate Aquifer are the Birds Hill, Sandilands and through thin tills in the Interlake region (see Figure 4.18). For the Sandstone Aquifer, the recharge is primarily in the Sandilands region (see Figure 4.19). Quantifying the amount of recharge was difficult due to lack of information in this area. One study investigated the rate of downward flow through the tills in the Sandilands area, however, the amount of water that actually reached the aquifer was not determined. Another study, determined recharge rates from temperature profiles with depth to bedrock. From these temperature profiles, recharge rates could be determined using type curves. This research determined an upper limit of $1x10^{-6}$ m/s of recharge to the aquifers in the Sandilands region (Ferguson et al., 2001). No research has been conducted in either the Bird's Hill or Interlake region. All recharge rates were determined in the calibration process.

Several sinks were present in the groundwater system being studied. The first is natural discharge to lakes and streams present throughout the modeling region. The major discharge zones are Lake Manitoba and Lake Winnipeg in the northern part of the region.

Average monthly lake levels were obtained for every year from 1920 forward from MWB (see Figures 4.20 and 4.21). The construction of the Red River Floodway (a flood diversion channel) around the city of Winnipeg caused a reduction in overburden units above the Carbonate Aquifer. The excavation caused locations where groundwater is discharging (approximately 0.14 m^3/s) from the Carbonate Aquifer into the Floodway (Render, personal communication, 2001).

All large pumping rate wells (pumping rate > 25,000 L/day) require a permit. The Carbonate Aquifer has numerous wells with a permit, whereas the Sandstone Aquifer has none. From the permits, pumping period, maximum allowable volume of water per annum and type of well (industrial, irrigation, etc.) were obtained (see Figure 4.22). As the maximum allocated volume of water was reported, some assumptions were required to obtain the actual pumping rate. For industrial users, the maximum rate was assumed as pumps are generally left on at the maximum rate. For irrigation wells, however, the quantity of pumping varies from year to year and season to season. Therefore, a reasonable average of 50% of the maximum allowable pumping rate was assumed. Agricultural wells were assumed to run at 100% of maximum, as the rate should not vary significantly. Wells assigned a type as 'other' were assigned 100% of the maximum rate.

Within Manitoba, there are approximately 80,000 water wells reported in GWDrill that do not require a permit. The bulk of these wells are most likely in the South portion of the province. The approach taken was to assign an average pumping rate for each township and range within the study area. This average was obtained by first

determining the number of wells from GWDrill within each township and range for both aquifers. To obtain the average flow rate, the quantity of wells was multiplied by an assumed pumping value per well based on usage types (see Table 4.3). The average flow rates were assigned UTM coordinates, which were placed at the center of each respective township and range (see Figure 4.23). This was considered to be the best method of accounting for these wells.

Another issue that is considered is that a number of wells are screened over both the Carbonate and Sandstone Aquifers. This results in exchange of water between these two systems. In the Southern portion of the province, the Sandstone Aquifer is under greater heads than the Carbonate Aquifer, and therefore water will flow up into the well from the Sandstone Aquifer and into the Carbonate Aquifer. This causes the Sandstone Aquifer to lose water (i.e. lose pressure) over time and result in cross-contamination between aquifers in locations where the Sandstone Aquifer has inferior water quality. The wells screened over both aquifers were determined by investigation of well logs in GWDrill (see Figure 4.24). There were a total of 493 wells that were screened across both aquifers.

Table 4.3 – Average flow rate per well based on different usages (Linsley et al., 1992).

Usage	**Average Flow per unit**	**Assumed Unit**	**Assumed average flow rate**
Domestic	150 L/cap.day – 300 L/cap.day	1-7 capita	150 L/d – 1800 L/d
Irrigation	0.37 – 2.29 m/year	½ mi^2 = 647,497 m^2	656,000 – 4060,000 L/d
Agricultural	150 – 10,000 L/day	---	150 – 10,000 L/d
A/C	50 – 10,000 L/day	---	50 – 10,000 L/d

4.6 Summary

This chapter presented the data collection that was carried to gather the hydrogeological properties and parameters that were required to construct the model. The transmissivity (or hydraulic conductivity) data will be used to generate statistics for interpolation purposes. The other data is used to assign other hydrogeological properties or for assessment of the model results.

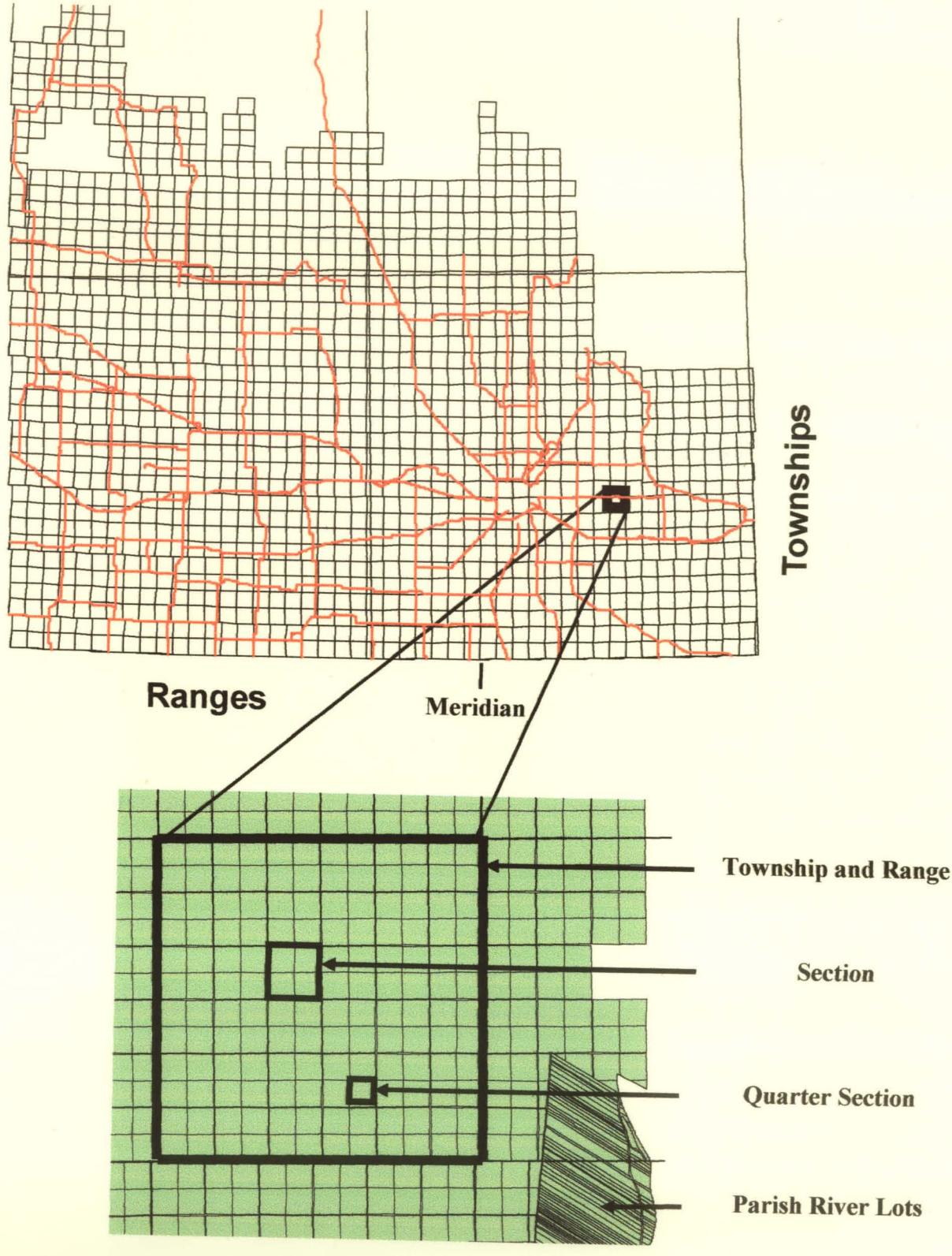

Figure 4.1 – Figure showing the Townships and Ranges of Southern Manitoba.

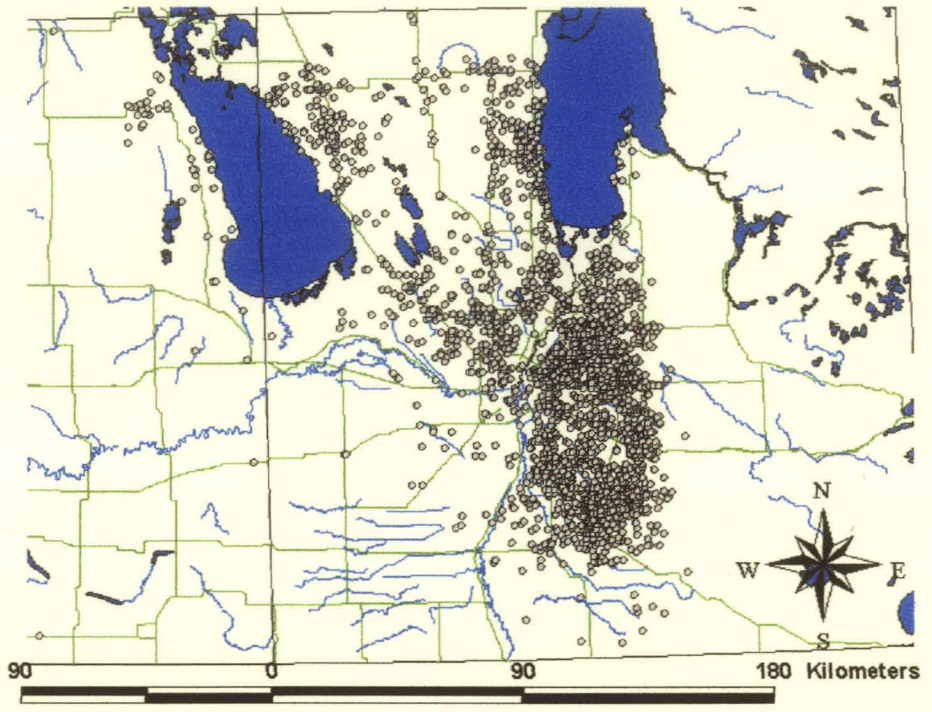

Figure 4.2 – Map showing location of transmissivity measurement points for Carbonate Aquifer.

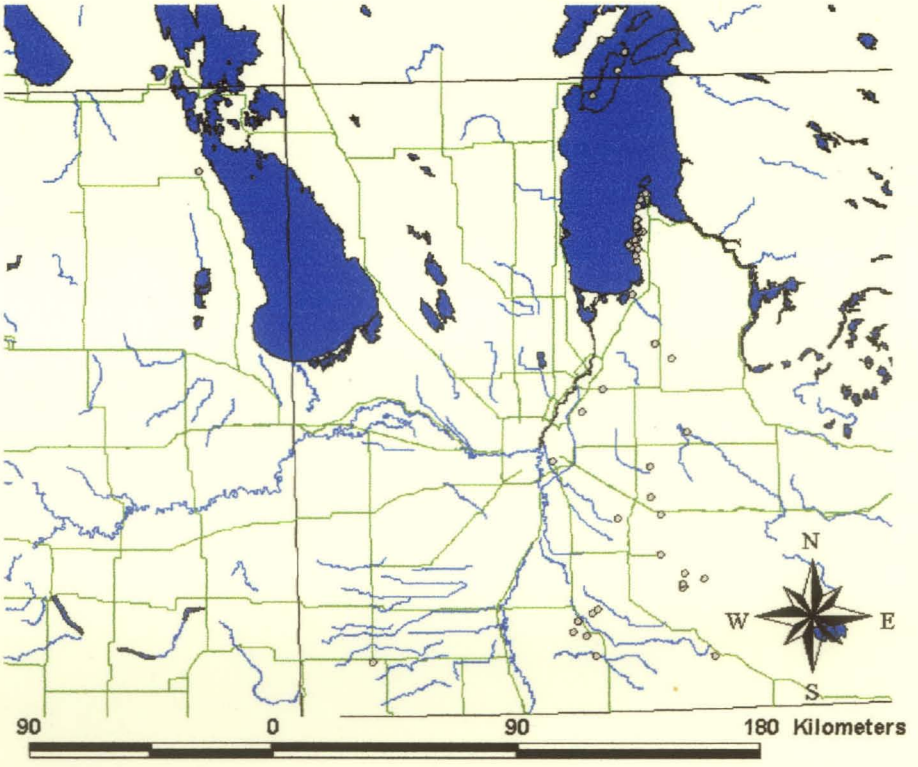

Figure 4.3 – Map showing location of transmissivity measurement points for Sandstone Aquifer.

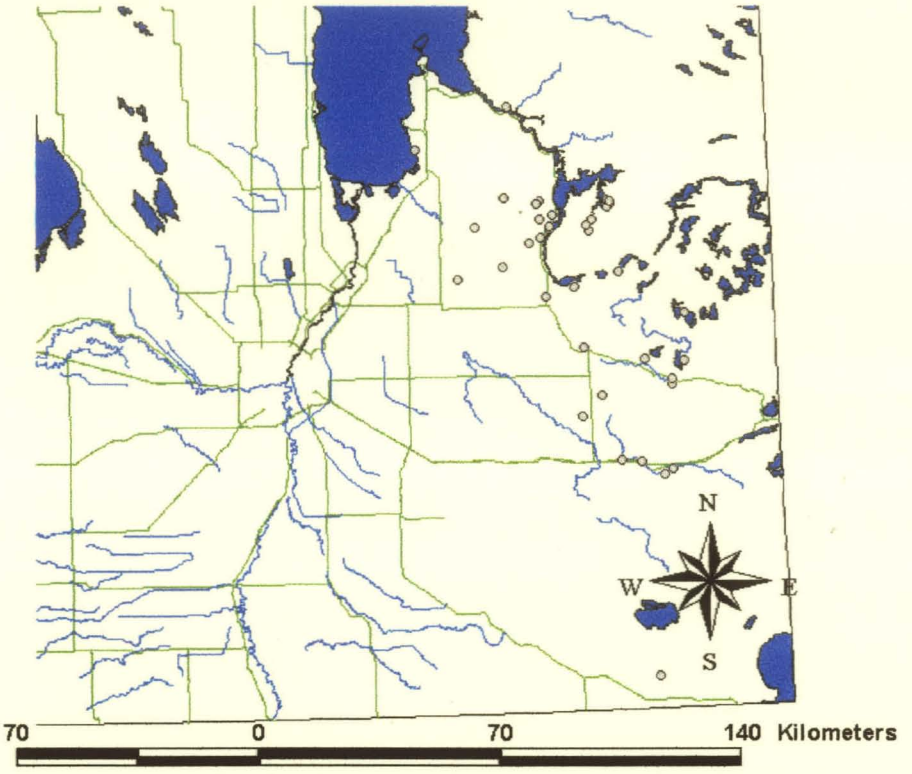

Figure 4.4 – Map showing location of transmissivity measurement points for Precambrian.

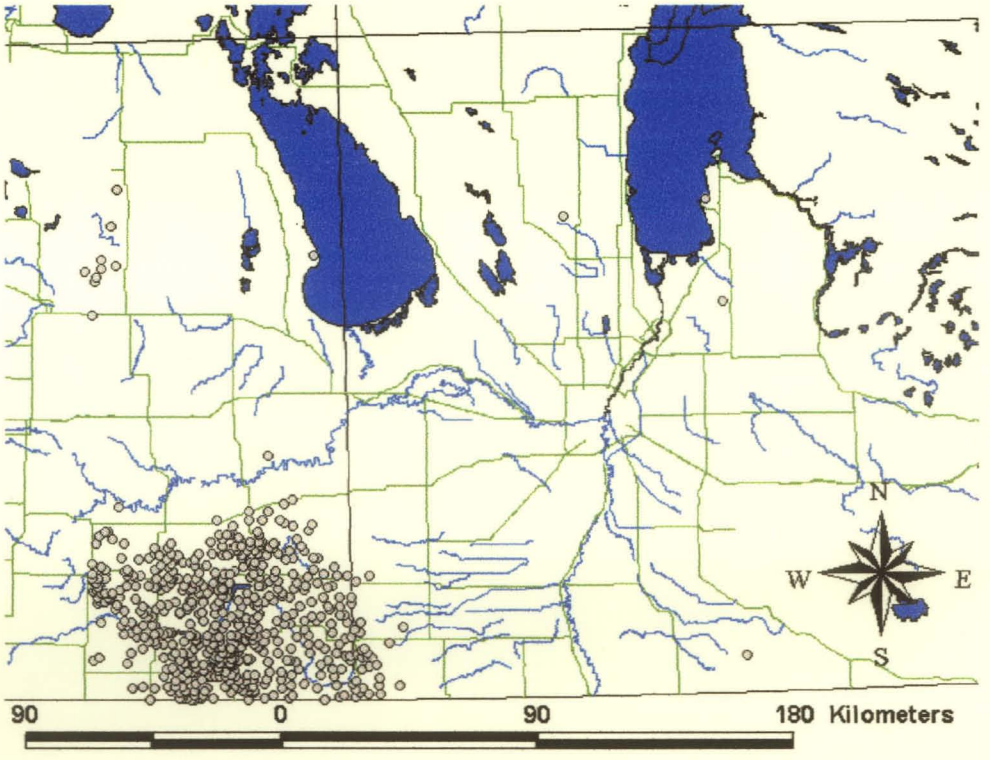

Figure 4.5 – Map showing location of transmissivity measurement points for shale.

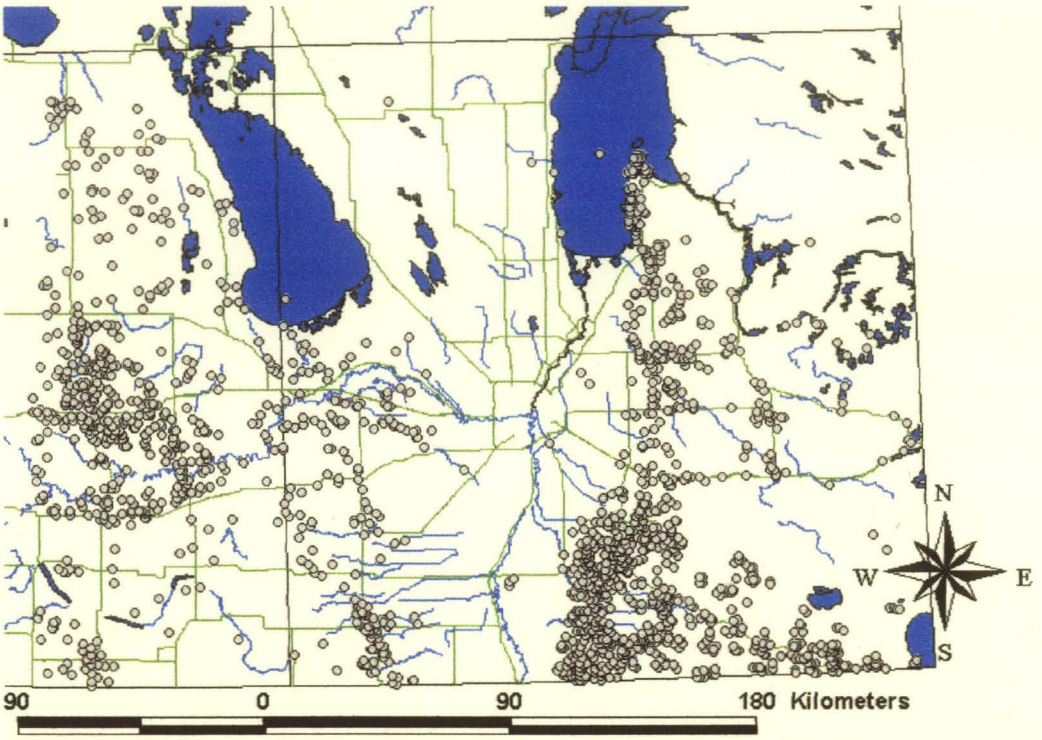

Figure 4.6 – Map showing location of transmissivity measurement points for sand and gravel.

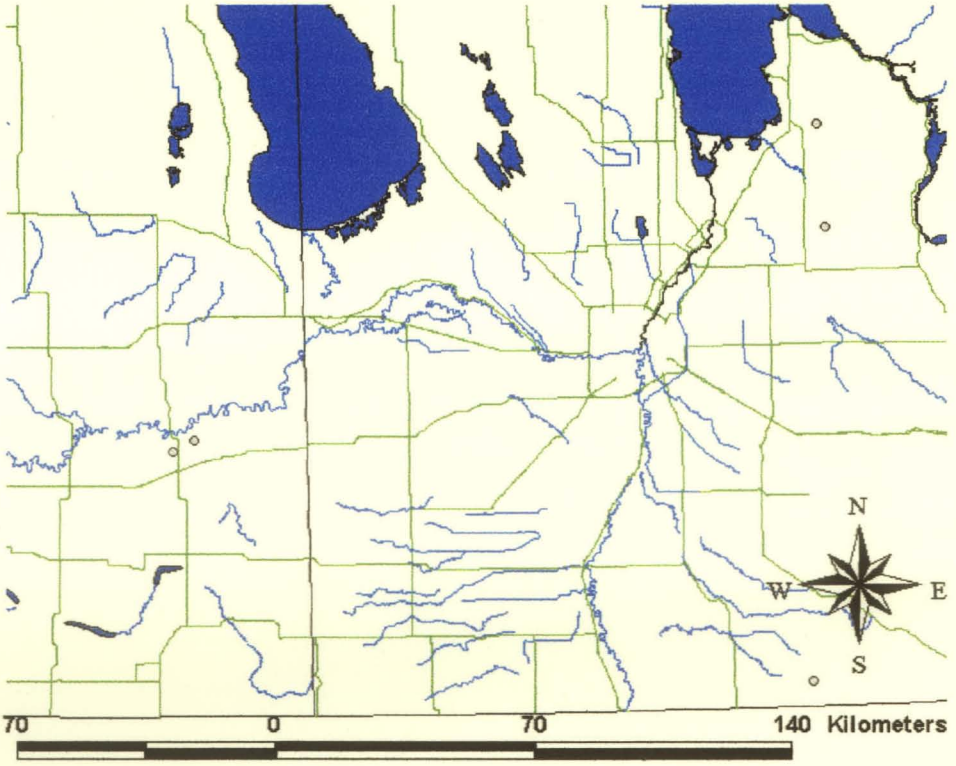

Figure 4.7 – Map showing location of transmissivity measurement points for silt.

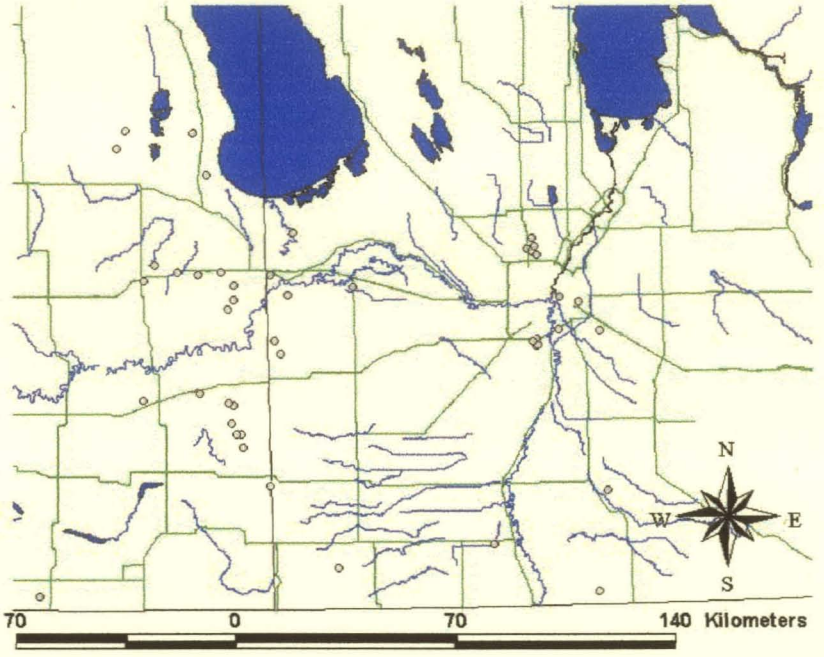

Figure 4.8 – Map showing location of hydraulic conductivity measurement points for clay.

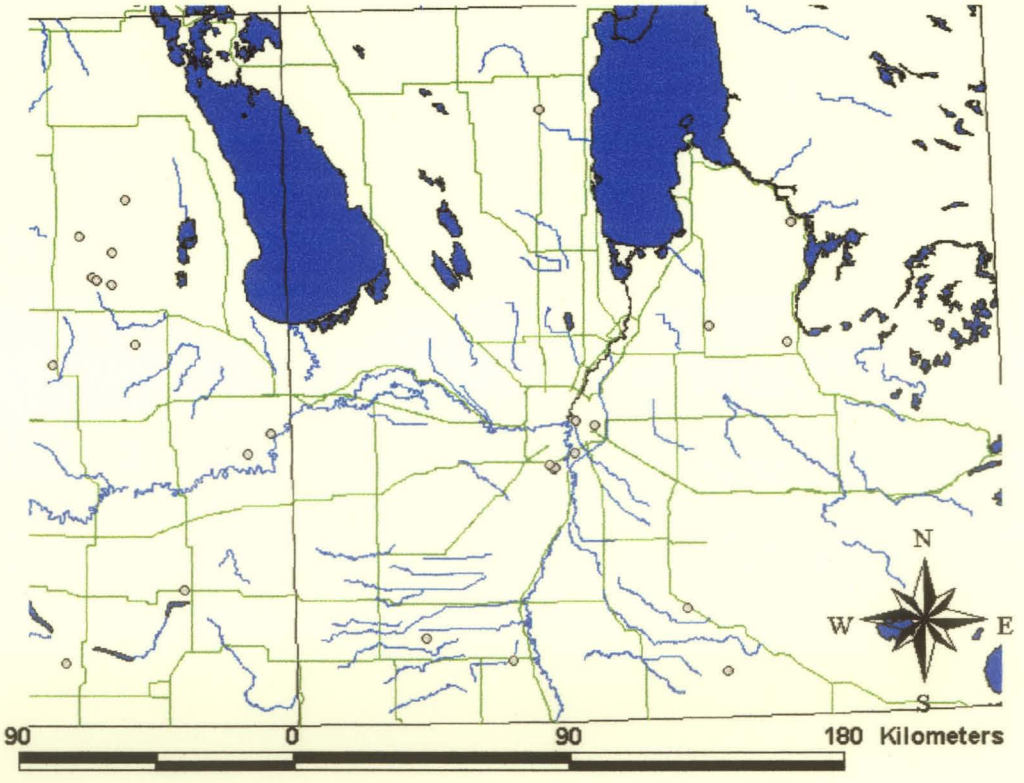

Figure 4.9 – Map showing location of hydraulic conductivity measurement points for till.

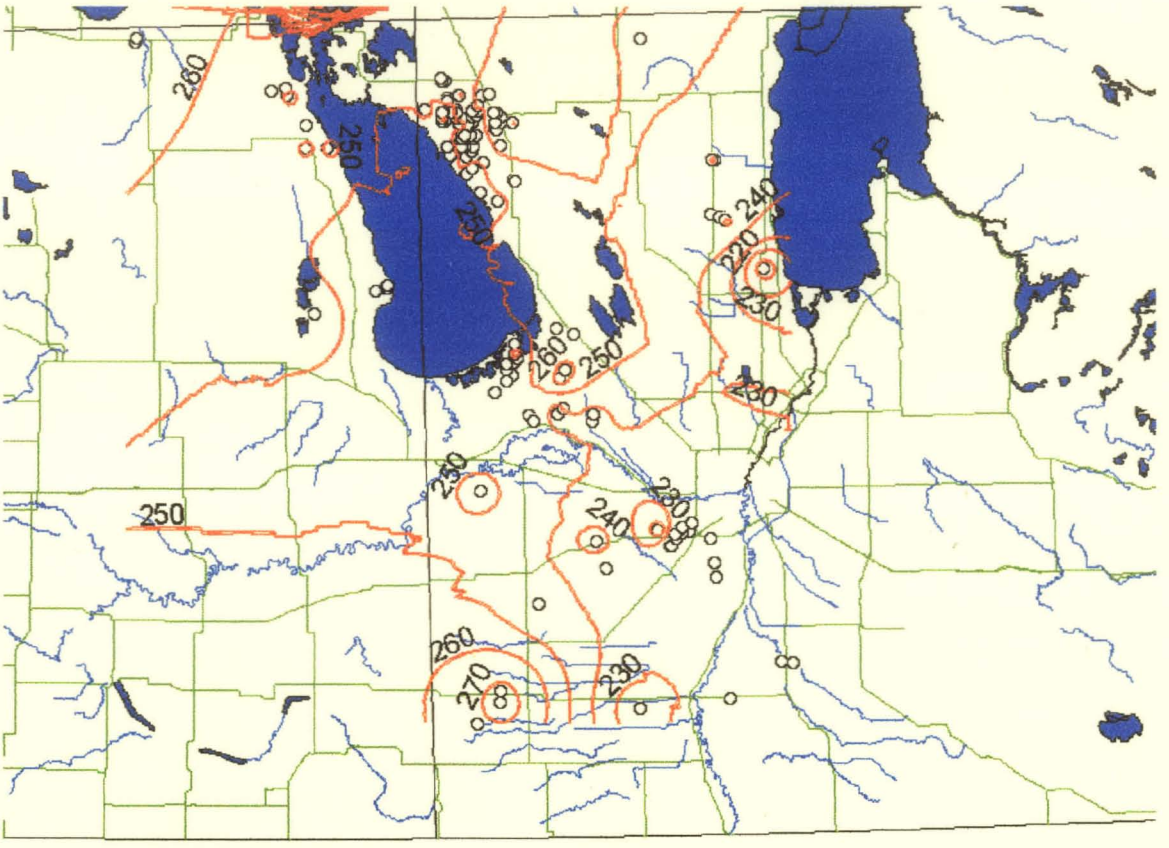

Figure 4.10 – Map showing location of historic water levels in meters above sea level and piezometric surface for the Carbonate Aquifer (1920).

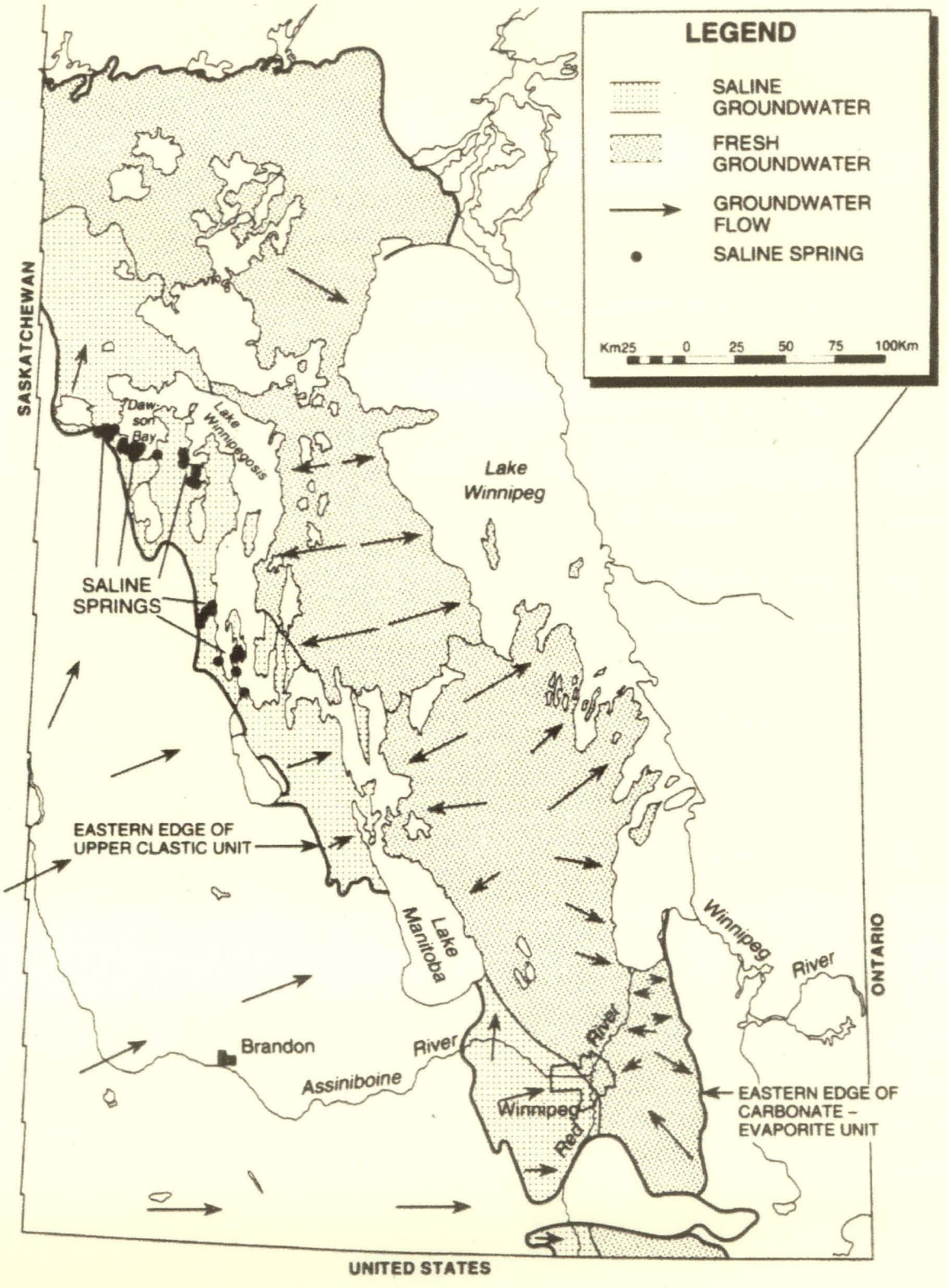

Figure 4.11 – Carbonate Aquifer regional flow system. (Taken from Betcher et al., 1995).

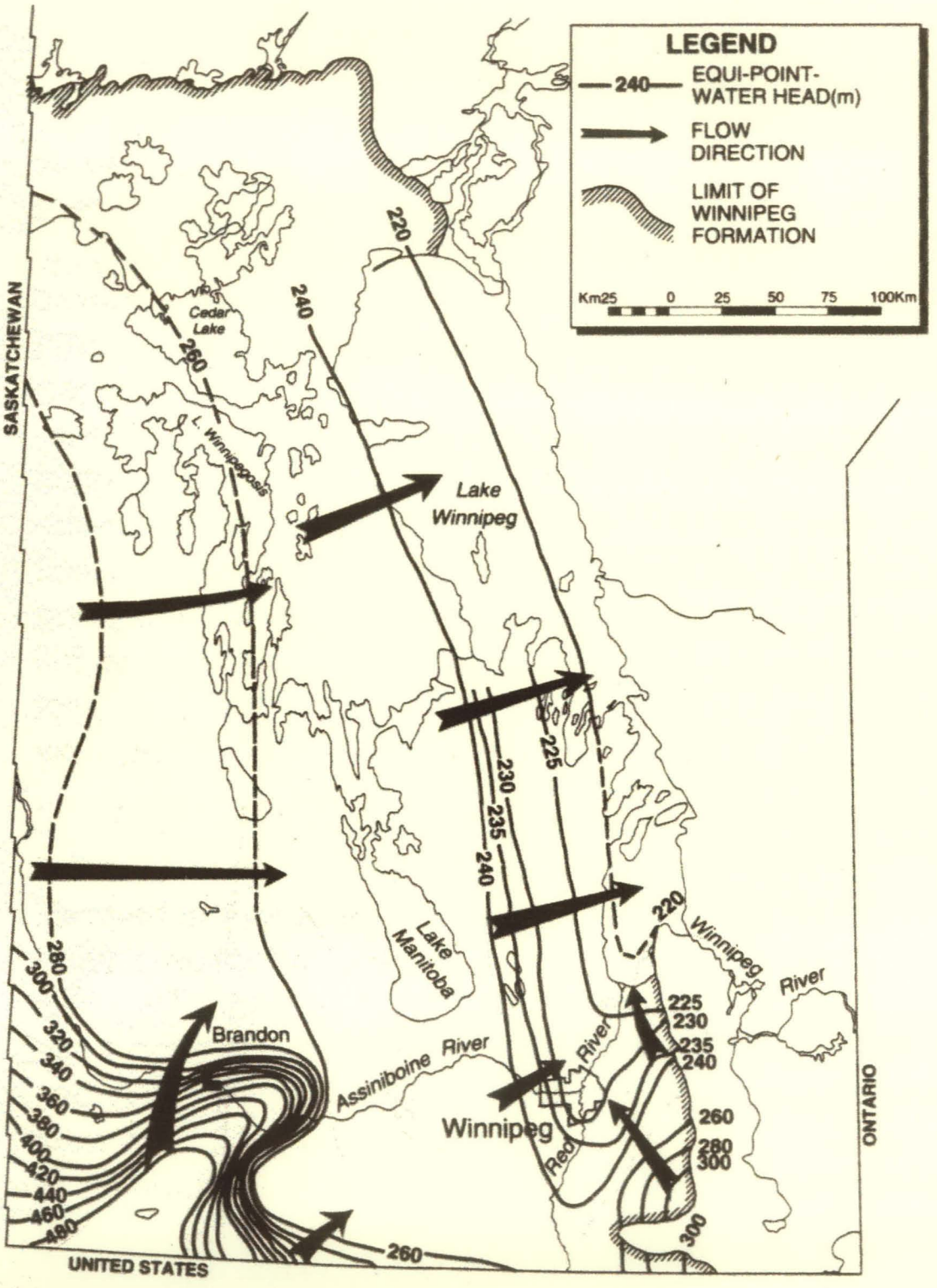

Figure 4.12 – Equivalent fresh water head and regional groundwater flow in Sandstone Aquifer (taken from Betcher et al., 1995).

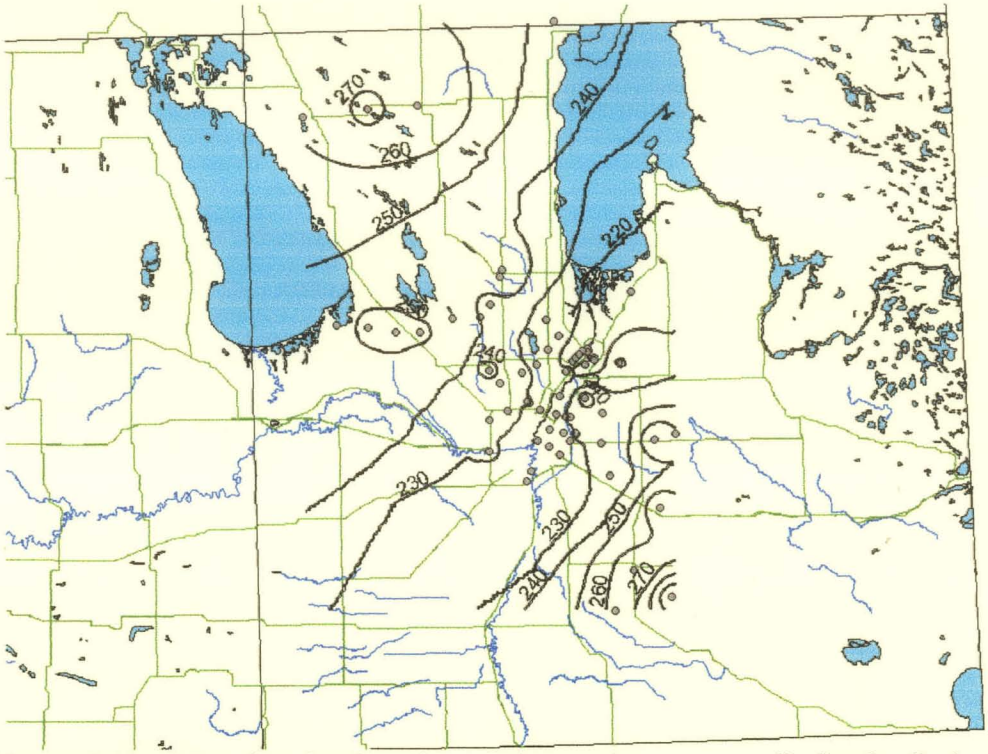

Figure 4.13 – Map showing location of observation water wells for the Carbonate Aquifer and instantaneous piezometric surface on January 1, 1999.

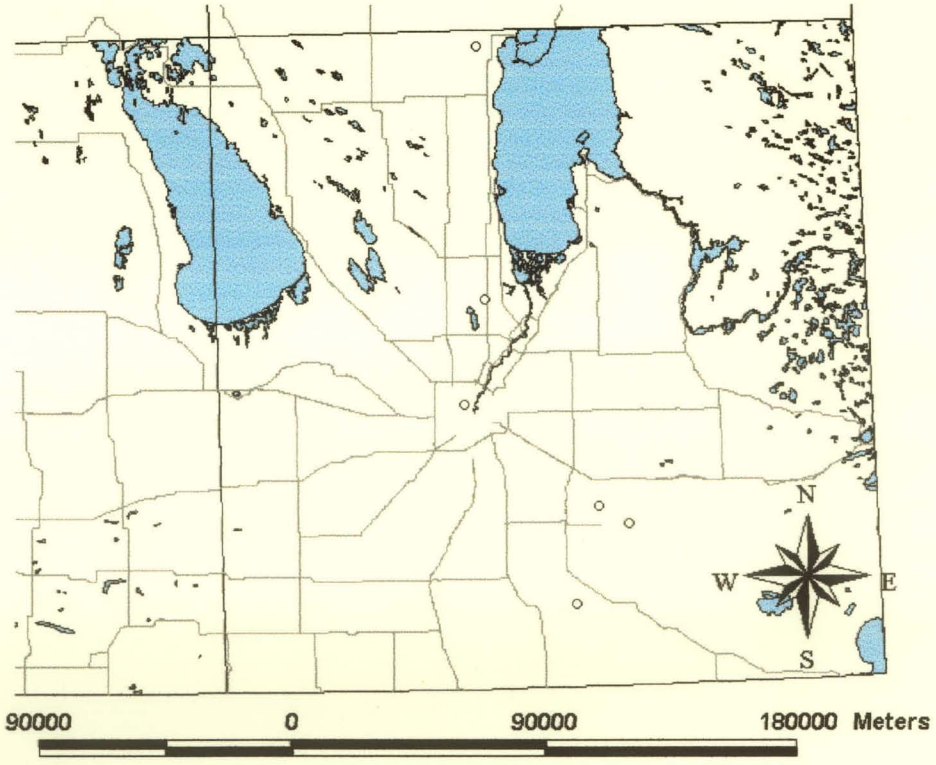

Figure 4.14 – Map showing location of observation water wells for the Sandstone Aquifer.

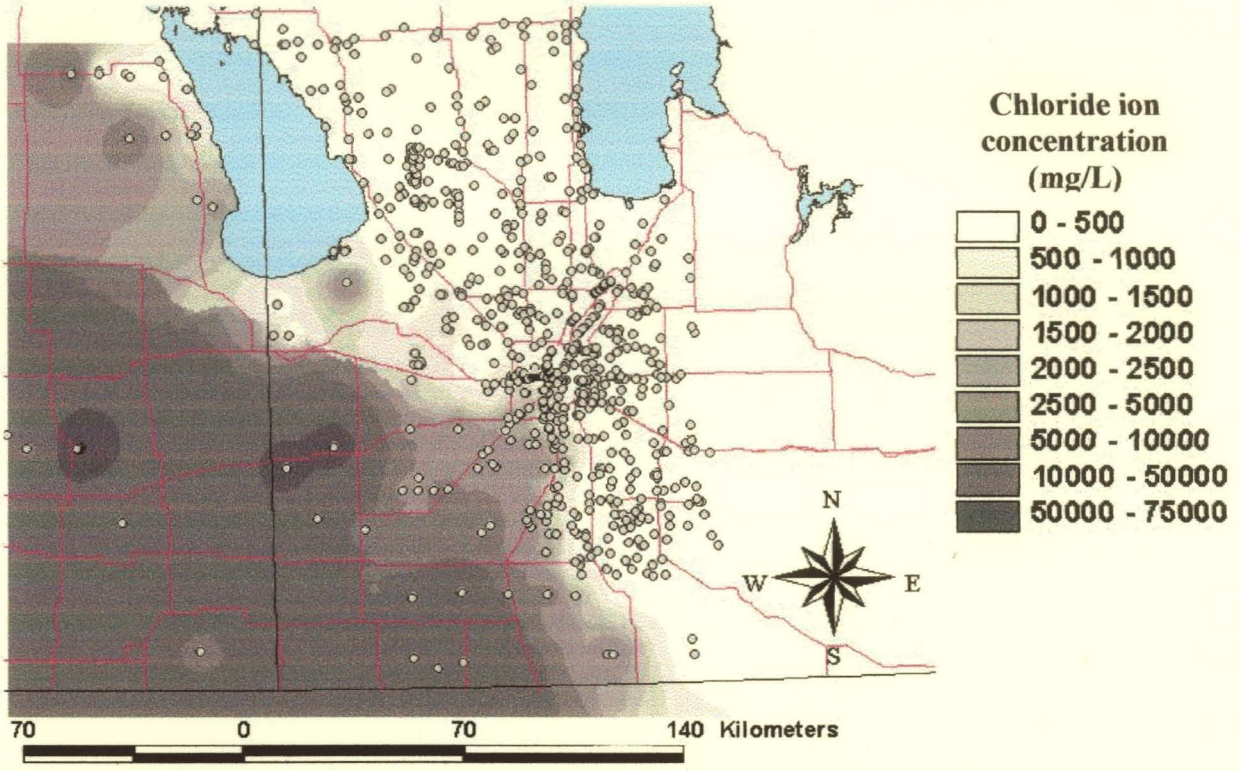

Figure 4.15 – Map showing location of chemistry sample points in Carbonate Aquifer and interpolated chloride ion concentration contours.

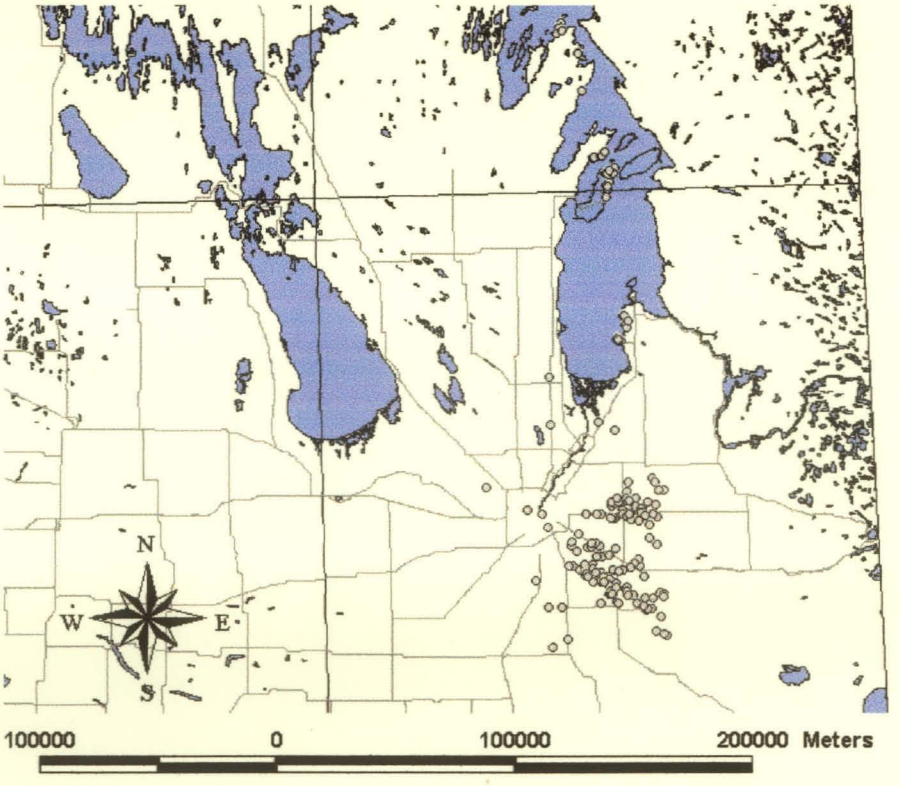

Figure 4.16 – Map showing location of chemistry measurements in Sandstone Aquifer.

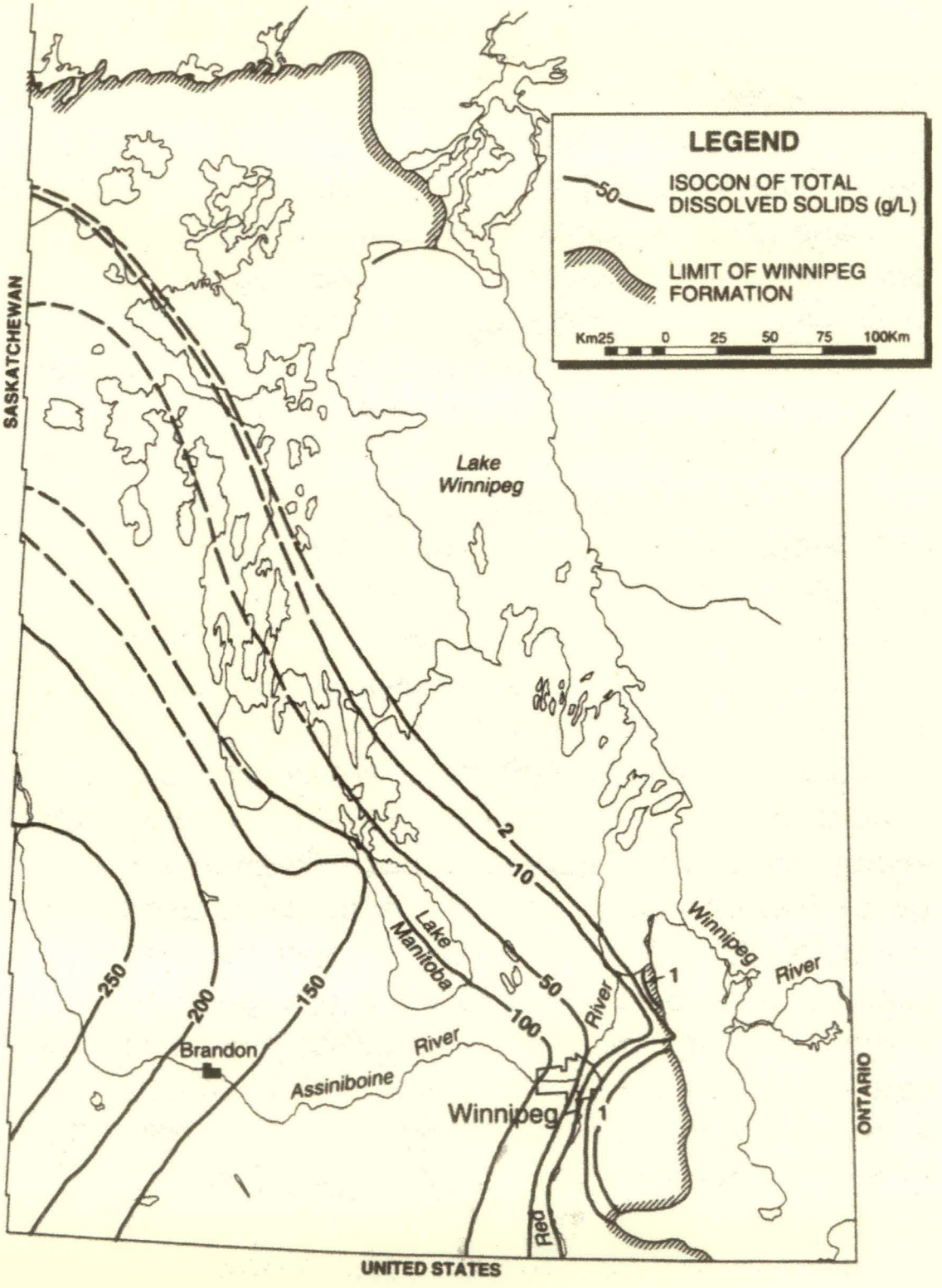

Figure 4.17 – Total dissolved solids (TDS) of Sandstone Aquifer groundwater (g/L) (Taken from Betcher et al., 1995).

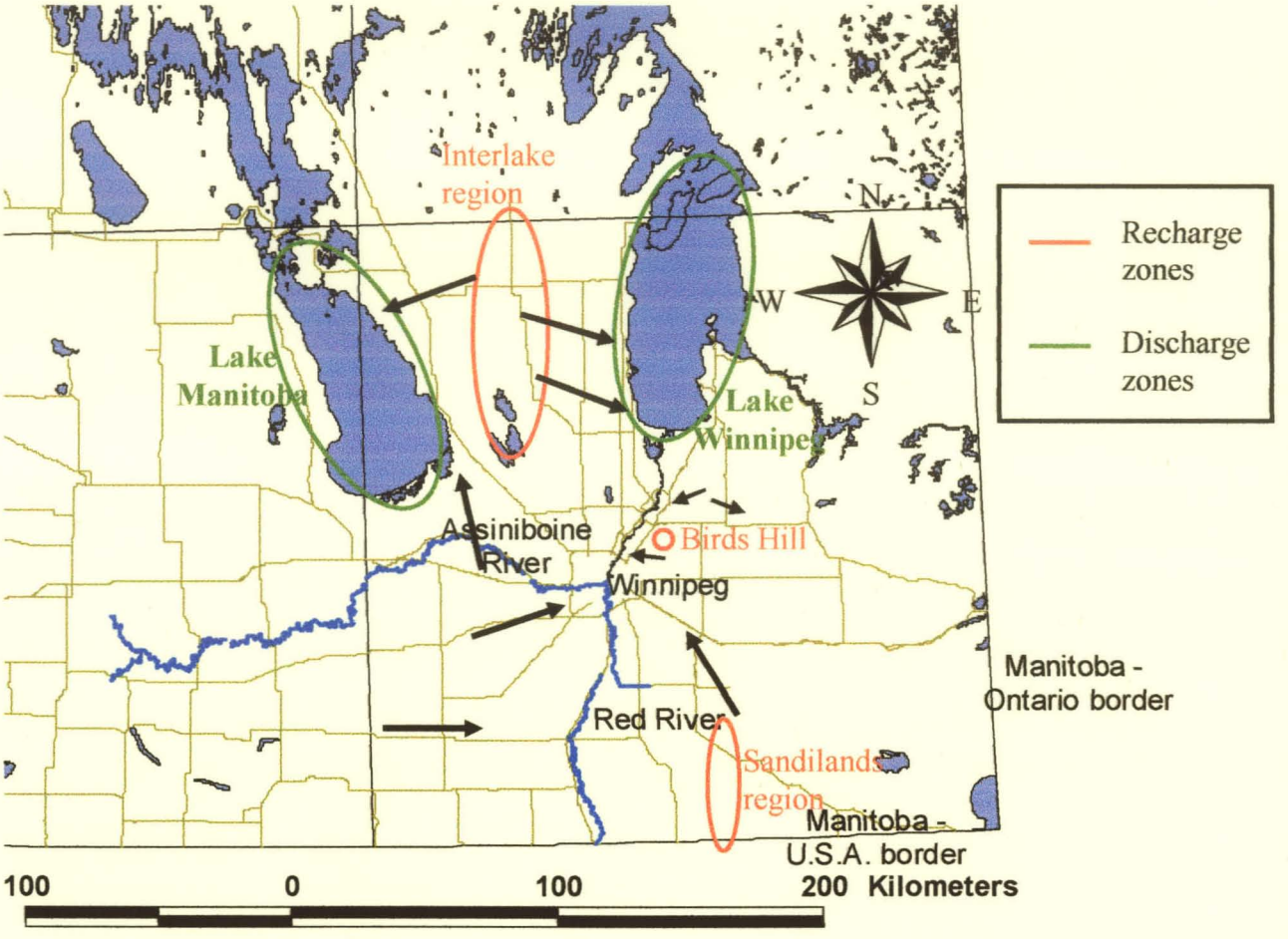

Figure 4.18 – Carbonate Aquifer approximate flow direction, recharge and discharge zones.

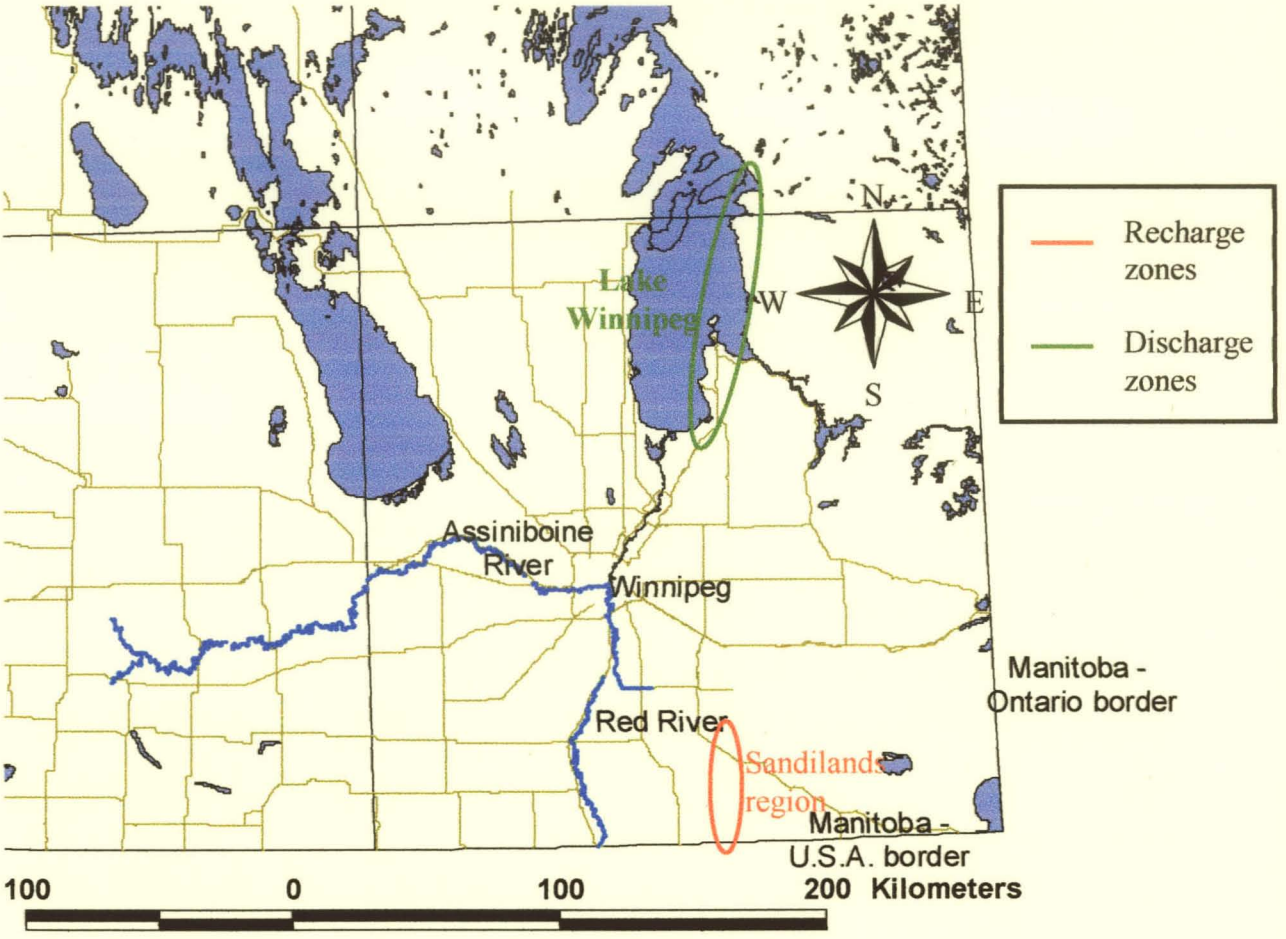

Figure 4.19 – Sandstone Aquifer recharge and discharge zones.

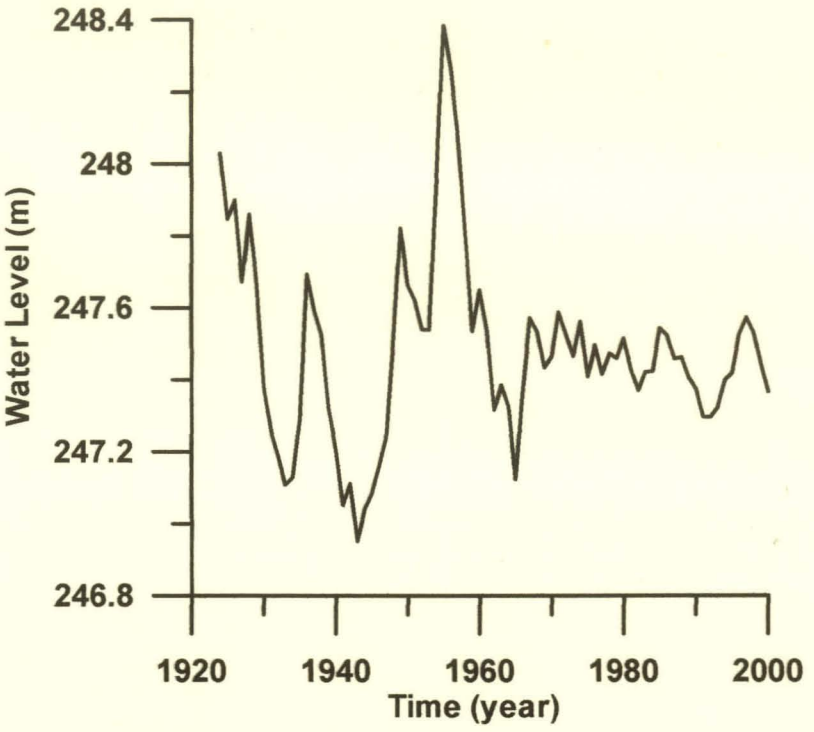

Figure 4.20 – Lake Manitoba water levels.

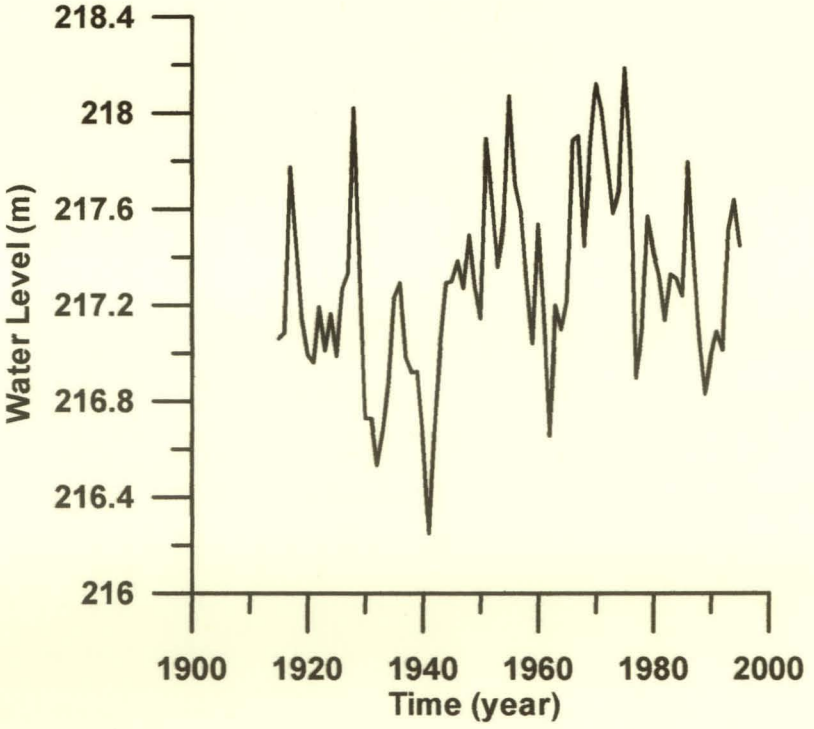

Figure 4.21 – Lake Winnipeg water levels.

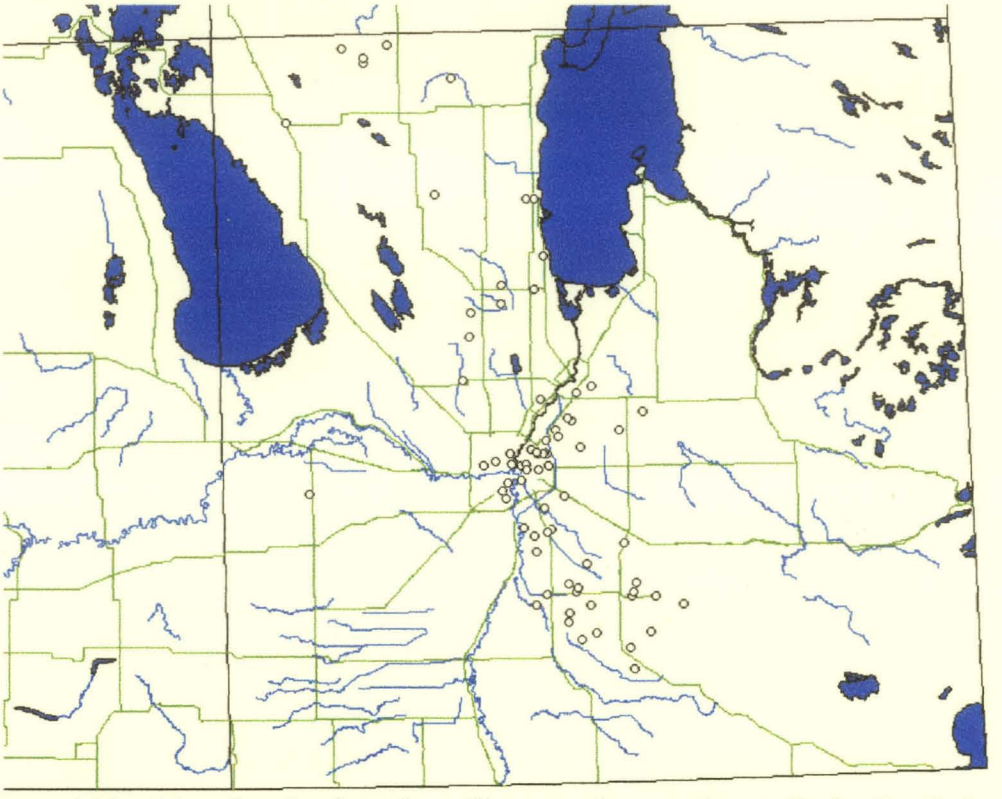

Figure 4.22 – Map showing location of large-scale pumping wells for the Carbonate Aquifer.

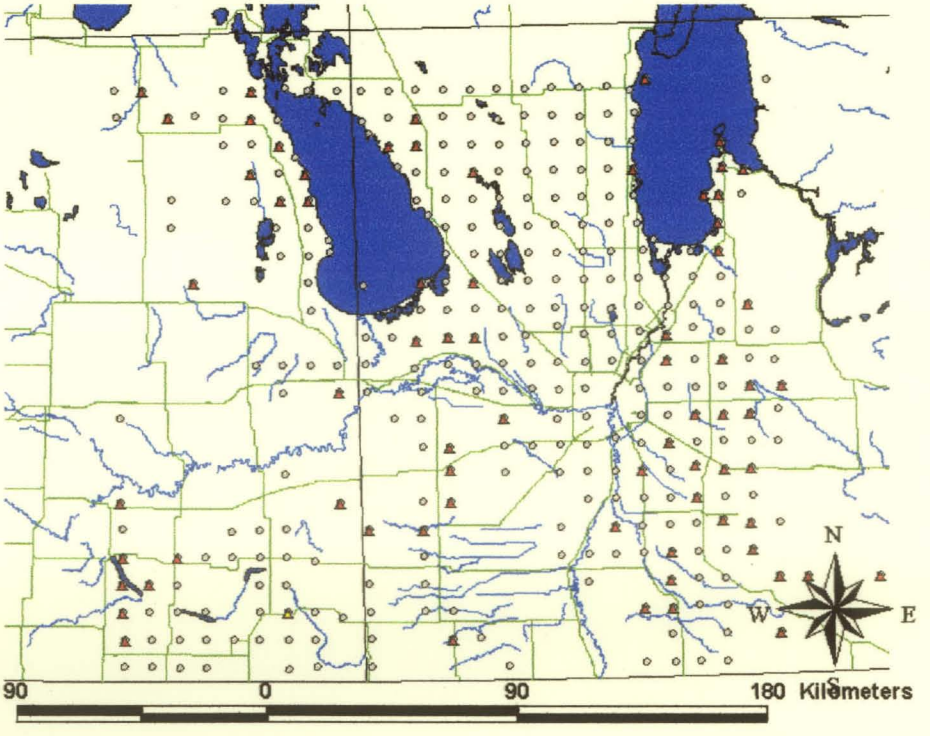

Figure 4.23 – Map showing location of small-scale pumping wells for the Carbonate (open circles) and Sandstone (filled triangles) Aquifers.

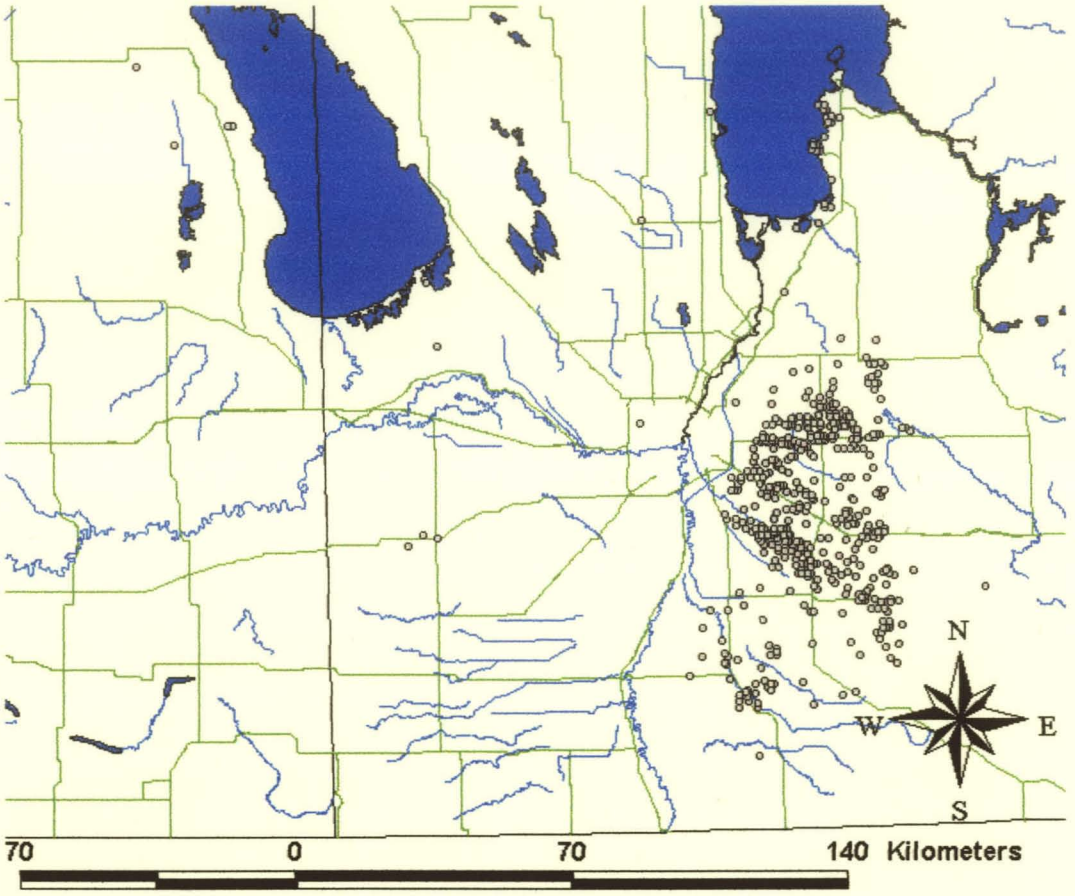

Figure 4.24 – Map showing location of wells screened over both the Carbonate and Sandstone Aquifers.

CHAPTER 5

GEOSTATISTICS

5.1 Introduction

As the final finite element model is fully heterogeneous in terms of transmissivity (hydraulic conductivity), each element is required to have an assigned transmissivity based on the data. Due to the paucity and quality of the data available (Chapter 4), it was not possible to directly assign values based on measurements. Bayesian Updating as described in Chapter 2 was used to interpolate transmissivity values to each element using the measured data and statistical properties of the underlying pdf. The Bayesian Updating method required that either the property, or transform of the property, follow a normal distribution. The correlation structure or some knowledge of the correlation structure for the parameter being interpreted, was also required. This chapter covers the determination of the distribution type and the different required statistical properties for subsequent interpolation of transmissivity. In the remainder of this thesis, where it is stated "log" will refer to the natural log.

In order to calculate the statistics from the measurements, some assumptions were required. The first was the ergodic hypothesis, which assumes that the statistics calculated from the single realization, are equal to the ensemble statistics. The stationarity assumption is also required, which assumes that the statistics are spatially invariant. The intrinsic hypothesis was also assumed for the variogram, in that the semi-variance is a function of the lag distance alone.

5.2 Carbonate Aquifer

Transmissivity values collected for the Carbonate Aquifer (Section 4.2.1) were used to analyse the geostatistics. It is known that transmissivity (hydraulic conductivity) is affected by changes in density and viscosity (equation 2.11). However, the transmissivity values were not corrected due to changes in density and viscosity as it is considered that these effects are negligible compared to the variability in the data. Initially the histogram of the raw data for the transmissivity of the Carbonate Aquifer was plotted (see Figure 5.1). The results show that the data are positively skewed. Therefore, a log transform was conducted on the data, and the histogram of the transformed data was constructed (see Figure 5.2). By visual examination of this plot, it appeared that the transformed data most likely followed a normal distribution. This postulation was tested by the chi square tests and normal scores plot test (see Section 2.7.2).

Prior to testing this postulation, the dataset had to be reduced such that the remaining data could be considered independent. One method was to ensure all data were at a separation greater than the integral scale, such that remaining values were only weakly correlated (Sudicky, 1986). An integral scale of 29,780 m was determined for the log transmissivity of the Carbonate Aquifer, as will be shown later in this chapter. Three different subsets were generated from the original dataset, ensuring all data were at a greater distance than the integral scale. A second method of generating an independent dataset was to randomly select values from the original dataset (Woodbury and Sudicky, 1991). The chi

square test and normal scores plot test were conducted on the original dataset and each of the subsets.

The null hypothesis for the chi square test is that there is no significant difference between log transmissivity frequency and the normal distribution. If the calculated chi square from the dataset is below some critical chi square (found in tables), then the null hypothesis is not rejected. The critical chi square is a function of DOF (number of bins minus one) and the significance level. Table 5.1 shows the calculated chi square values (χ^2) from each set and the critical chi square (χ_{crit}^2) at significance level of 0.05. It was observed that the chi square value generated from each subset is below the critical chi square, and therefore the null hypothesis can not be rejected.

Table 5.1 – Chi square test results for assessment of log normal distribution of transmissivity for Carbonate Aquifer.

Subset		**DOF (# bins – 1)**	χ_{crit}^2 **($\alpha = 0.05$)**	χ^2
All		29	42.5569	0.019
Subsets with correlation length removed	*1*	9	16.9190	0.25
	2	13	22.3621	0.19
	3	10	18.3071	0.22
Random subset		9	16.9190	0.42

To confirm the result of the chi square test, the normal scores plot test was also conducted. The normal scores plot involved plotting the log transmissivity versus the calculated normal score (see Figure 5.3). If the data follows a normal distribution, this plot should be linear with the mean of the data approximately equal to the intercept and standard deviation approximately equal to slope. The intercepts and slopes determined from the normal scores plot test for each subset are presented in Table 5.2. Comparison

of the mean to the intercept and standard deviation to the slope, show good results, satisfying the requirements of the normal scores test.

Table 5.2 – Normal Scores Plot Test results for assessment of log normal distribution of transmissivity for the Carbonate Aquifer.

Subset	Mean	Intercept	Standard Deviation	Slope	R^2
All	-7.15	-7.16	1.63	1.63	0.998
1	-7.03	-7.11	2.04	2.05	0.992
2	-7.38	-7.42	1.59	1.62	0.985
3	-7.62	-7.69	1.66	1.63	0.985
Random	-6.85	-6.90	2.14	2.08	0.935

The chi square and normal scores plot tests were satisfied for the entire dataset and each subset, indicating that the log transmissivity followed a normal distribution at the 0.05 significance level. Table 5.3 presents general statistics of log transmissivity for the Carbonate Aquifer.

Table 5.3 – General statistics of the natural log transmissivity for the Carbonate Aquifer.

Property	Dataset				
	All data	Subsets with integral scale removed			Random subset
		Subset 1	Subset 2	Subset 3	
Mean	-7.2	-7.0	-7.4	-7.6	-6.8
Standard Deviation	1.6	2.0	1.8	1.6	2.1
Variance	2.7	4.1	3.3	2.7	4.6
Range	11.5	7.9	8.4	7.8	9.5
Minimum	-12.5	-10.8	-11.5	-10.7	-10.9
Maximum	-0.9	-2.9	-3.1	-2.9	-1.4
n	2711	47	51	54	99

To ascertain the correlation structure of the transmissivity of the Carbonate Aquifer, the variogram was plotted in both the North-South and East-West directions (see Figure 5.4). To determine which variogram model was the best, the AIC was used (equation 2.33). Originally, both variograms were modeled, however according to the minimum AIC principle, the isotropic model was selected. Therefore, the isotropic variogram was

calculated and is presented in Figure 5.5. The semi-variance for this variogram was estimated using the Classical Estimator of Matheron (1962) and the Moving Window Estimator presented by Li and Lake (1994). The results from the Classical Estimator were highly variable at larger lag distances making any analysis difficult. The Moving Window Estimator results were smooth, with the semi-variance increasing from the value of the nugget at the origin and leveling off at a value approximately equal to the variance of the data (2.65). The exponential equation was applied in attempts to model the variogram and the best-fit model is shown in Figure 5.6. The RMS error of this model was 0.03, and at short lag distances (0 km to 25 km), the exponential model did not match the estimated semi-variance very well. The parameters of the best-fit model were a nugget (σ_0^2) of 2.0, a sill (σ_Y^2) of 2.65 and an integral scale (λ) of 29,780m. Other standard models, such as spherical, Gaussian and circular (Kitanidis, 1997) were also investigated, but the exponential model was found to have the best fit. Therefore, a nested model was investigated in attempts to improve the model. The nested model with the best fit was found to consist of a nugget plus an isotropic spherical model and an isotropic exponential model. This model had an RMS of 0.01 and fit the data well at all lag distances (see Figure 5.7). The equation of this resulting nested structure model is presented in Equation 5.1, where h_d is the lag distance in meters.

$$\gamma(h_d) = \gamma_{\text{nugget}} + \gamma_{\text{spherical\_model}} + \gamma_{\text{exponential model}}$$

$$\gamma_{\text{nugget}} = \sigma_0^2 = 1.81$$

$$\gamma_{\text{spherical\_model}} = (2.11-1.81)*\begin{cases} \frac{3}{2}\cdot\frac{h_d}{5757} - \frac{1}{2}\cdot\frac{h_d^3}{5757^3} & h_d < 5757 \\ 1 & h_d \geq 5757 \end{cases} \qquad \textbf{(5.1)}$$

$$\gamma_{\text{exponential\_model}} = (2.66-2.11)*\left(1-\exp\left(-\frac{h_d}{40022}\right)\right)$$

Note that the structure of the variogram model, in spite of the nested structure does not increase with increasing scale beyond the second nested structure. Self-similarity of the semi-variance was also not observed. Therefore, fractal nature of the correlation structure for log transmissivity was not observed for this dataset, agreeing with the observations of Hoeksema and Kitanidis (1985).

5.3 Sandstone Aquifer

The untransformed transmissivity histogram was prepared and found to be positively skewed (Figure 5.8). A log transform was conducted on the data, and the histogram is presented in Figure 5.9. The chi square test was conducted on the log transform of the transmissivity data as it appeared to be normally distributed. In a manner similar to the Carbonate Aquifer four subsets assuming an integral scale of 16,828 m of the original dataset were created. Table 5.4 shows the results of the chi square test and all $\chi^2 < \chi_{crit}^2$ at the 0.05 significance level, satisfying this test. The normal scores test was also conducted on each set and results are shown in Table 5.5. As the mean is approximately equal to the intercept and the standard deviation is approximately equal to the slope for all sets, the normal scores plot was satisfied. Both the chi square test and normal scores plot test confirmed that the log transmissivity of the Sandstone Aquifer followed a normal distribution. The general statistics of the log transmissivity of the Sandstone Aquifer are presented in Table 5.6.

Table 5.4 – Chi Square Test results for assessment of log normal distribution of transmissivity for Sandstone Aquifer.

Subset		DOF (# bins – 1)	χ_{crit}^2 ($\alpha = 0.05$)	χ^2
All		8	15.5073	0.30
Subsets with correlation length removed	*1*	9	16.9190	0.24
	2	9	16.9190	0.22
	3	9	16.9190	0.16
Random subset		9	16.9190	0.11

Table 5.5 – Normal Scores Plot Test results for assessment of log normal distribution of transmissivity for the Sandstone Aquifer.

Subset	Mean	Intercept	Standard Deviation	Slope	R^2
All	-7.96	-8.03	1.50	1.38	0.968
1	-8.01	-8.23	1.91	1.65	0.933
2	-8.14	-8.44	1.86	1.60	0.949
3	-7.99	-8.20	1.96	1.74	0.962
Random	-7.79	-7.95	1.33	1.29	0.956

Table 5.6 – General statistics of the natural log transmissivity for the Sandstone Aquifer.

Property	Dataset				
	All data	Subsets with integral scale removed			Random subset
		Subset 1	Subset 2	Subset 3	
Mean	-8.0	-8.0	-8.1	-8.0	-7.8
Standard Deviation	1.5	1.9	1.9	2.0	1.3
Variance	2.2	3.7	3.5	3.8	1.8
Range	10.4	10.4	10.4	10.4	5.1
Minimum	-12.4	-12.4	-12.4	-12.4	-10.0
Maximum	-2.0	-2.0	-2.0	-2.0	-4.9
Number	77	29	31	29	19

Inadequate data was available to plot variograms in both the East-West and North-South directions. Therefore, the isotropic variogram was plotted (see Figure 5.10). The best-fit exponential model with nugget of 0.56, integral scale of 16,828 m and sill of 2.9 is also presented in Figure 5.10. Due to the minimal amount of data available for analysis, the resulting variogram was slightly more sporadic than that generated for the Carbonate Aquifer, but a good variogram model was found. Reasonable upper and lower bounds of

the nugget, range and sill could be determined from the variogram assuming an exponential model.

5.4 Shale

Transmissivity was collected for shale through estimation of specific capacity. The histogram of untransformed data is presented in Figure 5.11. The histogram was skewed and therefore a natural log transform was conducted on the data (Figure 5.12). This transformed histogram appeared to follow a normal distribution and therefore the normal scores plot test and chi square test were conducted on the transformed dataset. Both tests were conducted on the entire dataset as well as three subsets generated using an integral scale of 20,800 m and a randomly generated subset. The results of the chi square test are presented in Table 5.7 and that of the normal scores plot test are presented in Table 5.8. Both tests were satisfied, therefore, it was determined that the transmissivity for the shale followed a log normal distribution. The general statistics for this log transformed dataset are presented in Table 5.9.

Table 5.7 – Chi Square Test results for assessment of log normal distribution of transmissivity for shale.

Subset		**DOF (# bins – 1)**	χ_{crit}^2 **($\alpha = 0.05$)**	χ^2
All		9	16.9190	0.097
Subsets with correlation length removed	*1*	9	16.9190	0.90
	2	9	16.9190	0.59
	3	9	16.9190	0.97
Random subset		9	16.9190	1.45

Table 5.8 – Normal Scores Plot Test results for assessment of log normal distribution of transmissivity for shale.

Subset	Mean	Intercept	Standard Deviation	Slope	R^2
All	-9.01	-9.03	1.42	1.40	0.980
1	-8.52	-8.71	1.62	1.52	0.877
2	-8.63	-8.81	1.83	1.83	0.935
3	-8.66	-8.84	1.88	1.89	0.934
Random	-8.85	-8.97	1.56	1.36	0.976

Table 5.9 – General statistics of the natural log transmissivity for shale.

Property	Dataset				
	All data	Subsets with integral scale removed			Random subset
		Subset 1	Subset 2	Subset 3	
Mean	-9.01	-8.52	-8.63	-8.66	-8.85
Standard Deviation	1.42	1.60	1.83	1.88	1.56
Variance	2.0	2.6	3.4	3.5	2.4
Range	9.7	5.8	6.0	6.3	8.8
Minimum	-12.4	-10.9	-11.1	-11.3	-11.4
Maximum	-2.7	-5.1	-5.1	-5.1	-2.7
Number	592	19	20	21	49

The variogram was required to determine the correlation with distance. The variogram was calculated using the Moving Window and Classical Estimators in the East-West and North-South directions (see Figure 5.13). As the variograms were similar in both directions, the isotropic variogram was calculated (Figure 5.14). The best fitting exponential model had a sill of 2.05, nugget of 1.8 and integral sale of 20,800 m (Figure 5.14). This model had an RMS of 0.03 and AIC of –708. The exponential model underestimated the semi-variance for integral scale less than 25 km and overestimated the semi-variance for integral scales between 25 and 50 km. Therefore, a nested model was considered. The nested model with best fit was two separate isotropic spherical models and a nugget (see Figure 5.15). The RMS of the nested model was 0.02 and AIC of –704. The RMS of the nested model was lower than that of the exponential model. However,

the AIC was lower for the exponential model, signifying that the exponential model was optimal fit between number of parameters and goodness of fit.

5.5 Carbonate Sequence

No data was collected for the carbonate unit, outside of the main Carbonate Aquifer. Therefore, ranges of values for hydraulic conductivity were determined from the literature. Limestone and dolostone rocks are reported to have hydraulic conductivity ranging between 1×10^{-9} and 6×10^{-6} m/s (Domenico and Schwartz, 1990).

5.6 Sand and Gravel

The histogram of untransformed transmissivity is presented in Figure 5.16. In order to obtain a normal distribution, a log transform was conducted on the transmissivity and the histogram is presented in Figure 5.17. Chi square and normal score plot tests were conducted on the full dataset, three subsets with the integral scale removed (41,228 m) and a subset generated from 100 randomly sampled points. The results of the tests are presented in Tables 5.10 and 5.11. Both tests were satisfied, signifying it could be assumed that the dataset followed a log-normal distribution. The general statistics of log transmissivity are presented in Table 5.12.

Table 5.10 – Chi Square Test results for assessment of log normal distribution of transmissivity for sand and gravel.

Subset		DOF (# bins – 1)	χ_{crit}^2 ($\alpha = 0.05$)	χ^2
All		20	31.4104	0.019
Subsets with correlation length removed	*1*	9	16.9190	0.065
	2	9	16.9190	0.50
	3	9	16.9190	0.19
Random subset		9	16.9190	0.11

Table 5.11 – Normal Scores Plot Test results for assessment of log normal distribution of transmissivity for sand and gravel.

Subset	Mean	Intercept	Standard Deviation	Slope	R^2
All	-8.01	-8.01	1.62	1.61	0.998
1	-7.62	-7.71	1.39	1.43	0.984
2	-10.89	-11.01	1.46	1.44	0.951
3	-8.28	-8.41	1.88	1.91	0.989
Random	-8.20	-8.25	1.92	1.92	0.985

Table 5.12 – General statistics of the natural log transmissivity for the sand and gravel.

Property	Dataset				
	All data	Subsets with integral scale removed			Random subset
		Subset 1	Subset 2	Subset 3	
Mean	-8.01	-7.62	-10.89	-8.28	-8.20
Standard Deviation	1.61	1.39	1.46	1.88	1.92
Variance	2.6	1.9	2.1	3.6	3.7
Range	11.0	6.0	5.1	7.5	9.0
Minimum	-12.9	-11.0	-12.9	-11.7	-12.4
Maximum	-1.9	-5.0	-7.8	-4.3	-3.3
Number	1714	31	27	32	99

The variograms of the log transmissivity calculated from the Moving Window and Classical Estimators were determined in the North-South and East-West directions (Figure 5.18). The variograms were similar and therefore the isotropic variogram was calculated (Figure 5.19). The variogram exhibits a hole effect, as evidence by the variogram leveling off at approximately 2.55 and then increases again to approximately 2.75.

5.7 Clay

For the clay unit, hydraulic conductivity values were reported. The histogram of the untransformed data is presented in Figure 5.20. By investigation of this plot, it appeared that a natural log transform would follow a normal distribution (Figure 5.21). The log

transformed histogram was bimodal, which may be a result of scale effects. A chi square test and normal scores plot test were conducted on the dataset to determine whether the data followed a log normal distribution. The results of these tests are presented in Tables 5.13 and 5.14. The general statistics of the log hydraulic conductivity are presented in Table 5.15.

Table 5.13 – Chi Square Test results for assessment of log normal distribution of hydraulic conductivity for clay.

Subset		DOF (# bins – 1)	χ_{crit}^2 ($\alpha = 0.05$)	χ^2
All		5	11.0705	0.19
Subsets with correlation length removed	*1*	5	11.0705	0.31
	2	5	11.0705	0.31
	3	5	11.0705	0.31
Random subset		5	11.0705	0.85

Table 5.14 – Normal Scores Plot Test results for assessment of log normal distribution of hydraulic conductivity for clay.

Subset	Mean	Intercept	Standard Deviation	Slope	R^2
All	-18.61	-18.71	4.21	4.07	0.91
1	-11.29	-11.68	4.17	4.34	0.89
2	-11.29	-11.68	4.17	4.34	0.89
3	-11.29	-11.68	4.17	4.34	0.89
Random	-19.26	-19.85	4.26	3.65	0.85

Table 5.15 – General statistics of the natural log hydraulic conductivity for the clay.

Property	Dataset				
	All data	Subsets with integral scale removed			Random subset
		Subset 1	Subset 2	Subset 3	
Mean	-18.61	-11.29	-11.29	-11.29	-19.26
Standard Deviation	4.21	4.17	4.17	4.17	4.26
Variance	17.71	17.39	17.39	17.39	18.15
Range	16.49	13.87	13.87	13.87	15.37
Minimum	-25.19	-19.36	-19.36	-19.36	-24.08
Maximum	-8.70	-5.49	-5.49	-5.49	-8.70
Number	99	16	16	16	19

The variogram of the log hydraulic conductivity was calculated from the Classical and Moving Window Estimators (Figure 5.22). Due to the small number of measurements the variogram only had three points on the plot.

5.8 Till

For till, the hydraulic conductivity was evaluated. The histogram of non-transformed hydraulic conductivity data is presented in Figure 5.23. It was decided that the data most likely followed a lognormal distribution and this histogram is presented in Figure 5.24. To test whether the dataset followed a log normal distribution, the chi square test and normal scores plot test was conducted on the entire dataset and four independent subsets, assuming an integral scale of 25,000 m. The results of the chi square test are presented in Table 5.16 and those of the normal scores plot are presented in Table 5.17. Both of these tests confirm that the dataset follow a normal distribution. The general statistics for the log hydraulic conductivity of the till are presented in Table 5.18.

Table 5.16 – Chi Square Test results for assessment of log normal distribution of hydraulic conductivity for till.

Subset		DOF (# bins – 1)	χ_{crit}^2 ($\alpha = 0.05$)	χ^2
All		10	18.3070	0.20
Subsets with correlation length removed	*1*	5	11.0705	0.35
	2	5	11.0705	0.31
	3	5	11.0705	0.29
Random subset		5	11.0705	0.25

Table 5.17 – Normal Scores Plot Test results for assessment of log normal distribution of hydraulic conductivity for till.

Subset	Mean	Intercept	Standard Deviation	Slope	R^2
All	-14.34	-14.52	2.74	2.76	0.98
1	-12.58	-12.88	2.35	2.37	0.93
2	-12.94	-13.27	2.81	2.92	0.94
3	-12.58	-12.86	2.26	2.28	0.95
Random	-11.16	-11.53	3.23	3.49	0.96

Table 5.18 – General statistics of the natural log hydraulic conductivity for the till.

Property	Dataset				
	All data	Subsets with integral scale removed			Random subset
		Subset 1	Subset 2	Subset 3	
Mean	-14.34	-12.58	-12.94	-12.58	-11.16
Standard Deviation	2.74	2.35	2.81	2.26	3.23
Variance	7.49	5.52	7.88	5.13	10.46
Range	11.36	7.03	10.45	7.03	10.95
Minimum	-19.75	-15.42	-18.83	-15.42	-17.36
Maximum	-8.39	-8.39	-8.39	-8.39	-6.41
Number	34	15	15	16	14

5.9 Summary

This chapter presented the geostatistical properties of the transmissivity or hydraulic conductivity of each of the hydrostratigraphic units. This included general statistics, distribution type and correlation structure. These geostatistical properties will be used in the next chapter when the transmissivity of each unit is interpolated using the Bayesian Updating method.

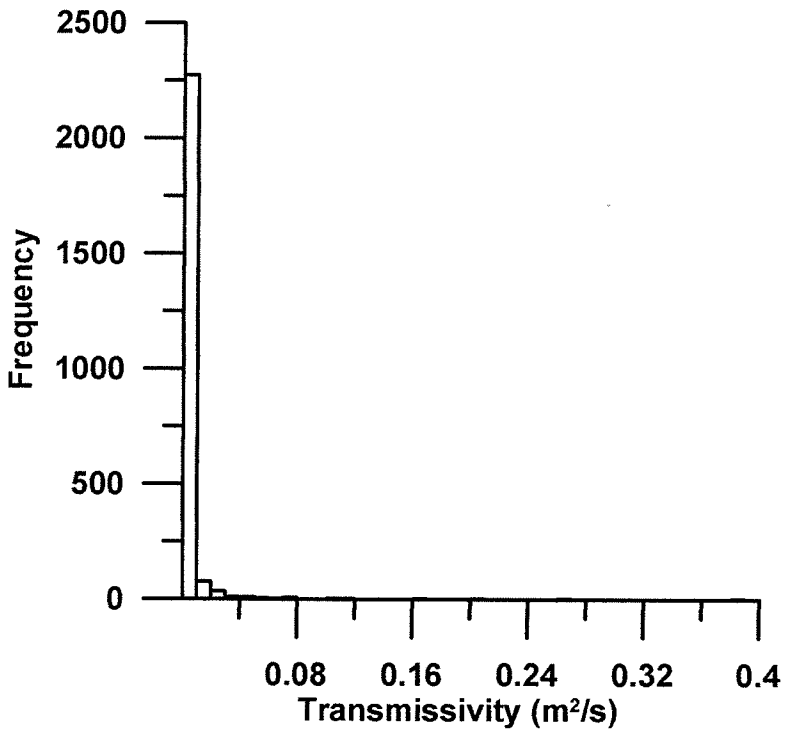

Figure 5.1 – Histogram of non-transformed transmissivity for the Carbonate Aquifer.

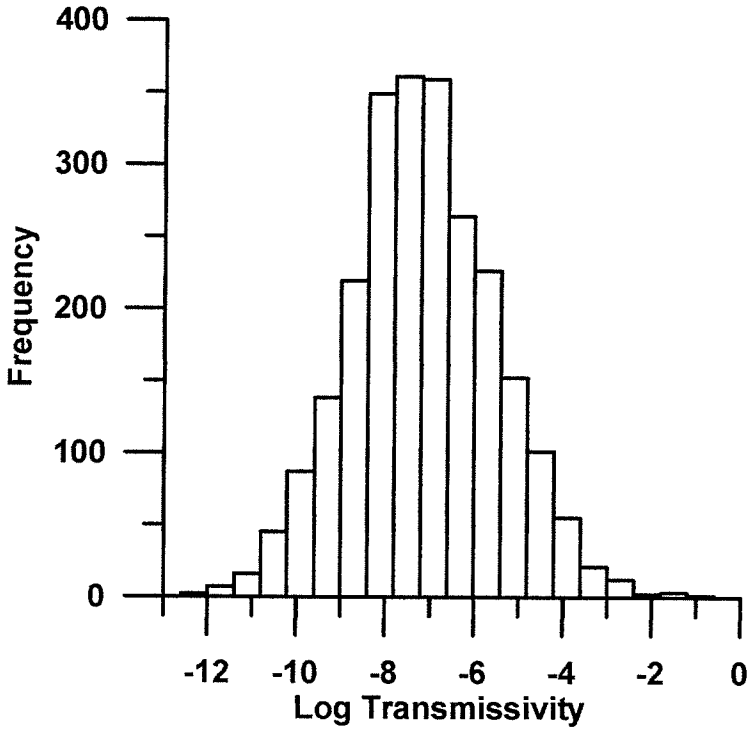

Figure 5.2 – Histogram of natural log transmissivity for the Carbonate Aquifer.

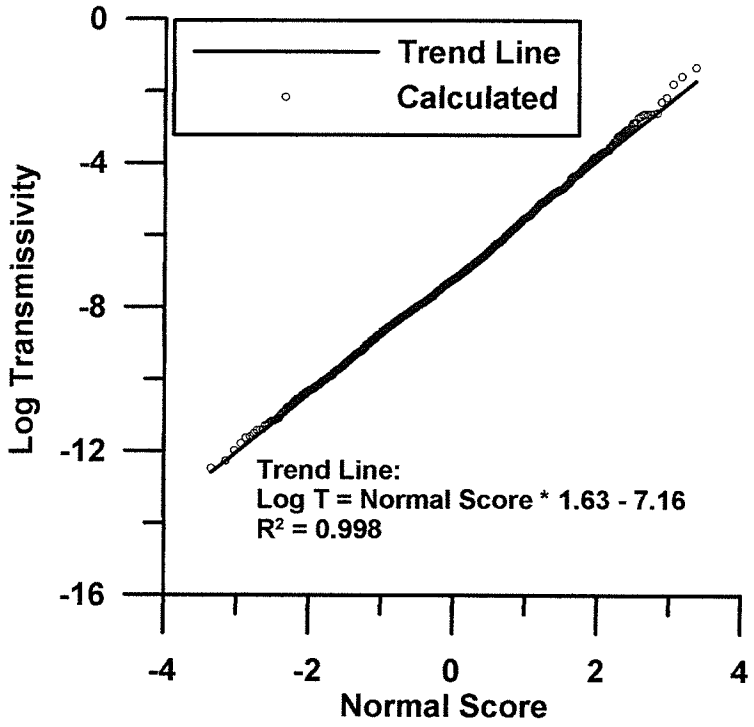

Figure 5.3 – Normal scores plot to determine if the natural log transmissivity in m^2/s for the Carbonate Aquifer follows a normal distribution.

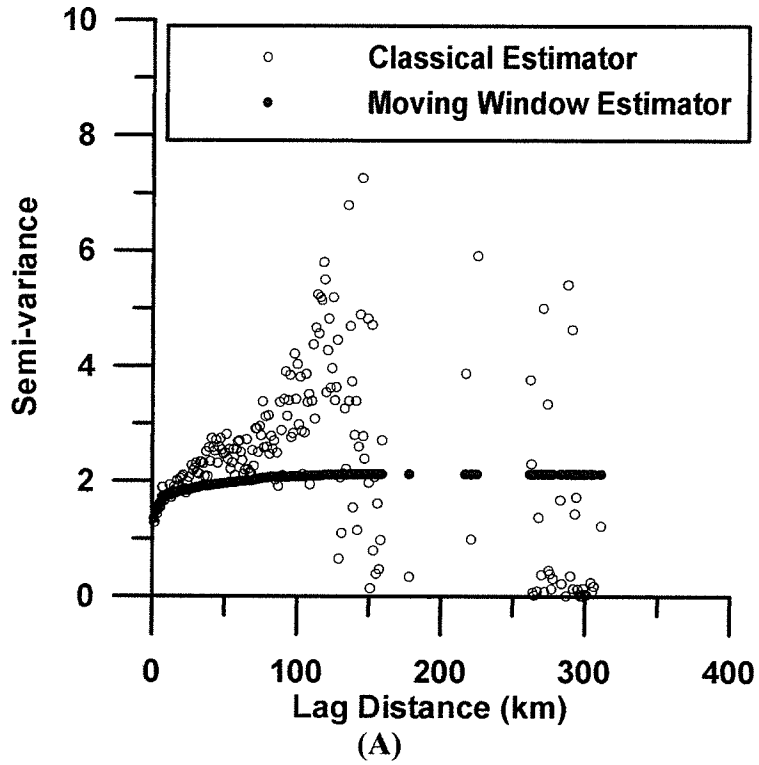

(A)

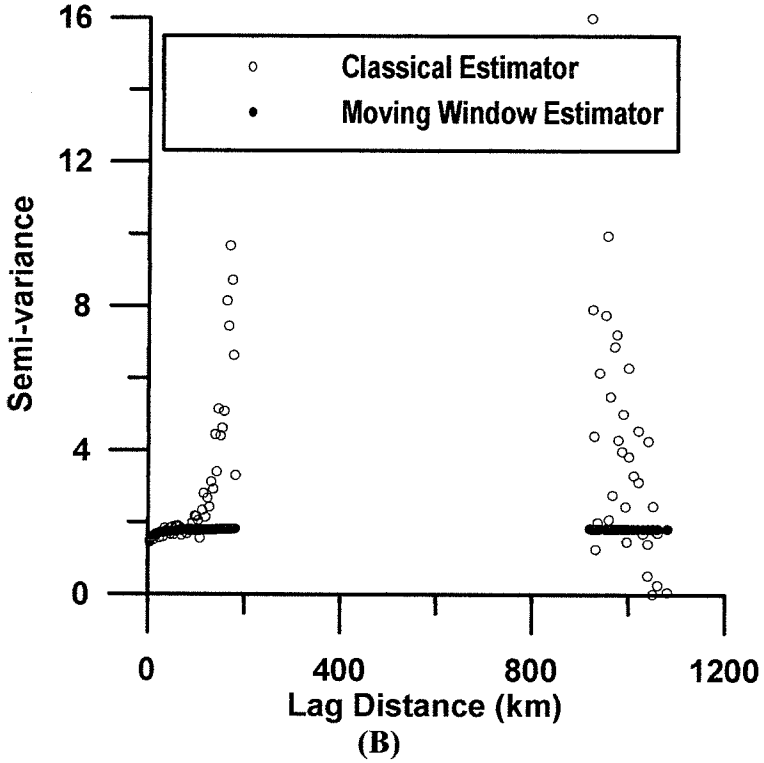

(B)

Figure 5.4 – Variogram in (A) East-West and (B) North-South direction of the natural log transmissivity for the Carbonate Aquifer determined using the Classical and Moving Window Estimators.

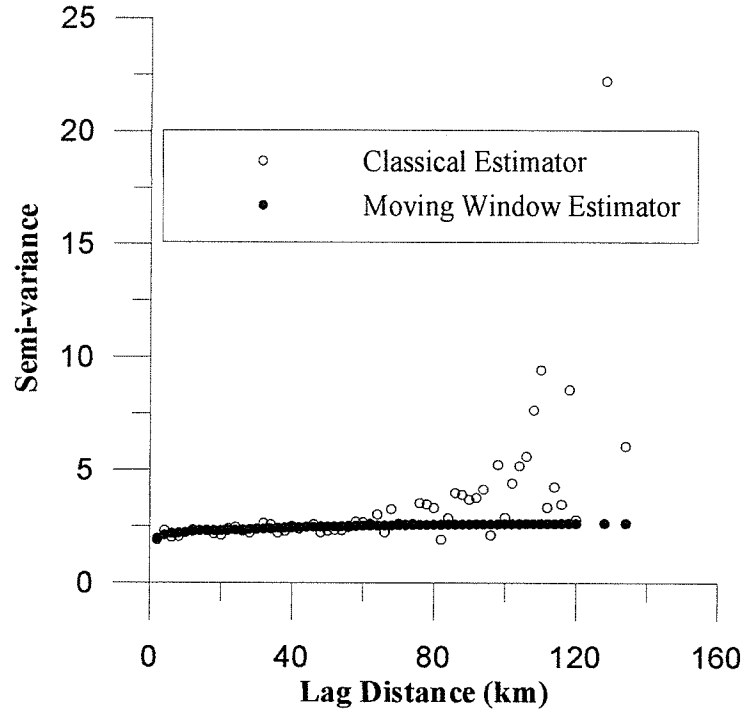

Figure 5.5 – Isotropic variogram for the log transmissivity of the Carbonate Aquifer estimated using the Moving Window and Classical Estimators.

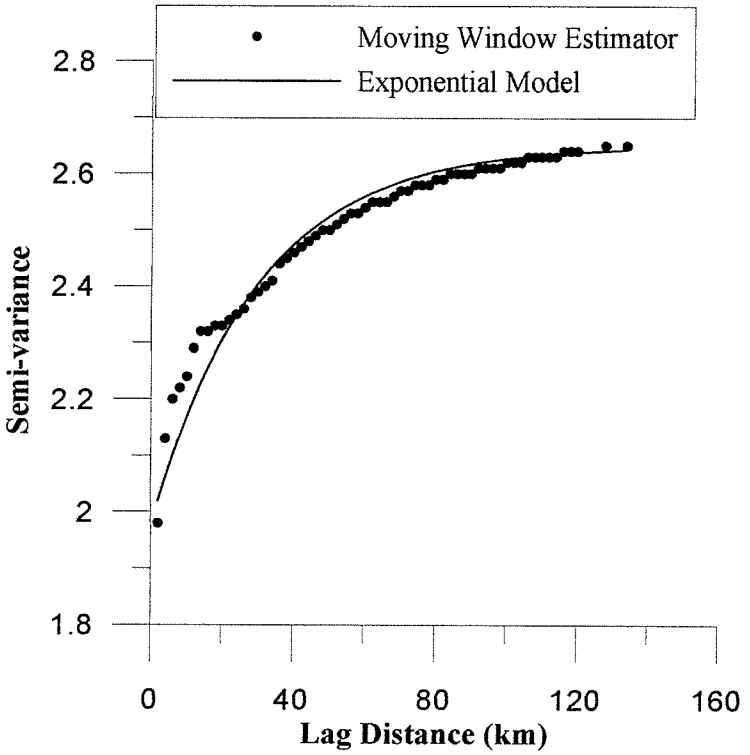

Figure 5.6 – Isotropic variogram for log transmissivity of the Carbonate Aquifer estimated using the Moving Window Estimator and the best fitting exponential model.

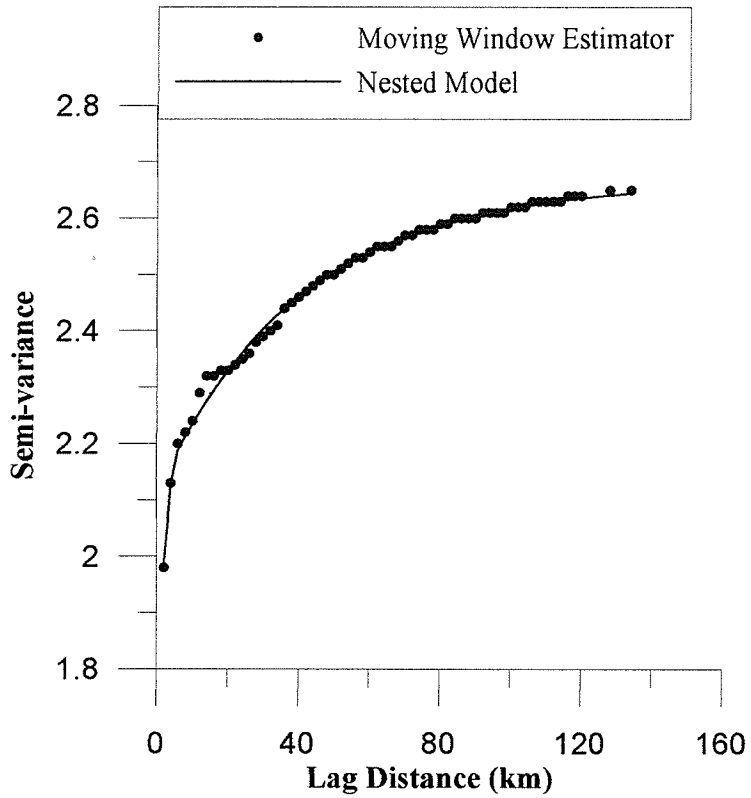

Figure 5.7 - Isotropic variogram for log transmissivity of the Carbonate Aquifer estimated using the Moving Window Estimator and the best fitting nested model.

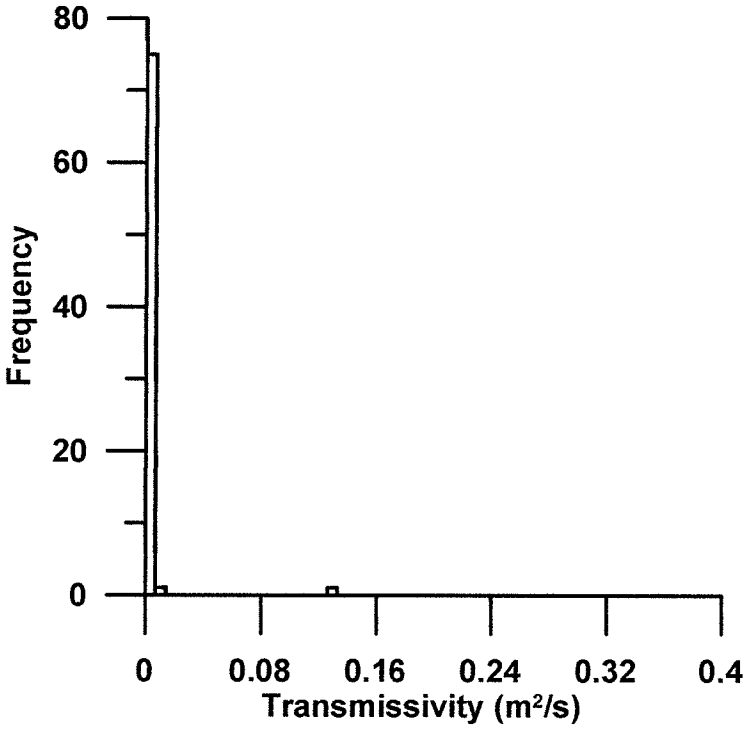

Figure 5.8 – Histogram of non-transformed transmissivity in the Sandstone Aquifer.

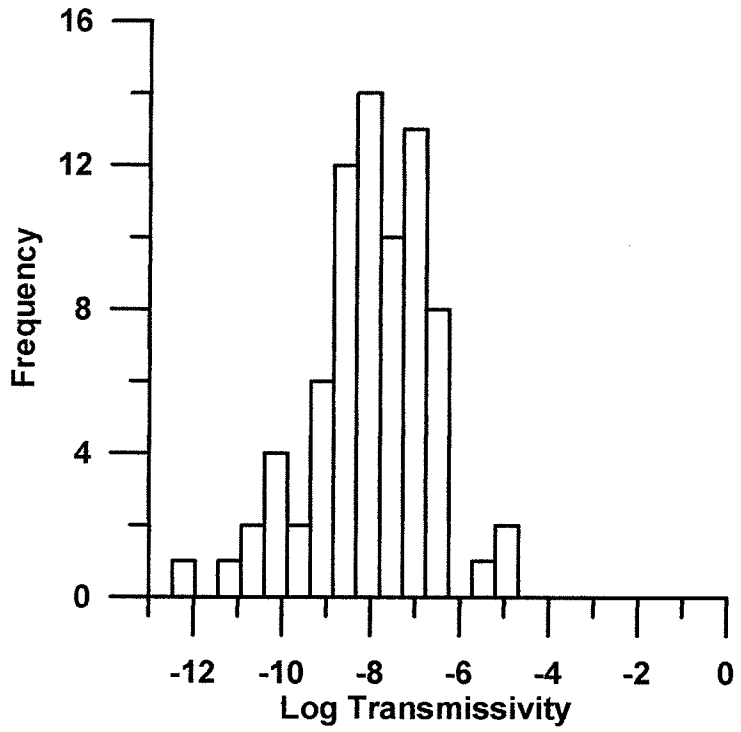

Figure 5.9 – Histogram of natural log transmissivity in m^2/s for the Sandstone Aquifer.

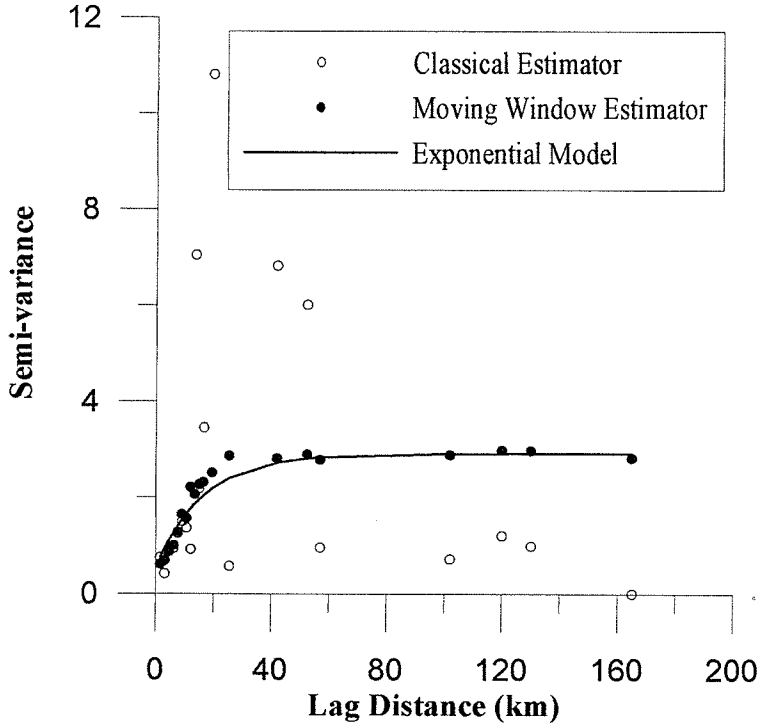

Figure 5.10 – Isotropic variogram of the natural log transmissivity in m^2/s for the Sandstone Aquifer using the Classical and Moving Window Estimators and the best fitting exponential model.

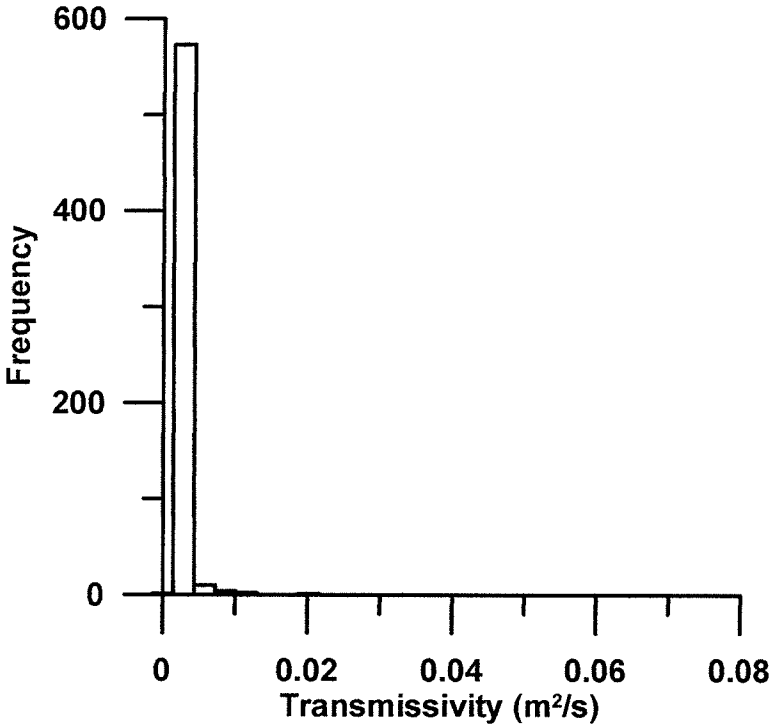

Figure 5.11 – Histogram of non-transformed transmissivity in m^2/s for the shale.

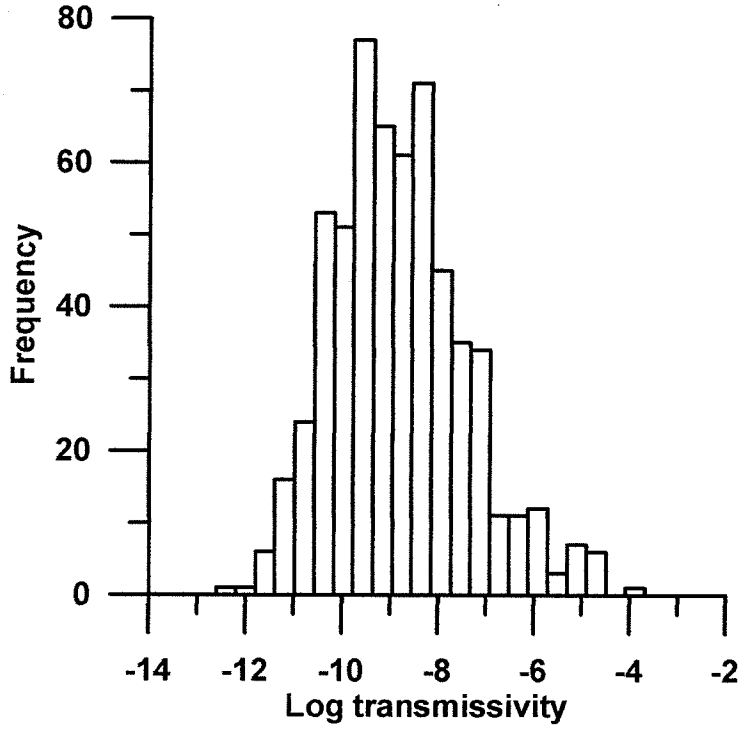

Figure 5.12 – Histogram of natural log transmissivity for the shale.

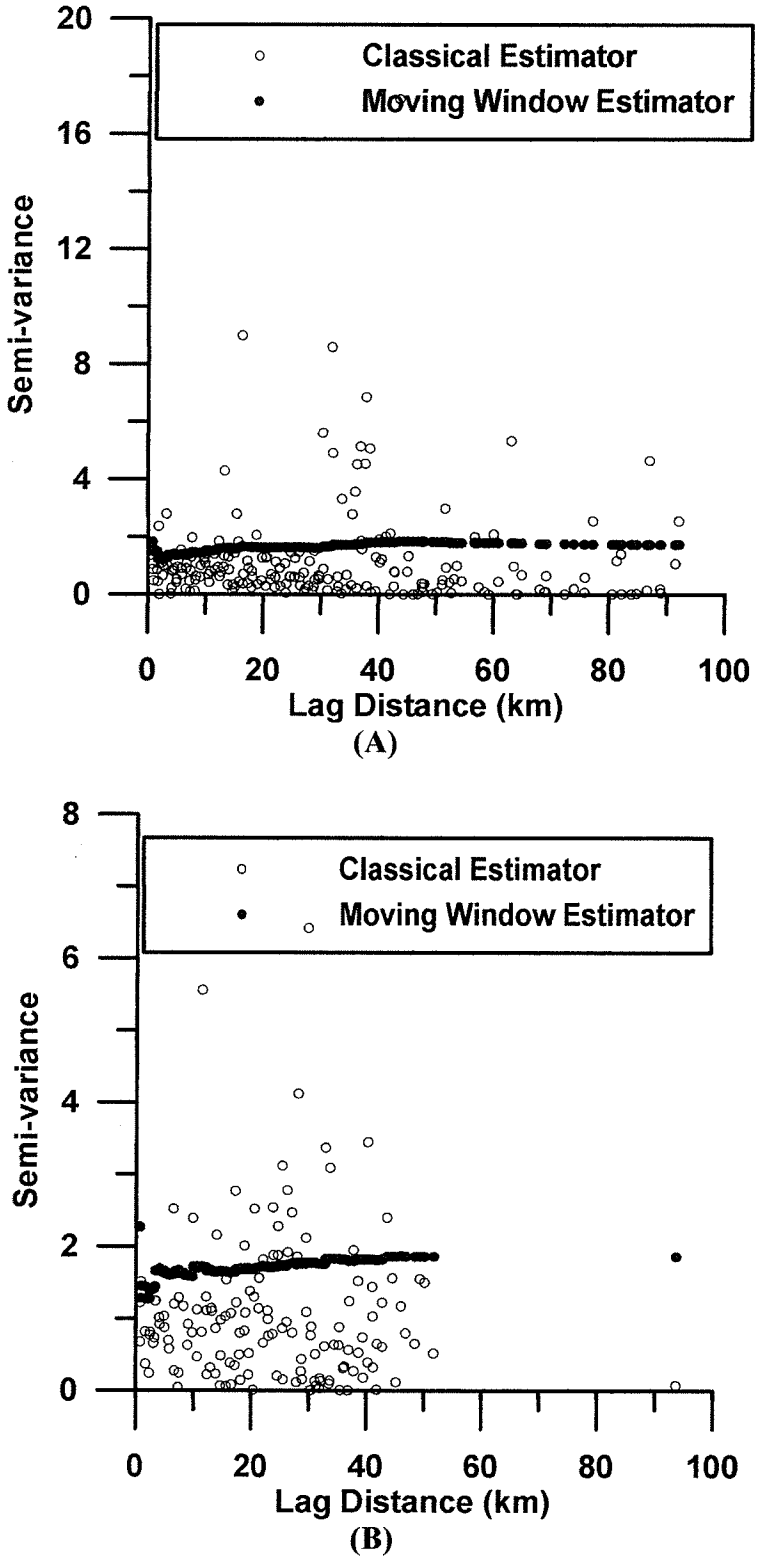

Figure 5.13 – Variogram in (A) East-West and (B) North-South direction of the natural log transmissivity for the shale determined using the Classical and Moving Window Estimators.

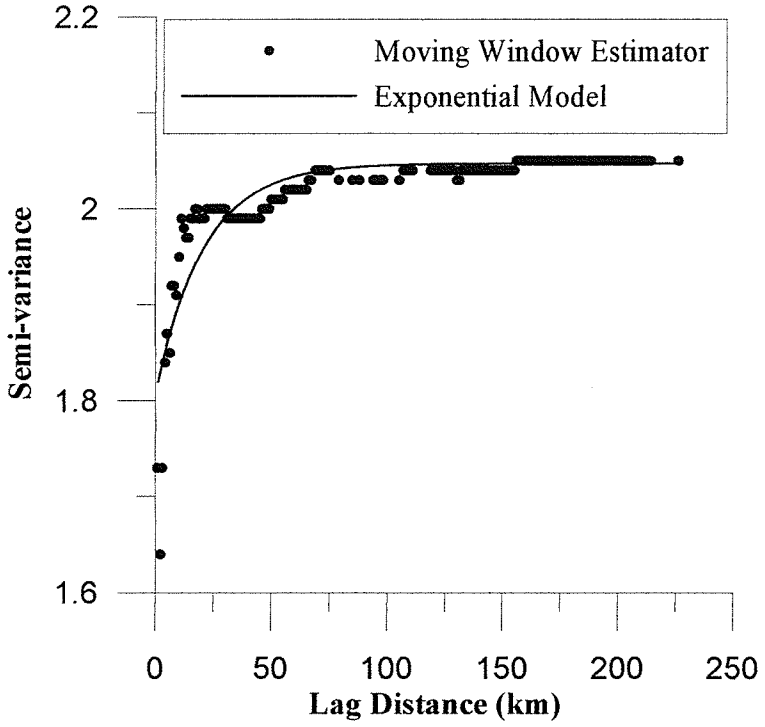

Figure 5.14 – Isotropic variogram for natural log transmissivity in m^2/s of shale estimated using the Moving Window Estimator and the best fitting exponential model.

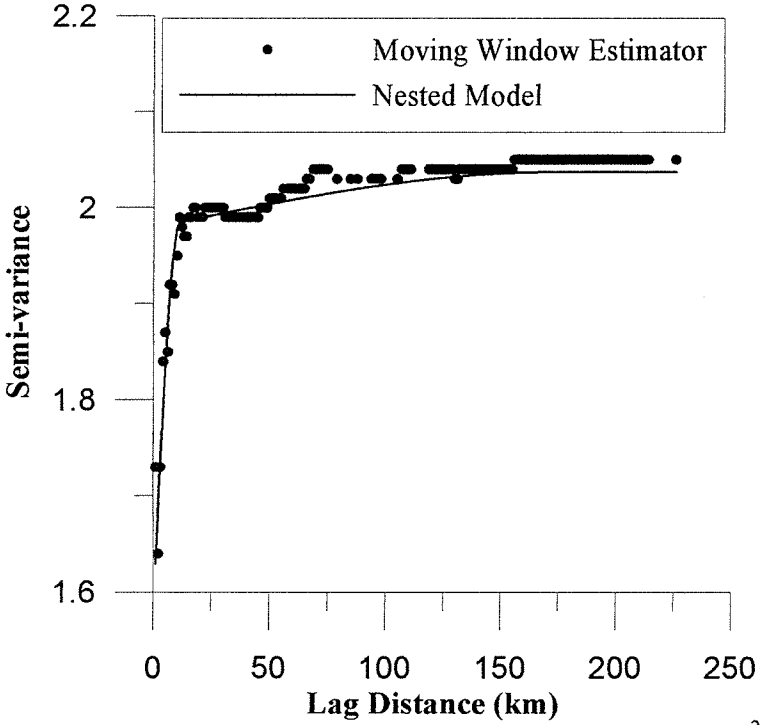

Figure 5.15 – Isotropic variogram for natural log transmissivity in m^2/s of shale estimated using the Moving Window Estimator and the best fitting nested model.

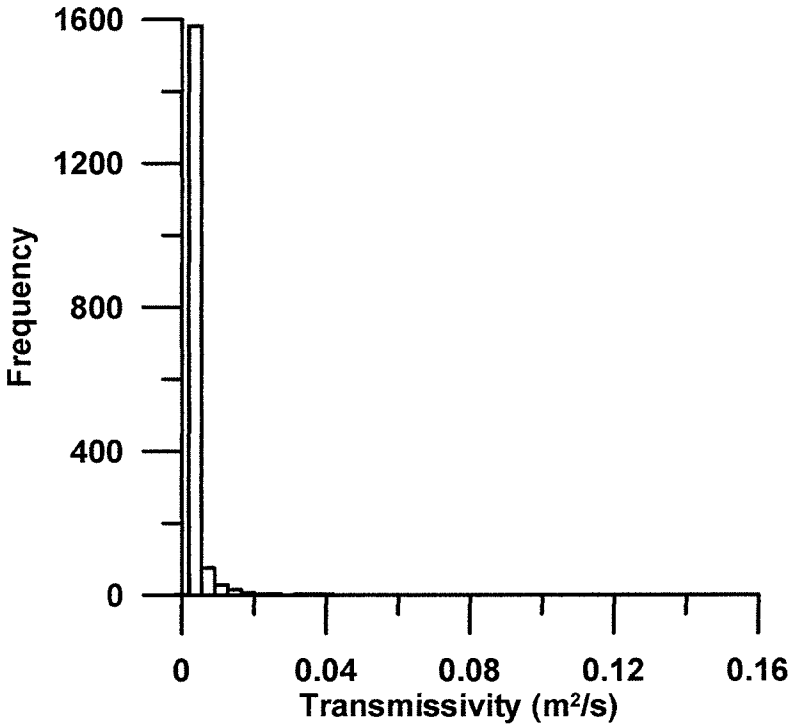

Figure 5.16 – Histogram of non-transformed transmissivity for the sand and gravel.

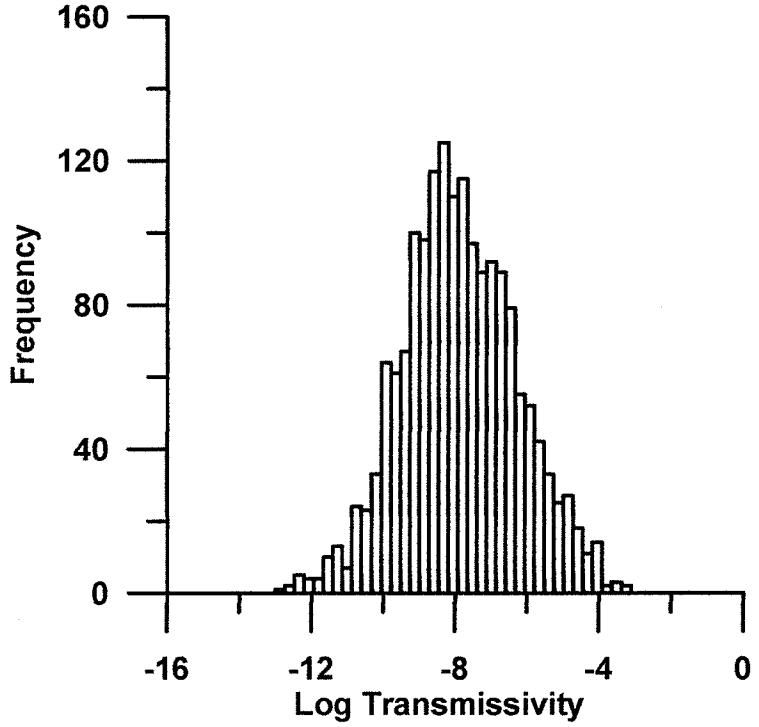

Figure 5.17 – Histogram of natural log transmissivity for the sand and gravel.

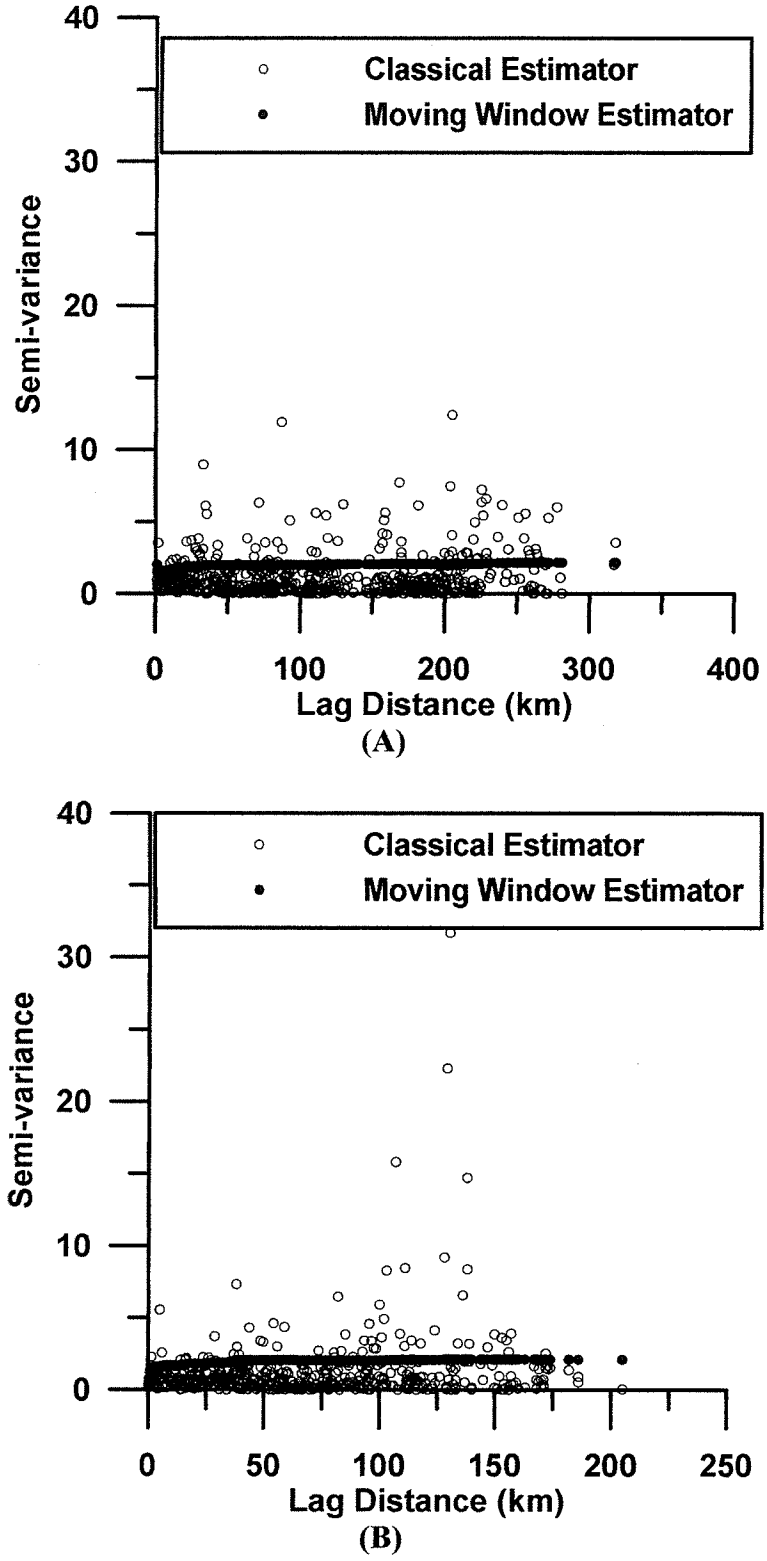

Figure 5.18 – Variogram in (A) East-West and (B) North-South direction of the natural log transmissivity in m^2/s for the sand and gravel using the Classical and Moving Window Estimators.

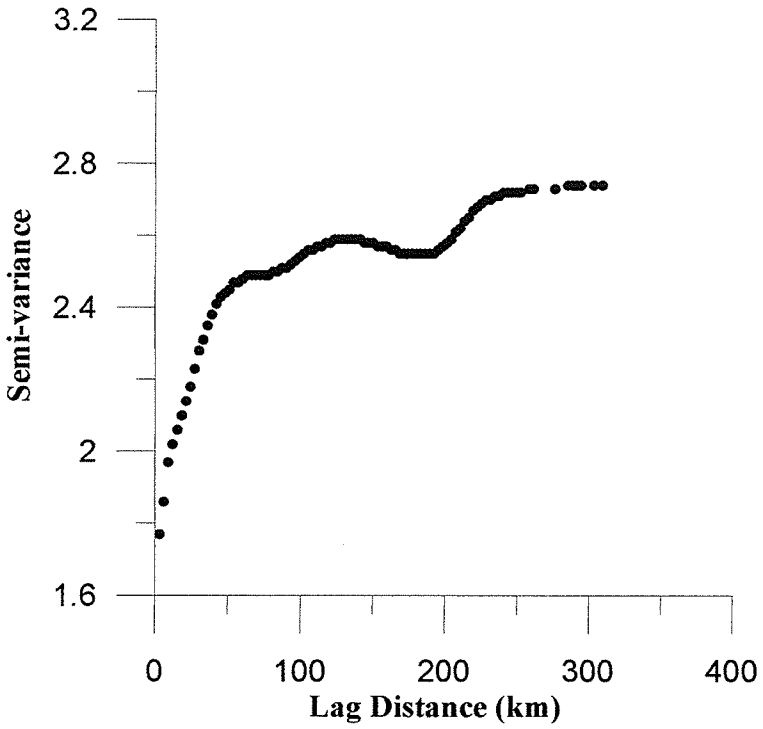

Figure 5.19 – Variogram of the log transmissivity of sand and gravel estimated using the Moving Window Estimator.

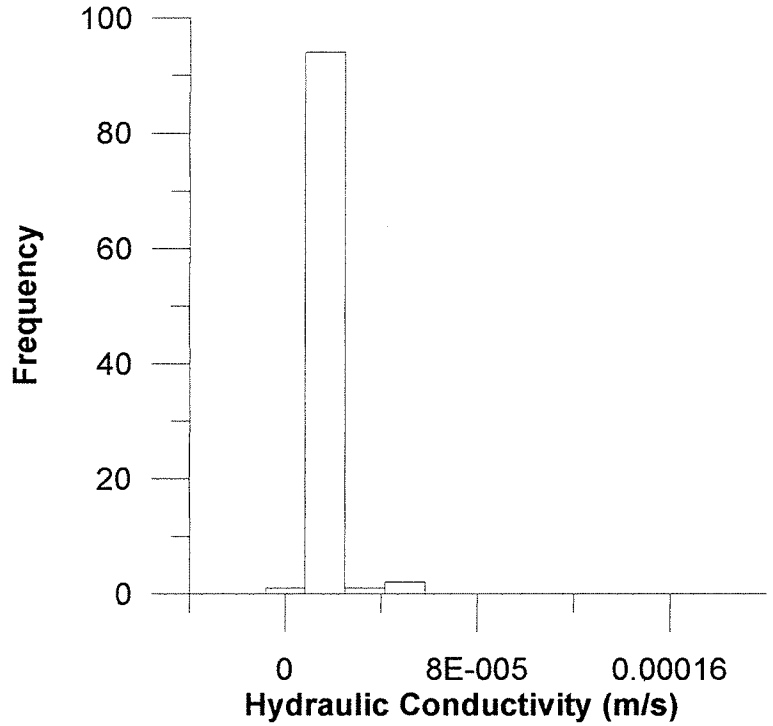

Figure 5.20 – Histogram of non-transformed hydraulic conductivity for the clay.

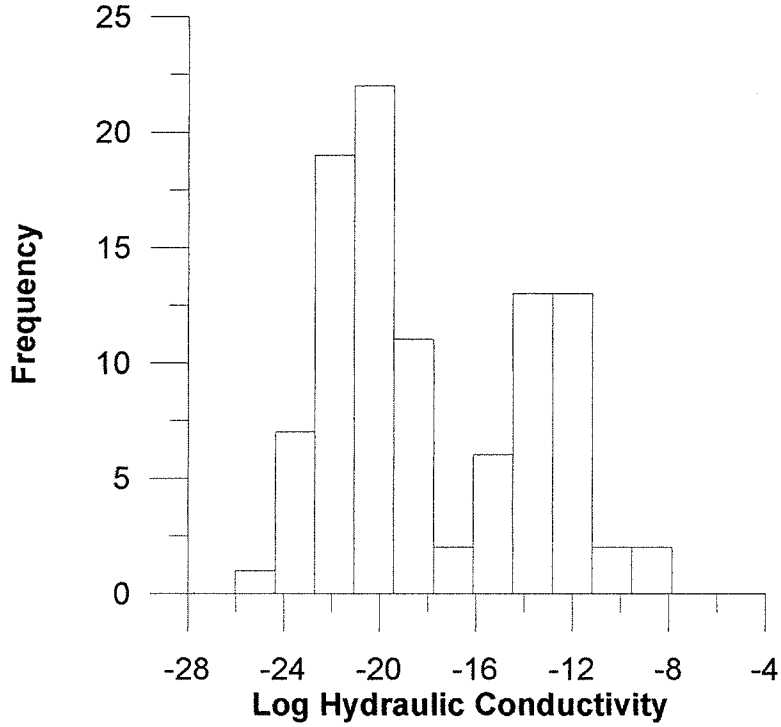

Figure 5.21 – Histogram of natural log hydraulic conductivity in m/s for the clay.

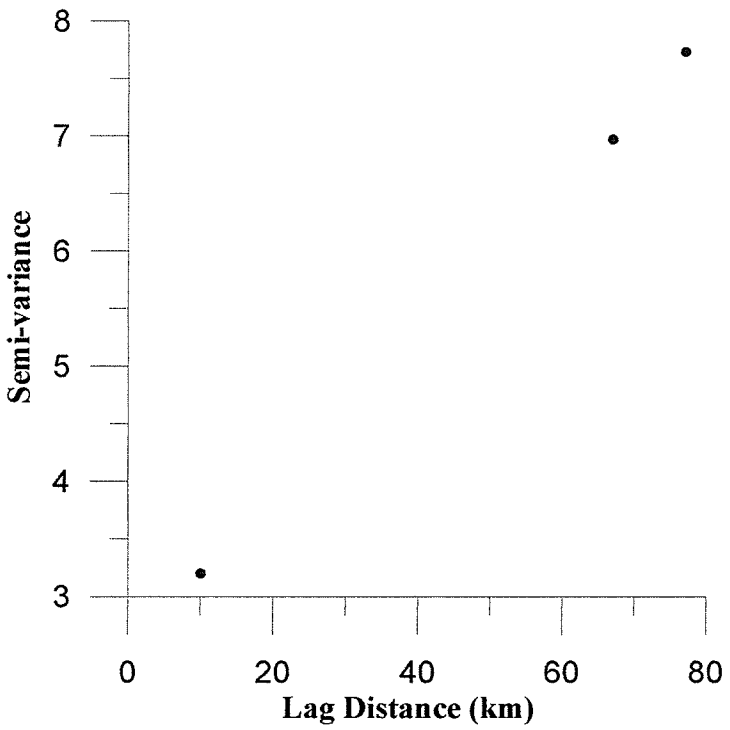

Figure 5.22 – Isotropic variogram of the natural log hydraulic conductivity for the clay determined using the Classical and Moving Window Estimators and the best fitting exponential model.

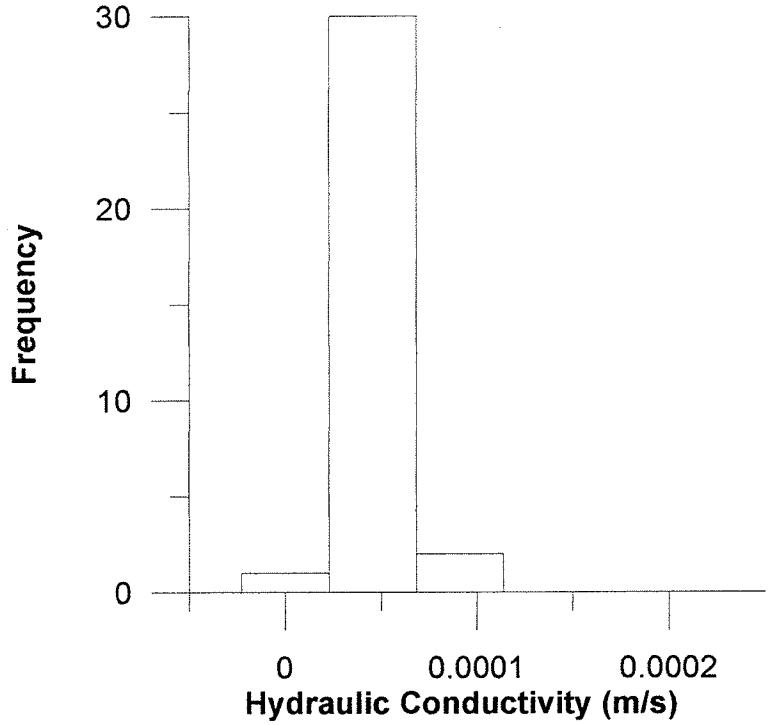

Figure 5.23 – Histogram of non-transformed hydraulic conductivity for the till.

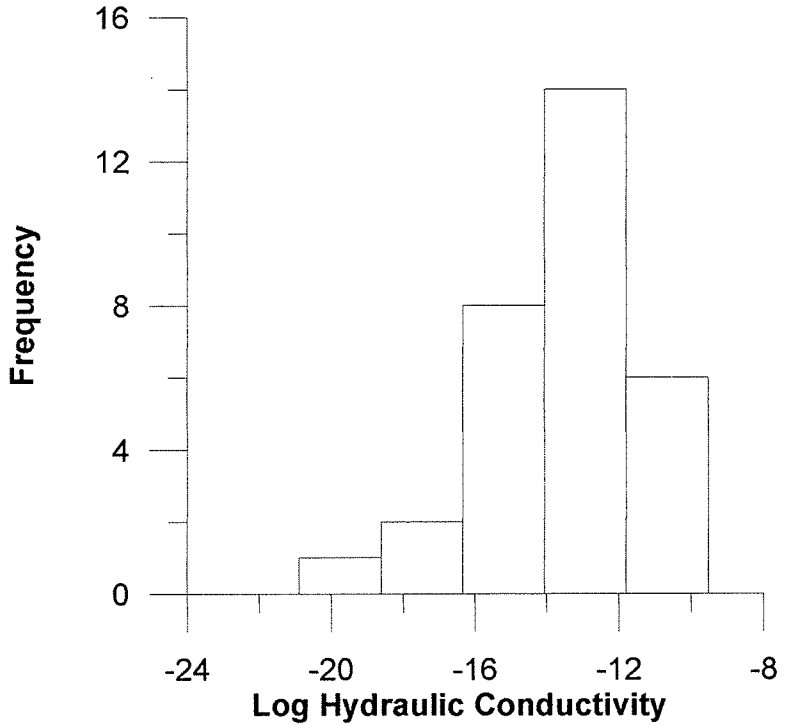

Figure 5.24 – Histogram of natural log hydraulic conductivity in m/s for the till.

CHAPTER 6

BAYESIAN UPDATING

The implementation of the Bayesian Updating methodology including numerical solvers into a numerical code is covered in this chapter. Precision and computational time checks between different scenarios are also evaluated and presented in this chapter. The resulting code was then used to interpolate the log transmissivity to each node within the finite element mesh, from the data presented in Chapter 4 and the geostatistics presented in Chapter 5.

6.1 Bayesian Updating Code Reformulation

To generate a heterogeneous transmissivity field from a limited dataset of uncertain data measurements, the Bayesian Updating Method presented in Section 2.8.2 was coded in Compaq Visual FORTRAN version 6.1. The initial code closely followed that originally developed according to Woodbury and Ulrych (2000). The code consisted of solving equations 2.53 and 2.54 for $\langle \mathbf{m} \rangle$ and $\mathbf{C}_q$, respectively.

In order to code equations 2.53 and 2.54, several aspects were addressed. The first component was the requirement of a numerical method to solve the integrals in the equations. Two different methods were assessed in the coding: Monte Carlo with and without Latin Hypercube Sampling (see Section 2.9). The second aspect was to determine which required parameters were unknown and should be treated as

hyperparameters. Different types of priors for these hyperparameters had to be incorporated into the final code (see Section 2.8.2.1). In cases where the variogram was well defined from the data, this variogram could be used in the solution; otherwise the parameters of the variogram were treated as hyperparameters. The third factor involved the requirement of a numerical method to solve the matrix equations that arose in the solution. For example, for equation 2.53, if $(\mathbf{GC_M G^T}+\sigma_d^2\mathbf{I})$ is denoted as **A** and **(d*-Gs)** as **b**, it is possible to represent the multiplication of these terms using these new variables ($\mathbf{A^{-1}b} = \mathbf{y}$). The vector of interest, **y,** is substituted back into equation 2.53. This matrix equation can be re-arranged, to $\mathbf{Ay} = \mathbf{b}$ and a numerical solver was required to determine **y**. Two different solvers were implemented into the code. One was the well known direct solver, Cholesky Decomposition and the second was the iterative Conjugate Gradient Method.

Once the code was programmed, it was found that it was fairly inefficient for large problems. Any excess arrays (lack of symmetry noted) or computations were removed to reduce operations and memory. The code was programmed with direct array allocation, meaning that each array was dimensioned to the exact size required, thereby eliminating excess memory and storage required to run the program. The code was also parallelized so that both processors of a dual processor machine would be used in the computations. This parallelization was conducted using a commercially available Visual KAP for OpenMP™.

6.1.1 Time Comparisons

In order to compare efficiency of the different sampling methods, numerical solvers and the effect of parallelization, different runs of the model were conducted and the time and precision were compared. A base run was conducted with 2258 interpolation nodes and 631 observations. The covariance function of the Carbonate Aquifer was used, but the mean (**s**) and noise (σ_d) were unknown and therefore marginalized out as hyperparameters (i.e. $\mathbf{u} = \mathbf{s}, \sigma_d$). A Gaussian pdf was used as the prior for the mean (**s**), with parameters of -7.15 and 1.7 for the mean and standard deviation, respectively. For the noise in the data, only upper and lower bounds could be assumed (0 and 12.5) and a truncated exponential was used as the prior. Latin Hypercube sampling with 100 iterations was used to solve the integral and Cholesky Decomposition to solve the matrix equation. This scenario was run on a computer with dual PIII 800 processors and 1 Gbyte RAM of memory. The precision was investigated at five nodes in the system and an average was taken in order to compare between scenarios. The time to run the base case was 2.31 hours with a precision of 0.029.

The first comparison to the base case was a scenario run under the exact same conditions, except that the code was not parallelized, i.e. only one processor. The time required to run this second scenario was 7.5 hours, over three times longer than the base case, as expected. The average precision was 0.029, which is the exact value from the base run as expected as the parallelization should only affect the speed of the solution.

The second comparison was a scenario the same as the base case, except that Monte Carlo sampling with 100 iterations was used to solve the integral. The time required for this scenario was 2.1 hours, which was slightly shorter than the base case. This was because some extra computations were required in the Latin Hypercube Sampling to separate the distributions into equal stratifications. The average precision was found to be 0.028. The precision was found to be slightly lower than that found with the Latin Hypercube Sampling, which was not as expected from the literature.

The final comparison was the same as the base case, except that the conjugate gradient solver was used to solve the matrix equation. This scenario took approximately 20.5 hours to run, which was significantly higher than all other cases. The average precision was found to be 1.55, which was also significantly higher than the other scenarios considered. Therefore, the Cholesky Decomposition solver was used for the remaining analysis.

6.2 Scale Considerations

Transmissivity was measured by various field tests, resulting in a database of values determined at different scales. A large quantity of the measurements was estimated from specific capacity (2261 for the Carbonate Aquifer and 50 for the Sandstone Aquifer) or by single-well drawdown tests (111 for the Carbonate Aquifer and 28 for the Sandstone Aquifer), which are considered point scale. This dataset comprised 88% and 100% of the transmissivity database for the Carbonate and Sandstone Aquifers, respectively. The remaining measurements were from multiple-well drawdown tests or where the test type

was unknown. However, these tests can be assumed to be point scale in comparison to the interpolation scale, which varied between 1,000 and 5,000 m. None of the pump tests were collected over large distances and were most likely less than 50 m in all cases. Therefore, the transmissivity measurements were all assumed to be point scale.

The Bayesian Updating methodology interpolates from point to point. Therefore, it can be used to interpolate from the point scale measurements to each node within the finite element mesh. In finite element modeling, transmissivity (or hydraulic conductivity) must be assigned to each element within the mesh, not to each node. Therefore, the interpolated transmissivity measurements at each node, had to be up-scaled to each element. The geometric mean was used to calculate the elemental transmissivity from the nodal transmissivities. Haverkamp and Vauclin (1979) investigated different averages for upscaling and found that the geometric mean resulted in the minimal error.

6.3 Carbonate Aquifer

The heterogeneous nature of the transmissivity of the Carbonate Aquifer was interpolated from the measurements (Chapter 4) and Geostatistics (Chapter 5) using Bayesian Updating. As described in Chapter 2, the data, or a transform of the underlying probability distribution function must follow a Gaussian distribution. As determined in Chapter 5, the natural log transform of the transmissivity measurements were found to follow a Gaussian distribution. Therefore, Bayesian Updating was used to interpolate the natural log transmissivity to each node in the finite element mesh. The first scenario considered assumed certain measurements ($\sigma_d^2 = 0$) and therefore the only unknown or

uncertain parameters required by equations 2.53 and 2.54 was the unconditional mean value at each point, $\mathbf{s}$ ($\mathbf{u} = (\mathbf{s})$). The hyperparameter $\mathbf{u}$ was marginalized out of the solution and prior probabilities were required. For the unconditioned mean ($\mathbf{s}$), a Gaussian probability distribution was assumed, as the mean and standard deviation of the mean were known from the data. The parameters used to assign priors to the hyperparameters are shown in Table 6.1. The other required parameters were those of the correlation structure of the data, which were known exactly from the nested variogram model (equation 5.1). The resulting log transmissivity field and associated uncertainty is presented in Figure 6.1. The standard deviation can be related to the confidence limits of the interpolated value. In the regions where many measurements were available, the standard deviation was low relative to areas where little or no data was present. The maximum standard deviation was 1.6, which is equal to the standard deviation of the data. The heterogeneous field was also approximated using kriging with SURFER™ (Golden Software Inc., Version 7) for comparison purposes (see Figure 6.2a). The same measurements and nested variogram (equation 5.1) were used in the kriging method as that in the Bayesian Updating method. The standard deviations of the kriging interpolation are presented in Figure 6.2b and were found to have a maximum of about 1.6. By comparing the transmissivity fields estimated by the two methods, it was observed that the same main features of high and low values occurred in the same regions. Comparing the standard deviation plots (Figures 6.1b and 6.2b) it was observed that the standard deviation, and therefore uncertainty in log transmissivity, was lower for the Bayesian Updating field than the kriging field.

Table 6.1 – Parameters and priors used in Bayesian Updating of log transmissivity of Carbonate and Sandstone Aquifers.

Medium	Parameter		Upper bound	Lower bound	Average	Standard Deviation	Type of prior
Sandstone Aquifer	**Mean**		-0.9	-12.5	-7.15	1.7	Gaussian
	Noise		12.5	0	1.7	--	TE
	Variogram Parameters	C_0	1.0	0	0.56	--	TE
		σ_Y^2	3	2.7	2.9	--	TE
		λ (m)	30,000	0	16,828	--	TE
Carbonate Aquifer	**Mean**		-0.9	-12.5	-7.15	1.7	Gaussian
	Noise		12.5	0	0.5	--	TE
	Variogram Parameters	C_0	--	--	1.93	--	--
		C_1	--	--	2.18	--	--
		C_2	--	--	2.56	--	--
		λ_1 (m)	--	--	12313	--	--
		λ_2 (m)	--	--	104488	--	--

*** TE – Truncated exponential**

The log transmissivity field of the Carbonate Aquifer was re-visited using Bayesian Updating, however in this case uncertainty in the data was considered. This was done by marginalizing the noise out of the solution, and therefore the set of hyperparameters for this case was $\mathbf{u} = (\mathbf{s}, \sigma_d^2)$. For noise in the data, only reasonable upper and lower limits could be assumed, leading to a prior based on a truncated exponential. The results of this case are presented in Figure 6.3. The result of adding noise to the measurements is that the log transmissivity field is smoother. In kriging, interpolation to a measurement point will return that exact same value. This may not be the best choice however, as that measurement may have an uncertainty associated with it. In Bayesian Updating, when the uncertainty is considered, the interpolated value may differ from the original measurement value. If an observed measurement was known with absolute certainty, this knowledge was incorporated into Bayesian Updating and in this case the interpolation would recover the exact observed value at that point.

6.4 Sandstone Aquifer

For the Sandstone Aquifer, the unknown parameters in Equations 2.53 and 2.54 were the unconditional mean at each node, the noise in the data, and the correlation structure parameters ($\mathbf{u} = \mathbf{s}$, λ, σ_Y^2, σ_0^2). For this case the exponential model was assumed for the correlation structure. Again, a Gaussian prior was assumed for the mean value, as both the mean and standard deviation of the pdf were known (see Table 6.1). As only upper and lower limits could be reasonably assumed for the sill and integral scale, the minimum relative entropy principle (Woodbury and Ulrych, 1998) was used to generate truncated exponential (see Chapter 2, Section 2.8.2.1.2). Initially the measurements were assumed exact and a noise (σ_d) of zero was incorporated. Bayesian Updating was then used to generate the log transmissivity field (see Figure 6.4a). The map of standard deviations from the Bayesian Updating interpolation is presented in Figure 6.4b. Note that for the Sandstone Aquifer, there were only 78 data points from which to interpolate, and most of this data was located in the eastern part of the province. Therefore, in the regions where measurements were present, some variability in log transmissivity was observed. However, in areas where no data was available within the integral scale, Bayesian Updating generated a value equal to the unconditional mean of the underlying distribution (-7.96). This was because there was insufficient information to alter the prior pdf. Note that a large transmissivity zone was created by the Bayesian procedure, which was not a reflection of any deterministic considerations, but was a natural outcome of updating a prior pdf with observations. The statistical model returns a result that was very reasonable; that is homogeneous in regions where little or no information was available to alter an initial state.

The log transmissivity field for the Sandstone Aquifer was also interpolated using kriging (Figure 6.5a) for comparison. The best-fit exponential model was used as the correlation structure in the interpolation. The standard deviations of the kriging interpolation are presented in Figure 6.5b. The resulting log transmissivity field from both methods is similar. The same high and low regions are observed in both cases. Comparing the standard deviation maps, the standard deviation is generally less for the log transmissivity generated by Bayesian Updating.

A second case was examined in which the log transmissivity field was generated using Bayesian Updating for the Sandstone Aquifer. In this case, the measurements were assumed uncertain and noise was incorporated in terms of upper and lower bounds. This resulted in the set of hyperparameters ($\mathbf{u} = \mathbf{s}$, σ_d^2, λ, σ_Y^2, σ_0^2). MRE was used to assign the prior for the noise, as only upper and lower bounds could be assumed. The resulting field is presented in Figure 6.6. Again, the results are smoother than that generated assuming exact measurements.

6.5 Summary

This chapter covered the development of the Bayesian Updating field that was subsequently used to generate heterogeneous log transmissivity fields for each hydrostratigraphic unit. These transmissivity fields will be used to assign hydraulic conductivity to the finite element mesh of the flow and transport model, in the next chapter.

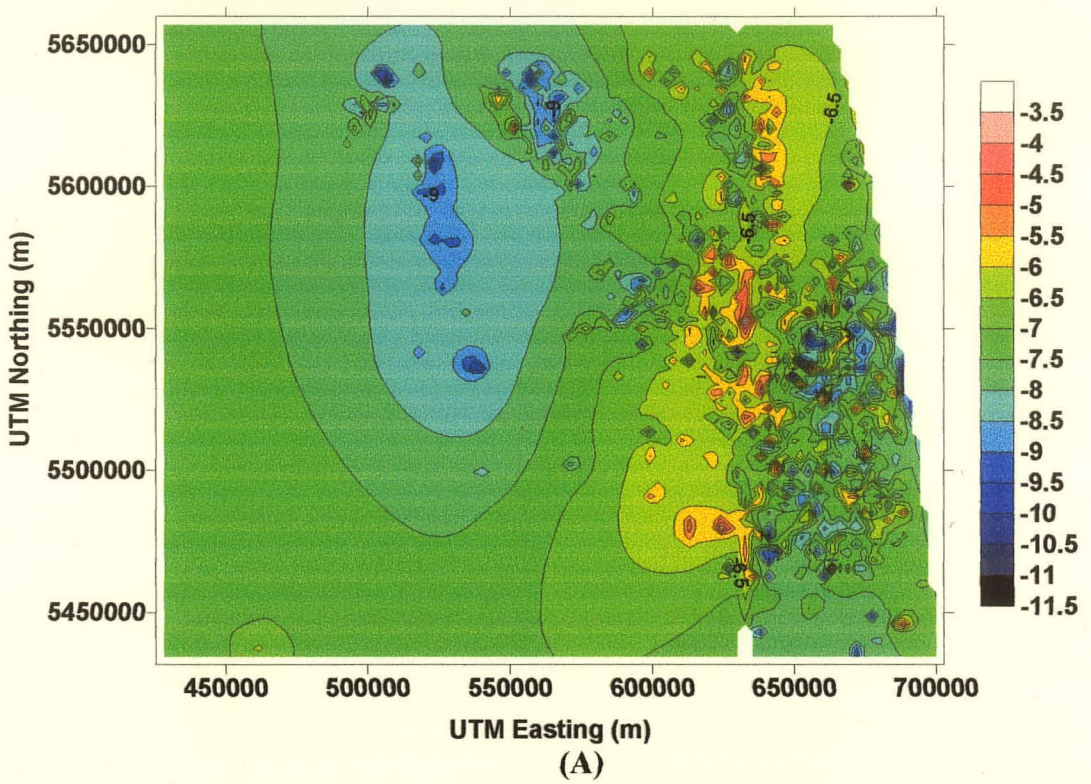

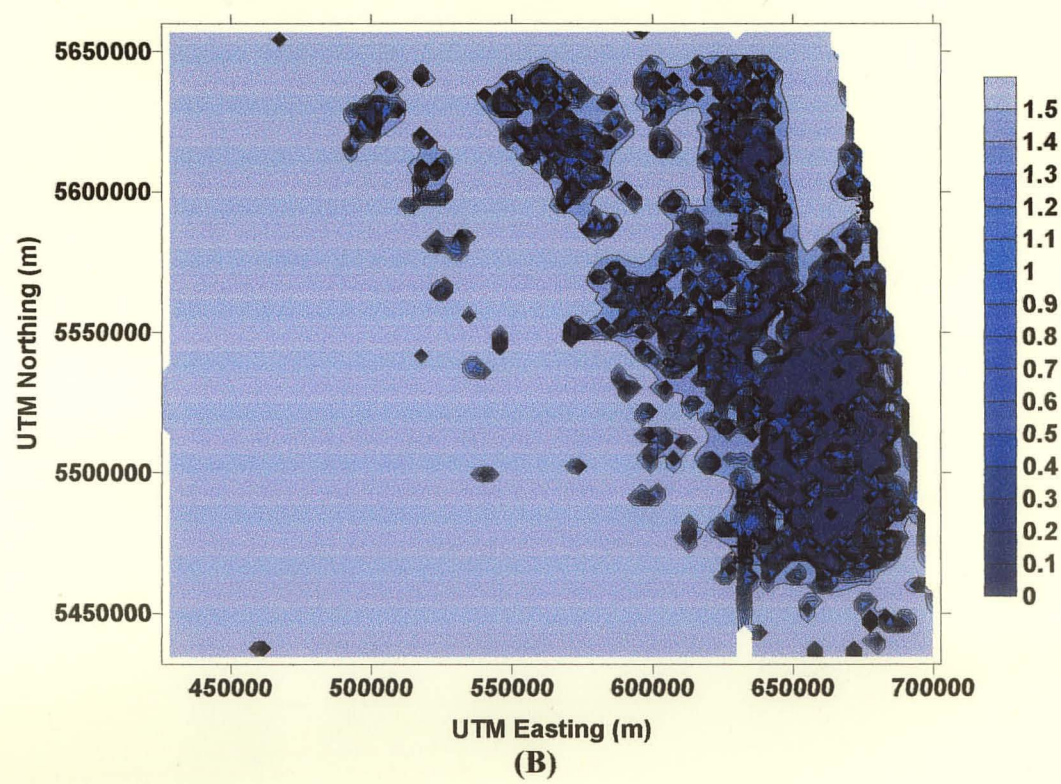

Figure 6.1 – Bayesian Updated log transmissivity for Carbonate Aquifer assuming certain measurements (no noise) (A) resulting log transmissivity and (B) associated uncertainty.

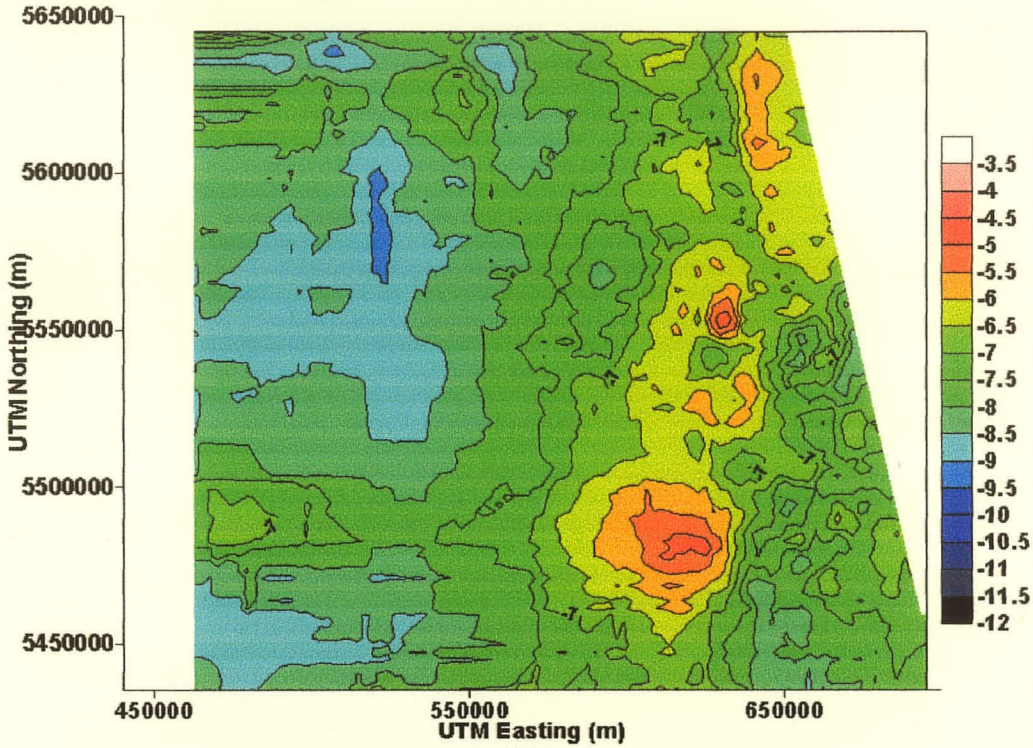

(A)

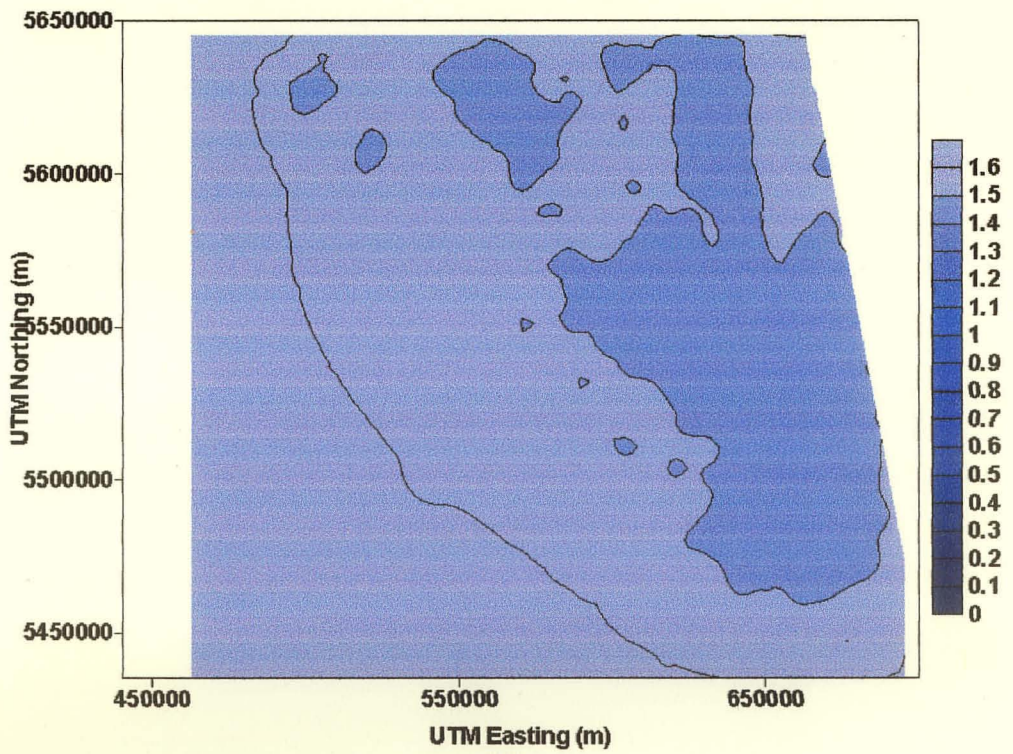

(B)

Figure 6.2 – (A) Log transmissivity field for Carbonate Aquifer assuming certain measurements generated using kriging and (B) associated uncertainty.

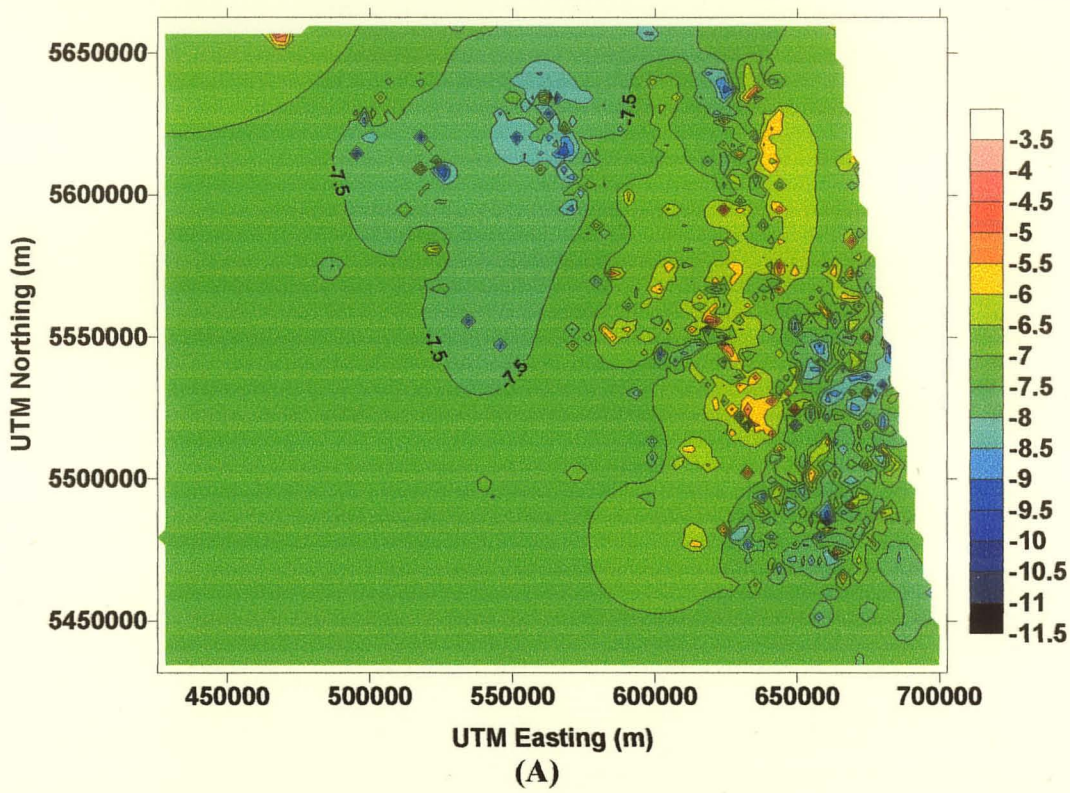

(A)

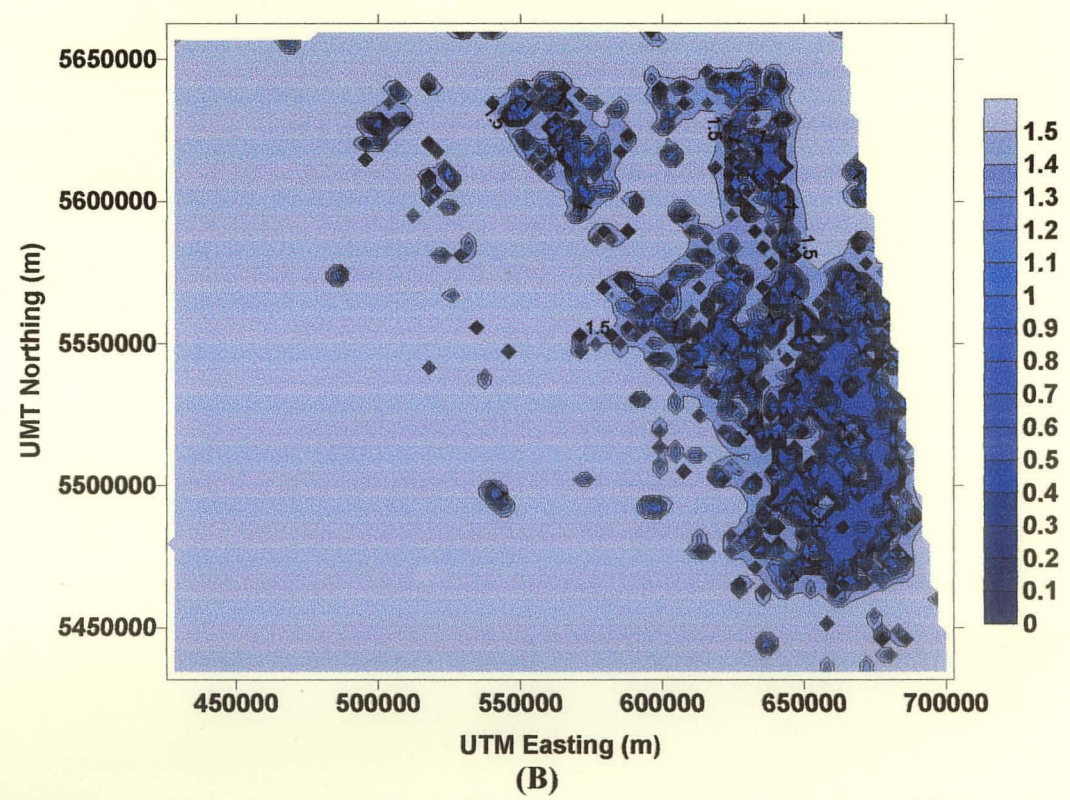

(B)

Figure 6.3 – (A) Log transmissivity field for Carbonate Aquifer generated from uncertain measurements using Bayesian Updating with 80 iterations of Latin Hypercube Sampling and (B) associated uncertainty.

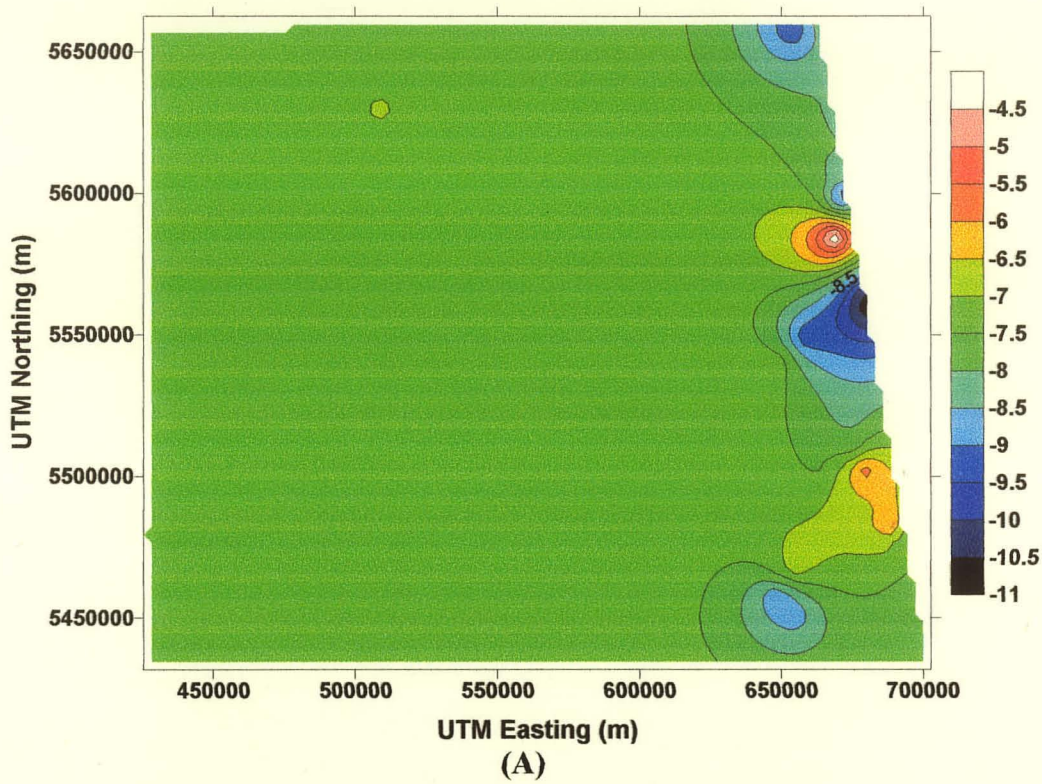

(A)

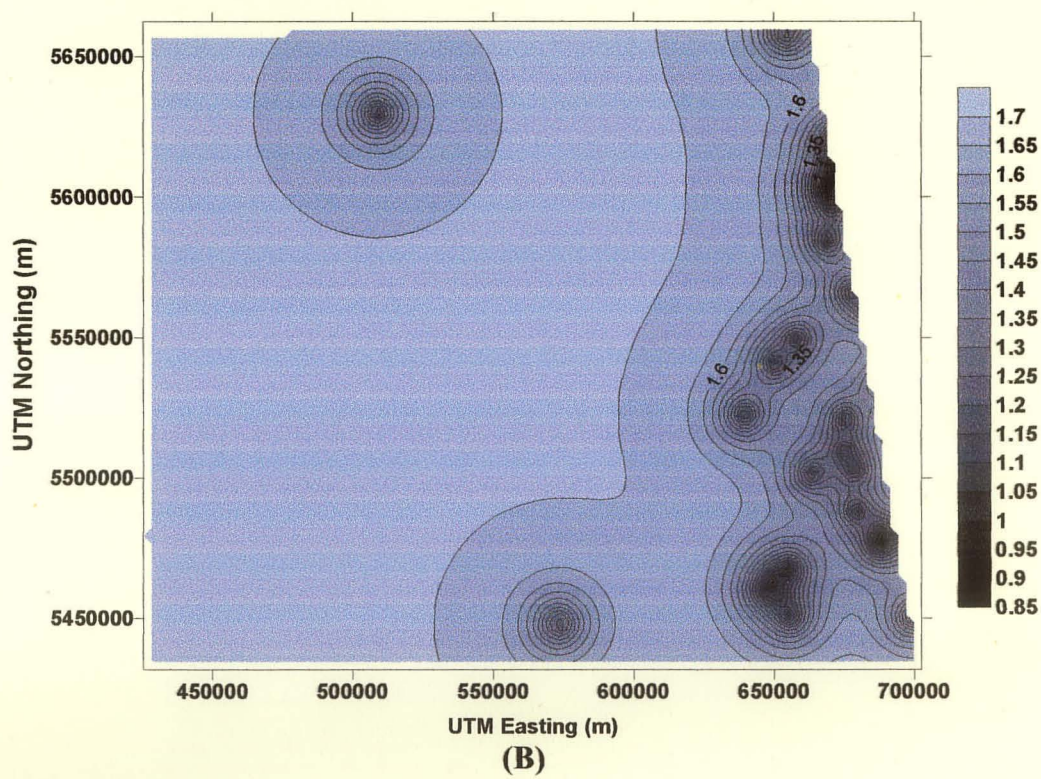

(B)

Figure 6.4 – (A) Log transmissivity field, assuming certain measurements, for Sandstone Aquifer generated using Bayesian Updating with 80 iterations of Latin Hypercube Sampling and (B) associated uncertainty.

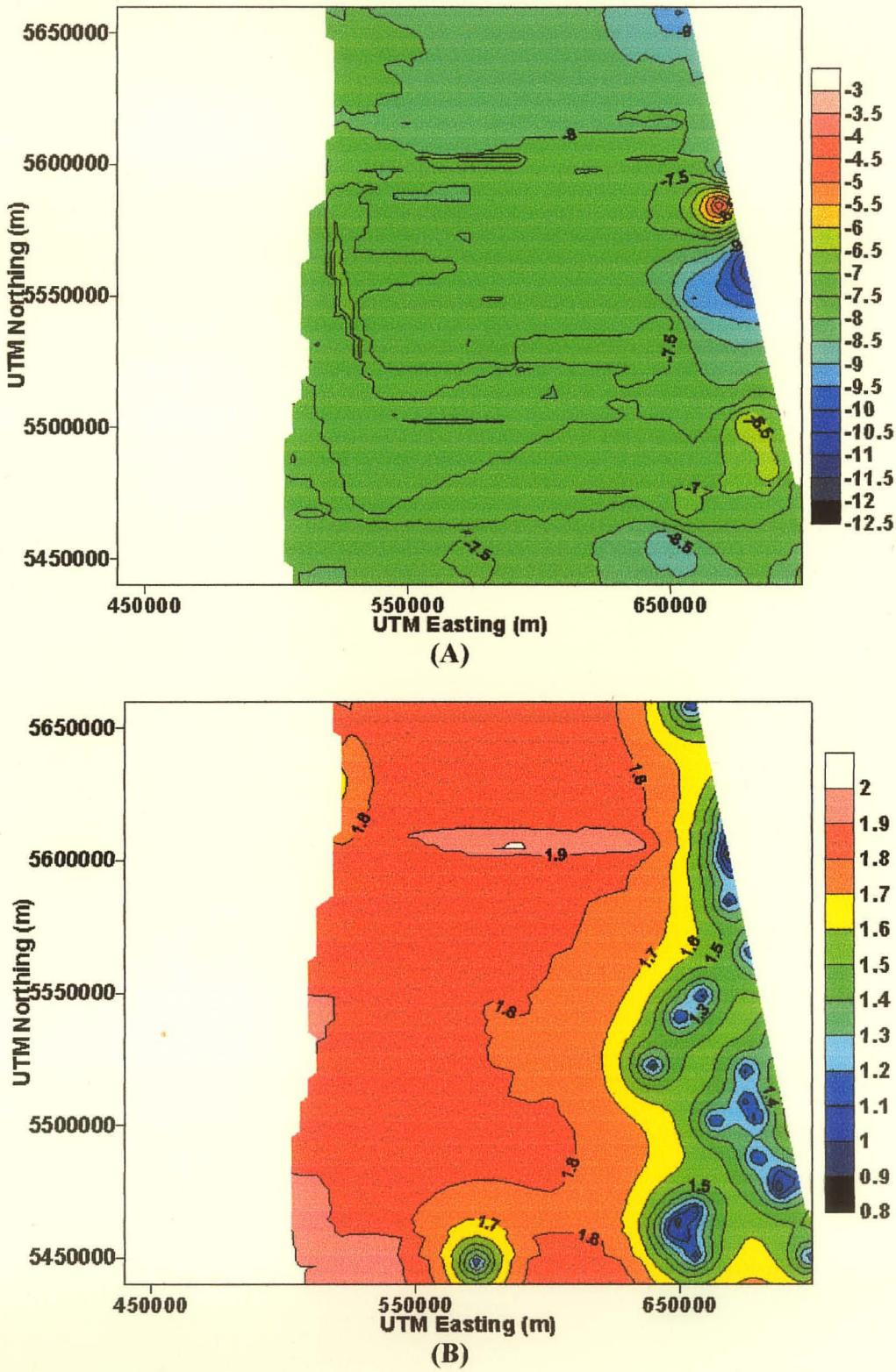

Figure 6.5 – (A) Log transmissivity field, assuming certain measurements, for Sandstone Aquifer generated using kriging and (B) associated uncertainty.

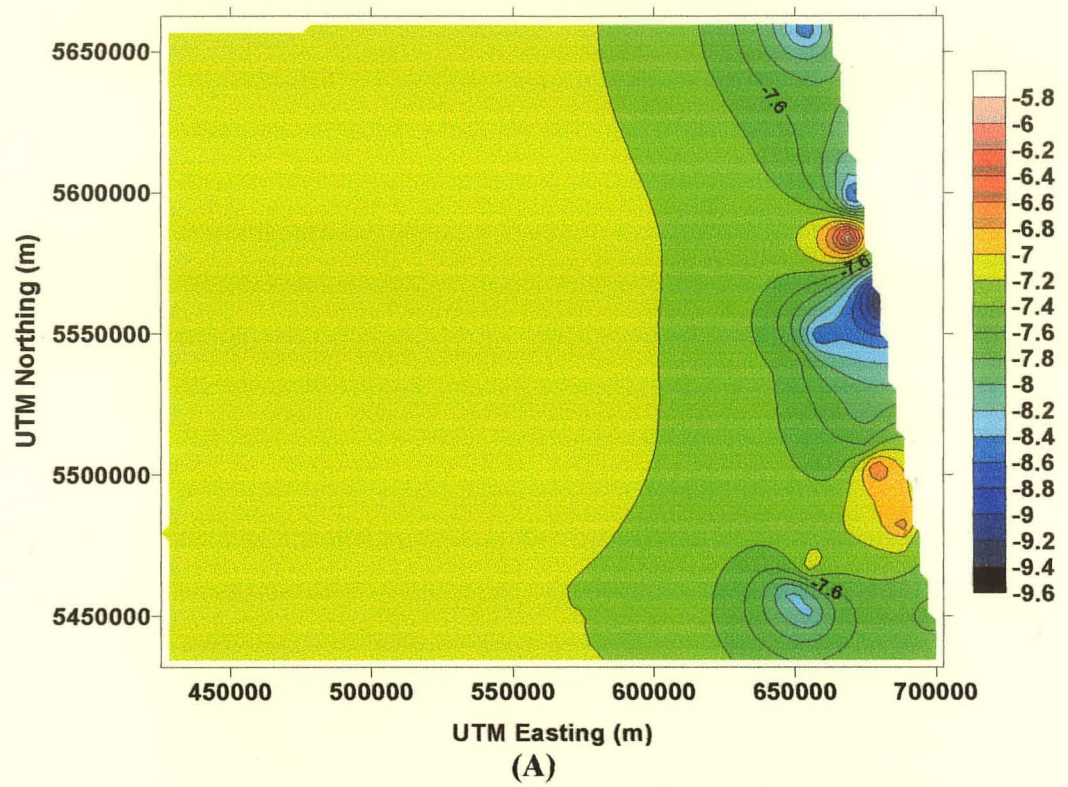

(A)

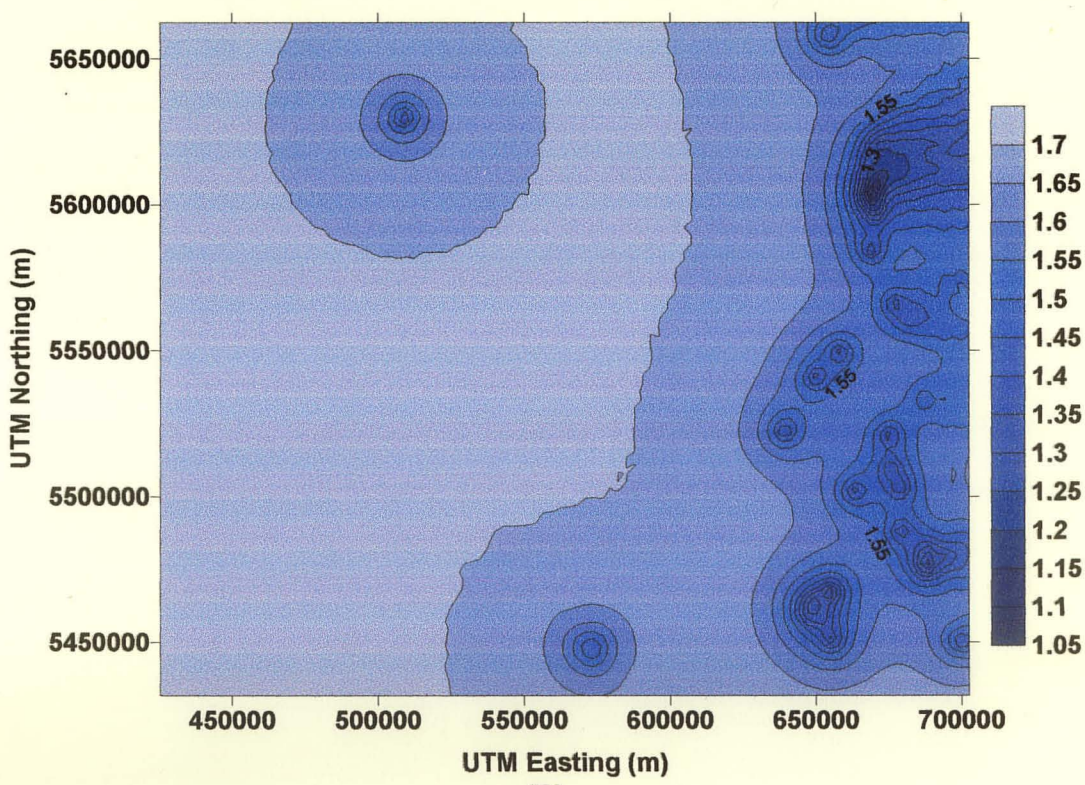

(B)

Figure 6.6 – (A) Log transmissivity field for Sandstone Aquifer generated from uncertain measurements using Bayesian Updating with 80 iterations of Latin Hypercube Sampling and (B) associated uncertainty.

CHAPTER 7

FLOW AND TRANSPORT MODEL DEVELOPMENT

7.1 Introduction

A numerical model of the flow and transport within the Carbonate Aquifer, Sandstone Aquifer and surrounding units was developed from the conceptual model presented in previous chapters. FRAC3DVS is a finite element flow and transport code, accounting for saturated/unsaturated conditions and variable density. The first section demonstrates the verification of the variable density aspect of this code. The next section covers the calibration targets used throughout the modeling exercise. The subsequent sections describe the construction of the flow and transport model of Southern Manitoba. Initially, two-dimensional models of each aquifer were constructed to ascertain hydrogeological properties and boundary conditions for both flow and transport. The three-dimensional model consisting of both aquifers and surrounding units was then constructed using this information. Finally, the sensitivity of model to different properties and boundary conditions was investigated.

7.2 Numerical Model and Code Verification

FRAC3DVS, modified to account for variable density flow, was used for model creation (Therrien and Sudicky, 1996). The numerical formulation and governing equations of this code were described in Chapter 2, Section 2.6. The code satisfied all of the requirements: finite element approach; allowed for heterogeneous transmissivity (or

hydraulic conductivity); solved both the solute transport and flow equations; and accounted for variable density effects on the solution.

The original code was verified for flow and transport as presented by Therrien and Sudicky (1996). However, the code was subsequently modified to account for variable density requiring this aspect to be verified. The model results were compared against the Henry problem; a salt dome problem; and compared against FEMWATER, an existing verified variable density code (Hsin-Chi, J.L. et al., 1997).

Henry (1964) approximated an analytical solution for steady state saltwater intrusion. The problem definition is presented in Figure 7.1 and consists of a rectangular area of 2.0 m by 1.0 m. No flow and no mass flux boundary conditions were implemented on the top and bottom. A constant freshwater influx of 6.6×10^{-5} m/s was imposed on the right boundary. The left side represented seaward conditions with a specified head boundary condition along the entire side and relative concentration equal to 1.0 from $z = 0$ to 0.8 m. To date, no numerical code has adequately simulated the Henry problem. The boundary condition on the left requires an abrupt change from salt to fresh water, which is physically improbable and numerically difficult to satisfy (Frind, 1982). However the problem is still used in most verification cases (Voss and Souza, 1987). For this thesis, the parameters as presented by Frind (1982) were used to evaluate the Henry problem (Table 7.1). The 0.5-isochlor results of Henry (1964) and the model results from Frind (1982) at steady state are presented in Figure 7.2. FRAC3DVS was used to solve this problem with 0.1 m square elements and results are presented in Figure 7.3. As no

previous numerical model has had a perfect match to the analytical solution of Henry, the FRAC3DVS results were thought to compare well.

Table 7.1 – Verification problem parameters

Parameter	Henry Problem	Salt Dome Problem	FEMWATER
K (m/s)	1.0×10^{-2}	1.1×10^{-5}	1.0×10^{-6}
D (m^2/s)	6.6×10^{-6}	1.39×10^{-8}	1.0×10^{-10}
Maximum density (kg/m^3)	1024.99	1200	1200
α_L *(m)*	0.0	20.0	2.0
α_T *(m)*	0.0	2.0	0.2
α_v *(m)*	0.0	0.0	0.0
n	0.35	0.2	0.2

The second verification case was a salt dome problem that was presented by Kolditz et al. (1998). The problem consisted of groundwater flow over a salt dome causing an addition of solute into the system, changing the density and affecting flow. The problem definition is presented in Figure 7.4 and consists of a rectangular region of 900 m x 300 m with properties presented in Table 7.1. On the top border, a specified head boundary condition that varied linearly from 20.456 m on the left to 10.228 m on the right was imposed. The remaining boundaries were all no flow boundary conditions. Freshwater inflow to the system was on the top left and was accounted for by assigning a relative concentration boundary condition equal to 0.0. The salt dome was placed in the middle 300 m of the bottom boundary with no mass fluxes allowed on either side. The results of the salt dome problem at steady state from modeling conducted by Kolditz et al. (1998) are presented in Figure 7.4. The FRAC3DVS code is not capable of directly solving for steady state solutions, for flow or transport. However, since steady state is the limiting condition for extremely long times, FRAC3DVS was simply run over a long time period (Figure 7.5). The results differed slightly from the model results presented by Kolditz et al. (1998). Both head distributions (Figures 7.4a and 7.5a) had approximately vertical

contours in freshwater regions and horizontal in saltwater regions with a bend occurring at saltwater/freshwater interface. The relative concentration contours (Figures 7.4c and 7.5b) show similar profiles with relative concentration contours dispersing towards the right. The results of FRAC3DVS and that of Kolditz et al., 1998 differed but had the same general form.

The results of FRAC3DVS were further verified by comparing with FEMWATER, an existing finite element, variably density flow and transport code. A simple problem of 100 m x 50 m with a constant head of 20 m and relative concentration of 1.0 on the left boundary and constant head of 10 m and relative concentration of 0.0 on the right (Figure 7.6). The parameters of the problem are presented in Table 7.1. Both codes were used to run the problem for 2×10^7 seconds from an initial condition of equivalent freshwater head and relative concentration equal to 0.0. The relative concentration contours of both models and a plot of FRAC3DVS results versus FEMWATER results is presented in Figure 7.7. The match between the results of the two models is quite good, verifying FRAC3DVS. A second case was examined in which only half of the left side had a relative concentration boundary condition of 1.0. The contours of both model results and plot of FRAC3DVS versus FEMWATER results is presented in Figure 7.8.

7.3 Hydrostratigraphic Model: Finite Element Mesh Construction

To model the system using the finite element method, a finite element mesh had to be constructed. For this case, the prism element type was used and the hydrostratigraphic model developed in Chapter 3 had to be subdivided into a system of elements and nodes.

In the solution of the model, the equivalent freshwater head and relative concentration were calculated at each node within the mesh. In the x-y plane, the element size was refined in areas where large changes in head or concentration were expected to occur, such as in the vicinity of wells (large head changes) and the saltwater interface (large concentration changes) (Figure 7.9). Changes in element size were done gradually so that neighbouring elements did not increase in size by more than 1.5 times. To create the three-dimensional mesh, FRAC3DVS used the two-dimensional plan mesh and nodal elevations of each layer. A simple example of the mesh development is shown in Figure 7.10. An x-y plane is shown with eight nodes in Figure 7.10a. The elevations of the model base and one layer are given and the resulting three-dimensional mesh is shown with one sublayer. This layer could be divided into any specified number of equal thickness sublayers.

The three-dimensional mesh for the model was constructed from the x-y plane and by assigning layer elevations from geology. A total of five main layers were used to construct the final three-dimensional mesh (see Figure 7.11). Layer 1 (Overburden units) had six evenly spaced sublayers with top defined by ground surface and bottom defined by the top of the Carbonate Aquifer. Layer 2 (Carbonate Aquifer) comprised three sublayers with bottom defined as the base of the Carbonate Aquifer. Layer 3 (Carbonate Unit) had six evenly spaced sublayers and bottom was defined as the top of the Winnipeg Formation. Layer 4 (Winnipeg Shale) was not subdivided and the bottom was assigned 1.5 m below top of Winnipeg Formation. Layer 5 (Sandstone Aquifer) was divided into three sublayers and the bottom was the top of the Precambrian.

Hydraulic conductivity was assigned to each finite element by using the hydrostratigraphic model to determine in which unit it was located. The hydraulic conductivity was then either calculated from the heterogeneous transmissivity field and the saturated thickness or was specified, creating a file of K_x, K_y and K_z. It was assumed for this model that $K_x = K_y$ and $K_z = 0.1 \cdot K_x$ (Domenico and Schwartz, 1990). The sensitivity of the model to this assumption is examined later in this chapter. The remaining hydrogeological properties were assumed homogeneous within each layer.

7.4 Calibration Targets

In order to calibrate and validate the model, the model results were compared against field observations. For flow, equivalent freshwater head values were compared. For the transport model, concentrations of chloride ion were compared. Chloride ion concentration was used to simulate the brine movement and was considered conservative. In order to assess the fit of the model results against these observations, a calibration target was specified prior to commencement of model simulations.

For calibration of the flow model, the steady state results were compared against historic water levels from 1920 (Chapter 4, Section 4.3). In an ideal situation, the observations would be error free and the goal would be a perfect match. However, the observed water levels do have an associated error and therefore the model results were assigned an allowable range to differ from the observations. The dataset of measured water levels was corrected for density effects to obtain observations in terms of equivalent freshwater

head. It was found that this correction was negligible as the bulk of the measurements are located within the freshwater zone where densities are approximately fresh. A model result within an interval of ±10 m from the observed historical water level is assumed due to following errors:

- Water levels were not instantaneous. The water level measurements for this dataset were taken at different times of day, season and year.
- Measurement error. For this historical dataset, the method of taking measurements and level of quality control was not known.
- Scaling effects. The wells were screened over a vertical distance affecting the observed water level. However, to compare with model results, the observations had to be assumed at a point.
- Location. The well locations as discussed previously are only approximately known.
- Interpolation error. In finite element modeling, the equivalent freshwater head was solved at each node. However, an observation point may not be located directly at any node. Therefore, the model results were interpolated to the observation location for comparison purposes.

To assess error across the region, the root mean square (RMS) error was used. For the Carbonate Aquifer, the total change in equivalent freshwater head across the study region was from 218 to 350 m. For the Sandstone Aquifer, the total head changed between 420 and 220 m, within the study region. An RMS error less than 10% of this maximum

change was assumed reasonable (13 m for the Carbonate Aquifer and 20 m for the Sandstone Aquifers) (Anderson and Woessner, 1992).

The model errors across the region were checked by plotting the computed versus observed equivalent freshwater head. The points should fall approximately along a one-to-one line. A regressed line through the points should result in a slope close to 1.0, an intercept of 0.0 and a high coefficient of correlation (R^2) value. To test statistically whether the slope and intercept of the regressed line are significantly different from 1.0 and 0.0, respectively, the t-test was used (Kennedy and Neville, 1976). The equation of the regressed line is $y = b \cdot x + a$. To test the slope, the t-test is applied against $|b-b_0|$ where b_0 is the theoretical value of the slope (in this case 1.0). The null hypothesis is that there is no significant difference between b and b_0. The t value is calculated from the following equation:

$$t = \frac{|b - b_0|}{s_b} = \frac{|b - 1|}{s_b} \qquad (7.1)$$

Where s_b is the standard deviation of the slope, b, determined through regression. Critical t-values can be obtained from tables at specified degrees of freedom (DOF) and chosen significance level. For this case the DOF is equal to number of points minus two. If the calculated t-value is greater than the critical t-value, the null hypothesis is rejected. This result draws the conclusion that there is a significant difference between the regressed slope and a value of 1.0. The t-test can also be conducted to determine whether the intercept is significantly different from 0.0 and on the R^2, to ensure that correlation exists. A plot of the residuals should show no trend and have a good scatter. These plots clearly show whether a region is being consistently over or under estimated.

To validate (or history match) the model, the results were compared against a second dataset collected under different stress conditions. In this case, the current water levels collected from MWB observation wells were used. The errors associated with the current dataset were the same as the historic ones, except that instantaneous piezometric surfaces could be created. The same targets used for calibration were kept for assessment of flow model validation.

For the solute transport model, concentrations of chloride ion were modeled. The maximum chloride concentration within the study area was measured as 75,000 mg/L. For both aquifers, only one dataset of chloride ion concentrations was available that was collected from water sampling conducted in the late 1990's. As no "steady-state" dataset was available, calibration could not be conducted. Therefore, only a history match was conducted. The errors associated with both datasets were measurement error, scaling effects, sampling location and interpolation error. Due to these errors, a calibration target of ±7.5 g/L is assumed. The maximum allowable RMS was 7.5 g/L, which was 10% of a possible change of 75 g/L over the study region.

7.5 Two-Dimensional Simulations: Carbonate Aquifer

Initially, a two-dimensional model of flow and transport within the Carbonate Aquifer was constructed. The purpose was to determine reasonable boundary conditions and hydrogeological properties for the Carbonate Aquifer. The finite element mesh for the Carbonate Aquifer had the same x-y plane as shown in Figure 7.9 with three layers, of a

thickness equal to 5 m each. The flow model was run to approximate steady state and calibrated against the historical head dataset (1920). The hydraulic conductivity was based on the Bayesian Updating interpolation (Figure 6.3) of transmissivity and an assumed 15 m saturated thickness. The other parameters are presented in Table 7.2. For this case, the Red River Floodway and wells screened over both the Carbonate and Sandstone Aquifers were ignored.

7.5.1 Two-Dimensional Simulations: Flow Calibration to 1920 (Carbonate Aquifer)

The boundary conditions for the steady state solution were assigned according to available information (see Figure 7.12 and Table 7.2). The Northern and Southern boundaries were parallel to streamlines (see Figure 4.11) and therefore were assigned no flow boundary conditions. A no flow boundary condition was imposed on the Eastern boundary, as this was where the Carbonate Aquifer subcropped. Water was known to flow into the region from the west and was incorporated using a specified head boundary condition of 270 m on the Western boundary. Discharge to Lake Manitoba and Lake Winnipeg were accounted for using specified head boundary conditions of 248 and 217 m, respectively (Section 4.5). The Red River, a region of discharge was accounted for using specified head boundary condition, with heads increasing from 217 m at Lake Winnipeg to 245 m at the South end. The river has a gradient of approximately 0.2 m per kilometer. The Assiniboine River was not incorporated into the model. The recharge to the Sandilands region was reported to have an upper limit of 1 x 10^{-6}m/s (Section 4.5) and was incorporated using a specified flux boundary condition. Ensuring that the flux

constraint was satisfied, the value of flux was determined through calibration. The other recharge zones, Birds Hill and Interlake region were incorporated in the same manner.

Table 7.2 – Calibrated parameters for Carbonate Aquifer flow and transport model.

Parameter			Value
Flow	**Properties:**	*Hydraulic Conductivity*	BU field and saturated thickness of 15 m
		Porosity	0.15
		Storativity	5×10^{-5}
	BCs:	*Western Boundary*	Type I BC $h_f = 270$ m
		Lake Manitoba	Type I BC $h_f = 248$ m
		Lake Winnipeg	Type I BC $h_f = 217$ m
		Red River	Type I BC varying h_f – approximately 0.2 m/km (≡ 1 ft/mi)
		Birds Hill	Flux BC = 1×10^{-8} m/s
		Sandilands	Flux BC = 5.2×10^{-10} m/s
		Interlake	Flux BC = varying between 2×10^{-11} to 2×10^{-10} m/s
Transport	**Properties:**	*Longitudinal dispersivity*	20,000 m
		Transverse dispersivity	2000 m
		Vertical dispersivity	200 m
		Diffusion coefficient	1×10^{-10} m/s
	BCs:	*Western Boundary*	Type I BC C = 0.75 to 75 g/L

Wells within the system were also accounted. Pumping rates for non-permit wells were determined for each township and range as described in Section 4.5. However, it is known that these pumping rates will vary between 1920 and 1999 as development occurs and demand changes. Information regarding the changes in pumping rates was not available and therefore it was assumed that pumping rates are directly related to changes in population. In other words, as the population grew from 1920 to 1999, the pumping rates increased accordingly. The population in Manitoba was collected from Canadian Census data at five year intervals (see Table 7.3 and Figure 7.13). For the steady-state model of 1920, these wells were assumed to be pumping at 53% of the total rate.

Table 7.3 – Manitoba population and rates of population increase.

Year	Manitoba population	Percentage of 1999 population
1921	610,118	53
1926	639,056	56.2
1931	700,139	61.6
1936	711,216	62.6
1941	729,744	64.2
1946	726,923	64.0
1951	776,541	68.3
1956	850,040	74.8
1961	912,686	81.1
1966	963,066	84.8
1971	988,247	87.0
1976	1,021,506	89.9
1981	1,026,241	90.3
1986	1,063,016	93.6
1991	1,091,942	96.1
1996	1,113,898	98.0
1999[1]	1,136,176	100

[1] No census data available for 1999, therefore a 2% increase was assumed from 1996.

The calibrated model results of equivalent freshwater head for the Carbonate Aquifer at steady state are presented in Figure 7.14. On Figure 7.14a, the observation points are shown with an associated error bar. If the error was within the calibration target (± 10 m), the error bar was shown in green. If the error bar was pointing downward, then the model was underestimating the equivalent freshwater head and if the error bar was pointing upward, the model was overestimating the equivalent freshwater head. Figure 7.14b shows filled contours of the freshwater equivalent heads, which were found to compare well with those in Figure 4.11. Figure 7.14c shows a plot of the computed versus observed equivalent freshwater head versus observed. The RMS error was 6.10 m, which was within the calibration target of 13 m. The linear regression gave a slope of 1.00 and R^2 of 0.73. The total number of data points in the interpolation was 126, giving

a DOF of 124. The critical t-value for a significance level of 0.05 is 1.98. The t-values calculated for the slope and intercept were 0.039 and 0.112, respectively. Therefore, it can be concluded that there is no significant difference between the regressed slope and 1.0 and the regressed intercept and 0.0. The correlation coefficient was also tested against a value of 0.0. If the calculated t-value is greater than the critical t-value, then correlation is said to exist. In this case, the t-value was calculated to be 18.2, indicating that correlation exists between the calculated and observed equivalent freshwater heads. The scatter of residuals is presented in Figure 7.14d and does not appear to exhibit any trend. Upper and lower bound limits of ±10 m show one point above + 10 m and seven observations below – 10 m residual, indicating these points were outside the calibration target. However, no combination of parameters was found to get all observations within this assigned target.

7.5.2 Two-Dimensional Simulations: Flow Model History Match to 1999 (Carbonate Aquifer)

The flow and transport model was run from 1920 to 1999, incorporating any change in stress on the system. The steady state flow solution was used as an initial condition for the flow aspect of the model.

The pumping rate of the non-permit pumping wells were increased in proportion to population change as described in Section 7.5.2. The wells which have permits were incorporated during the reported period. The initial time-step was one second and was then increased or decreased by no more than a factor of 10 for each subsequent step. The

amount of change depended on the maximum change in equivalent freshwater head or concentration that occurred in the previous time step.

The history match of flow model results for 1999 is shown in Figure 7.16 and was compared against the dataset of 1999 water levels. From Figure 7.16a, it was evident that the model was underestimating the equivalent freshwater head in the Sandilands region as a result of a low flux rate. Therefore, the Sandilands recharge would have to be increased when incorporated into the larger three-dimensional flow model. Figure 7.16b showed that the equivalent freshwater head contours did not change significantly from the steady-state solution indicating that increased stress had small effect on the flow regime on the regional scale. The plot of computed versus observed equivalent freshwater head (Figure 7.16c) shows a larger number of points that are underestimated, as previously discussed. The RMS error for this model run was 12.27 m, which was double that of the steady state run but was still within the 13 m target. The regressed line had a slope of 0.71; intercept of 65.3 an R^2 value of 0.59. The calculated t-values for the slope and intercept were 3.61 and 3.45, respectively. For a DOF of 71, the critical t-value for a two-tailed test is 2.0 at the 0.05 significance level and 3.46 at the 0.001 significance level. For a 0.05 significance level, neither the slope nor intercept satisfy the test. At the 0.001 significance level, the intercept is satisfied and the slope is very close. For the correlation coefficient, the calculated t-value was 10.0, which is greater than the critical t-value and signifies correlation at the 0.05 significance level. The plot of residual versus observed equivalent freshwater head (Figure 7.16d) illustrates an increase in model results that are outside the ±10 m zone.

7.5.3 Two-Dimensional Simulations: Solute Transport History Match to 1999 (Carbonate Aquifer)

Concentrations of the chloride ion concentration were used to examine movement of the salt water/fresh water interface. Only one dataset of chloride ion concentration was available and was from sampling done in 1999. Therefore, the concentrations in 1920 were unknown and calibration could not be conducted. An initial condition for transient analysis was obtained by running the model over a long time period. The model was subsequently run from 1920 to 1999 using the approximated initial conditions. A history match was conducted between the model results and the dataset of chloride ion concentrations.

By investigation of the chloride ion concentrations in Figure 4.15, a specified concentration boundary condition varying from 75 g/L on South end to 0.75 g/L on North end was imposed on the western boundary (see Figure 7.15). Type II boundary conditions were used on Lake Manitoba and Lake Winnipeg to account for the discharge zones. The north, south and east boundaries were assigned a no flux boundary condition.

The value of unconditional longitudinal dispersivity was estimated from equation 2.4 assuming the second and third terms were negligible ($\alpha_L = \sigma^2 \cdot \lambda_e$). From Chapter 5, Section 5.2.1, it was determined that the variance of log transmissivity in the Carbonate Aquifer was 2.7 and the integral scale of the exponential correlation structure was 29,000 m. The unconditional longitudinal dispersivity was therefore estimated as 78,000 m,

which is extremely high. Comparison of this estimated value with that of Neuman (1990) and Gelhar et al. (1992) (Figure 2.5) required the scale of the problem. To determine the scale of the model, the source of brine in the aquifers is required (the scale equals distance between source and plume location). The cause or source of saltwater within the aquifers is not well understood and therefore defining the location of the source was not possible. A comparison could therefore not be conducted with the results of this research and that of Neuman (1990) and Gelhar et al. (1992).

The effect of variable density due to movement of solute was also considered. From the geochemistry dataset, it was determined that the maximum density within the study area was 1150 kg/m^3, and this was used to calculate densities at varying concentrations (equation 2.13). For the transport model, the hydrogeological parameters are shown in Table 7.2. A longitudinal dispersivity of 20,000 m was found to give a good fit between model results and observations. This conditional value (20,000 m) is lower than the unconditional estimate (78,000 m). However, as Neuman (1990) stated, conditioned values of longitudinal dispersivity will decrease as the knowledge of heterogeneous hydraulic conductivity increases. As the hydraulic conductivity for the Carbonate Aquifer is fully heterogeneous, this observed difference was thought reasonable. The transverse dispersivity was assumed to be one order of magnitude lower (2000 m) than the longitudinal dispersivity and vertical dispersivity another order of magnitude lower (200 m).

The transport model results from year 1999 were compared against the observed concentrations of chloride ion (see Figure 7.17). Concentration contours are presented in Figure 7.17a, presenting only those observation points having an absolute residual greater than 0.75 g/L. The observation measurements show increased error, as evidenced by the yellow and red error bars, within the plume to the west. The problem, however, was that where one observation would indicate that it was being overestimated (arrows pointing up), another observation close by was indicating that it was being underestimated (arrows pointing down).

Investigation of the chloride ion dataset provided some insight into this problem. First, a large proportion of the wells had sampling regions which were not entirely within the Carbonate Aquifer. The smallest concentration contour shown on the plan view is 1.0 g/L. Comparing the concentration contours from the model (Figure 7.17a) with those generated from the measurements (Figure 4.15), shows the 1.0 g/L (or 1000 mg/L) contour to be similarly located. Figure 7.17b shows those observations that had sampling regions located entirely within the Carbonate Aquifer. Second, a plot of concentration versus depth (Figure 7.18) shows some interesting results. Those samples taken from oil wells (marked with a square) were sampled at depths greater than 200 m while the remaining wells had sample locations at depths less than 200 m. The oil wells had higher concentrations and were the only wells that were sampled within the plume of saltwater in the Carbonate Aquifer. A plot of computed versus observed concentrations is presented in Figure 7.17c. The regressed line had a slope of 0.30, intercept of 0.014 and R^2 value of 0.24. The slope and intercept had calculated t-values of 19.5 and 4.97,

respectively. The critical t-value for a DOF of 602 at a 0.05 significance level was 1.96. As the t-values were greater than critical t-values, it was concluded that there was a significant difference between the slope and 1.0 and the intercept and 0.0. The calculated t-value for R^2 was 13.7, which is greater than the critical t-value indicating that correlation between the computed and observed concentration values exists. A large proportion of the observations are at very low concentration values. To observe what was occurring in the low concentration region, the results were plotted on a log-log scale (Figure 7.17d). The slope and intercept of the new regressed line was 1.17 and 0.25, respectively, with an R^2 of 0.26. The t-value calculated for slope and intercept was 2.15 and 0.91, respectively. The t-value for the slope still showed a significant difference from 1.0, but is much closer to satisfying the constraint. At a significance level of 0.01, the critical t-value is 2.576, indicating that the slope is not significantly different from 1.0 at this level. A plot of the calculated versus observed concentrations for those observations taken entirely within the Carbonate Aquifer is presented in Figure 7.17e. The plot of residuals for all observations is shown on a log scale in Figure 7.17f.

7.6 Two-Dimensional Simulations: Sandstone Aquifer

A two-dimensional model of the Sandstone Aquifer was constructed to obtain hydrogeological properties and boundary conditions. The finite element mesh was constructed using the same x-y plane as shown in Figure 7.9. The boundary conditions are shown in Figure 7.19 and Table 7.4. The hydrogeological properties are also presented in Table 7.4. A Type I (specified equivalent freshwater head) boundary condition was implemented on the Western and Southern boundary. As the aquifer

outcrops beneath Lake Winnipeg, a Type I boundary condition was implemented on the nodes beneath the lake on the edge of the finite element mesh. Recharge to the system was through the Sandilands region and therefore a Type II boundary condition was incorporated in that region.

7.6.1 Two-Dimensional Simulations: Flow Calibration to 1920 (Sandstone Aquifer)

For the Sandstone Aquifer, no historical water levels were available. Therefore, calibration of the flow model could not be conducted. For transient analyses, an initial condition was required. An equivalent freshwater head profile was obtained (Figure 4.12). The equivalent freshwater head measurements used to create this profile were obtained just prior to 1986. Therefore, this was not necessarily representative of pre-1920 conditions. However, this was used qualitatively to provide reasonable model results that could be subsequently used as an initial condition for the transient simulations.

Transmissivity measurements for the Sandstone Aquifer were concentrated in the eastern part of the province. Therefore, when BU was used to generate the heterogeneous log transmissivity field, the result in the west was essentially homogeneous log transmissivity equal to the mean. This solution makes sense, as the field could not be altered from its original state without any new information, i.e. measurements in the west. When the hydraulic conductivity was assigned to the model based on this BU field and saturated thickness of the unit, the model could not provide equivalent freshwater heads with the desired profile. This result is a function of limited measurements of transmissivity that

are concentrated in one section of the region. It was decided to divide the aquifer into 32 zones, which would contain homogenous hydraulic conductivity (see Figure 7.19). The values of hydraulic conductivity for each zone were determined through calibration (Table 7.4). These zones were chosen in a manner that would provide an acceptable solution. The boundary conditions for flow and the other hydrogeological properties are presented Figure 7.19 and Table 7.5. The flow model results are presented in Figure 7.20. Through visual examination, the profiles of Figure 7.20 and Figure 4.12 compare well.

Table 7.4 – Hydraulic conductivity values for each zone in calibrated Sandstone Aquifer flow and transport model.

Zone	K (m/s)	Zone	K (m/s)	Zone	K (m/s)
1	7×10^{-6}	*12*	1×10^{-6}	*23*	1×10^{-4}
2	3×10^{-8}	*13*	1×10^{-6}	*24*	4×10^{-5}
3	1×10^{-8}	*14*	5×10^{-7}	*25*	5×10^{-7}
4	1×10^{-9}	*15*	2×10^{-7}	*26*	5×10^{-7}
5	5×10^{-9}	*16*	2×10^{-6}	*27*	2×10^{-4}
6	5×10^{-6}	*17*	1×10^{-7}	*28*	2×10^{-4}
7	5×10^{-6}	*18*	1×10^{-7}	*29*	5×10^{-6}
8	1×10^{-6}	*19*	4×10^{-7}	*30*	1×10^{-5}
9	1×10^{-6}	*20*	2×10^{-7}	*31*	1×10^{-5}
10	1×10^{-6}	*21*	5×10^{-7}	*32*	9×10^{-8}
11	3×10^{-8}	*22*	5×10^{-5}		

7.6.2 Two-Dimensional Simulations: Flow Model History Match to 1999 (Sandstone Aquifer)

To simulate the period from 1920 to 1999, the model was run accounting for variable density effects and changes in pumping rates. A maximum density of 1150 kg/m^3 was used and pumping rates for wells were incorporated similarly to the Carbonate Aquifer.

Table 7.5 – Calibrated parameters for flow and transport Sandstone Aquifer model.

Parameter			Value
Flow	**Properties:**	*Hydraulic Conductivity*	Zoned
		Porosity	0.15
		Storativity	5×10^{-5}
	BCs:	*Western Boundary*	Type I BC: h_f ranging between 260 m and 420 m
		Lake Winnipeg	Type I BC: $h_f = 217$ m
		Sandilands	Flux BC = 1.4×10^{-10} m/s
Transport	**Properties:**	*Longitudinal dispersivity*	15,000 m
		Transverse dispersivity	1500 m
		Vertical dispersivity	150 m
		Diffusion coefficient	1×10^{-10} m/s
	BCs:	*Western Boundary*	Type I BC: C = 75 g/L

The flow model results in the year 1999 are presented in Figure 7.21. Five water level observations were available for 1999 and were used to assess the model results, as shown on Figure 7.21a. A plot of computed versus observed equivalent freshwater head values are presented in Figure 7.21b. The RMS error was 7.31 m, which was within the 20 m target, and the regressed line had a slope of 0.83, intercept of 44.1 and a R^2 value of 0.96. The critical t-value for a DOF of 3 and significance level of 0.05 was 3.182. The t-values for the slope, intercept and R^2 were 1.13, 1.2 and 8.7, respectively. Therefore, the slope was not significantly different from 1.0 and intercept from 0.0. As the t-value for the R^2 was greater than the critical t-value, it can be concluded that correlation exists. A residual plot is presented in Figure 7.21c and shows that all but one observed value was within ±10 m.

7.6.3 Two-Dimensional Simulations: Solute Transport History Match to 1999 (Sandstone Aquifer)

For the transport model, the chloride ion concentration was again used to simulate brine movement. As for the Carbonate Aquifer, only one dataset of chloride ion concentrations was available from sampling conducted in late 1990's. However, in this case the measurements are located in the freshwater region only. A Type I boundary condition with concentration equal to 75 g/L was established on the entire western boundary (Figure 7.15 and Table 7.5).

The unconditional longitudinal dispersivity was estimated from equation 2.4. The variance of the log transmissivity was 2.2 and integral scale was 16 km, giving an unconditioned longitudinal dispersivity of 35 km. The model was run over a long period of time to approximate the conditions in 1920. The same adaptive time steps used for the Carbonate Aquifer model were used. The hydrogeological parameters are presented in Table 7.5.

The transport model results for the year 1999 are presented in Figure 7.22. Again the conditioned longitudinal dispersivity (15,000 m) was below the unconditioned estimate (35,000 m). Figure 7.22a shows the contours and observation points. The observations are primarily located within the freshwater zone and therefore the saltwater portion of the plume could not be assessed. Comparison of the 1.0 g/L chloride ion concentration line (Figure 7.22a) with the 1.0 g/L TDS contour line from Betcher et al. (1995) (Figure 4.17) showed that the contour lines were in similar locations. Figure 7.22b shows a plot of

computed versus observed concentrations. The RMS error was 0.45 g/L, which was well within the 7.5 g/L calibration target. The regressed line had a slope of 0.06, an intercept of 0.0018 and an R^2 value of 0.0003. For a DOF of 161 and significance level of 0.05, the critical t-value was 1.96. The t-values calculated for the slope and intercept were 2.9 and 3.40, respectively. As the t-values are greater than the critical t-value, there is a significant difference between the slope and 1.0 and the intercept and 0.0. The critical t-value at significance level of 0.001 is 3.291, which satisfies the requirement for the slope and is close to that of the intercept. The t-value calculated for R^2 was 0.22, which is less than critical t-value indicating no correlation. The plot of calculated versus observed concentration was constructed on a log-log scale (Figure 7.22c). This plot shows significant scatter around the one-to-one line. The regressed line had a slope of 0.04 and intercept of 3.5. The calculated t-values for the slope and intercept were 13.7 and 13.6, respectively. A plot of the residuals on a log plot is shown in Figure 7.22d. With a lack of data in the higher ranges of concentration, it was difficult to improve these results.

7.7 Three-Dimensional Model

Using the boundary conditions and hydrogeological properties determined in the individual aquifer modeling exercise, the three-dimensional model was constructed. The Carbonate and Sandstone Aquifers were combined into one three-dimensional model, incorporating the surrounding units of the hydrostratigraphic model.

7.7.1 Flow Calibration to 1920

Hydrogeological properties were assigned to each element within the finite element mesh. For the calibrated model, the Carbonate Aquifer hydraulic conductivity was assigned using the Bayesian Updating field and assumed saturated thickness of 15 m. The Sandstone Aquifer was assigned using the same zones and hydraulic conductivity values as that for the individual two-dimensional model. The hydraulic conductivity values for the sand and gravel, clay, till, Winnipeg Shale and carbonates were assumed homogeneous and were given a value of 10^{-3}, 10^{-6}, 7.8×10^{-6}, 10^{-10} and 10^{-9} m/s, respectively. The other hydrogeological parameters, such as porosity, were assumed homogeneous and are presented in Table 7.6 and boundary conditions in Table 7.7 and Figure 7.23.

Boundary conditions were assigned (see Figure 7.23 and Table 7.7) using the individual aquifer model results. A Type I boundary condition was implemented on the west boundary at both the Carbonate and Sandstone Aquifers. Lake Manitoba, Lake Winnipeg and the Red River were incorporated using Type I boundary conditions with values measured in the field. The recharge zones within the Interlake, Sandilands and Birds Hill regions were assigned Type II boundary conditions with values determined through calibration.

Cross-contamination between the Carbonate and Sandstone Aquifers can occur in locations where wells are open or screened across both aquifers. The water can then transfer between aquifers causing contamination and potential decrease in water quality.

The wells that were determined to have screens along both aquifers (Section 4.5) were incorporated with an assumed pumping rate of 1.2×10^{-5} m^3/s (0.2 USGPM).

The steady state model results were compared against the historical water level measurements (1920) (see Figure 7.24). Figure 7.24a shows the plan view of the fresh-water equivalent head contours and the observation points with associated error interval. Cross-sections along lines A-A′ and B-B′ as shown in Figure 7.24a are presented in Figures 7.24b and c. A plot of computed versus observed equivalent freshwater head measurements are shown in Figure 7.24d. The RMS error of the model results to observations is 7.49 m, which is well within the lower target of 13 m. A linear regression through the points gave a slope of 0.92, intercept of 23.6 and R^2 of 0.75. The t-values calculated for the slope, intercept and R^2 were 1.14, 1.43 and 19.2, respectively. The critical t-value for a DOF of 124 at significance level of 0.05 was 1.98. The t-test indicates that the slope and intercept are not significantly different from 1.0 and 0.0, respectively and that correlation exists. The residual plot (Figure 7.24e) shows a good scatter of points around the zero line. Approximately thirteen points were outside the ±10 m target. No combination of parameters was found in which every observation was within this target.

Table 7.6 – Calibrated hydrogeological properties used in the three-dimensional model.

Unit	Hydraulic Conductivity (m/s)	Porosity	Storativity	α_L(m)	α_T (m)	α_v (m)
Sandstone Aquifer	Zoned	0.015	$5x10^{-5}$	15,000	1500	150
Winnipeg shale	10^{-10}	0.1	10^{-6}	15,000	1500	10
Carbonate	10^{-9}	0.01	10^{-5}	20,000	2000	10
Carbonate Aquifer	BU field	0.01	10^{-4}	50,000	2000	200
Overburden	Sand and gravel = 10^{-3} Till = $7.8x10^{-6}$ Clay = 10^{-6}	0.4	10^{-3}	15,000	1500	150

Table 7.7 – Boundary conditions assigned to the three-dimensional model.

Parameter		Value
Flow	*Western Boundary on Carbonate Aquifer*	Type I BC h_f = 270 m
	Western Boundary on Sandstone Aquifer	Type I BC h_f = 260 to 420 m
	Lake Manitoba	Type I BC h_f = 248 m
	Lake Winnipeg	Type I BC h_f = 217 m
	Red River	Type I BC varying h_f – approximately 0.2 m/km (≡ 1 ft/mi)
	Birds Hill	Flux BC = 1.0×10^{-8} m/s
	Sandilands	Flux BC = 6.0×10^{-9} m/s
	Interlake	Flux BC = 2.0×10^{-10} m/s
	Red River Floodway (from 1968 forward)	Type I BC – head base of Floodway
Transport	*Western Boundary on Carbonate Aquifer*	Type III BC C = 0.75 to 75 g/L
	Western Boundary on Sandstone Aquifer	Type III BC C = 75 g/L

7.7.2 Flow Model History Match to 1999

The model was subsequently history matched for both flow and transport. The flow and transport model was run from 1920 to 1999 through time accounting for variable density, with a maximum density of 1150 kg/m^3.

In 1968, the Red River Floodway was constructed. The Floodway is used in times of flooding to divert water from the Red River around the City of Winnipeg. The construction of the Floodway was known to have an effect on the flow regime and was therefore incorporated into the model. The Floodway was accounted for in the model from 1968 to 1999 using Type I boundary conditions with head values equal to the ground level.

The results of the transient flow model (Figure 7.25) were compared against equivalent freshwater head observations from 1999. Figure 7.25a shows the plan view of the equivalent freshwater head distribution with observations. Cross-sections along lines C-C′ and D-D′ are presented in Figures 7.25b and c. A plot of computed versus equivalent freshwater head was plotted and compared against a one-to-one line (Figure 7.25d). The RMS error was 10.4 m, which was within the calibration target and linear regression gave a slope of 1.13, intercept of -28.1 and R^2 value of 0.82. For a DOF of 76 and significance level of 0.05, the critical t-value was 2.0. The t-values of the slope, intercept and R^2 were 2.00, 1.83 and 18.4, respectively. This result indicates no significant difference between the slope with 1.0 and intercept with 0.0 and that correlation exists. A plot of the residual versus observed equivalent freshwater head shows thirteen points outside of the calibration target of ±10 m (Figure 7.25c). There is a slight trend evident within the residuals.

The quantity of discharge to the Red River Floodway in the field was assigned the approximate values of 0.14 m^3/s. The model computed the discharge to the Floodway to

be 0.16 m^3/s. As the discharge rate in the field is only approximate, these values were thought to be reasonably close.

7.7.3 Solute Transport History Match to 1999

The transport boundary conditions were accounted for using Type III boundary conditions on the western boundary at the aquifer locations. A Type I BC was initially used, but was found to cause irregularities in the west. To assign an initial condition for transient analyses, the initial conditions generated in the individual (two-dimensional) transport models were used for the (three-dimensional) transport model. Type I boundary conditions were used to generate these initial conditions in the two-dimensional models. Even though Type III boundary conditions were used in the three-dimensional model, the initial condition from the two-dimensional models was thought to be representative and was therefore used. Type III boundary conditions were incorporated using the flow rate across the border and the concentration. The transport parameters required for the three-dimensional model were assumed constant within each unit (Table 7.6). The values of the dispersivity were similar to those of individual aquifer models, with the exception of the Carbonate Aquifer longitudinal dispersivity which was increased to 50,000 m from 20,000 m as this was found to increase stability.

The solute transport model results in 1999 are shown in Figure 7.26. The plan view of concentrations with observations having an absolute residual greater than 0.75 g/L, is shown in Figure 7.26a. Into the salt-water zone, the observations are more sporadic as evidenced by the variability in observation intervals. It was difficult to improve

calibration as one point can show very good agreement, while a nearby observation shows very poor agreement. Cross-sections were prepared along lines E-E′, F-F′ and G-G′ are shown in Figures 7.26b, c and d. The cross-section shows a higher concentration in the western corner that decreases while moving eastwards. A plot of computed versus observed concentration values showed good agreement at lower concentrations but the concentrations were underestimated at higher ranges (Figure 7.26e). The RMS error of the fit was 2.55 g/L, which is below the target of 7.5 g/L. A linear regression through the points gave a slope of 0.64, intercept of 0.0014 and R^2 of 0.57. For a DOF of 769 and significance level of 0.05, the critical t-value was 1.96. The t-values for the slope and intercept were 15.1 and 0.98, respectively. As the t-value of the slope is greater than the critical t-value, the slope is significantly different from 1.0. The plot of computed versus observed concentration on log-log scale is presented in Figure 7.26f. This plot shows a better scatter of points around the one-to-one line. This observation may be a result of increased measurement error at lower concentration ranges. A residual plot showed a trend of decreasing residual with increasing concentration (Figures 7.26f and h). No matter what parameters or boundary conditions were used, the results were not improved. Lack of information made any further improvement difficult.

Variable density was considered in the final model. To determine whether consideration of variable density had a significant effect, a comparison was conducted between model results in which variable density was considered and that in which it was ignored. For both the Carbonate and Sandstone Aquifers, the head and concentration were compared between the two models. For the Carbonate Aquifer, the RMS error between the two

models results for the head and concentration was 0.63 m and 1.5 g/L, respectively. The effect on head is not that significant, however, the change in concentration is quite large. For the Sandstone Aquifer, the RMS error for the head and concentration is 0.87 m and 4.8×10^{-3} g/L, respectively. The effect on head and concentration for the Sandstone Aquifer is not that high and is below the RMS error of the model itself.

To determine whether the three-dimensional transport model showed a significant improvement over the individual two-dimensional models, the absolute value of residuals between computed versus observed values for both models were compared. The means of residuals between models were tested to determine whether the means were the same or significantly different. The null hypothesis is:

$$H_0: \mu_1 = \mu_2$$

Where μ_1 is the mean of the absolute value of residuals from the two-dimensional models and μ_2 is the mean of the absolute value of residuals from the three-dimensional model. The alternate hypothesis is that the mean from the three-dimensional model is significantly lower than the two-dimensional model.

$$H_A: \mu_1 \geq \mu_2$$

To compare two means, the t-test can be used. The t-value is calculated and compared against critical t-value at specified significance level.

$$t = \frac{(y_1 - y_2)}{s_p \sqrt{\frac{1}{n_1} + \frac{1}{n_2}}} \qquad (7.2)$$

Where y_1 is the sample mean of absolute value of residuals from two-dimensional models, y_2 is the sample mean of absolute value of residuals from the three-dimensional

model, n_1 is the number of points in the two-dimensional models, n_2 is the number of points in three-dimensional model and s_p is the pooled variance. The pooled variance is calculated from the following equation.

$$s_p = \frac{(n_1 - 1)\cdot s_1^2 + (n_2 - 1)\cdot s_2^2}{n_1 + n_2 - 2} \tag{7.3}$$

Where s_1^2 is the variance from the two-dimensional models and s_2^2 is the variance from the three-dimensional model. The critical t-value is found in tables at a DOF of n_1+n_2-2 and chosen significance level. If $t < t_{crit}$ then the null hypothesis can not be rejected.

For this case, the t-value calculated from the residuals of the two models is 40.0. The critical t-value for a DOF of 762 and significance level of 0.05 for a one-tailed test was found equal to 1.645 from tables. As the t-value is greater than the critical t-value, it can be concluded that there is a significant difference between the two means.

The variance of the two model scenarios can be compared via the variance ratio test using the F-distribution. For this test, the null and alternate hypotheses are as follows:

$$H_o : \frac{\sigma_1^2}{\sigma_2^2} = 1$$

$$H_A : \frac{\sigma_1^2}{\sigma_2^2} > 1$$

Where σ_1^2 is the variance of the two-dimensional models and σ_2^2 is the variance of the three-dimensional model. The sample variances are used to calculate the ratio, $\frac{s_1^2}{s_2^2}$. The ratio is compared against critical F-value determined from tables with $\nu_1 = n_1-1$, $\nu_2 = n_2 -$

1, which are the DOF of the numerator and denominator, respectively. If the ratio is greater than the critical F-value, then s_1^2 is deemed significantly larger than s_2^2.

The ratio of sample variances was determined equal to 1.76. The critical F-value for a DOF of 761 in the numerator and 761 in the denominator and at a significance level of 0.05 was found in the tables to be less than 1.25. The exact value at the desired DOF was not present in the table. However, the ratio of sample variances is greater than the critical F-value, and therefore it can be concluded that σ_1^2 is significantly greater than σ_2^2.

Through all of the statistical analyses comparing the means and the variances, showed a significant difference between the two-dimensional models and the three-dimensional model. The mean of the residuals of the three-dimensional model was found to be significantly lower than the mean of residuals of the two-dimensional models. Also, the variance of the residuals showed that the variance of the three-dimensional model was significantly lower than that of the two-dimensional models.

The difference between the two-dimensional and three-dimensional models is that the surrounding units and the cross-contamination between the aquifers are considered in the three-dimensional model. To determine whether the cross contamination between aquifers had an effect on the model results, two runs were conducted. One run ignores cross-contamination and the other considers cross-contamination. The runs were compared by determining the RMS error between the head and concentration for each model. For the Carbonate Aquifer, the RMS error between the head and concentration

results of the two models were 1.4 m and 7.2 mg/L, respectively. For the Sandstone Aquifer the RMS error for the head and concentration was 5.7 m and 0.13 mg/L.

The statistical analysis shows that there is a significant improvement from the three-dimensional model and the two-dimensional models. Comparing the models with and without the consideration of cross contamination shows that large changes occur in the heads within both the Carbonate and Sandstone Aquifers. The change in concentration is not that large at 7.2 mg/L and 0.13 mg/L for the Carbonate and Sandstone Aquifers, respectively. Therefore, it is concluded that the three-dimensional model is required to successfully model the region.

7.8 Sensitivity Analysis

To investigate how sensitive the final model was to the different boundary conditions and properties, the variables were investigated individually. For the flow model parameters, the assumed boundary conditions were varied while other conditions were maintained constant. The steady state flow results were determined and the RMS was calculated. By comparison of the RMS value with that of the initial model, the sensitivity of the model to the different parameters could be determined.

The value of the specified head on the western boundary of the Carbonate Aquifer was uncertain. The specified head was varied by 10% and 20% in both directions. A plot of the percent change in RMS versus percent change in equivalent freshwater head is presented in Figure 7.27. This plot illustrates that the flow results were significantly

affected by the value of the specified head on the western boundary condition. Decrease in equivalent freshwater head showed minimal change. However, an increase in equivalent freshwater head resulted in a significant increase in RMS.

The specified boundary condition on the west and south borders of the Sandstone Aquifer were investigated. The RMS of the overall three-dimensional model did not vary significantly as a result of the change in this boundary condition. However, as there were no historical observations for the Sandstone Aquifer, it was not surprising that the overall RMS did not change significantly. Therefore, the effect of this boundary was thought to be more significant than this test showed.

The specified flux boundary condition in the Birds Hill region was investigated and found to have no effect on steady state model. The Birds Hill recharge zone was localized, which may explain why this parameter had such small effect. The value of the specified flux boundary condition in the Interlake region was found to have an effect on the final model. This zone is quite extensive and is a major source of recharge to the aquifers. The percent change in RMS as a result of change in the value of the specified flux in the Interlake area is shown in Figure 7.28. Increases in Sandilands recharge were also found to have an effect on the flow model (see Figure 7.29), as this is also a significant recharge zone.

For the model, the K_z value was assumed to be 0.1 times the value of K_x. The effect of this assumption was evaluated on the steady-state flow model. Figure 7.30 shows a plot

of the percent change in RMS as a result of change in factor multiplied by K_x to calculate K_z. A value of $K_z = K_x$ was found to have a very slight effect on the resulting RMS. However, decreasing the factor used to calculate K_z was found to cause an increase in RMS. The lower value of K_z would cause a reduction in the vertical flow rate causing a decrease in the amount of recharge that reaches the aquifers.

To evaluate the sensitivity of the contaminant transport parameters, two cases were examined. The first was to examine the effects on the individual aquifers as these were used to assign initial conditions to the three-dimensional model. The second scenario investigated effects on the three-dimensional model stepping from 1920 to 1999, using the same initial condition.

The Carbonate Aquifer was found significantly affected by changes in longitudinal dispersivity. Effects of changing longitudinal dispersivity on the RMS error on the results are illustrated in Figure 7.31. The plot of percent change in RMS versus longitudinal dispersivity showed that a decrease in value did not have as much effect as when the value was increased. The transverse and vertical dispersivity values were not found to have an effect on this single aquifer scenario.

For the Sandstone Aquifer, it was also determined that the longitudinal dispersivity had an effect on the solute transport results. In a similar manner to that observed with the Carbonate Aquifer, a decrease in the longitudinal dispersivity had less effect than an increase (see Figure 7.31). The transverse dispersivity was found to have a slight effect

on the results (Figure 7.32). The vertical dispersivity was found to have no effect on the resulting solute transport model.

For the three-dimensional runs, the values of longitudinal, transverse and vertical dispersivities in the Carbonate and Sandstone Aquifers were found to have only a very slight effect. Since the model is stepping forward from the same initial condition, this result makes sense. The dispersion on the plume would not be greatly affected over such a short period in geological time. It was found that if the values of dispersivity were too low (< 100 m), then the model results were meaningless (relative concentration values greater than 1.0 and less than 0.0).

7.9 Summary

FRAC3DVS was the finite element code chosen to model the flow and transport in Southern Manitoba. The code was verified to ensure that the variable density aspect had been coded successfully.

Calibration targets were established prior to modeling. Individual models of both aquifers were constructed to provide approximate boundary conditions and hydrogeological parameters that were used in subsequent three-dimensional modeling.

The three-dimensional model was constructed accounting for all units. The Carbonate Aquifer hydraulic conductivity was assigned based on the Bayesian Updated field of transmissivity values and was fully heterogeneous. A lack of transmissivity

measurements in the Sandstone Aquifer resulted in a smooth BU field that could not reproduce the observed flow regime. Therefore, the region was zoned and hydraulic conductivity values were determined through calibration. The other units all had homogeneous hydraulic conductivity values. The remaining properties: porosity, storativity and dispersivity values were all homogeneous.

The flow model has very good results with an RMS error of 7.49 m for the steady state calibration and 10.4 m for the transient validation. This error was well within the allowable error of 20 m for the Sandstone Aquifer and 13 m for the Carbonate Aquifer. The residuals showed good scatter and very few data were outside the allowable interval. The transport model was within the allowable calibration target with a RMS of 2.9 g/L for the transient calibration. The model results within the higher ranges of the saltwater region however underestimated the concentration consistently. A summary of the different t-tests and RMS values are presented in Table 7.8.

Table 7.8 – Summary of RMS values and t-tests for each model calibration and history match.

	Carbonate Aquifer			**Sandstone Aquifer**		**3D Model**		
	Steady-state flow (1920)	**Flow History Match (1999)**	**Transport (1999)**	**Flow History Match (1999)**	**Transport (1999)**	**Steady-state flow (1920)**	**Flow History Match (1999)**	**Transport (1999)**
RMS	6.10 m	12.3 m	5.3 g/L	7.31 m	0.42 g/L	7.49 m	10.4 m	2.9 g/L
Slope (log)	1.00	0.71	0.30 1.17	0.83	0.06 0.04	0.92	1.13	0.64 0.50
Intercept	-1.56	65.3	0.014 0.25	44.1	0.0018 3.5	23.6	-28.1	0.0014 -1.40
R^2	0.73	0.59	0.24 0.26	0.96	0.0003	0.75	0.82	0.57 0.20
DOF	124	71	602	3	161	124	76	771
$t_{crit}(\alpha/2)$ (log)	1.96 (0.025)	1.96 (0.025) 3.46 (0.005)	1.96 (0.025) 3.46 (0.005)	3.182 (0.025)	1.96 (0.025) 3.46 (0.005)	1.98 (0.025)	2.0 (0.025)	1.96 (0.025)
t_{slope} (log)	**0.039**	3.61	19.5 *2.15*	**1.13**	*2.9* 13.7	**1.13**	**2.00**	15.1 12.1
$t_{intercept}$ (log)	**0.112**	*3.45*	4.97 **0.91**	**1.2**	*3.40* 13.6	**1.43**	**1.83**	**0.98** 11.3
t_{R2}	**18.2**	**10.0**	**13.68**	**8.73**	0.22	**19.24**	**18.4**	**32.2**

- Numbers marked in bold indicate that t-test is passed at 0.05 significance level.
- Numbers in italics indicate that t-test is passed at 0.001 significance level.

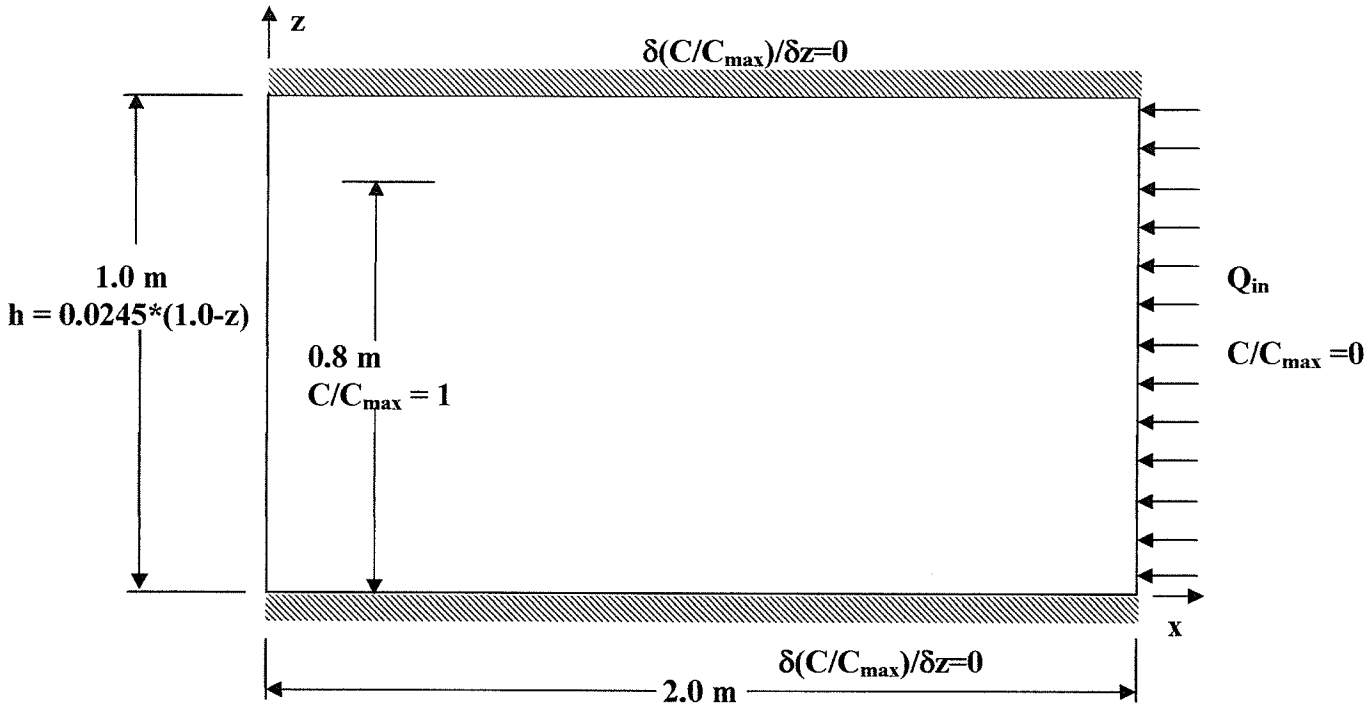

Figure 7.1 – System definition for Henry's problem.

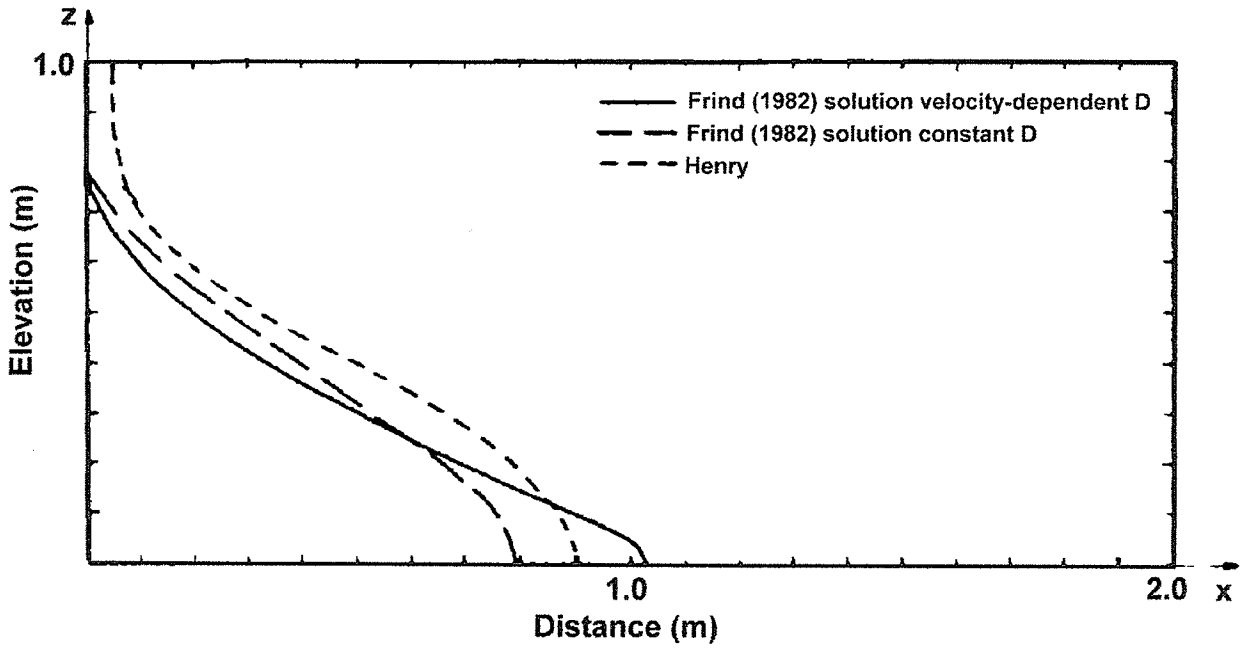

Figure 7.2 – Henry problem results from analytical solution of Henry and Frind (1982) solution (taken from Frind (1982)).

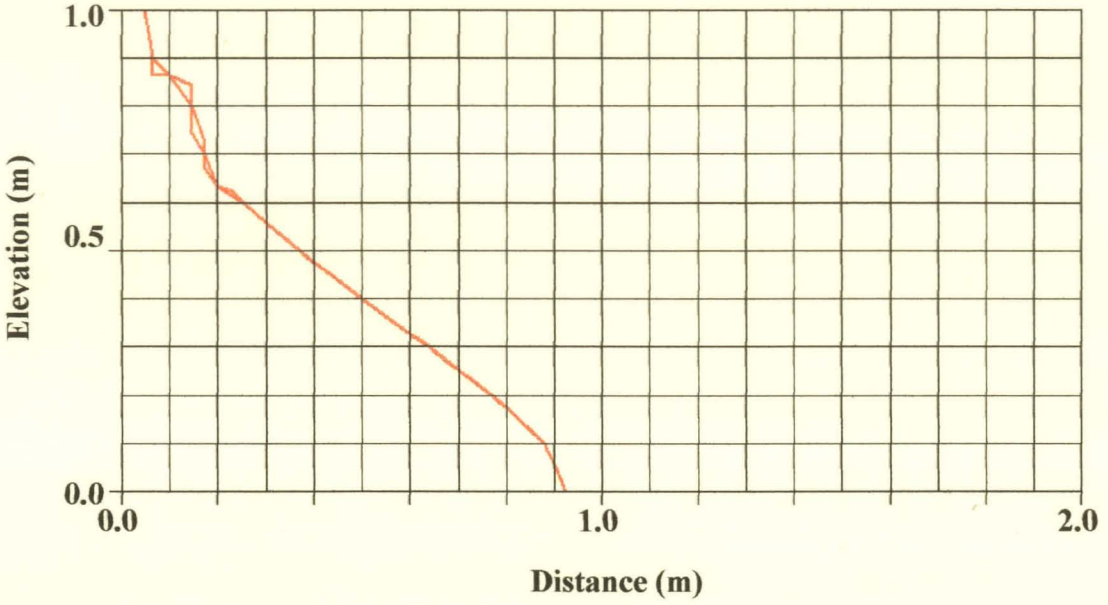

Figure 7.3 – Position of 0.5 isochlor at steady state with a 0.1 m grid generated from FRAC3DVS.

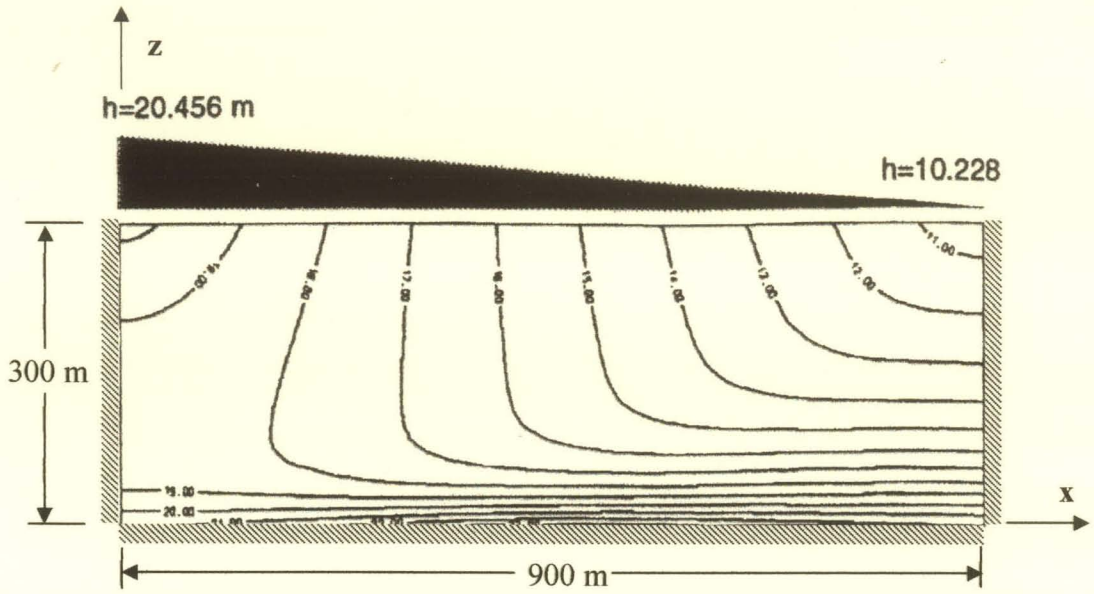

(A)

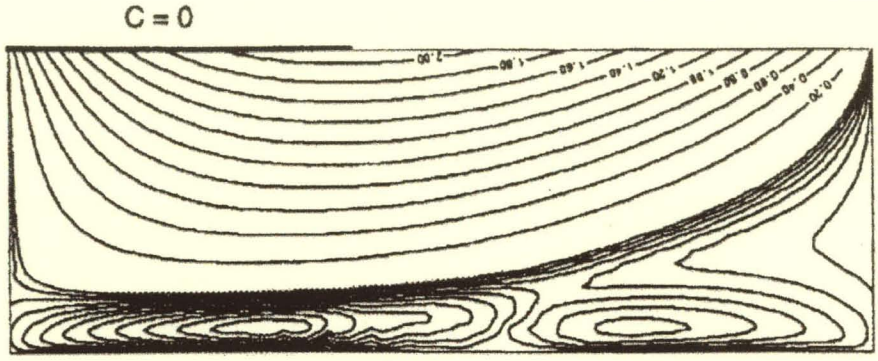

(B)

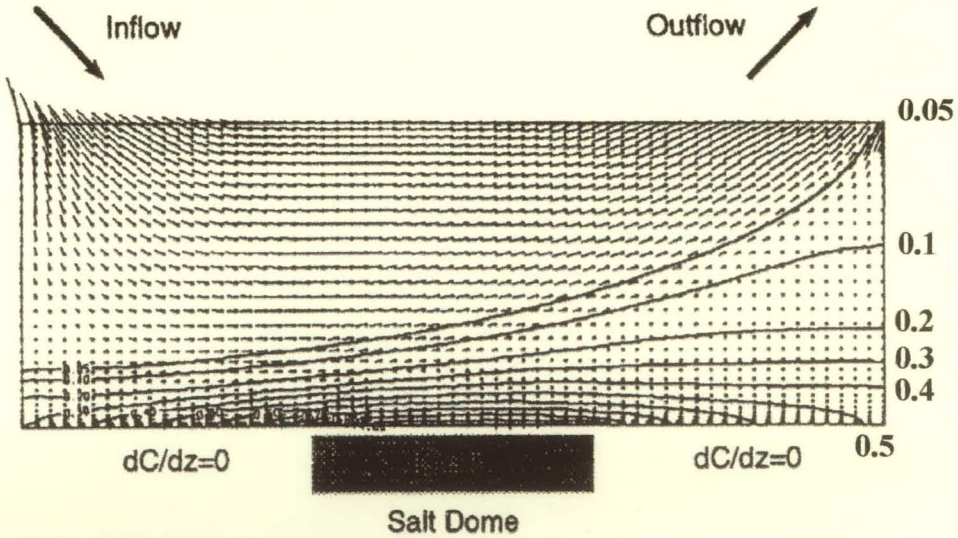

Figure 7.4 – Salt dome problem, showing domain and boundary conditions: (A) hydraulic head; (B) streamline; (C) velocity and relative concentration contours (taken from Kolditz et al., 1998).

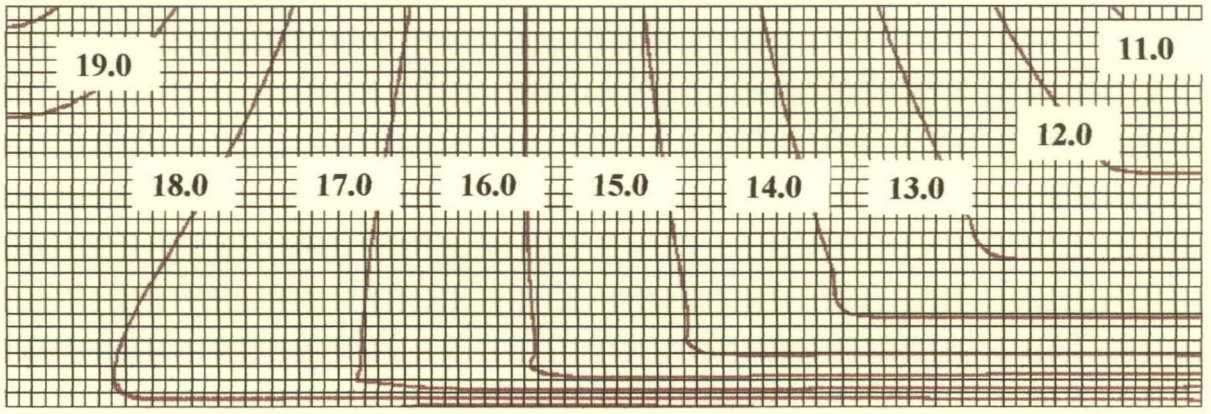

(A)

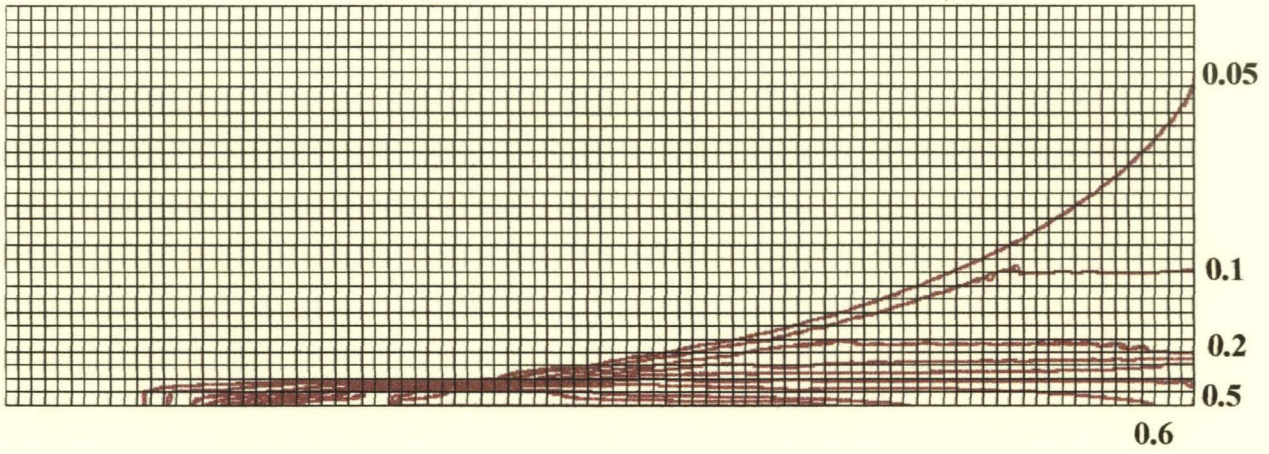

(B)

Figure 7.5 – Salt dome problem (A) total head contours and (B) relative concentration contours from FRAC3DVS.

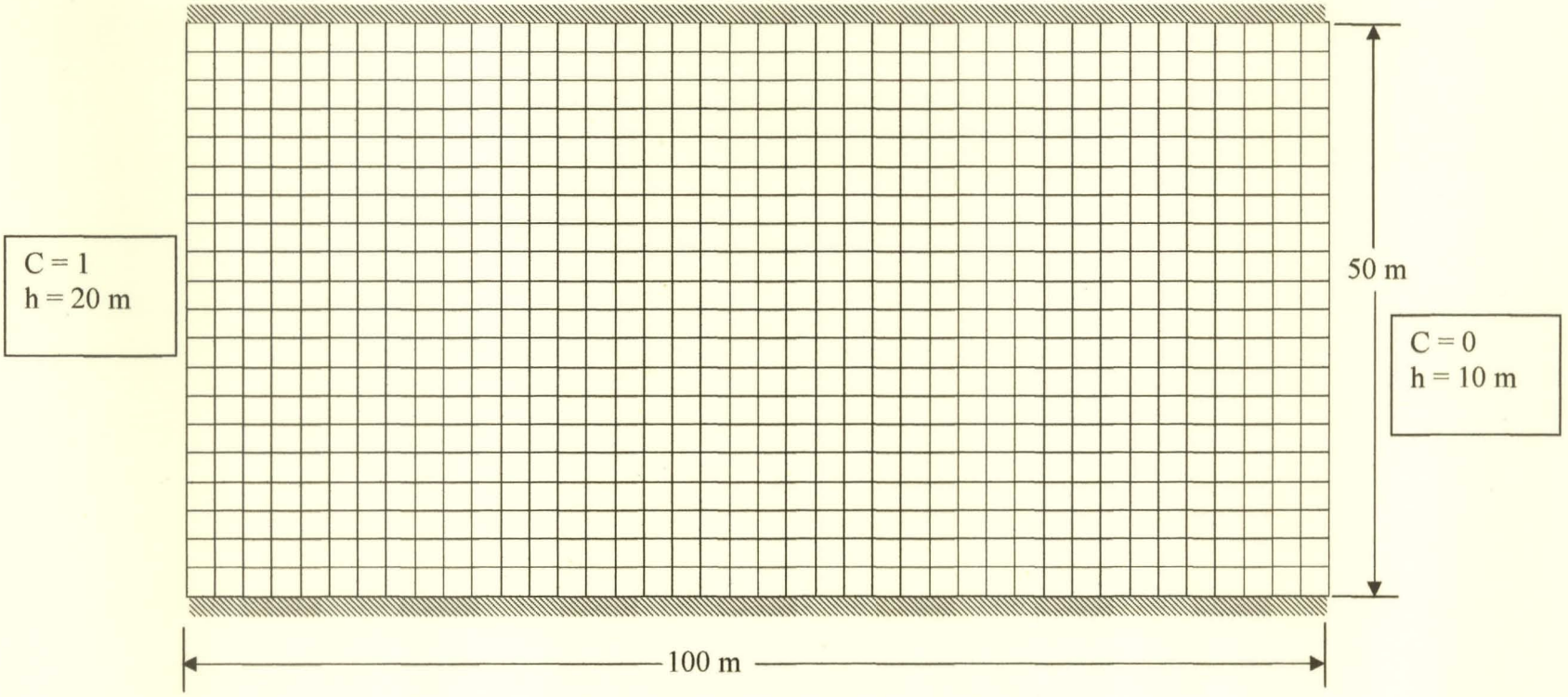

Figure 7.6 – Geometry of problem used for comparison between FEMWATER and FRAC3DVS.

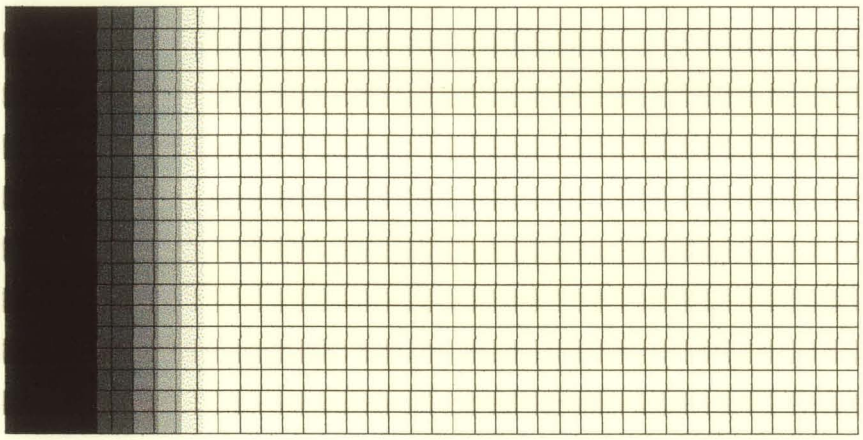

(A)

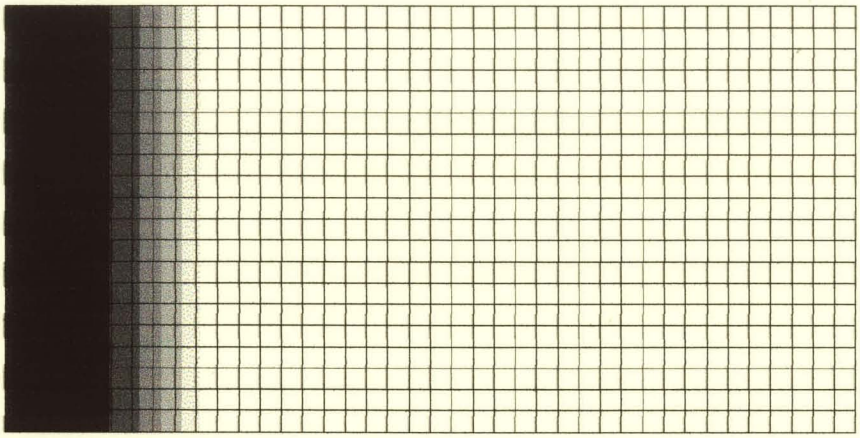

(B)

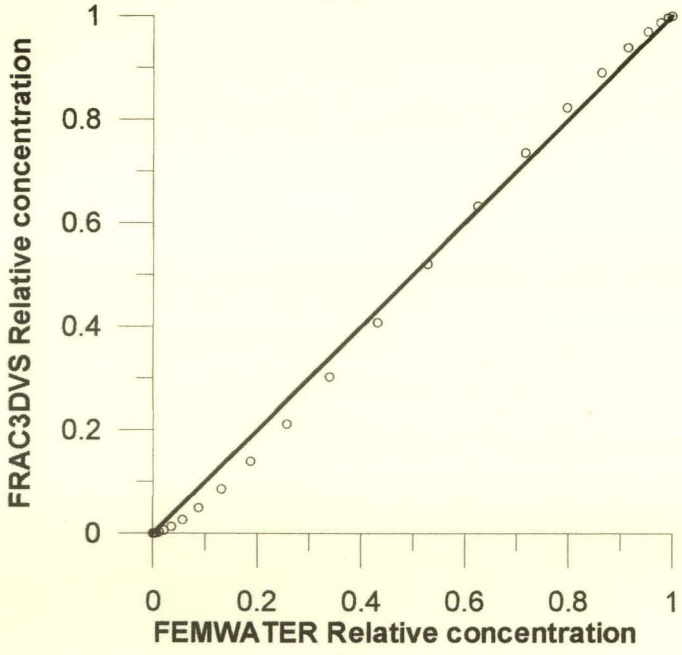

(C)

Figure 7.7 – FEMWATER and FRAC3DVS results for comparison for first examined case.

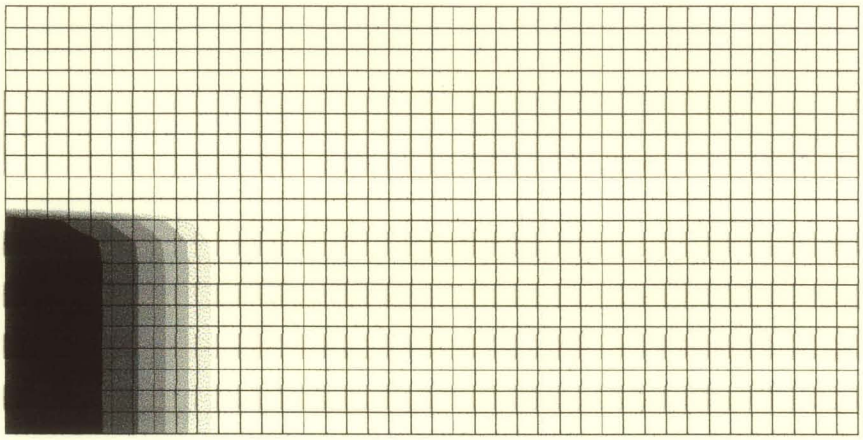

(A)

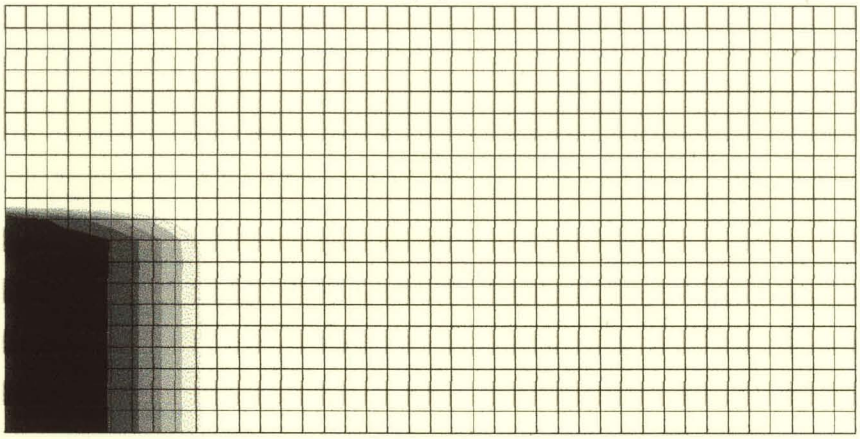

(B)

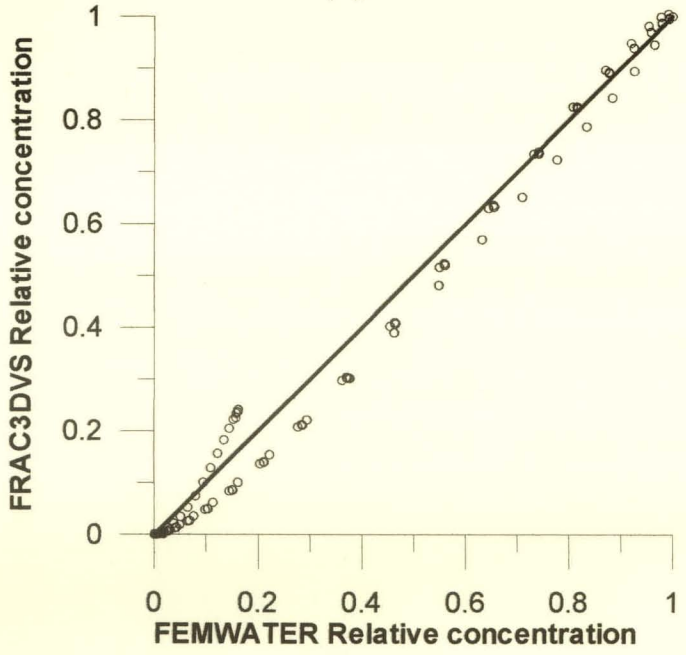

(C)

Figure 7.8 - FEMWATER and FRAC3DVS results for comparison for second examined case.

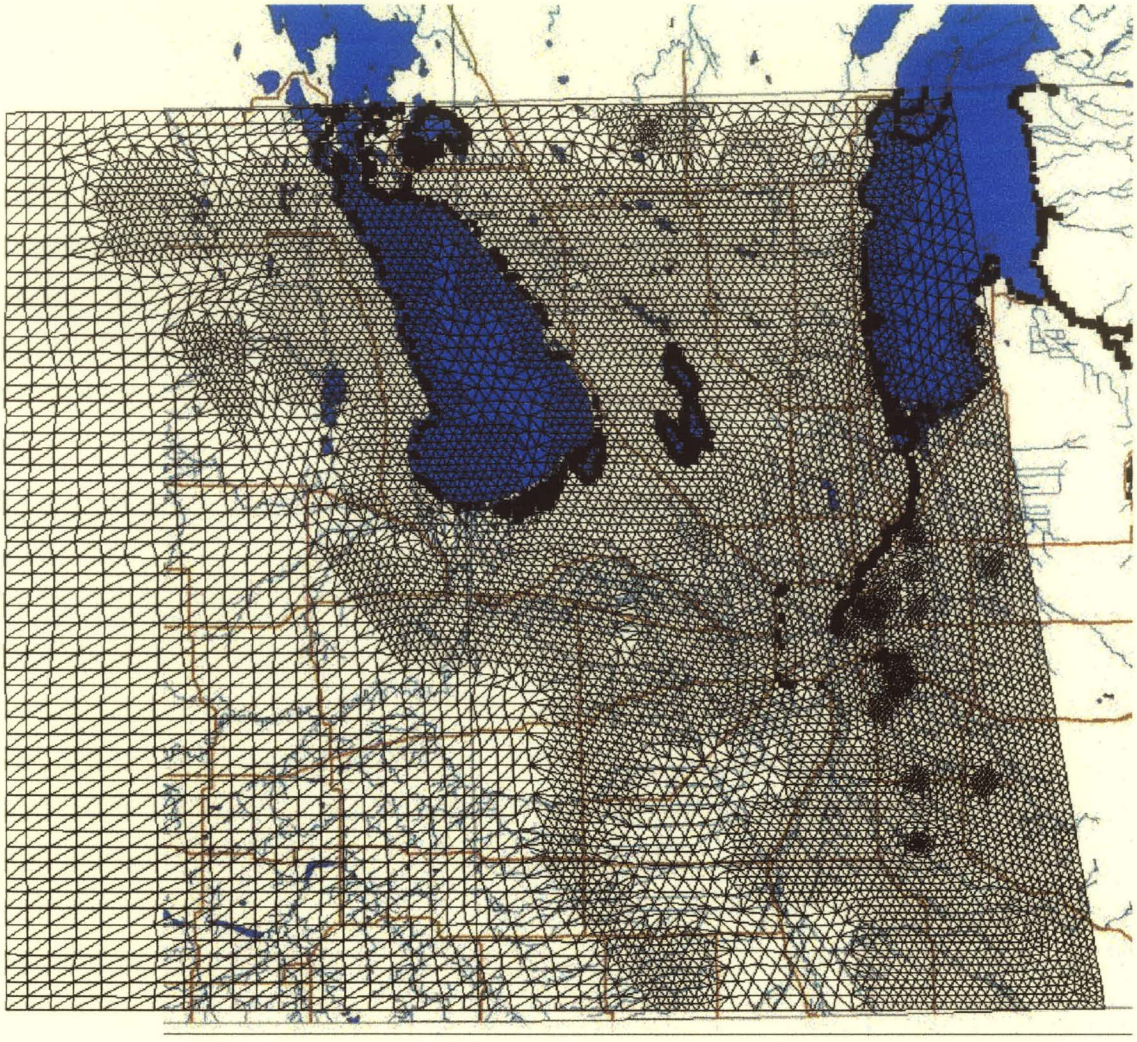

Figure 7.9 – Plan view of the finite element mesh.

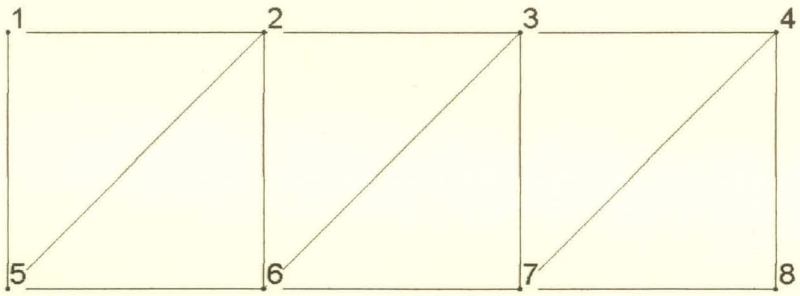

(A)

Node	1	2	3	4	5	6	7	8
Bottom	-1.0	0.0	2.0	3.0	-1.0	0.0	2.0	3.0
Top of Layer 1	2.0	2.0	3.5	5.0	2.0	2.0	3.5	5.0

(B)

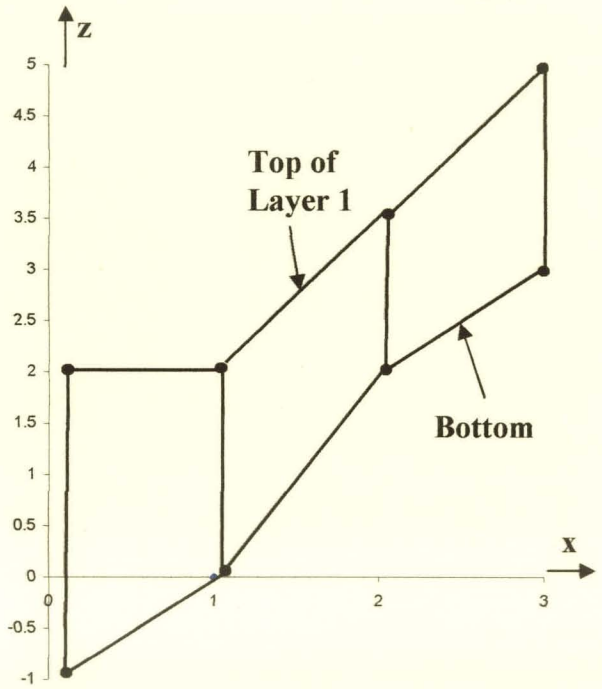

(C)

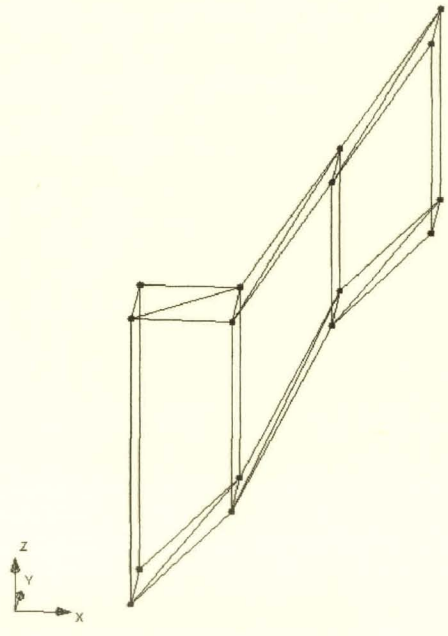

(D)

Figure 7.10 – Example of 3D mesh construction. (A) Initial 2D mesh with node numbers; (B) Table showing elevations of each node for a one layer 3D mesh; (C) Side view of resulting 3D mesh with elevations; and (D) Final 3D mesh.

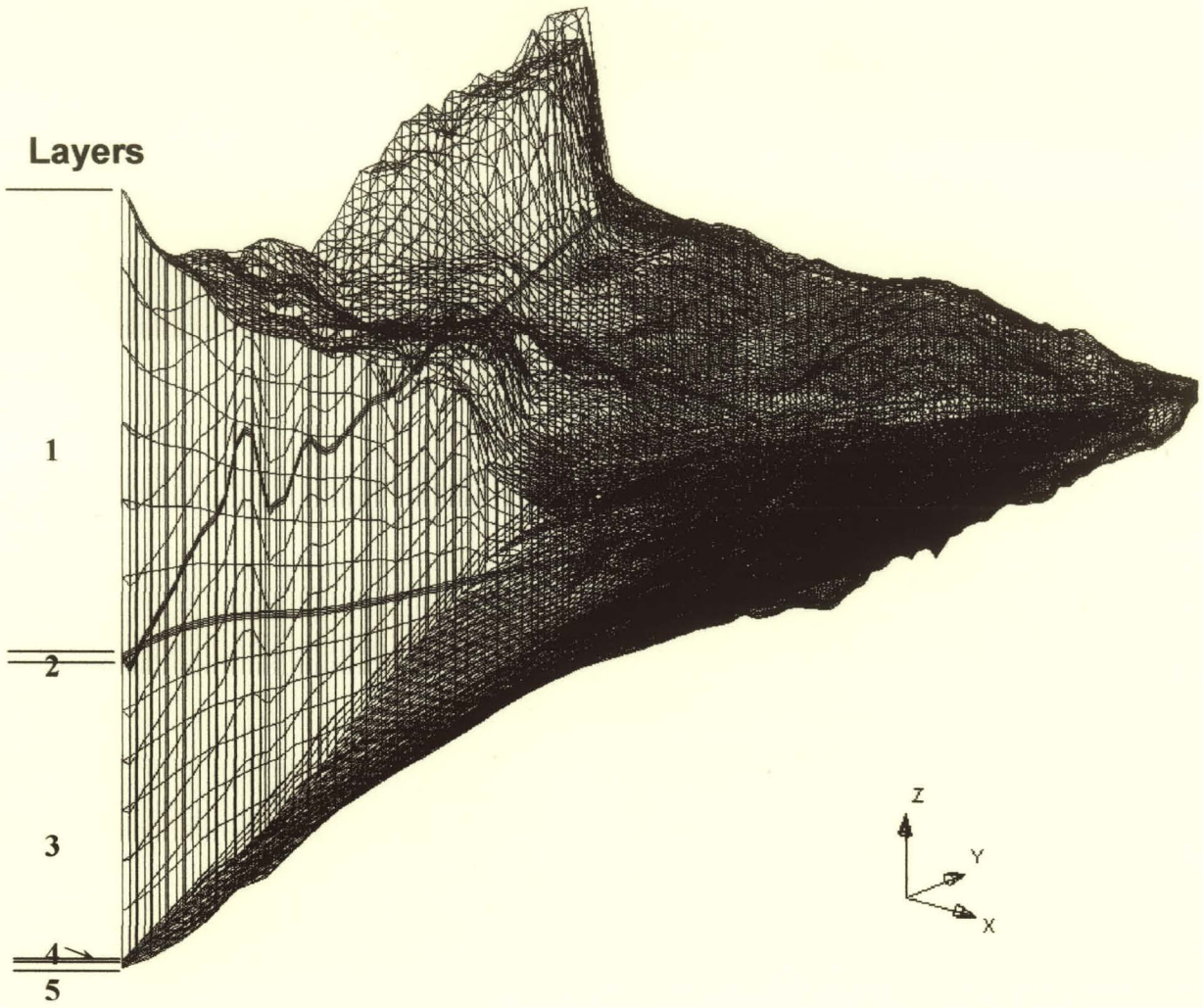

Figure 7.11 – Three-dimensional finite element mesh with 150x vertical exaggeration.

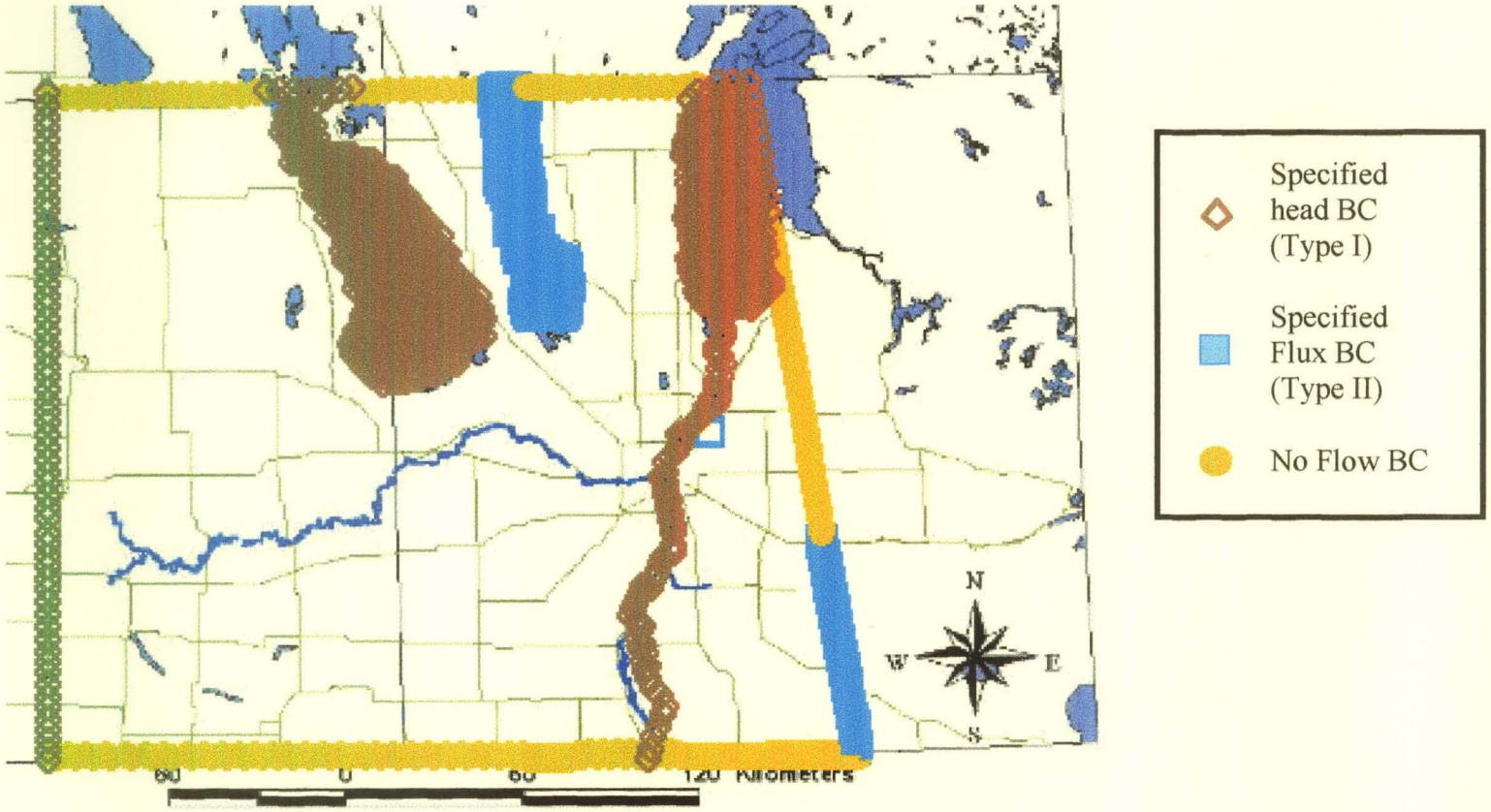

Figure 7.12 – Carbonate Aquifer boundary conditions used in flow model.

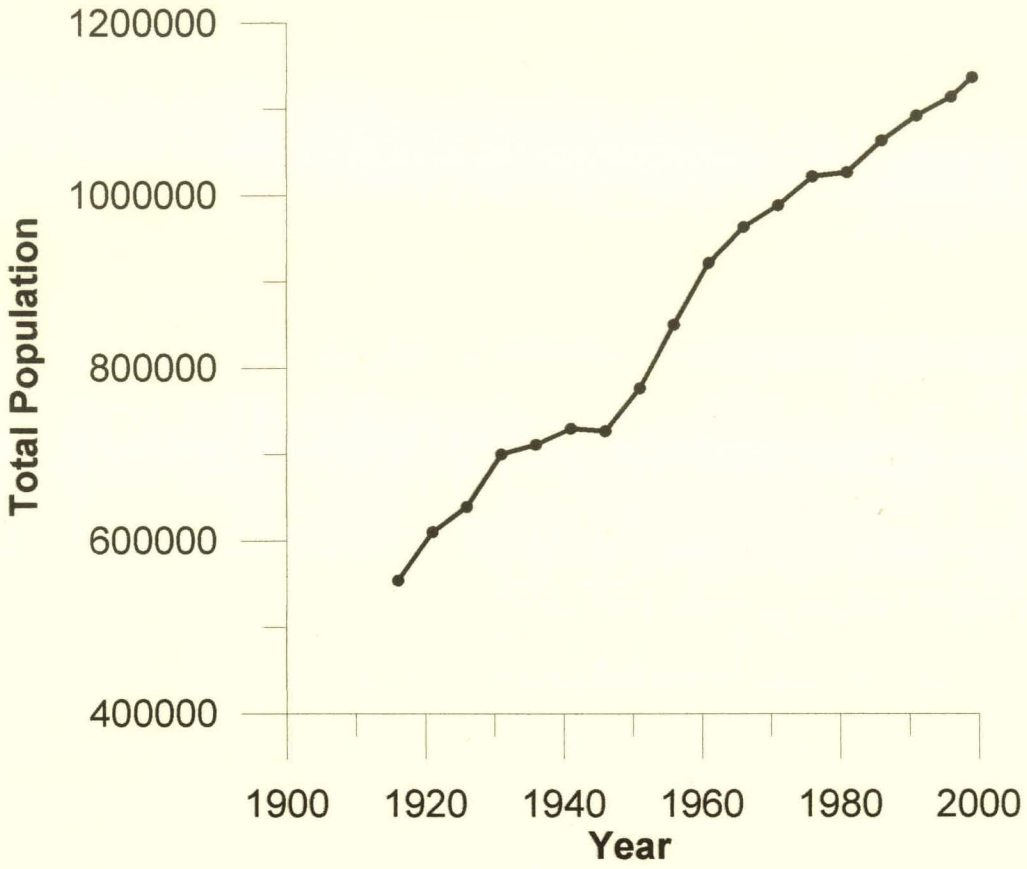

Figure 7.13 – Population of Manitoba between 1916 and 1999 from Census Data.

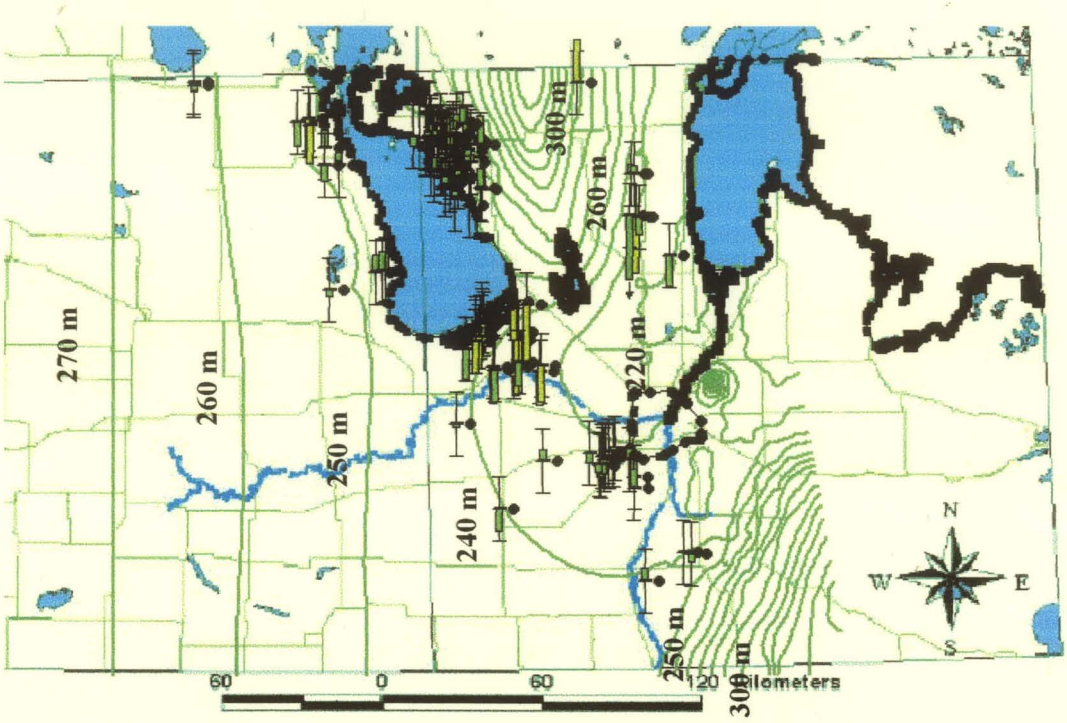

(A)

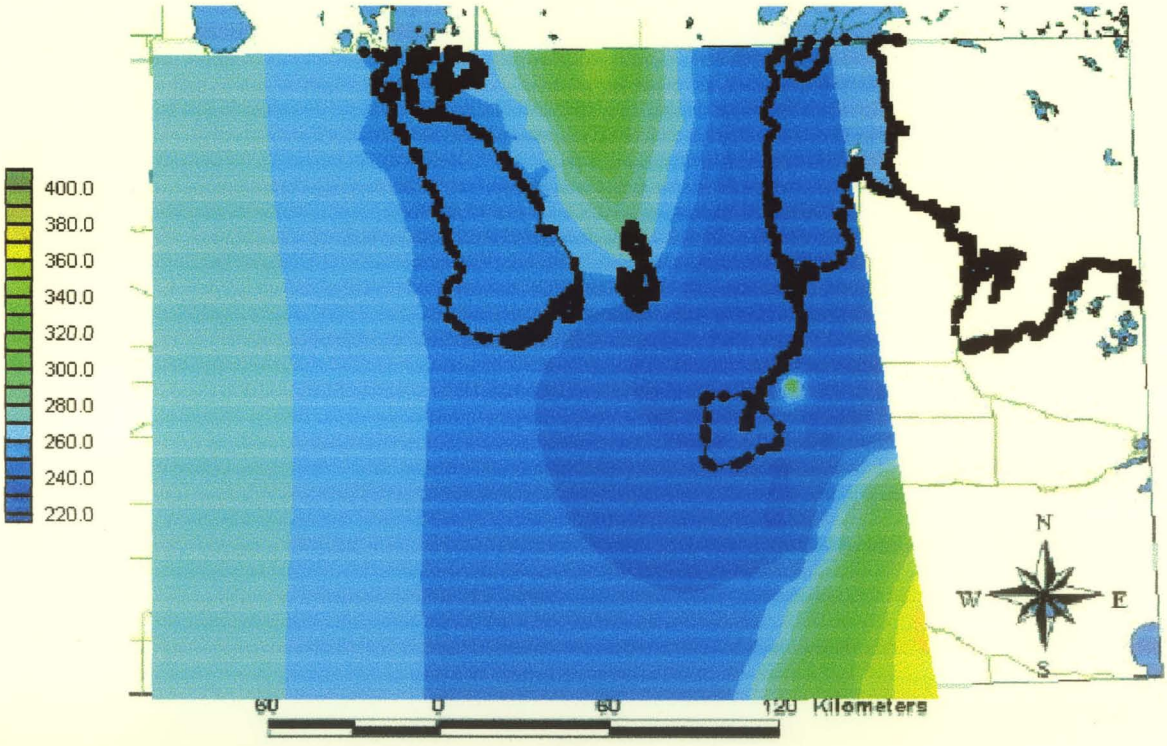

(B)

Figure 7.14 – Carbonate Aquifer steady state (Year = 1920) equivalent freshwater head results. (A) Contours with observation points; (B) Flow directions; (C) Plot of computed versus observed values; and (D) Plot of residuals (RMS = 6.10 m, R^2 = 0.7279, slope = 1.0022, and intercept = -1.5632).

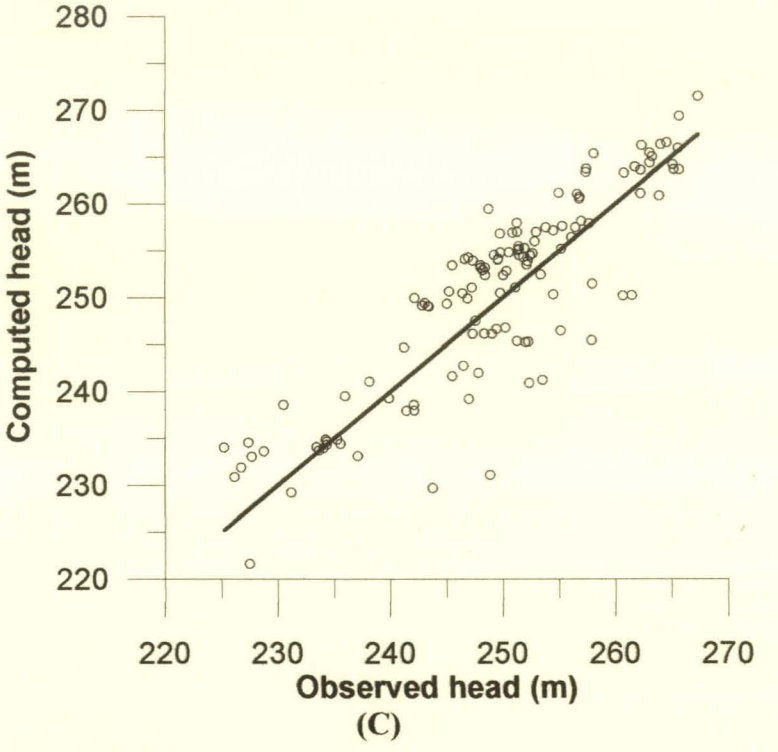

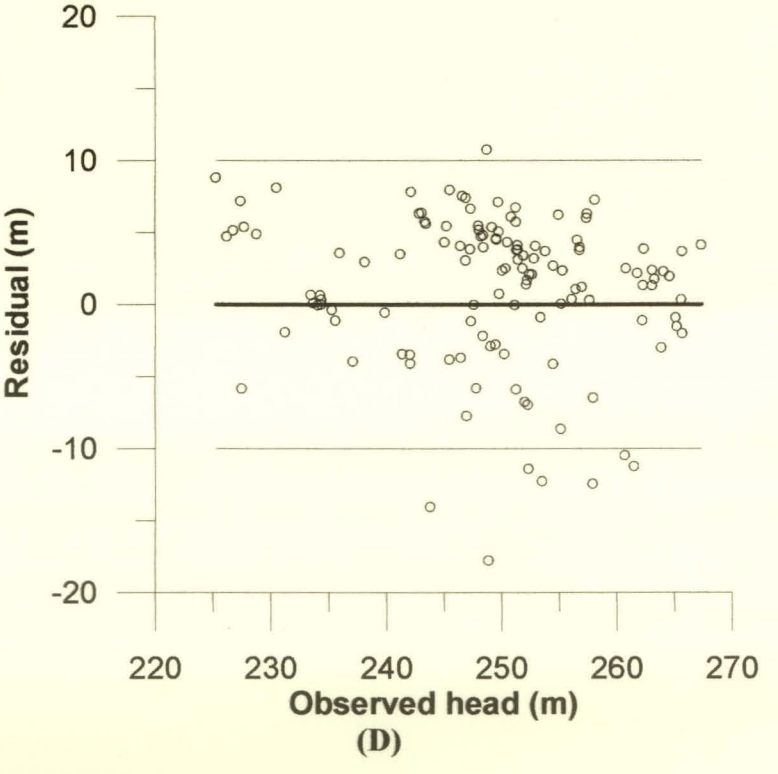

Figure 7.14 (continued) – Carbonate Aquifer steady state (Year = 1920) equivalent freshwater head results. (A) Contours with observation points; (B) Flow directions; (C) Plot of computed versus observed values; and (D) Plot of residuals (RMS = 6.10 m, R^2 = 0.7279, slope = 1.0022, and intercept = -1.5632).

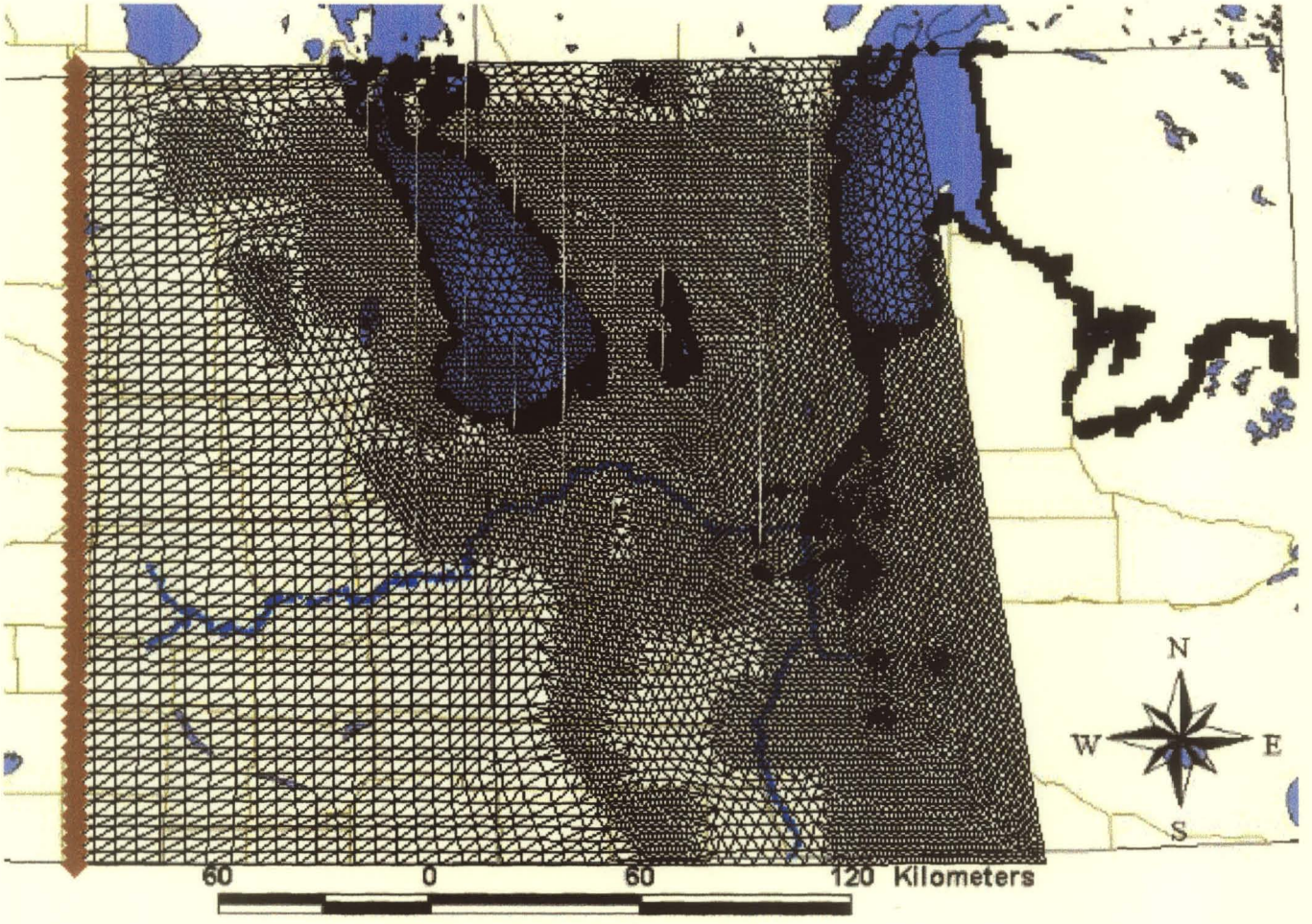

Figure 7.15 – Carbonate and Sandstone Aquifers solute transport boundary conditions for two-dimensional models.

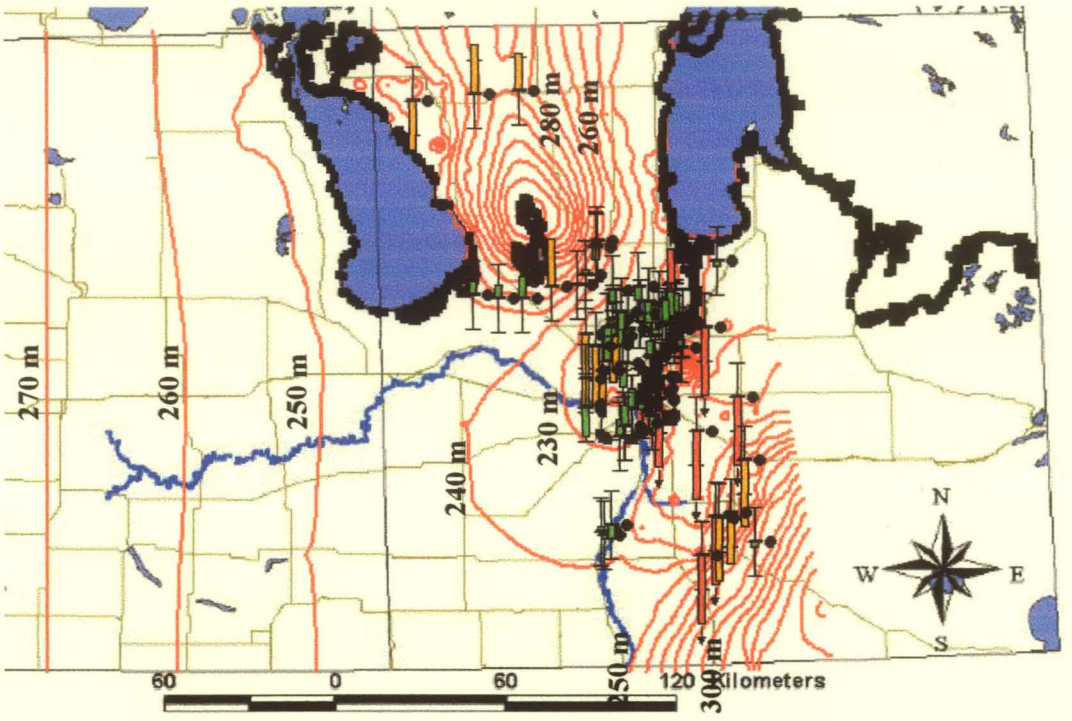

(A)

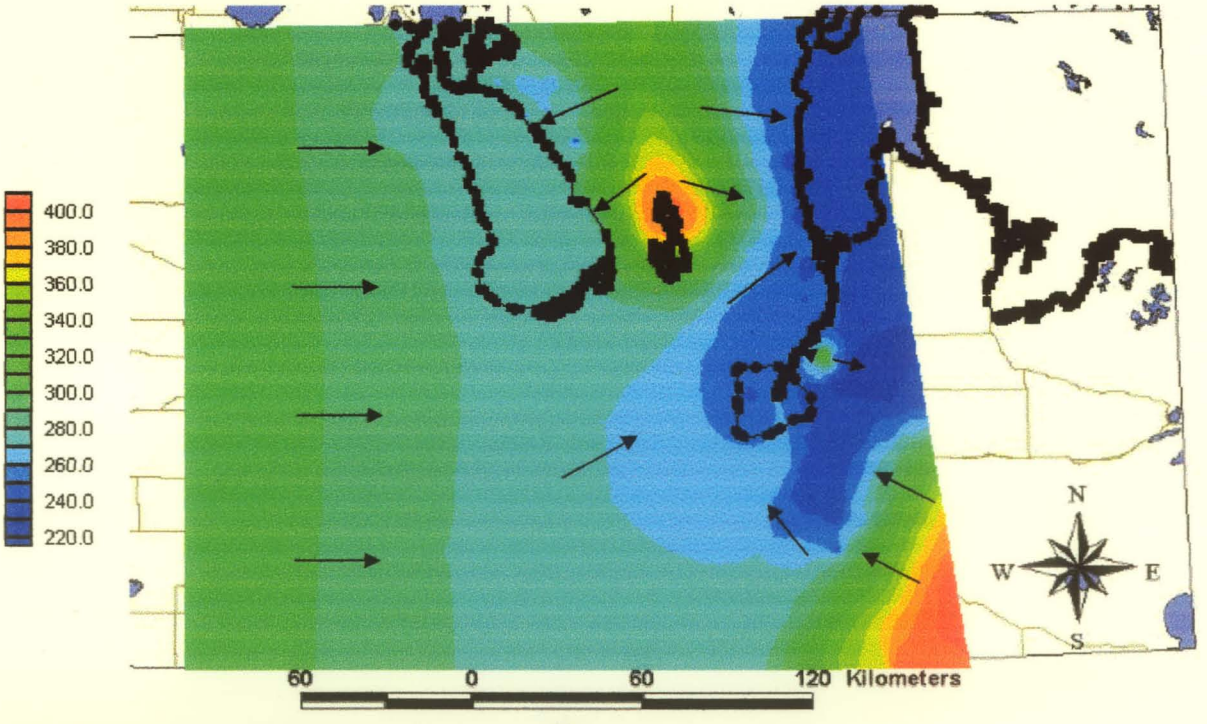

(B)

Figure 7.16 – Carbonate Aquifer equivalent freshwater head results at 1999. (A) Contours with observation wells; (B) Flow directions; (C) Plot of computed versus observed values; and (D) Plot of residuals (RMS = 12.27 m, R^2 = 0.5864 and slope = 0.7092).

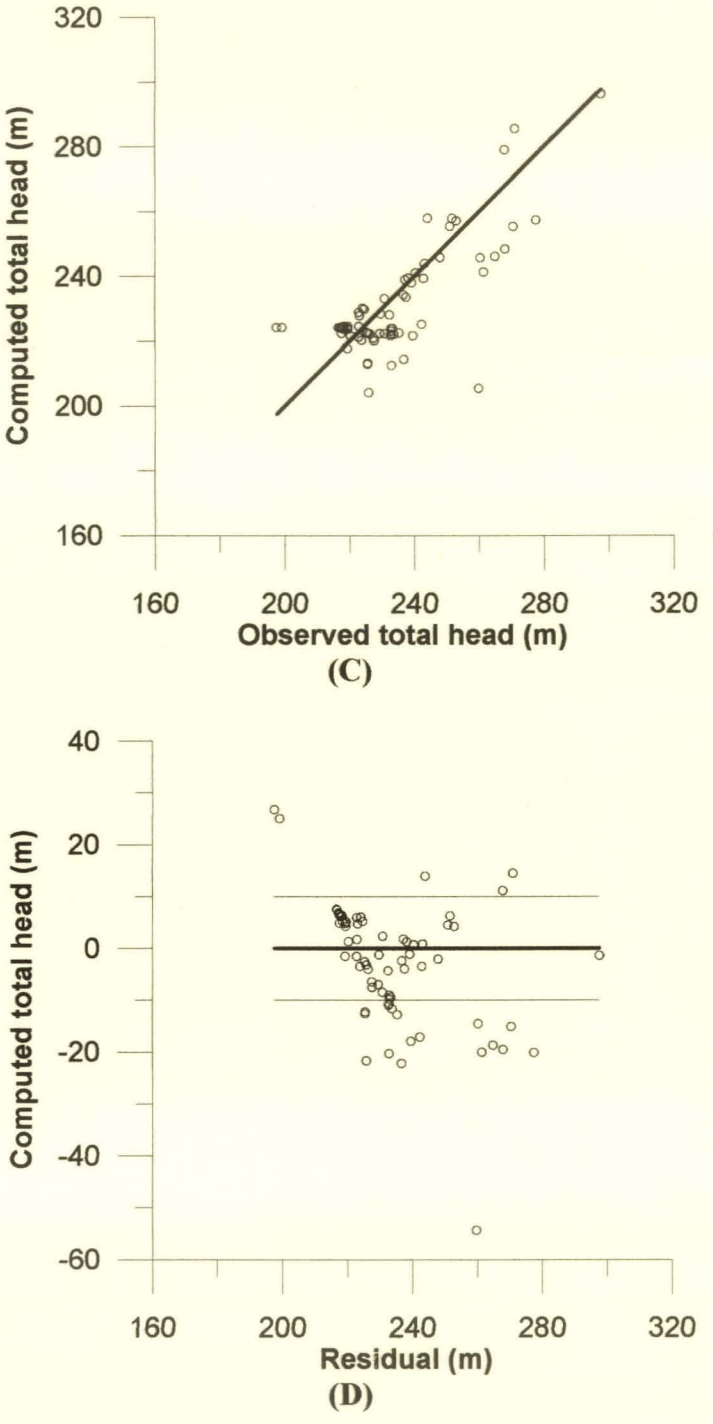

Figure 7.16 (continued) – Carbonate Aquifer equivalent freshwater head results at 1999. (A) Contours with observation wells; (B) Flow directions; (C) Plot of computed versus observed values; and (D) Plot of residuals (RMS = 12.27 m, R^2 = 0.5864 and slope = 0.7092).

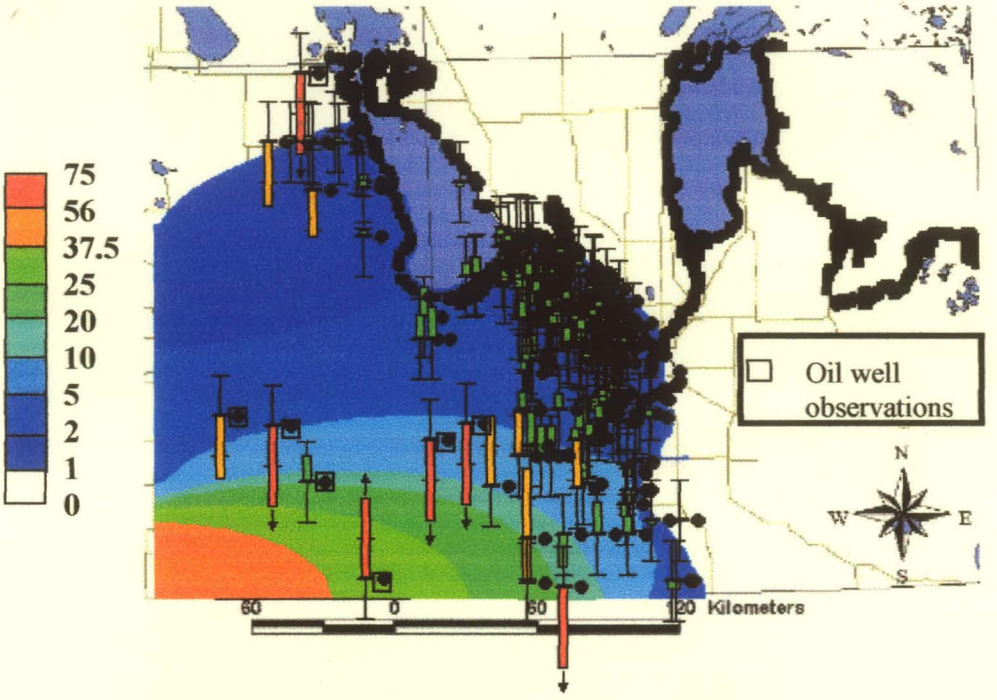

(A)

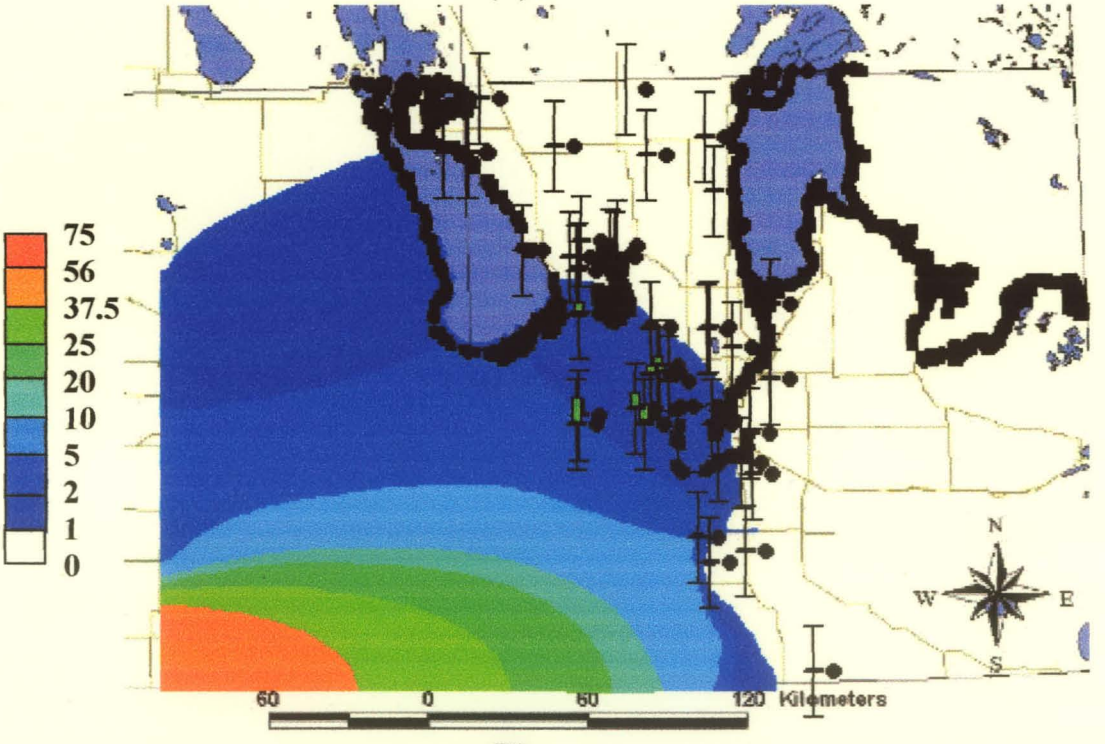

(B)

Figure 7.17 – Carbonate Aquifer concentration (g/L) results for year 1999 for transient calibration; (A) Filled contours with observations that have absolute residual greater than 7.5 g/L; (B) Contours with observation intervals that are within the aquifer alone; (C) Plot of computed versus observed values; (D) Plot of computed versus observed values on log-log scale; (E) Plot of computed versus observed values for wells within aquifer alone on log-log scale; and (F) Residual plot on log scale (RMS = 5.25 g/L).

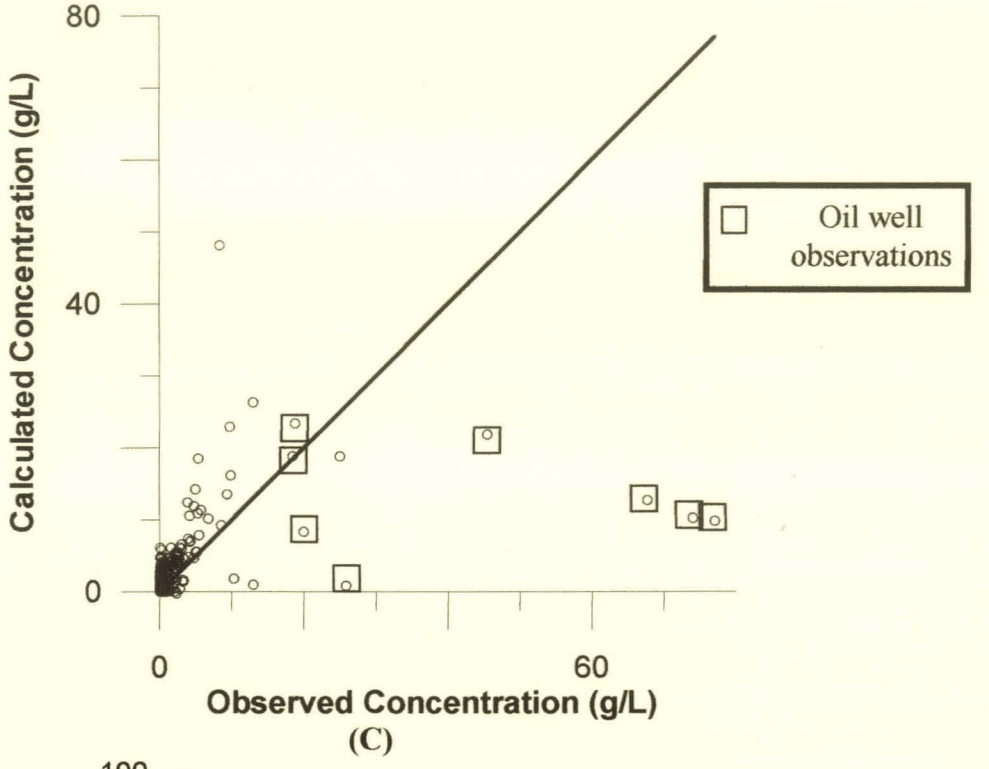

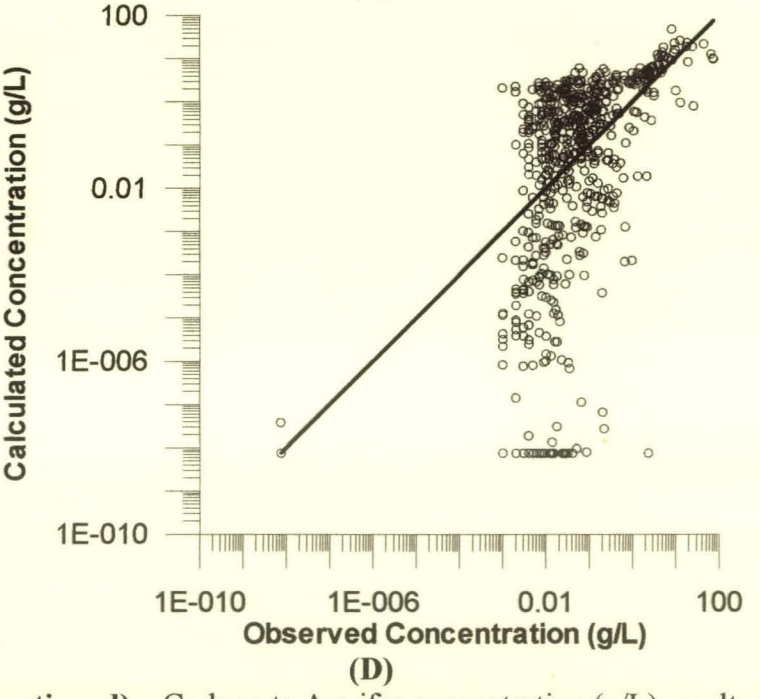

Figure 7.17 (continued) – Carbonate Aquifer concentration (g/L) results for year 1999 for transient calibration; (A) Filled contours with observations that have absolute residual greater than 7.5 g/L; (B) Contours with observation intervals that are within the aquifer alone; (C) Plot of computed versus observed values; (D) Plot of computed versus observed values on log-log scale; (E) Plot of computed versus observed values for wells within aquifer alone on log-log scale; and (F) Residual plot on log scale (RMS = 5.25 g/L).

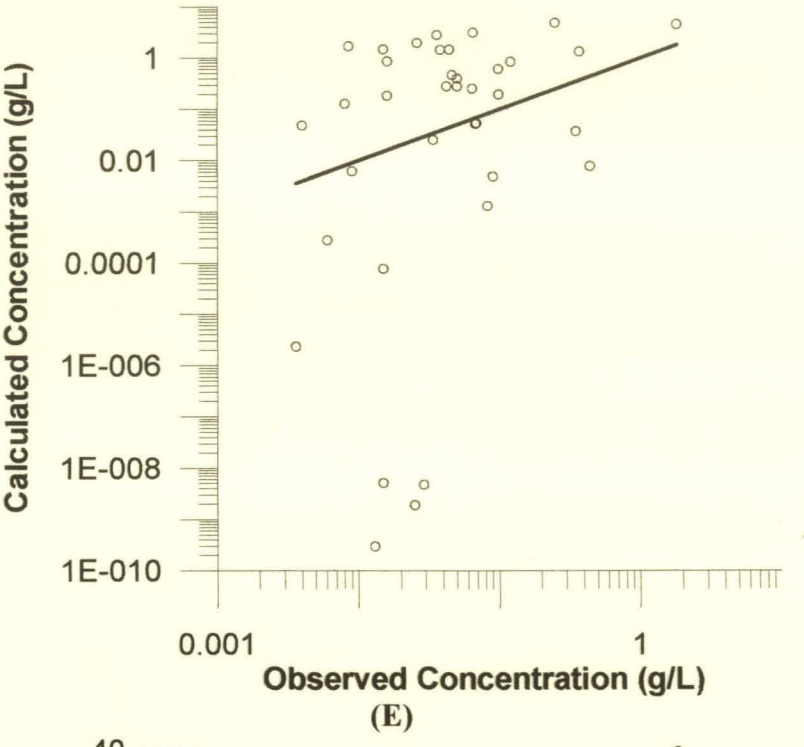

(E)

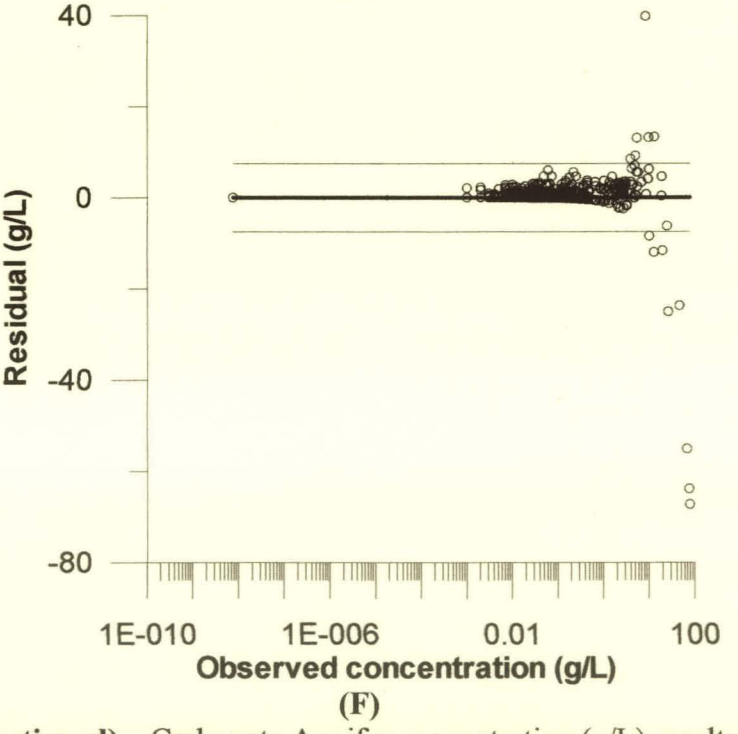

(F)

Figure 7.17 (continued) – Carbonate Aquifer concentration (g/L) results for year 1999 for transient calibration; (A) Filled contours with observations that have absolute residual greater than 7.5 g/L; (B) Contours with observation intervals that are within the aquifer alone; (C) Plot of computed versus observed values; (D) Plot of computed versus observed values on log-log scale; (E) Plot of computed versus observed values for wells within aquifer alone on log-log scale; and (F) Residual plot on log scale (RMS = 5.25 g/L).

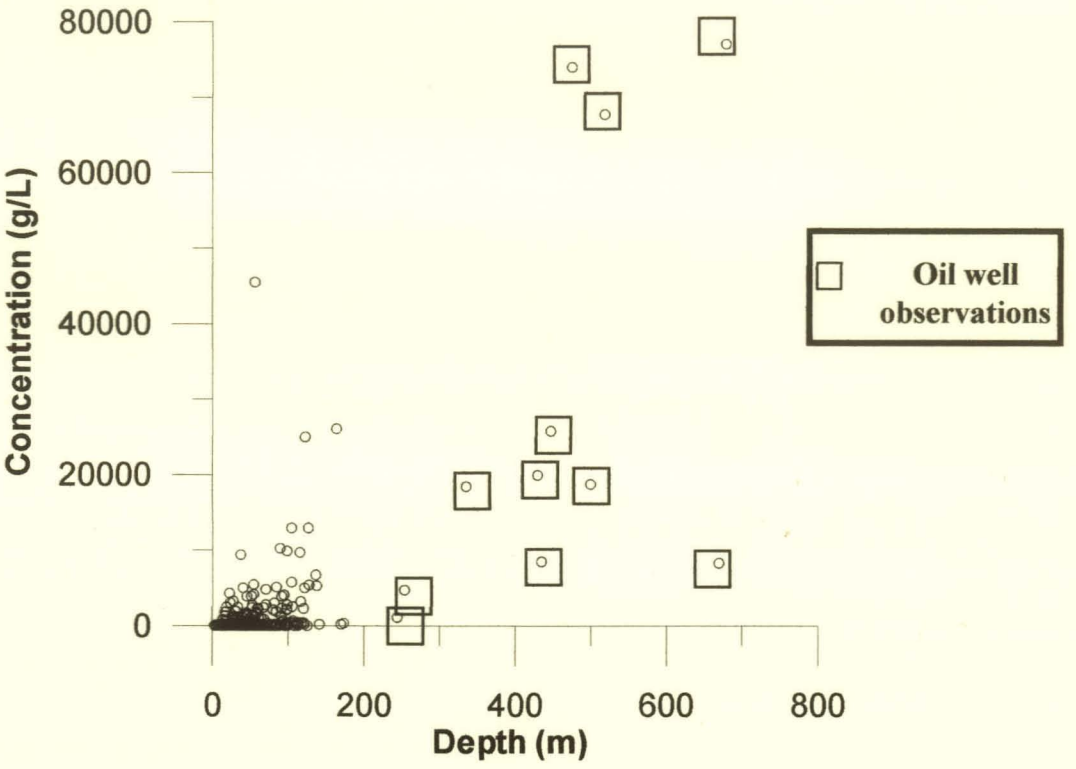

Figure 7.18 – Concentration measurements from Carbonate Aquifer as a function of sampling depth.

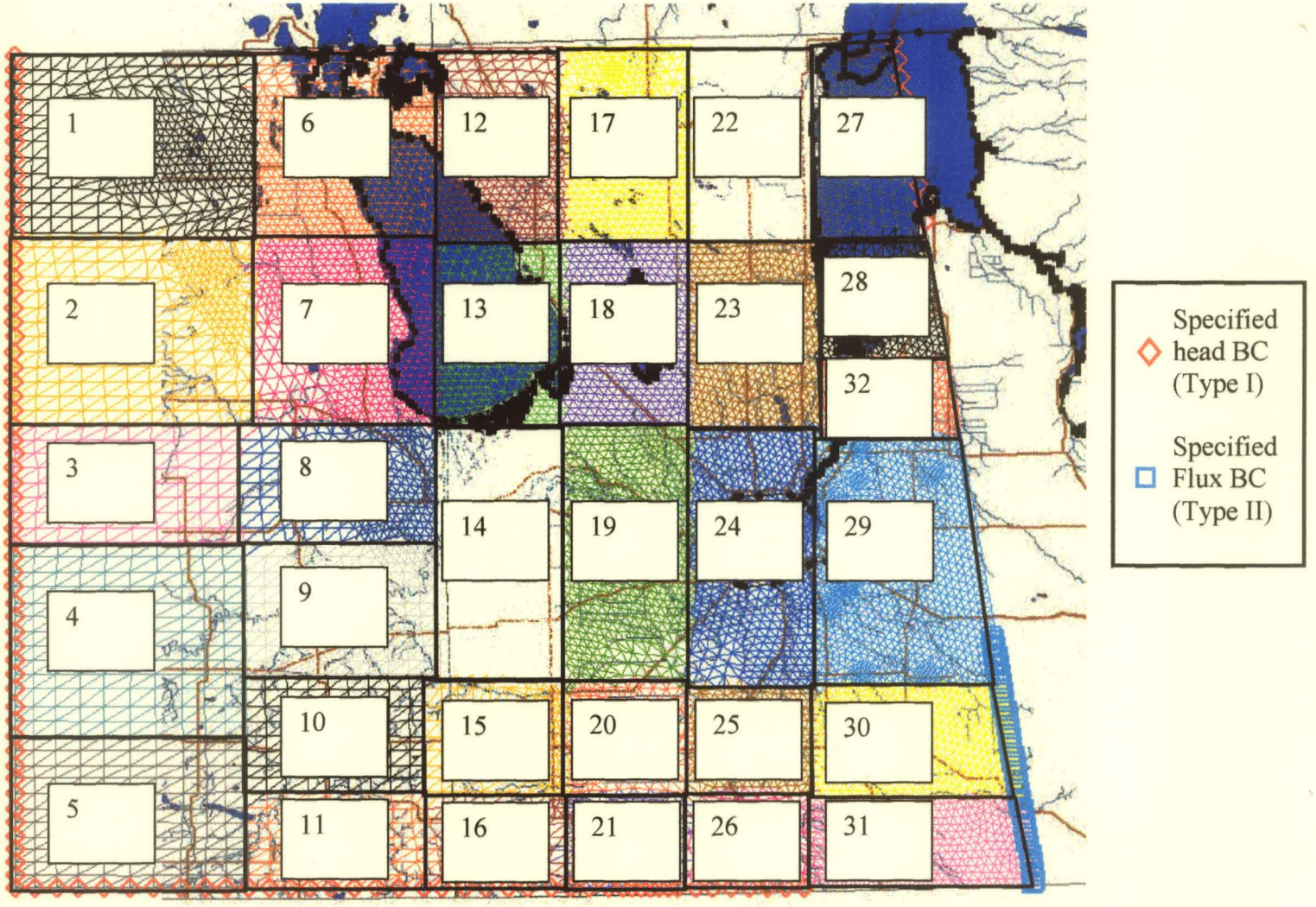

Figure 7.19 – Sandstone Aquifer flow boundary conditions and hydraulic conductivity zones.

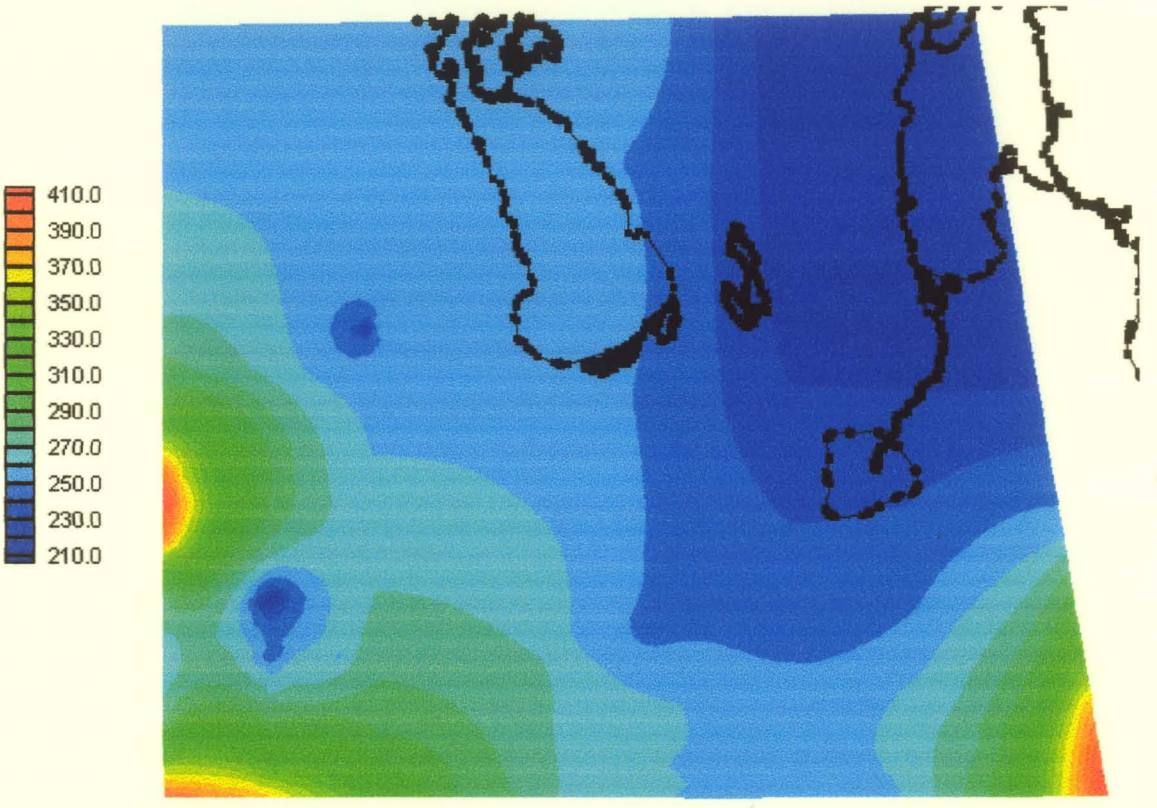

Figure 7.20 – Sandstone Aquifer equivalent freshwater head contours at steady state.

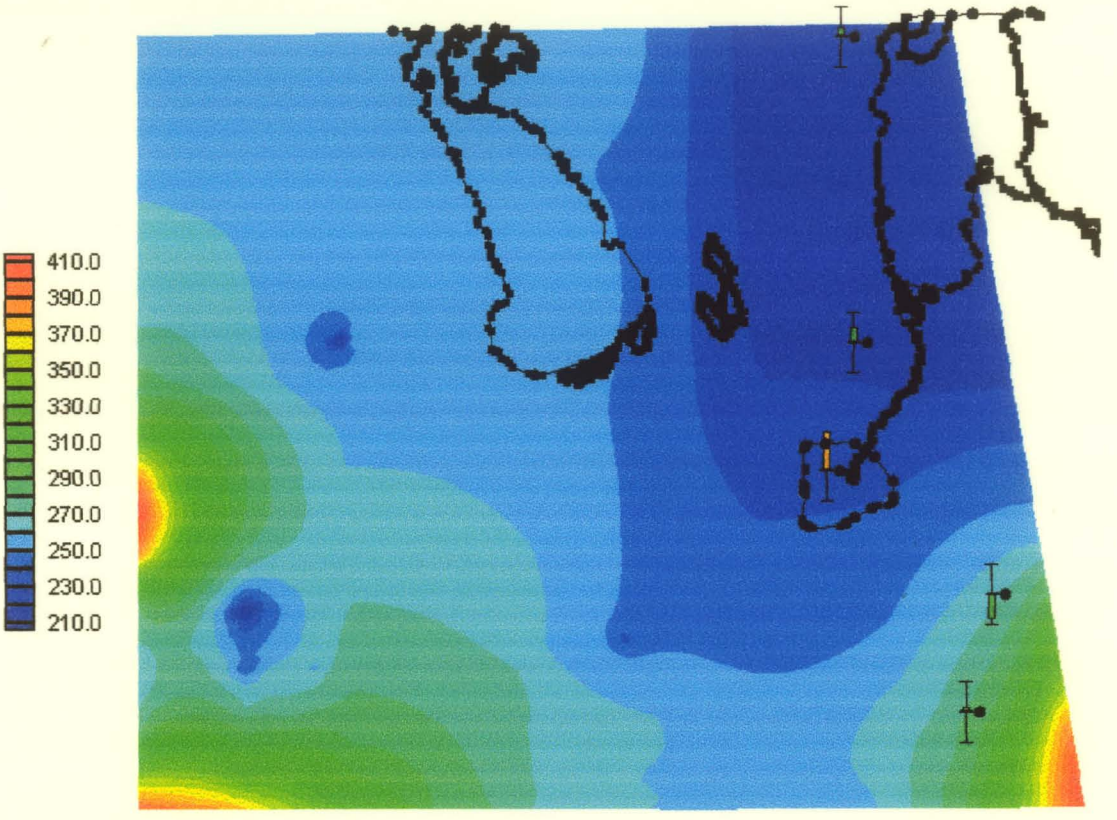

(A)

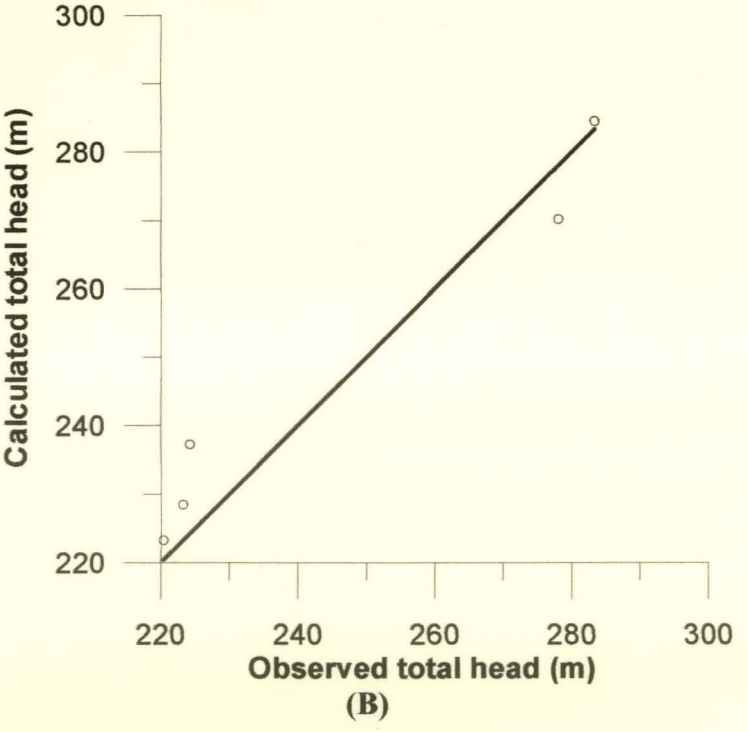

(B)

Figure 7.21 – Sandstone Aquifer equivalent freshwater head model results at T= 1999, showing (A) Contours with observation points; (B) Plot of computed versus observed values and (C) Plot of residuals (RMS = 7.31 m, R^2 = 0.96, slope = 0.832, intercept = 44.16).

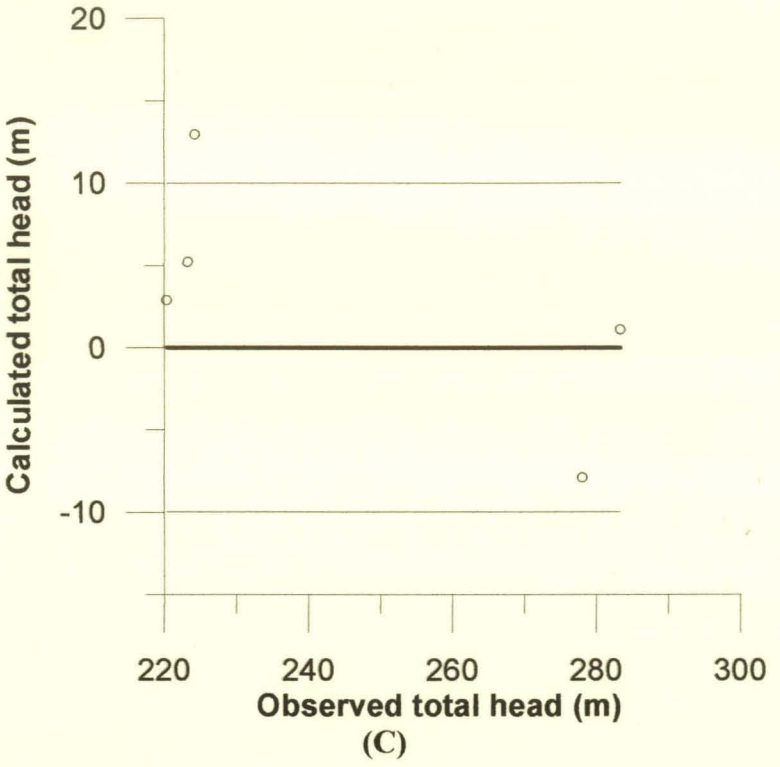

Figure 7.21 (continued) – Sandstone Aquifer equivalent freshwater head model results at T= 1999, showing (A) Contours with observation points; (B) Plot of computed versus observed values and (C) Plot of residuals (RMS = 7.31 m, R^2 = 0.96, slope = 0.832, intercept = 44.16).

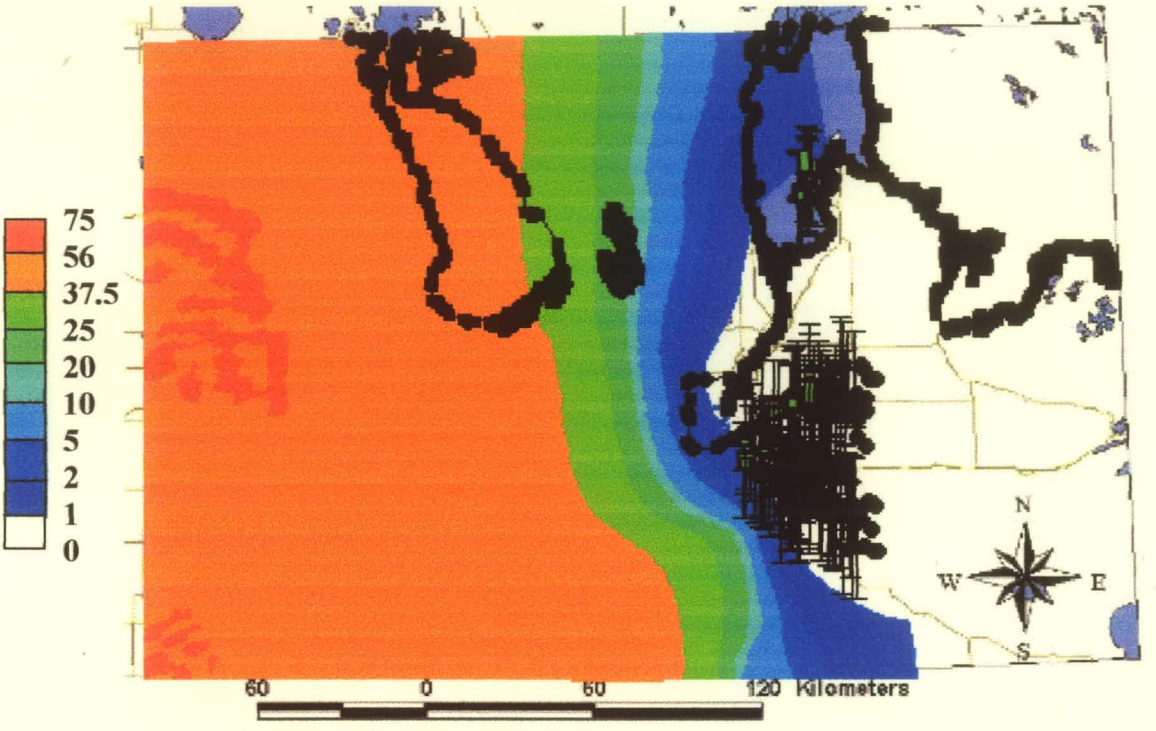

(A)

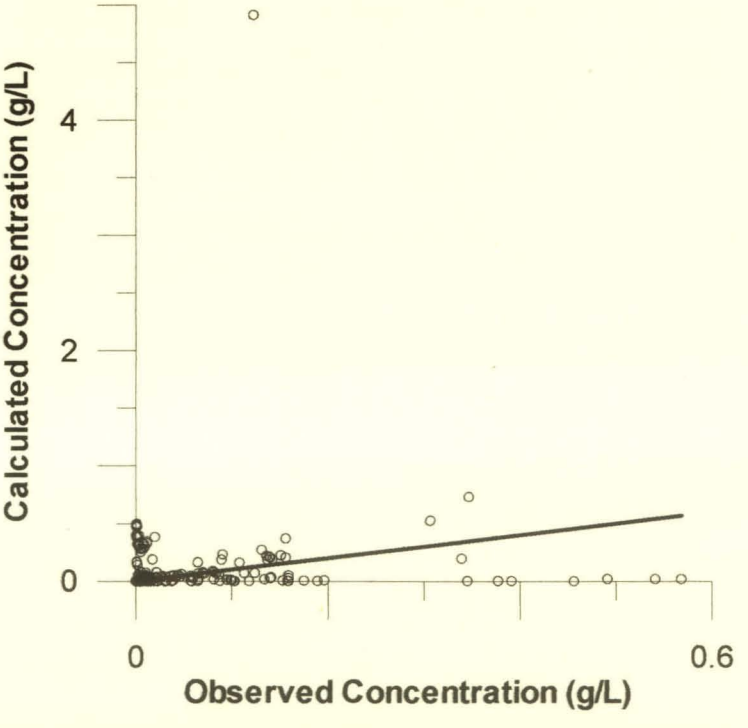

(B)

Figure 7.22 – Sandstone Aquifer concentration results for year 1999; (A) Contours with observation points and intervals; (B) Plot of computed versus observed values; (C) Plot of computed versus observed values on a log-log scale; and (D) Residual plot on log scale (RMS = 0.45 g/L).

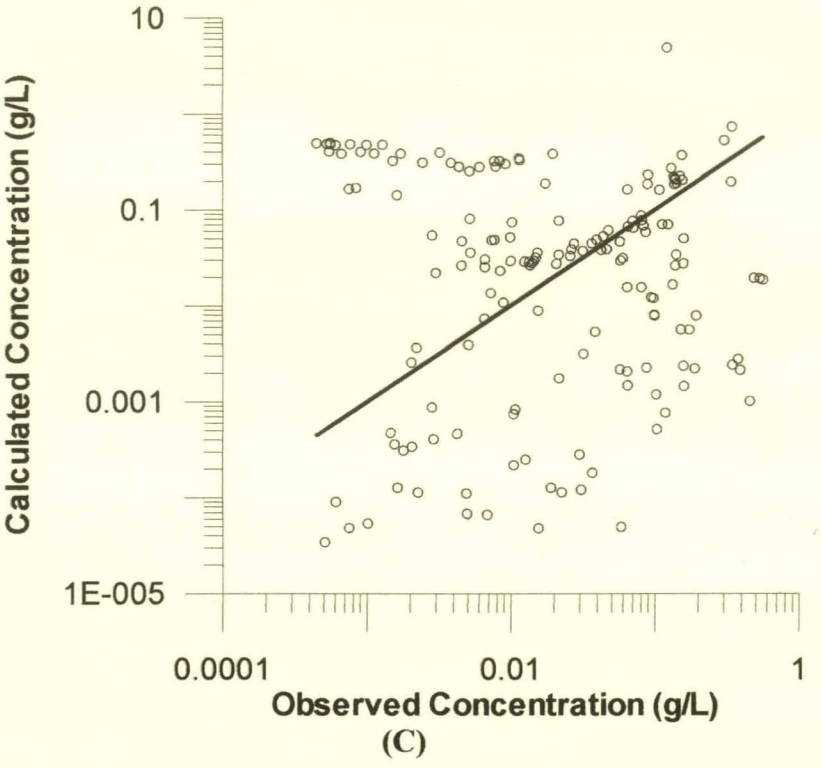

(C)

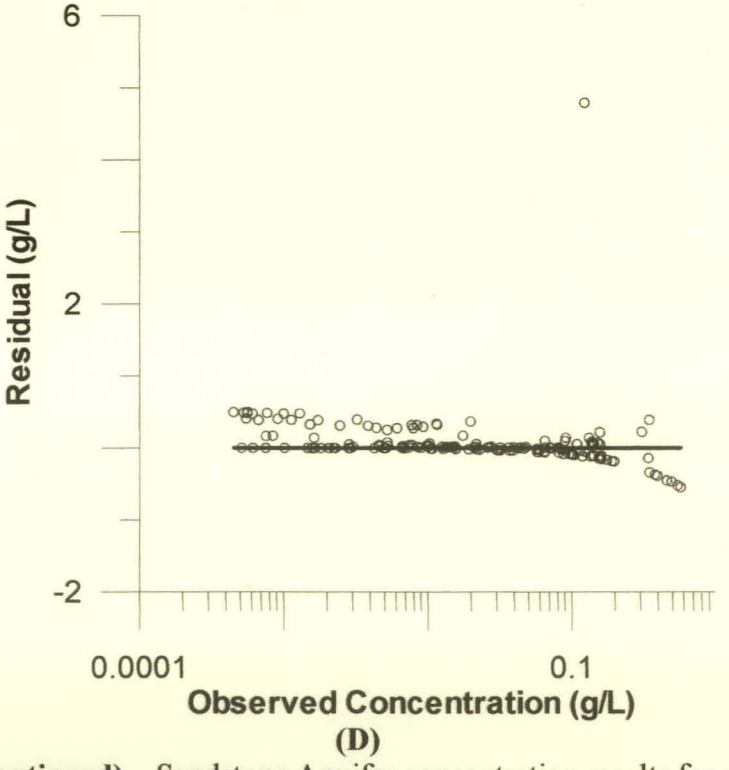

(D)

Figure 7.22 (continued) – Sandstone Aquifer concentration results for year 1999; (A) Contours with observation points and intervals; (B) Plot of computed versus observed values; (C) Plot of computed versus observed values on a log-log scale; and (D) Residual plot on log scale (RMS = 0.45 g/L).

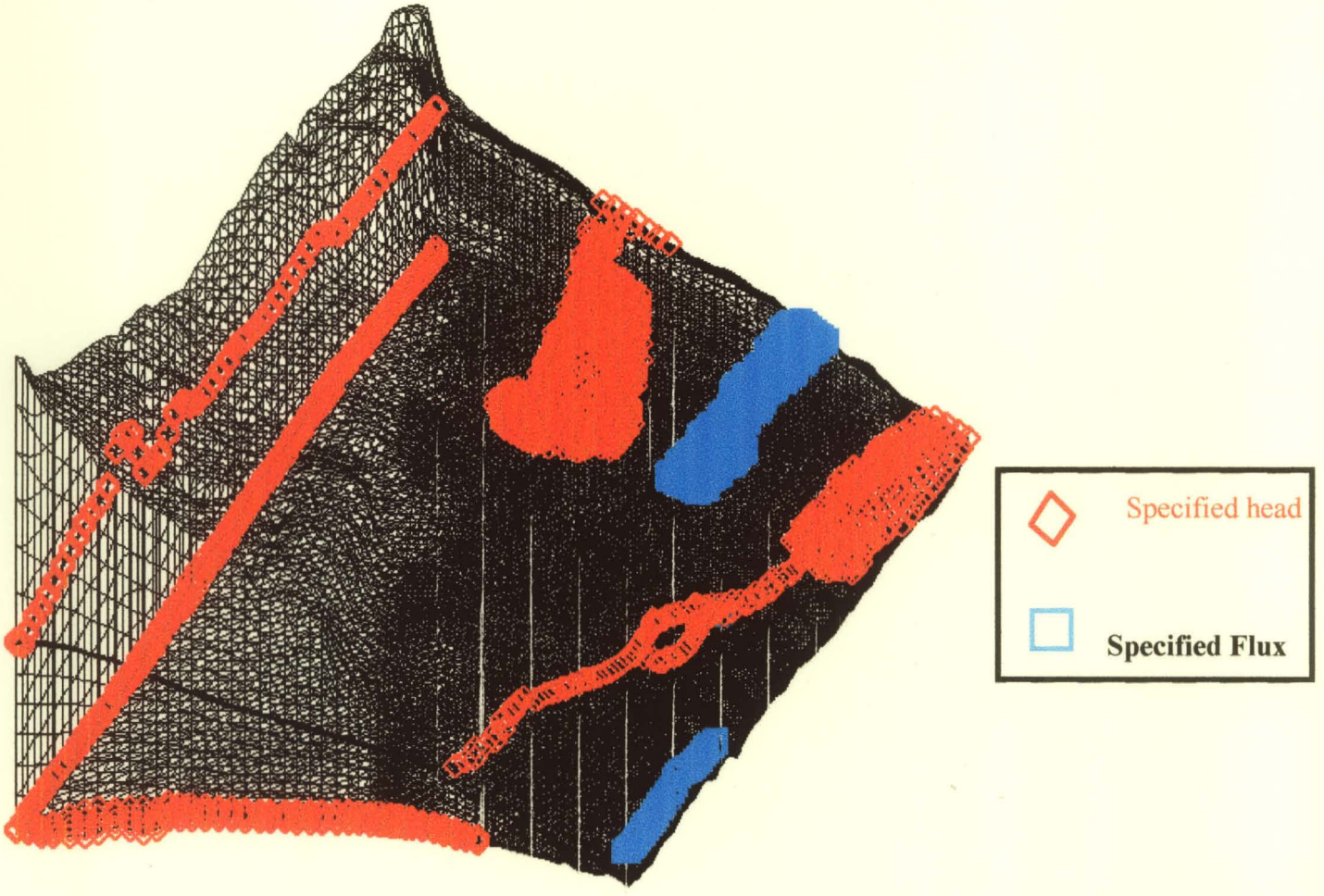

Figure 7.23 – 3D flow model boundary conditions.

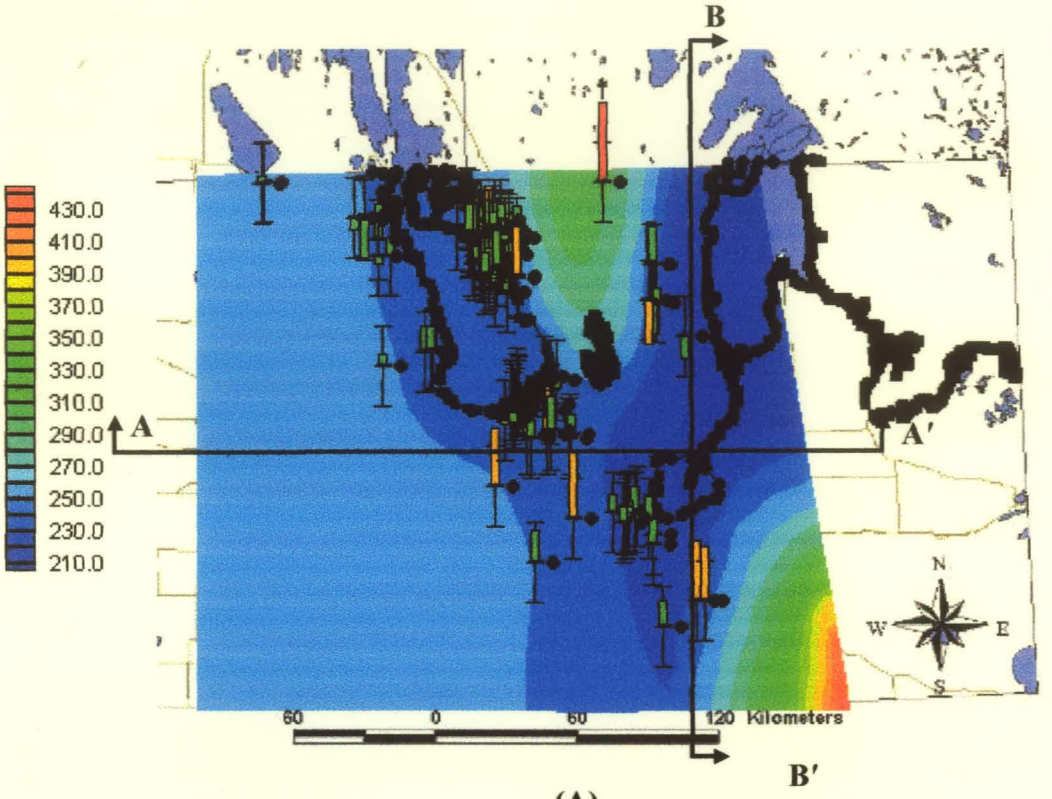

(A)

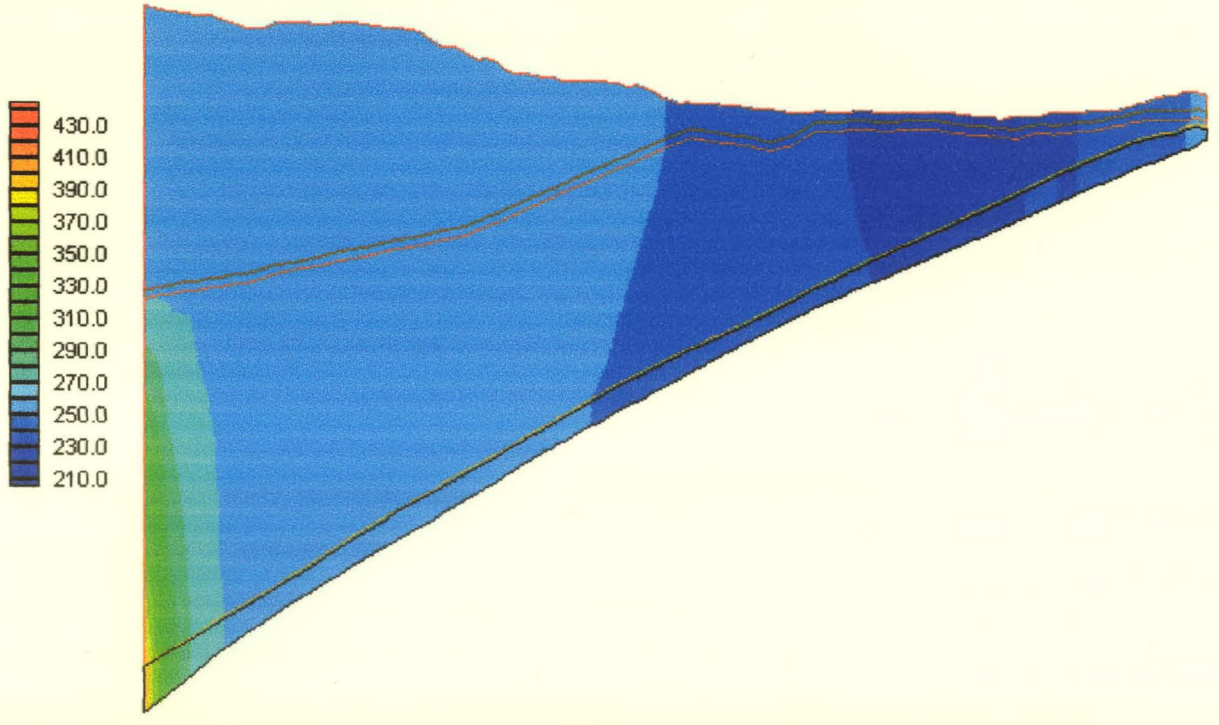

(B)

Figure 7.24 – Steady flow equivalent freshwater head results of three-dimensional model. (A) Plan view with observation points; (B) Cross-section through line A-A′; (C) Cross-section through line B-B′; (D) Plot of computed versus observed values; and (E) Residual plot (RMS = 7.22, slope = 0.92, intercept = 23.6, $R^2 = 0.75$).

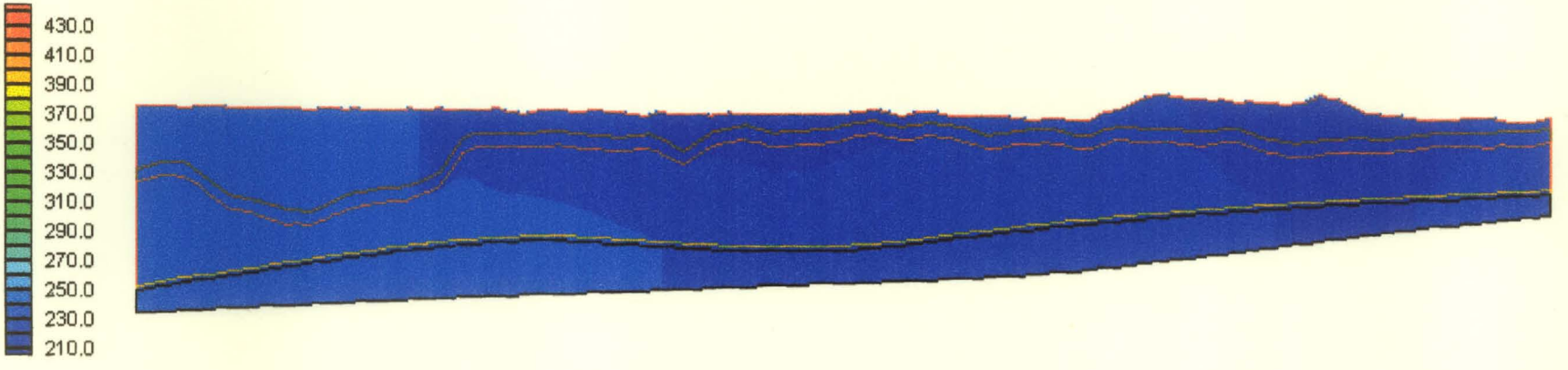

(C)

Figure 7.24 (continued) – Steady flow equivalent freshwater head results of three-dimensional model. (A) Plan view with observation points; (B) Cross-section through line A-A′; (C) Cross-section through line B-B′; (D) Plot of computed versus observed values; and (E) Residual plot (RMS = 7.22, slope = 0.92, intercept = 23.6, R^2 = 0.75).

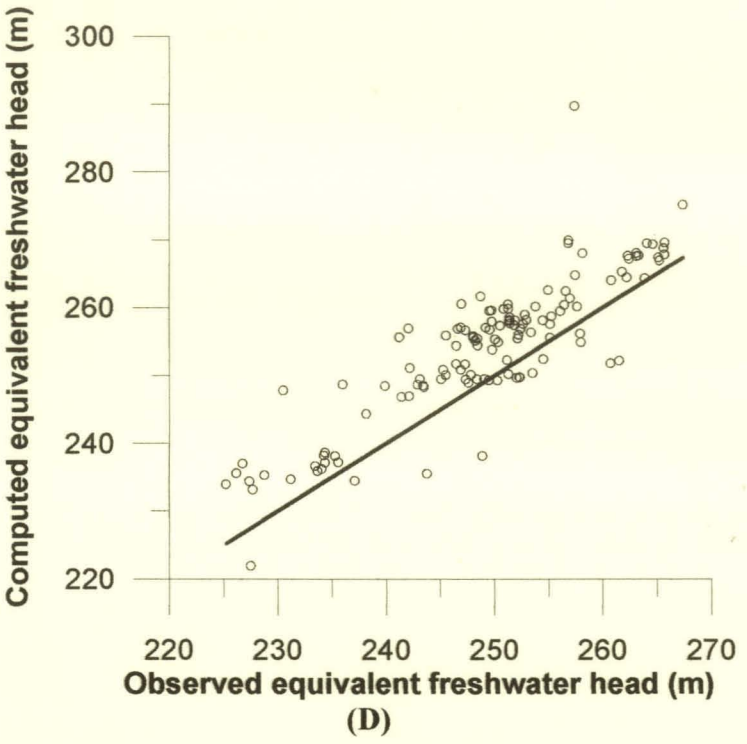

(D)

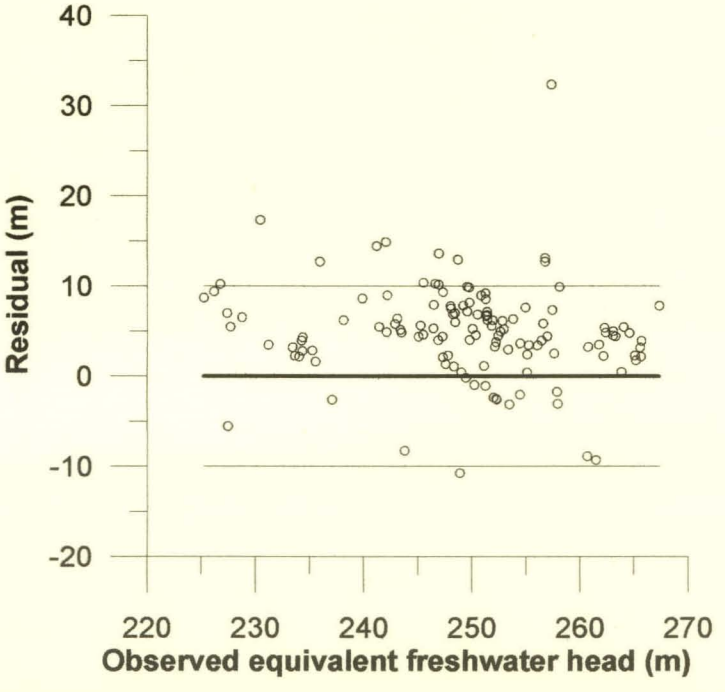

(E)

Figure 7.24 (continued) – Steady flow equivalent freshwater head results of three-dimensional model. (A) Plan view with observation points; (B) Cross-section through line A-A′; (C) Cross-section through line B-B′; (D) Plot of computed versus observed values; and (E) Residual plot (RMS = 7.22, slope = 0.92, intercept = 23.6, $R^2 = 0.75$).

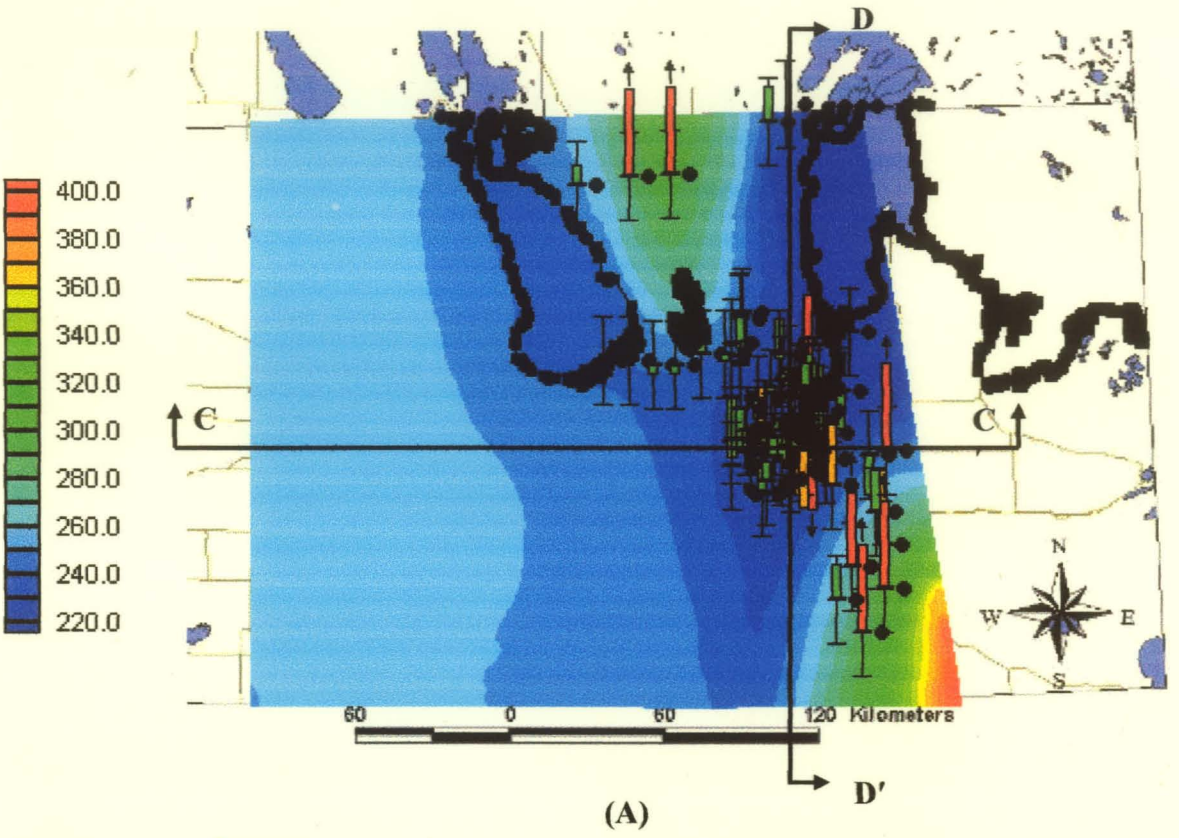

(A)

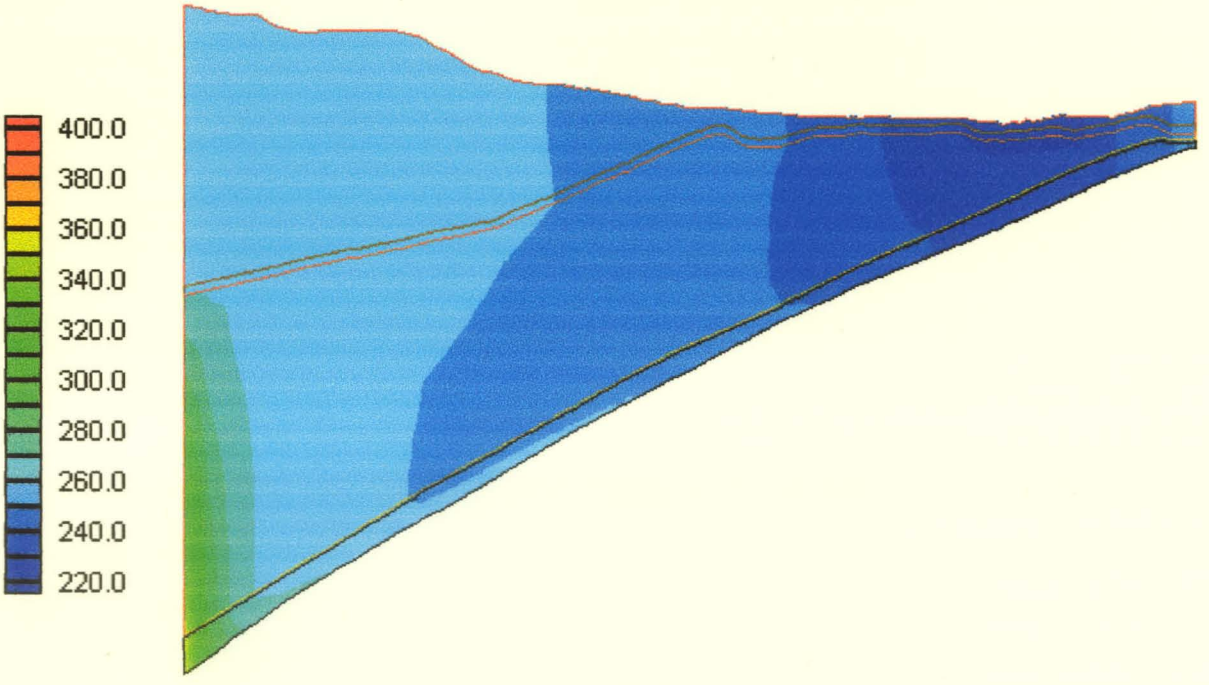

(B)

Figure 7.25 – Equivalent freshwater heads from flow model results at 1999. (A) Plan view with observation points; (B) Cross-section through line C-C′; (C) Cross-section through line D-D′; (D) Plot of computed versus observed values; and (E) Residual Plot (RMS = 10.4, slope = 1.13, intercept = -28.1, R^2 = 0.82).

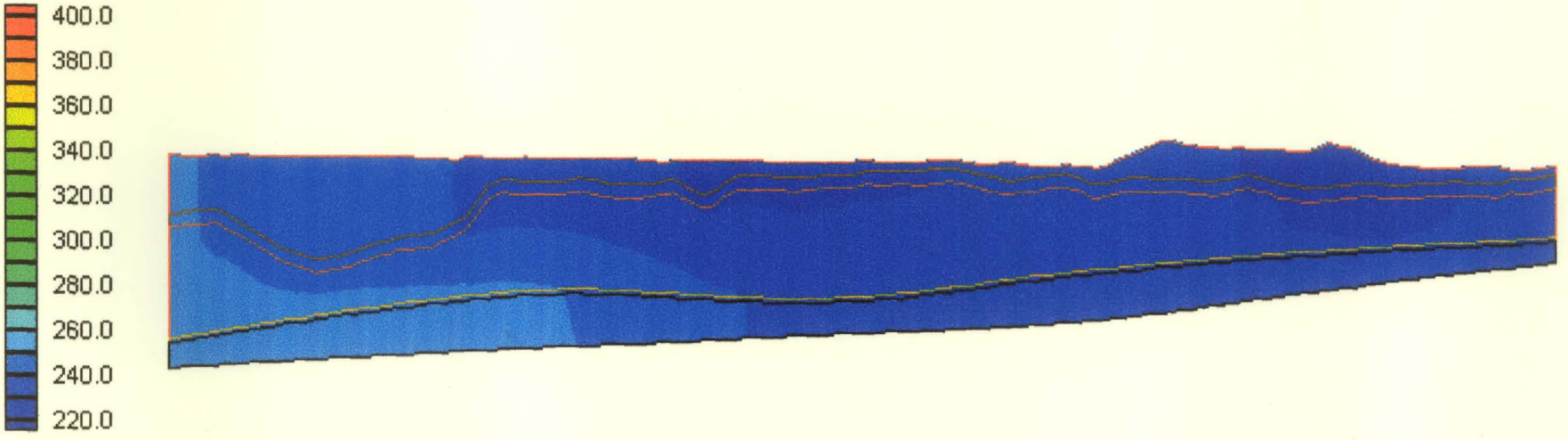

(C)

Figure 7.25 – Equivalent freshwater heads from flow model results at 1999. (A) Plan view with observation points; (B) Cross-section through line C-C′; (C) Cross-section through line D-D′; (D) Plot of computed versus observed values; and (E) Residual Plot (RMS = 10.4, slope = 1.13, intercept = -28.1, $R^2 = 0.82$).

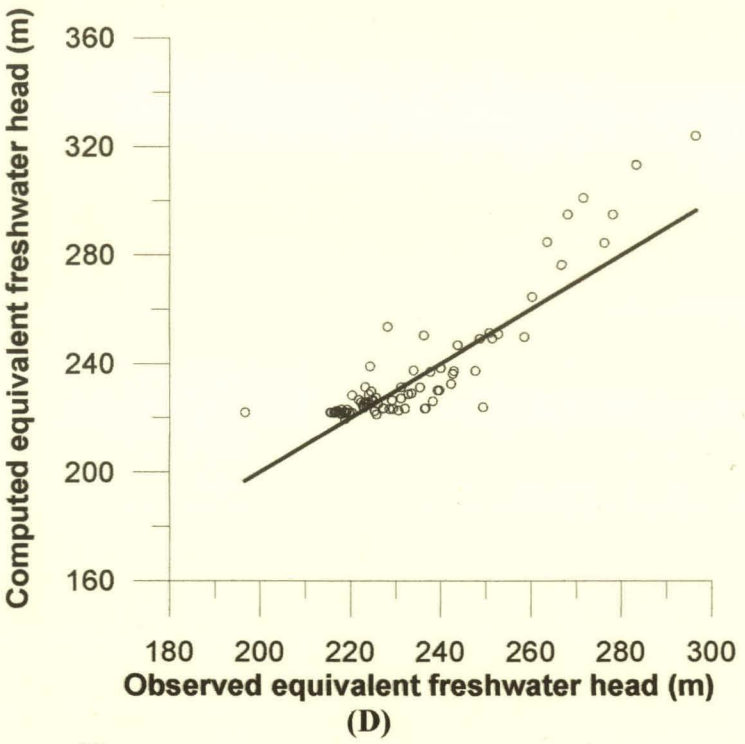

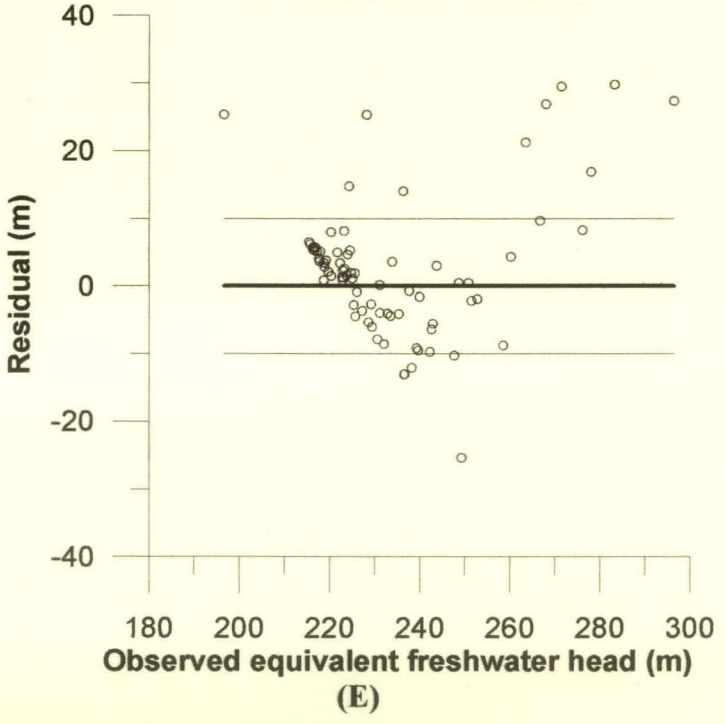

Figure 7.25 – Equivalent freshwater heads from flow model results at 1999. (A) Plan view with observation points; (B) Cross-section through line C-C′; (C) Cross-section through line D-D′; (D) Plot of computed versus observed values; and (E) Residual Plot (RMS = 10.4, slope = 1.13, intercept = -28.1, R^2 = 0.82).

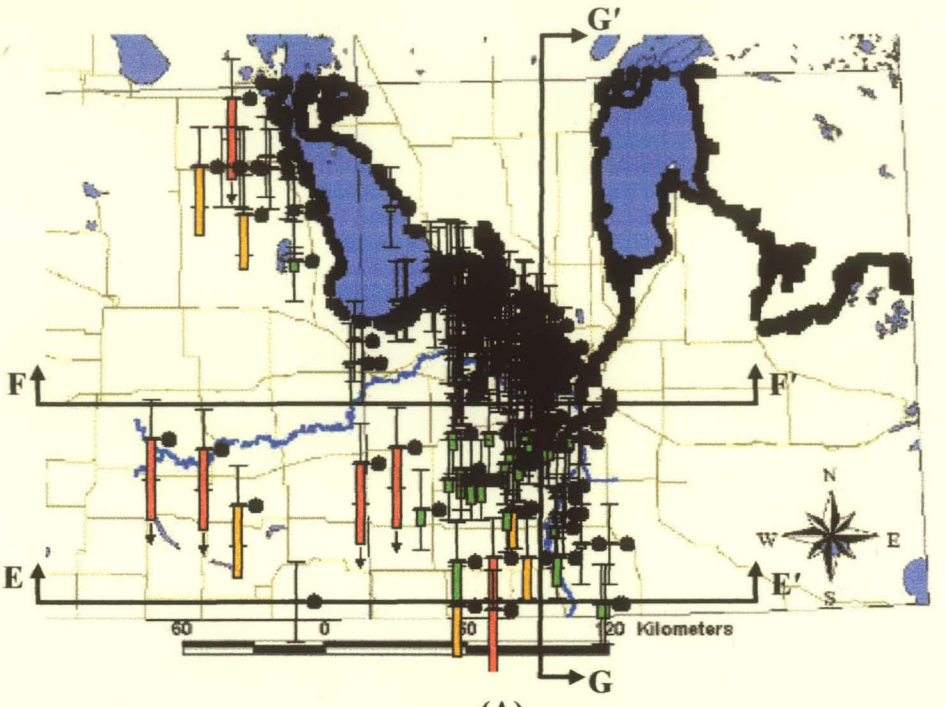

(A)

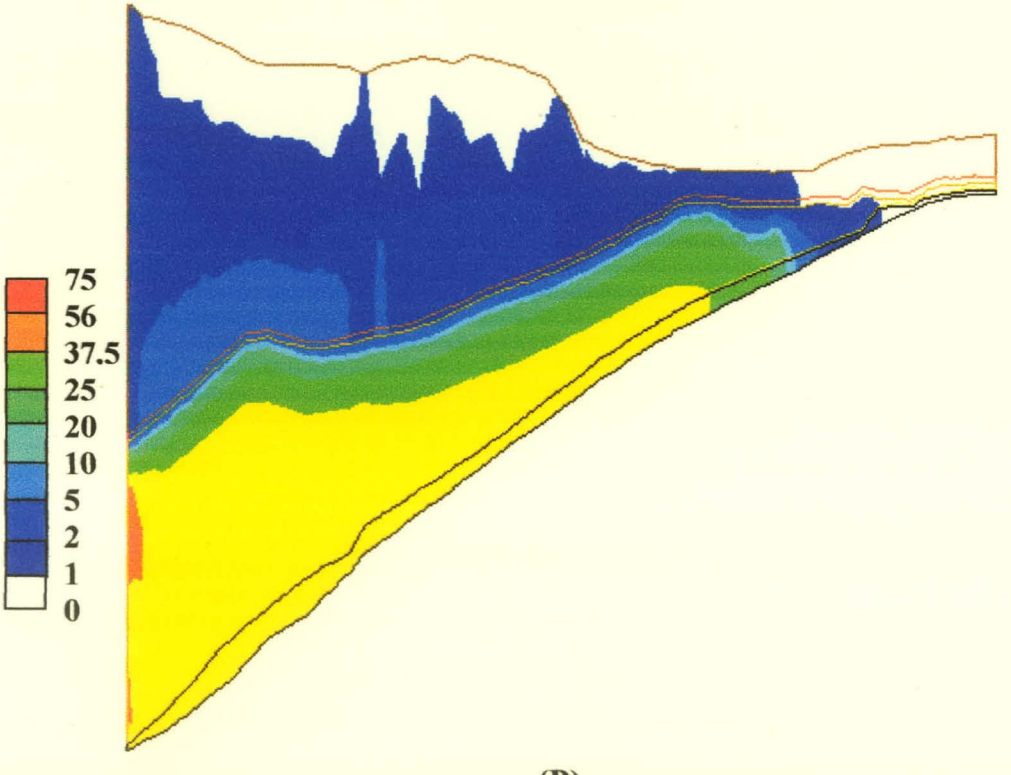

(B)

Figure 7.26 – Concentration (g/L) results in 1999. (A) Plan view of observation points with residual greater than 0.75 g/L; (B) Cross-section through line E-E′; (C) Cross-section through line F-F′; (D) Cross-section through line G-G′; (E) Plot of computed versus observed values; (F) Plot of computed versus observed values on log-log scale; (G) Residual plot; and (H) Residual plot on log scale (RMS = 2.85 g/L, slope = 0.642, intercept = 0.0014, R^2 = 0.574).

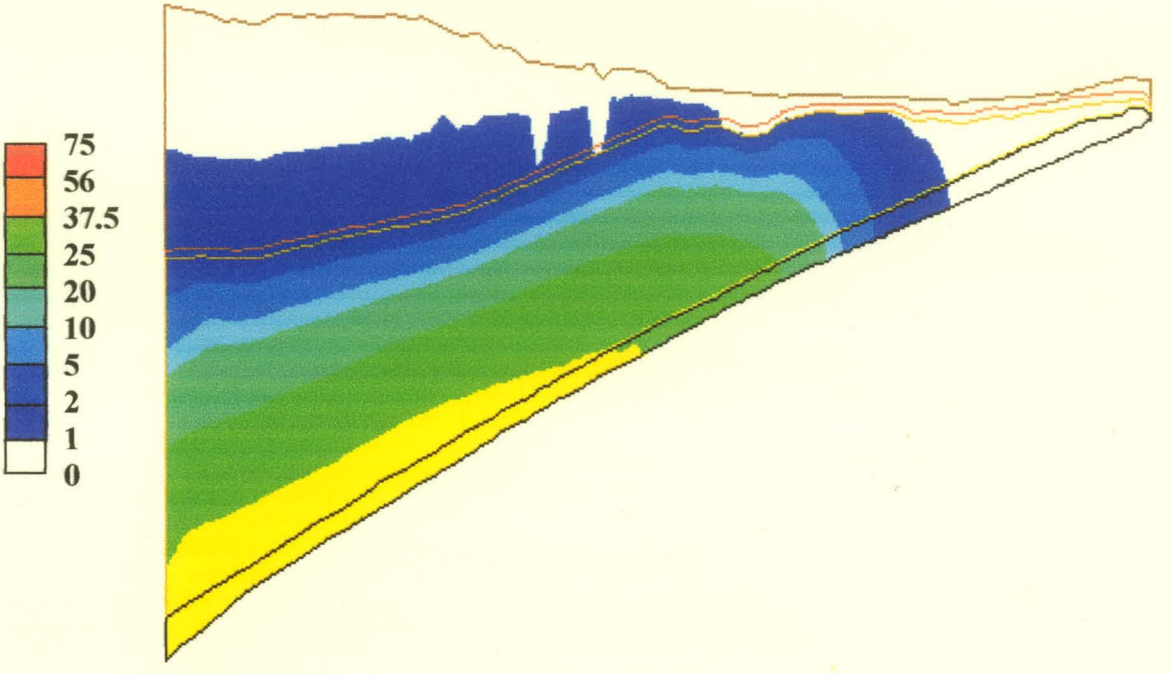

(C)

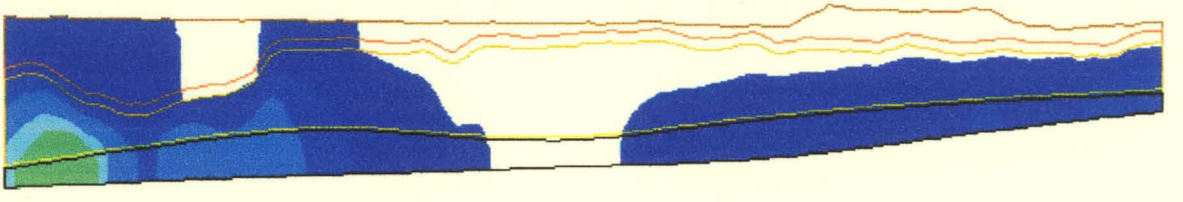

(D)

Figure 7.26 (continued) – Concentration (g/L) results in 1999. (A) Plan view of observation points with residual greater than 0.75 g/L; (B) Cross-section through line E-E′; (C) Cross-section through line F-F′; (D) Cross-section through line G-G′; (E) Plot of computed versus observed values; (F) Plot of computed versus observed values on log-log scale; (G) Residual plot; and (H) Residual plot on log scale (RMS = 2.85 g/L, slope = 0.642, intercept = 0.0014, $R^2 = 0.574$).

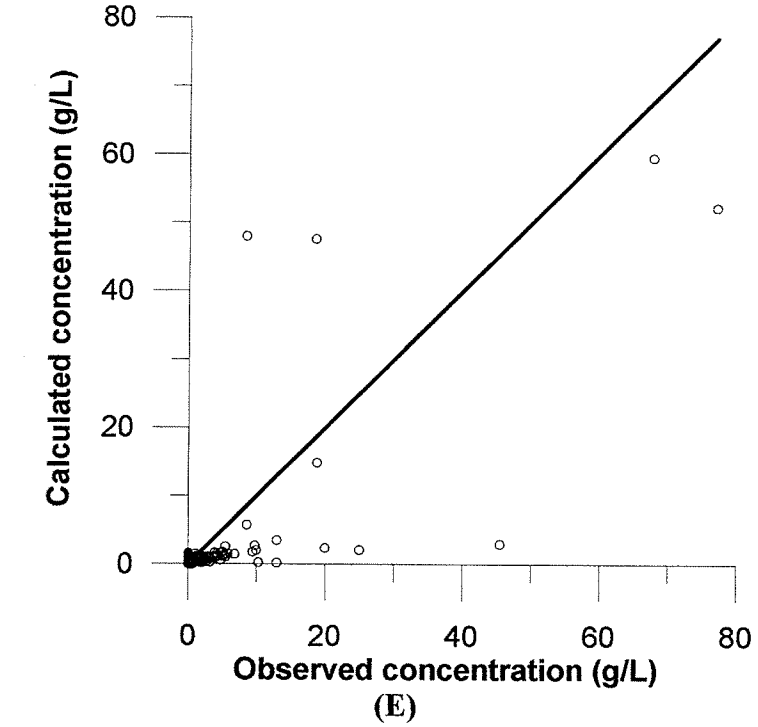

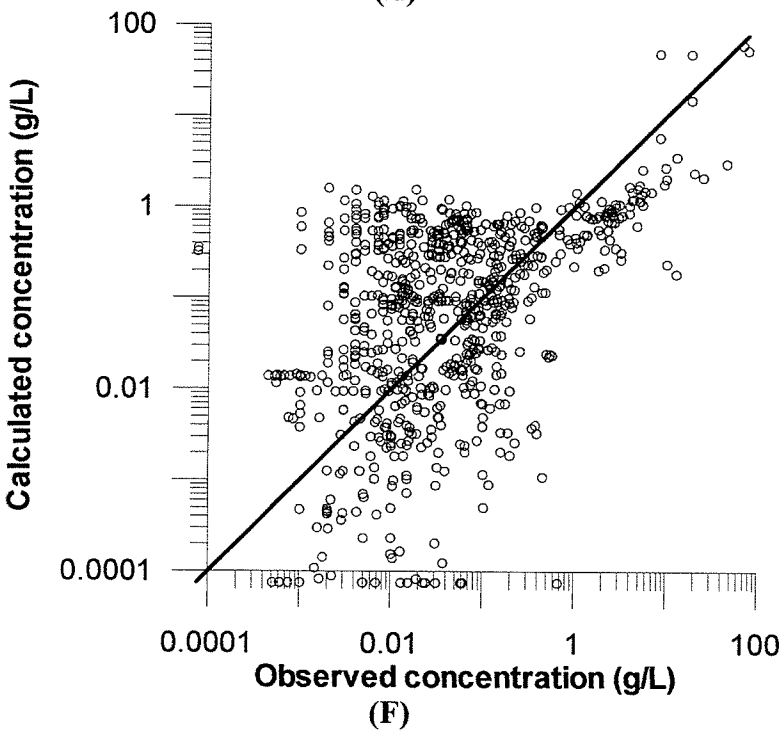

Figure 7.26 (continued) – Concentration (g/L) results in 1999. (A) Plan view of observation points with residual greater than 0.75 g/L; (B) Cross-section through line E-E′; (C) Cross-section through line F-F′; (D) Cross-section through line G-G′; (E) Plot of computed versus observed values; (F) Plot of computed versus observed values on log-log scale; (G) Residual plot; and (H) Residual plot on log scale (RMS = 2.85 g/L, slope = 0.642, intercept = 0.0014, $R^2 = 0.574$).

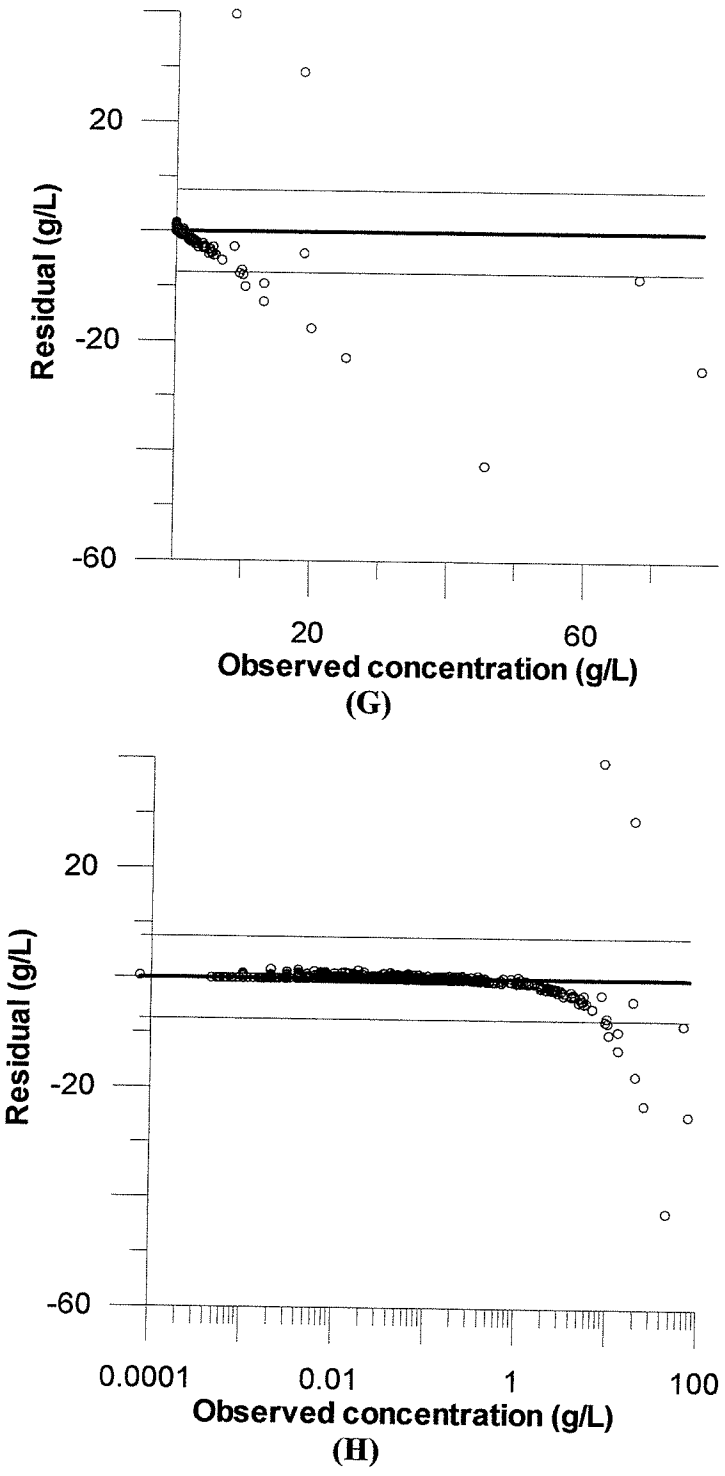

Figure 7.26 – Concentration (g/L) results in 1999. (A) Plan view of observation points with residual greater than 0.75 g/L; (B) Cross-section through line E-E′; (C) Cross-section through line F-F′; (D) Cross-section through line G-G′; (E) Plot of computed versus observed values; (F) Plot of computed versus observed values on log-log scale; (G) Residual plot; and (H) Residual plot on log scale (RMS = 2.85 g/L, slope = 0.642, intercept = 0.0014, $R^2 = 0.574$).

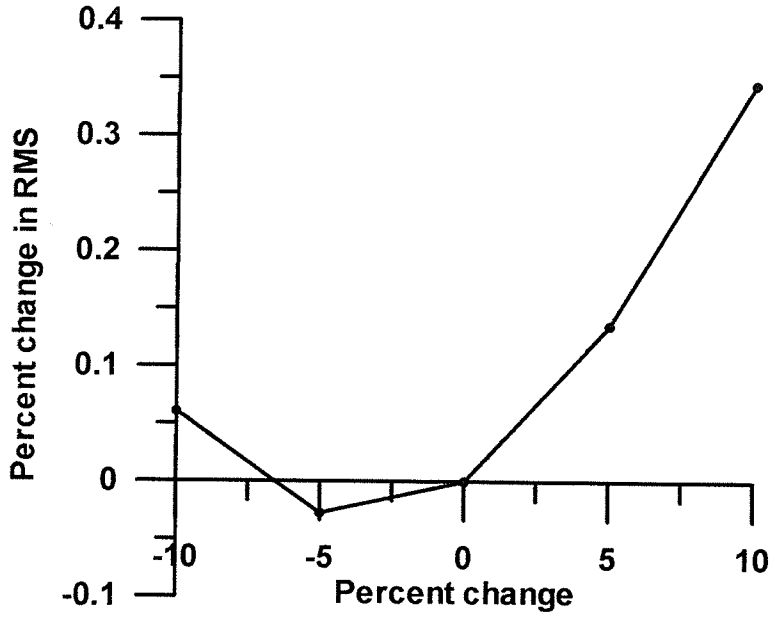

Figure 7.27 – Percent change in RMS as a result of change in specified head on the Western boundary of the Carbonate Aquifer.

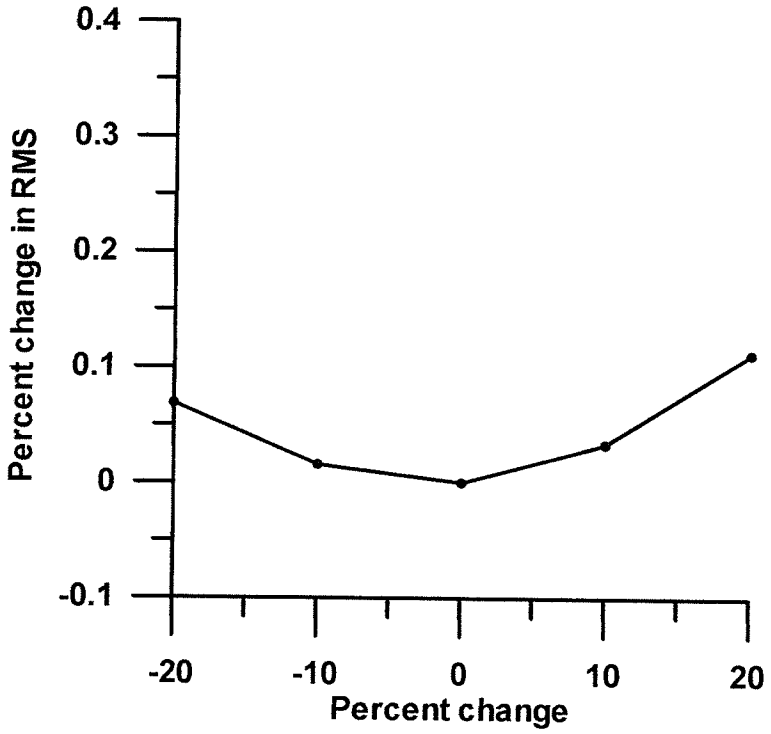

Figure 7.28 – Percent change in RMS due to changes in specified flux in Interlake region.

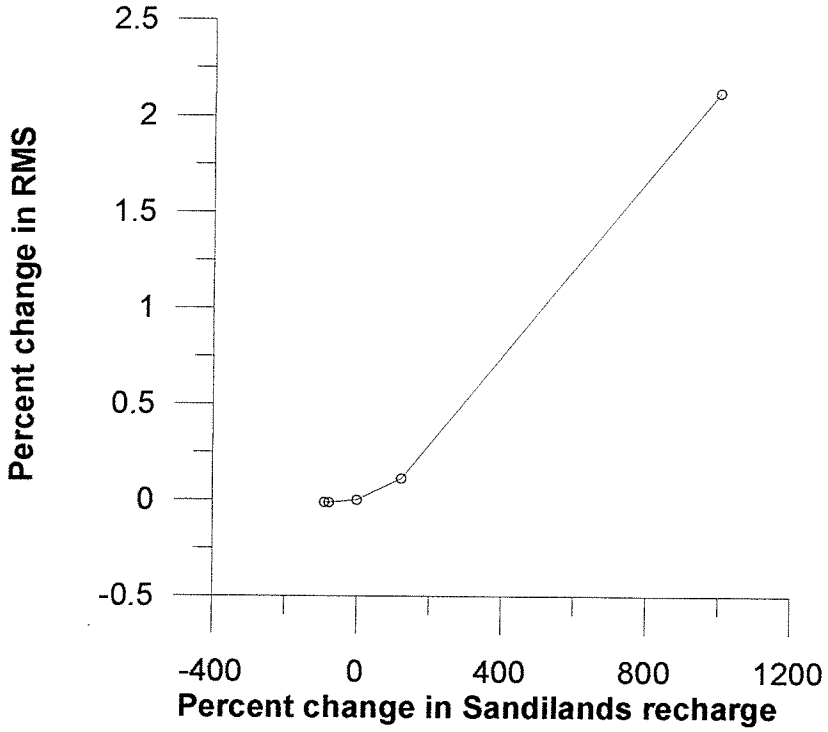

Figure 7.29 – Sensitivity of flow model to Sandilands recharge

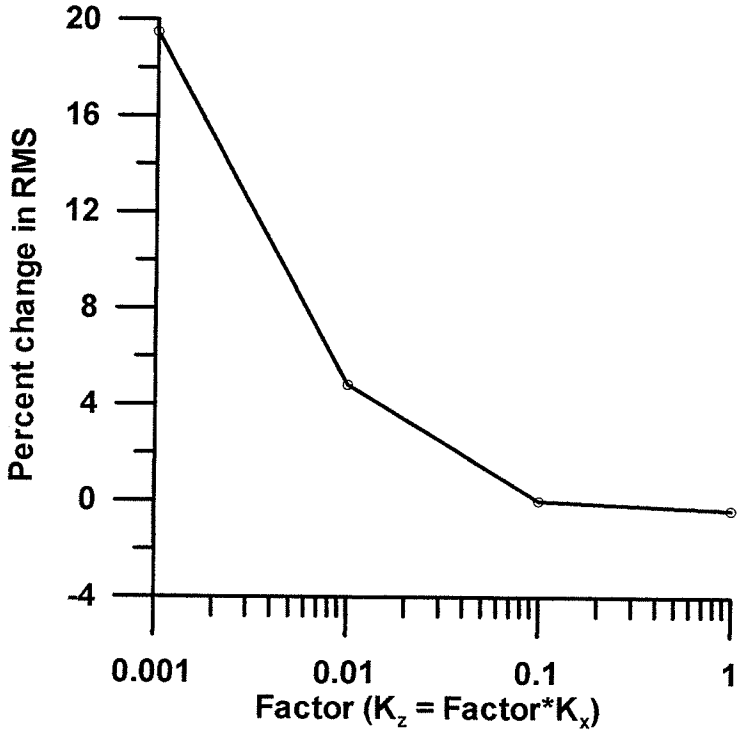

Figure 7.30 – Sensitivity of flow model to changes in K_z.

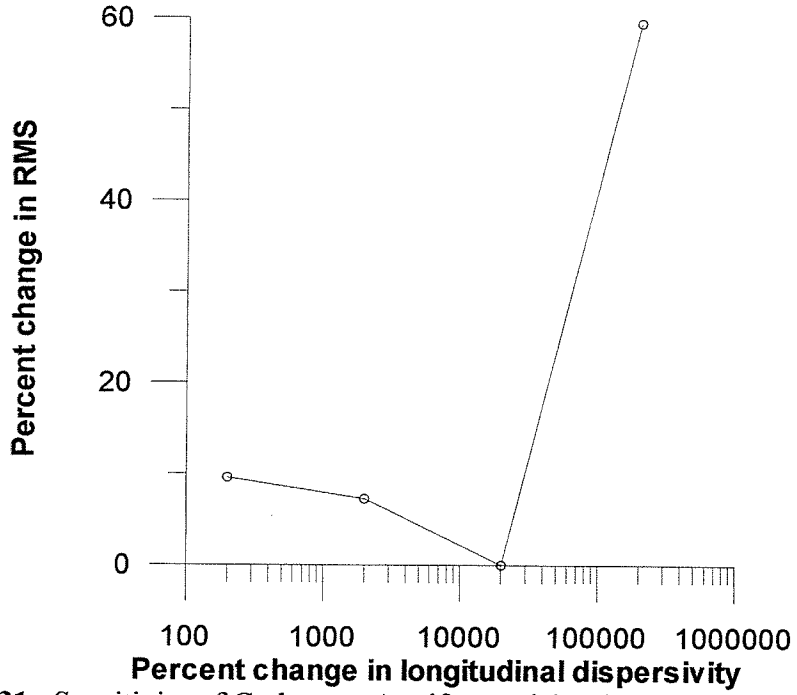

Figure 7.31– Sensitivity of Carbonate Aquifer model to longitudinal dispersivity.

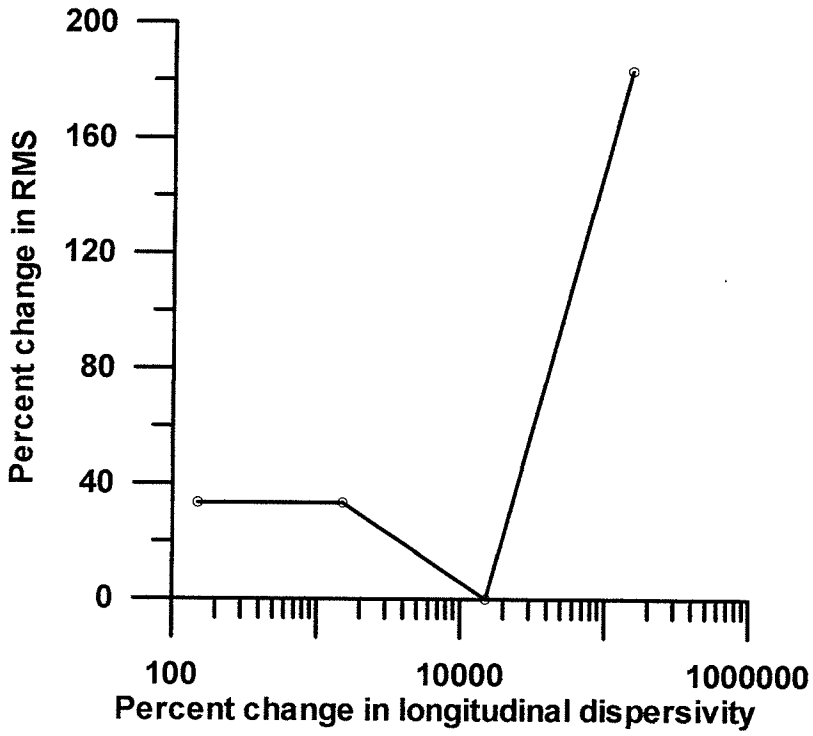

Figure 7.32– Sensitivity of Sandstone Aquifer model to longitudinal dispersivity.

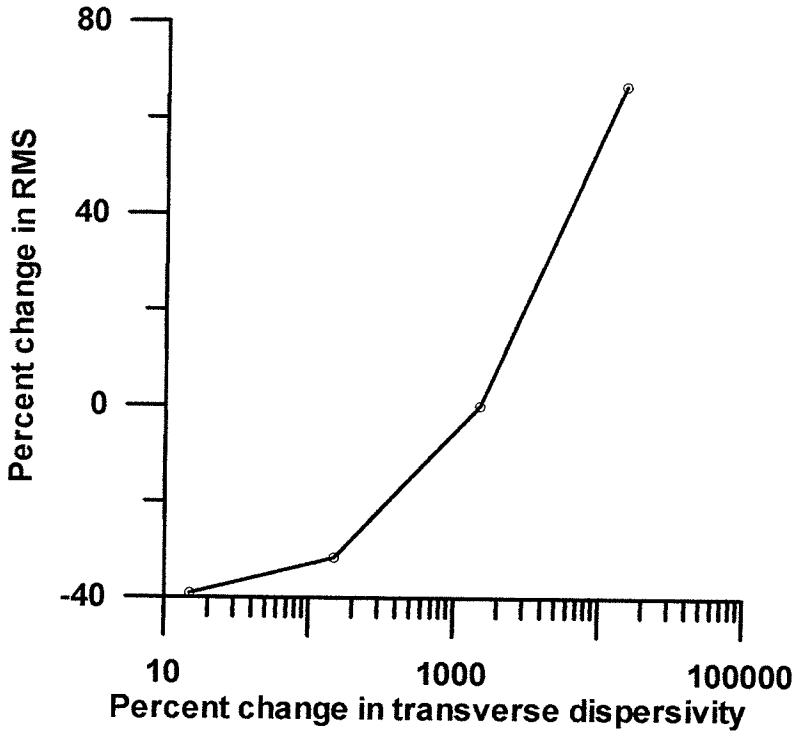

Figure 7.33– Sensitivity of Sandstone Aquifer model to transverse dispersivity.

CHAPTER 8

WATER RESOURCES ENGINEERING APPLICATIONS

8.1 Introduction

The groundwater flow and transport model constructed in Chapter 7 was used to evaluate several water resources engineering applications. The base sustainability of the system was evaluated by running the model while maintaining pumping rates constant. The sustainability considering increased development was subsequently considered by raising pumping rates over time. The model was then used to evaluate the effects on the system due to a flood and conversely due to a drought. The final problem was to observe the effect of a pumping centre in the Carbonate Aquifer in the City of Winnipeg.

Sustainability of groundwater systems is important for management decisions regarding development of these systems. Domenico and Schwartz (1990) state a general strategy for development is to obtain the largest quantity of water, without compromising the stability of the system. The "safe yield" of water withdrawal from the system was defined by Meinzer (1923) as "the rate at which water can be withdrawn from an aquifer for human use without depleting the supply to the extent that withdrawal at this rate is no longer economically feasible". Conkling (1946) altered this definition to make it more practical and useable. This new definition of safe yield was an allowable annual removal of water that does not:

1. Exceed average annual recharge.
2. Lower the water table so that the permissible cost of pumping is exceeded.

3. Lower the water table so as to permit intrusion of water with undesirable quality.

Banks (1953) added a fourth condition of safe yield, which is the protection of existing water rights. Many different definitions of safe yield or sustainable development have been made by different researchers. For this thesis, the sustainability of the system was evaluated by examining several factors. If the percentage of recharge that was removed through well extraction was less than 50% then the system was deemed sustainable. If the hydraulic head drops below the top of the aquifer in any location then dewatering of the aquifer may occur, signifying that the system is not sustainable. A continued decline in hydraulic head at the end of simulation time may signify an unsustainable system. Finally examination of water quality changes to determine if any decline in quality occurs.

8.2 Base Sustainability Case

The base sustainability of the system was evaluated by predicting the system response from 1999 forward, while maintaining all pumping rates at the 1999 levels. The model was run over a period of twenty years. For comparison purposes, values of hydraulic head at selected times were compared against 1999 levels to observe changes. The change in hydraulic head with time was then examined in both the Carbonate and Sandstone Aquifers. The change in hydraulic head within the Carbonate Aquifer after twenty years is presented in Figure 8.1. All observed changes in hydraulic head occur in the vicinity of the City of Winnipeg. Within the city an increase in hydraulic head is observed. Wells requiring a permit were incorporated at the time specified on the permit. Some of these wells were no longer permitted for pumping in the late 1990's. Therefore,

the groundwater level may be rebounding as a result of the decreased stress. East and north of the City of Winnipeg, decreases in the hydraulic head are observed with the maximum decline occurring in the Southern Interlake. This decrease may be a result of increased development that occurred just before 1999. Figure 8.1b presents a plot of change in hydraulic head versus time for the Carbonate Aquifer. This figure illustrates that on average, an almost linear decrease in hydraulic head is occurring with time to 0.17 m at 20 years. The maximum decline in hydraulic head was also found to increase with time to almost -1.5 m. If the decline continues to increase without bound, then this may signify future problems in a small portion within the Carbonate Aquifer in terms of water supply. The approximate region over which this decline is predicted to occur is 5 square kilometers. The maximum increase in hydraulic head was found to increase and then level off at later times. There were some regions in which the hydraulic head dropped below the top of the Carbonate Aquifer after twenty years (Figure 8.2). This region is where dewatering may occur, which is in the Interlake region and west of Lake Manitoba.

The effect on water levels within the Sandstone Aquifer is shown in Figure 8.3. After a twenty year period, it was observed that west of the City of Winnipeg, there is a slight increase in hydraulic head and east of the City of Winnipeg, and there is a decrease in hydraulic head. The observed increase in hydraulic head is very slight, less than 0.75 m. The decrease in hydraulic head is probably due to the system reacting to an increase in pumping rates prior to 1999. On the western boundary, an anomalous thin line showing a decrease in hydraulic head is evident. This anomalous zone does not coincide with the decrease in hydraulic head observed over a large region east of the boundary. A Type I

boundary condition was used on the western boundary of the Sandstone Aquifer. As a decrease in hydraulic head occurs east of the boundary, this condition may have caused this irregularity. The other possibility resulting in this decrease in hydraulic head on the border is that the grid is too coarse. The maximum decline in hydraulic head occurs southeast of the City of Winnipeg. A plot of change in hydraulic head versus time is presented in Figure 8.3b. The average change in hydraulic head was found to decrease with time to 0.12 m at 20 years. The maximum increase in hydraulic head increased linearly to 0.7 m and the maximum decline was found to increase linearly to -2.2 m, after 20 years. The hydraulic head did not drop below the top of the aquifer in any location.

A mass balance on the entire area simulated at twenty years had an inflow of 20.1 m^3/s, which consisted of 18 m^3/s to Type I boundaries and 1.9 m^3/s to Type II boundaries. The outflow was -20.7 m^3/s with -20 m^3/s to Type I boundaries and -0.60 m^3/s to extraction wells. The withdrawal from storage in the system was 0.6 m^3/s. For this case, the percent of recharge that is lost to well extraction is 32%.

The change in concentration in the Carbonate Aquifer is presented in Figure 8.4. Figure 8.4a shows the concentration contour of 1 g/L at 1999 (beginning of simulation) and 2019 (after 20 years simulation). The results show that the plume has moved slightly northeast with time. The average change in concentration is approximately nil (Figure 8.4b). The maximum increase in concentration is approximately 600 mg/L (C/C_0 = 0.008). The changes in concentration observed over the model area were very slight (~ 2%) in comparison to the maximum concentration (75,000 mg/L). The RMS error of the transport model is 3.9% (Chapter 7). It is thought with the available data for the transport

model, the finite element mesh and by the finite element method that the model could not accurately predict such small changes in concentration. It is thought that the model may be capable of simulating large movement of brine, but is not capable of accurately predicting small changes in concentration. However, in this particular system the flow rate is small and the transition is thought to be at equilibrium, resulting in only small changes of concentration. Therefore, it was thought that the model could not simulate any small movement of the transition zone.

For the Sandstone Aquifer, the concentration contour of 1 g/L showed a slight movement eastward (Figure 8.5). In the literature, it states that the freshwater/saltwater transition zone is moving at a rate of 1 m/year eastward (Betcher et al., 1995). The model is showing some movement in this direction. South of the City of Winnipeg, the transition zone has moved slightly and north of the city, negligible movement was observed. The movement was not observed due to the discretization of the finite element mesh.

In terms of sustainability, the maximum decline in hydraulic head for the Carbonate Aquifer was less than 2 m. However, there is a region north of the City of Winnipeg in which the hydraulic head dropped below the top of the aquifer signifying dewatering. This result indicates potential problems for the water supply within the Carbonate Aquifer north of the City of Winnipeg. The estimated percentage of recharge going to well extraction is 32% which is less than 50%. The changes in concentration predicted by the model, is less than the accuracy of the model. Therefore, the system is sustainable except for those regions in which dewatering may occur in the Carbonate Aquifer.

8.3 Sustainability with increased development

In Section 8.2, the system under current stress conditions was evaluated over time. However, with increased population and development it is most likely that the stresses on the groundwater system may continue to increase. To account for this increase in stress, the non-permit pumping rates were increased with time. The pumping rates were assumed to increase by 2% every five years, which was the average increase in population between 1921 and 1996 (Chapter 7, Table 7.3). The model was then run over a twenty year period.

Changes in hydraulic head were compared against 1999 levels. The effect on hydraulic heads in the Carbonate Aquifer is presented in Figure 8.6. The plan view of the change in hydraulic head after twenty years is shown in Figure 8.6a. Similarly to the base sustainability case, the changes in hydraulic head are only observed in the vicinity of the City of Winnipeg. An increase in hydraulic head is observed in the west part of the City of Winnipeg and is most likely a result of permit pumping wells turned off in the late 1990's. The decrease in stress results in water levels rebounding and hence an increase in hydraulic head. A decrease in hydraulic head is observed east of the City of Winnipeg, and as expected is more significant than that predicted by the base sustainability case, due to increased pumping. The maximum decline in hydraulic head occurred just east of the City of Winnipeg. A plot of change in hydraulic head versus time is presented in Figure 8.6b. The average change in hydraulic head is found to decrease with time to -0.25 m. The maximum increase in hydraulic head is found to increase with time to 5.2 m. The

maximum decline in hydraulic head increases with time to -6.0 m at 20 years, as compared to -1.5 m found for the base sustainability case. Figure 8.7 shows the region in which the hydraulic head dropped below the top of the Carbonate Aquifer, which is slightly larger than that of the base sustainability case.

The changes in hydraulic head within the Sandstone Aquifer are presented in Figure 8.8. The plan view of change in hydraulic heads after twenty years shows an increase in hydraulic head towards the west (Figure 8.8a). A significant decrease in hydraulic head was observed southeast of the City of Winnipeg just north of Sandilands region. The decline in hydraulic head is fairly significant with a magnitude of approximately -7 m. A plot of change in hydraulic heads with time is presented in Figure 8.8b. The average change in hydraulic head is found to increase slightly to 0.3 m. The maximum increase in hydraulic head is found to increase with time to 11 m. The maximum decline in hydraulic head at twenty years is found to increase significantly to approximately -36 m. This maximum decline in hydraulic head is located just north of Sandilands region. Even with the large decline in hydraulic head, the hydraulic head did not drop below the top of the aquifer at any location. On the southwest corner of the province a decrease in hydraulic head was predicted. Just east of this location, the model predicted an increase in hydraulic head across a large portion of the region. This result is similar to the results obtained for the base sustainability case. Again it was thought that this effect near the border of the model was due to boundary conditions or grid refinement in that region.

The mass balance of the entire model showed an inflow of 20.1 m^3/s, with 19 m^3/s to Type I boundaries and 1.2 m^3/s to Type II boundaries. The outflow was -20.6 m^3/s with -20 m^3/s from Type I boundaries and -0.65 m^3/s through extraction wells. The amount of water removed from storage was at a rate of -0.50 m^3/s. In this case, the percent of recharge going to extraction wells was found equal to 55%. The percent of recharge lost to pumping increased from the base sustainability case (32%).

The effect of increased development on the concentrations within the Carbonate Aquifer is presented in Figure 8.9. The concentration contour of 1 g/L shows that the predicted values for the year 2019 show that with increased development the plume moves slightly further towards the east. For the Carbonate Aquifer, it was observed that on average there was a very slight increase in concentration to 28.7 mg/L at twenty years (Figure 8.9b). The maximum increase in concentration was found to increase with time to 575 mg/L at 20 years. This maximum increase is greater than that determined for base sustainability case. The maximum increase in concentration was found to occur in the northern Interlake. A fairly large region of the Carbonate Aquifer is affected by a slight increase in concentration.

For the Sandstone Aquifer, the movement 1 g/L concentration contour was not different than that observed for base sustainability case (Figure 8.10a). Figure 8.10b shows that the average change in concentration was found to decrease to -575 mg/L. The maximum increase was found to increase with time to 1500 mg/L. The maximum decrease was found to increase with time to -4500 mg/L, which is significant. The changes in

concentration are less than 5% of maximum concentration. As explained for base sustainability case it was not though that the model could accurately predict such small changes.

In terms of sustainability, there remains a region where the heads dropped below the top of aquifer and dewatering may occur. Also the percent of recharge taken by well extraction has increased to 55% from the base sustainability case. This value is greater than the specified value 50%, indicating that the system is no longer sustainable. With increased development it is predicted that the groundwater system may become less sustainable with time.

8.4 Flood Effects

The effect of a flood on the system was evaluated to determine the change in water levels and relative concentration with time. The nodes within the region flooded during the Flood of 97 were assigned constant hydraulic head boundary conditions (Figure 8.11). The flood was assumed to last for a period of one month, with the flood occurring instantaneously and then stopping instantaneously. The model and was run for a period of 50 years to observe the long-term effects. All wells in the model were assumed to pump throughout the simulation period, including those open across both aquifers. The change in hydraulic head in the Carbonate Aquifer is presented in Figure 8.12. After one month (end of the flood period) a distinct increase in hydraulic head is observed south of the City of Winnipeg. After 2.6 years, the water levels within the Carbonate Aquifer are still elevated, and the affected region has grown larger. The plot of the change in

hydraulic head with time shows that the maximum increase in hydraulic head increases at early times after flooding and then declines over time.

The effects on the concentration within the Carbonate Aquifer are presented in Figure 8.13. The plan view of concentration shows an increase in concentration in the region south of the City of Winnipeg after a one-month period. Therefore, the Carbonate Aquifer water quality is degraded as a result of flooding. In actuality, after the Flood of 97, increases in concentration within the Carbonate Aquifer were observed (Betcher, personal communication 2002). However, whether this increase was due to increased heads through overburden or contamination through wells is not known.

The effects on the Sandstone Aquifer were found to be negligible in terms of both hydraulic head and concentration.

8.5 Drought Effects

A drought can be of concern on groundwater systems when lack of precipitation results in decreased spring runoff and rainfall. This change in precipitation will cause a reduction in the amount of recharge reaching the aquifers. A global climate model was investigated to determine if a prolonged drought may be a concern on groundwater systems in Manitoba. Global precipitation trends between 1900 and 1994, show that in general the amount of precipitation has increased at higher altitudes and has decreased at lower altitudes (Scientific American website: http:/www.sciam.com/0597issue/ 0597karl.html)

(Figure 8.14). From Figure 8.14, it appears that for Southern Manitoba the quantity of precipitation is not changing significantly over time.

Even though a long-term drought may not be of significant concern in Southern Manitoba, model simulations were conducted for completeness. The effect of a drought on the aquifer system was investigated by decreasing the recharge rates and running the model for a period of three years with the reduced recharge. The recharge rates were decreased by 0%, 10%, 25%, 50%, 75% and 100% to observe the effects on the system. The run with 0% reduction in recharge was used for comparison of hydraulic heads and concentrations after three years. The remaining parameters, such as pumping rates, were maintained the same.

The effect on the hydraulic head within the Carbonate Aquifer and Sandstone Aquifer after three-years with a 50% reduction in recharge is displayed in Figure 8.15. The plan view of change in hydraulic head for the Carbonate Aquifer shows a decline in hydraulic head within the Sandilands region southeast of the City of Winnipeg and within the Interlake region with maximum decline occurring in the Sandilands (Figure 8.15a). This is the expected result as these locations are the two major recharge zones to the Carbonate Aquifer. For the Sandstone Aquifer, the decline in hydraulic head is only observed in the Sandilands region (Figure 8.15b).

The maximum decline in hydraulic head as a function of reduction in recharge is presented in Figure 8.16. This plot shows that the effect of a drought on the Carbonate

Aquifer is much more significant than that on the Sandstone Aquifer. The maximum decline for the Sandstone Aquifer varies between -0.05 and -0.53 m. For the Carbonate Aquifer, the maximum decline varies between -0.8 and -7.6 m.

The effect of a drought on the concentration was found to be negligible. Therefore, in times of drought the concern within the aquifer system should be towards maintaining the water levels within the Carbonate Aquifer.

8.6 Effect of a pumping centre within the Carbonate Aquifer

The transition zone between fresh and salt water in the Carbonate Aquifer runs north-south through the City of Winnipeg. It is thought that a large drawdown caused by a pumping centre just east of the transition zone within the freshwater region may cause the transition zone to be drawn further east. One well within the Carbonate Aquifer was incorporated into the model to simulate the presence of a pumping centre. The Carbonate Aquifer was chosen as this is where all permitted wells with larger pumping rates are currently located. For permit wells, the maximum pumping rate was equal to 0.056 m^3/s. Therefore, four pumping rates in the same order of magnitude of this maximum pumping value were chosen for examination. The well was located just east of the saltwater/freshwater transition zone within the City of Winnipeg. The model was run over a three years and compared against runs that did not contain the new well.

The changes in hydraulic head within the Carbonate Aquifer due to the pumping centre are presented in Figure 8.17. A plan view of change in hydraulic head for a pumping rate

of 0.05 m^3/s (≡ 792.5 USGPM) after three years shows a drawdown cone within the City of Winnipeg. This result is expected with the maximum change in hydraulic head at the middle of the drawdown cone. The drawdown cone covers a radius of approximately 10,000 m. In Figure 8.17b, a plot of maximum decline in hydraulic head versus pumping rate, shows the obvious result of increased maximum decline with increased pumping rate. For an extremely large pumping rate of 0.5 m^3/s (≡ 7925 USGPM), caused the hydraulic head to drop below the top of the Carbonate Aquifer.

The effect on the hydraulic heads within the Sandstone Aquifer due the pumping well screened over the Carbonate Aquifer is presented in Figure 8.18. The plan view of the change in hydraulic head shows that there are only minimal effects on the Sandstone Aquifer. The effect on the Sandstone Aquifer is to the east of the drawdown cone that developed in the Carbonate Aquifer. This may be a result of better connection between the aquifers at that location, or perhaps the presence of a well screened over both aquifers.

The effect on the concentration within the Carbonate Aquifer is presented in Figure 8.19. It is observed that there is an increase in the concentration east of the Red River in the region of the well. The maximum increase in concentration is 28 mg/L, which is 0.04% of the maximum concentration. It is thought that the model is not capable of modeling such small changes in concentration.

The analysis of this problem illustrates that a pumping well within the City of Winnipeg should be examined closely to ensure that the water level will not decline significantly and that the concentration does not increase significantly.

8.7 Summary

The model was used to evaluate several problems that could be encountered in the management of the groundwater systems in Southern Manitoba. The model was found to provide good solutions for evaluating: base sustainability; future sustainability; effects of a flood; effects of a drought; and effects of a pumping well.

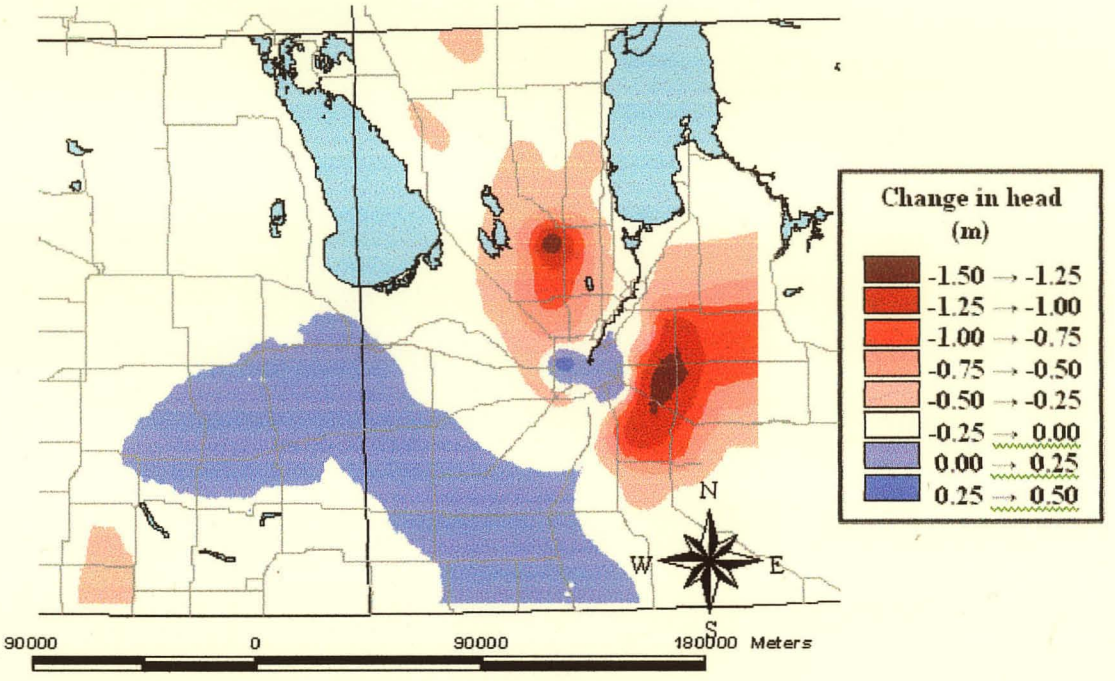

(A)

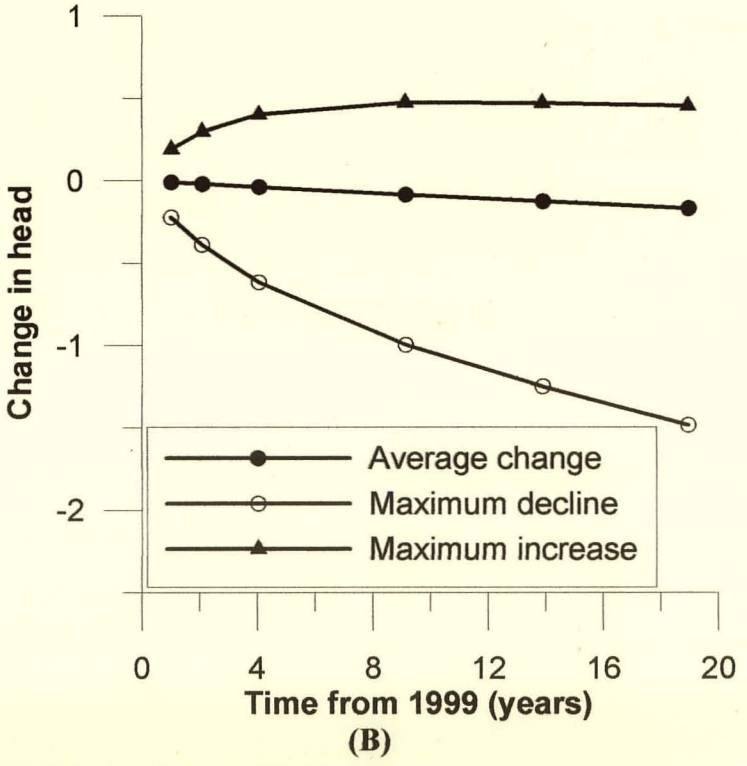

(B)

Figure 8.1 – Change in head in Carbonate Aquifer with time, maintaining pumping rates at 1999 levels: (A) After 20 years; and (B) Plot of change in head versus time.

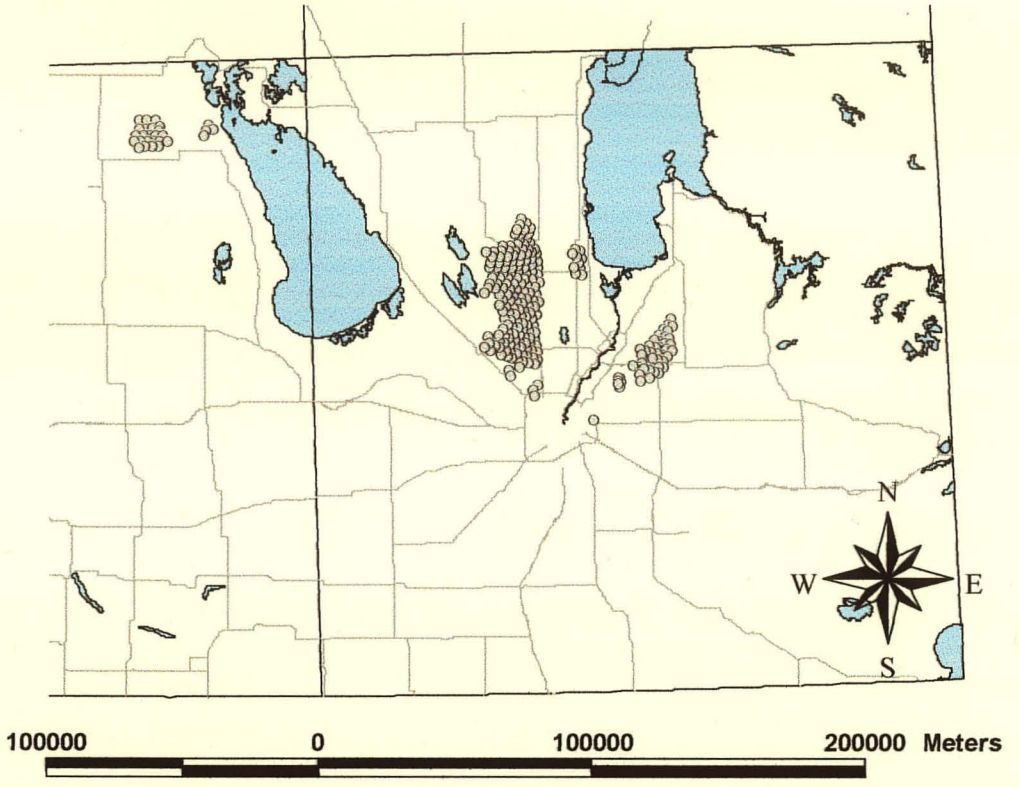

Figure 8.2 – Nodes in which the head dropped below the top of the Carbonate Aquifer after twenty years under the current sustainability conditions.

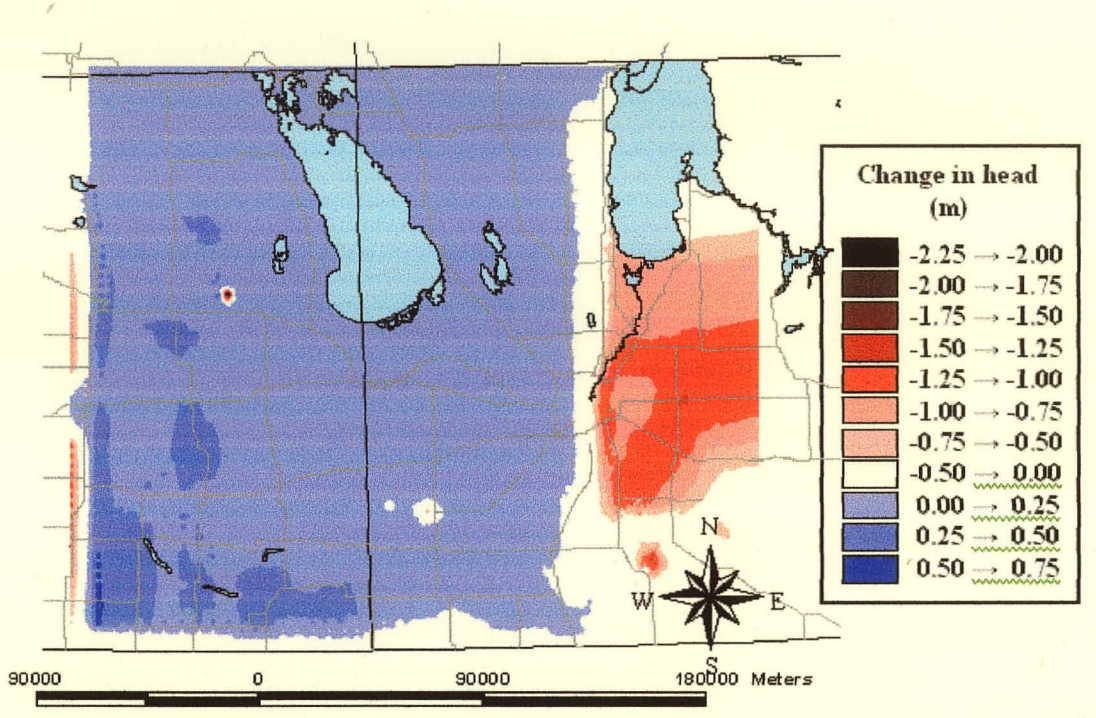

(A)

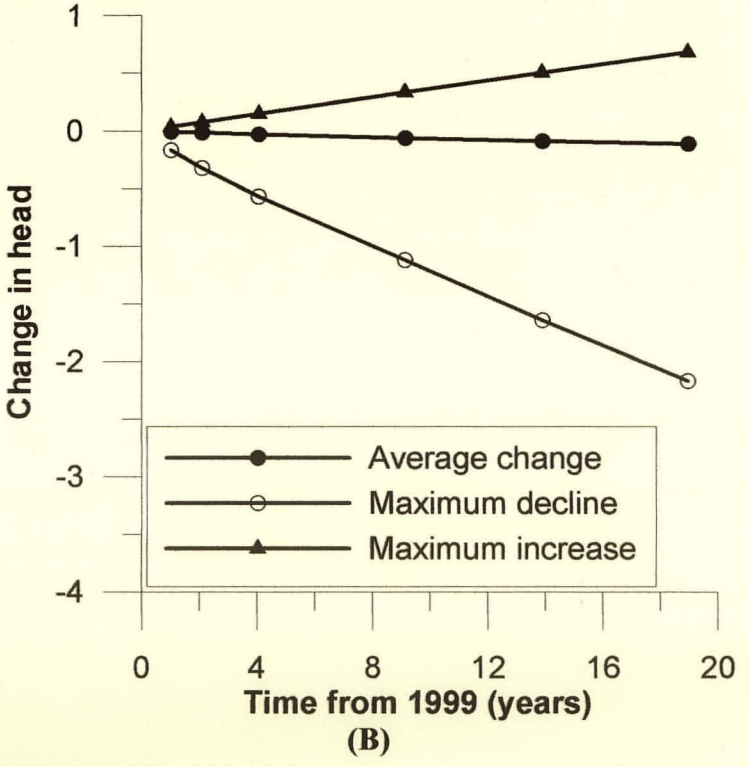

(B)

Figure 8.3 – Change in head in Sandstone Aquifer with time, maintaining pumping rates at 1999 levels: (A) After 20 years; and (B) Plot of change in head versus time.

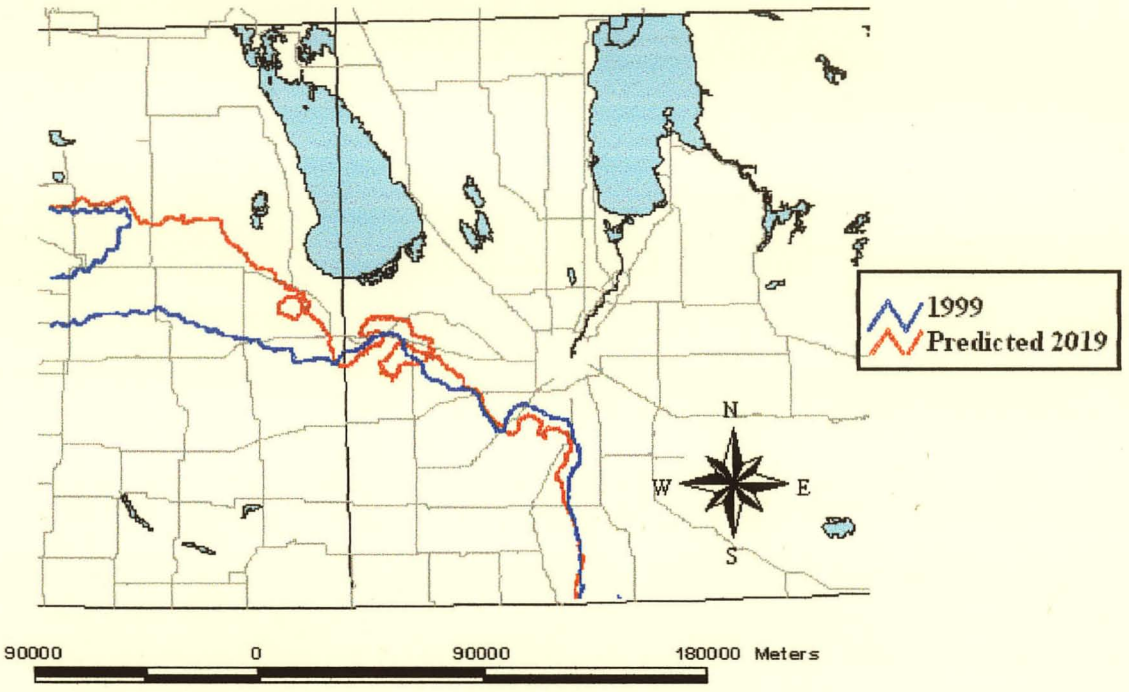

(A)

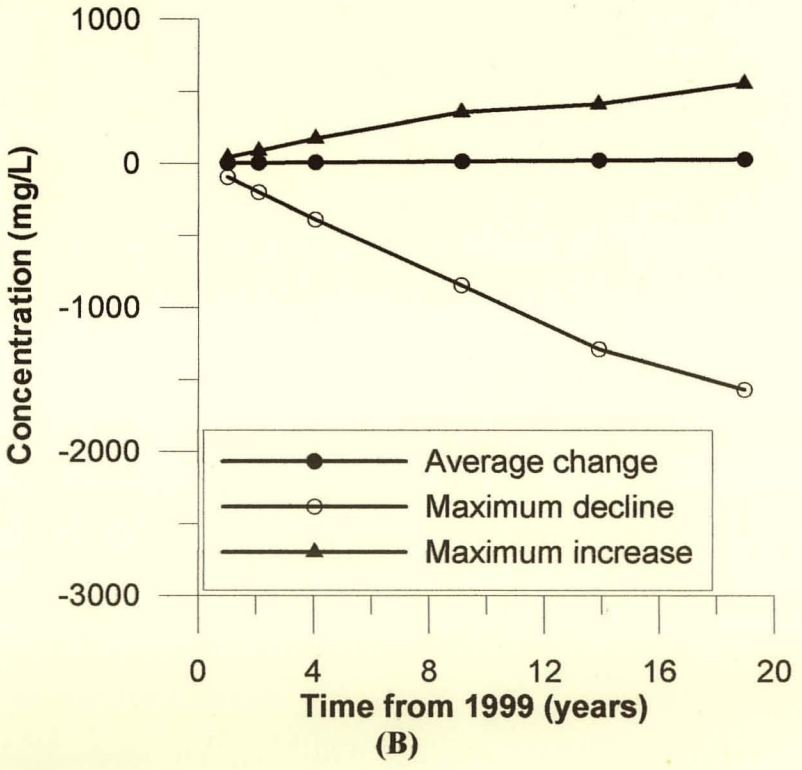

(B)

Figure 8.4 - Change in concentration in Carbonate Aquifer, maintaining pumping rates at 1999 levels: (A) C = 1 g/L contours; and (B) Plot of change in concentration versus time.

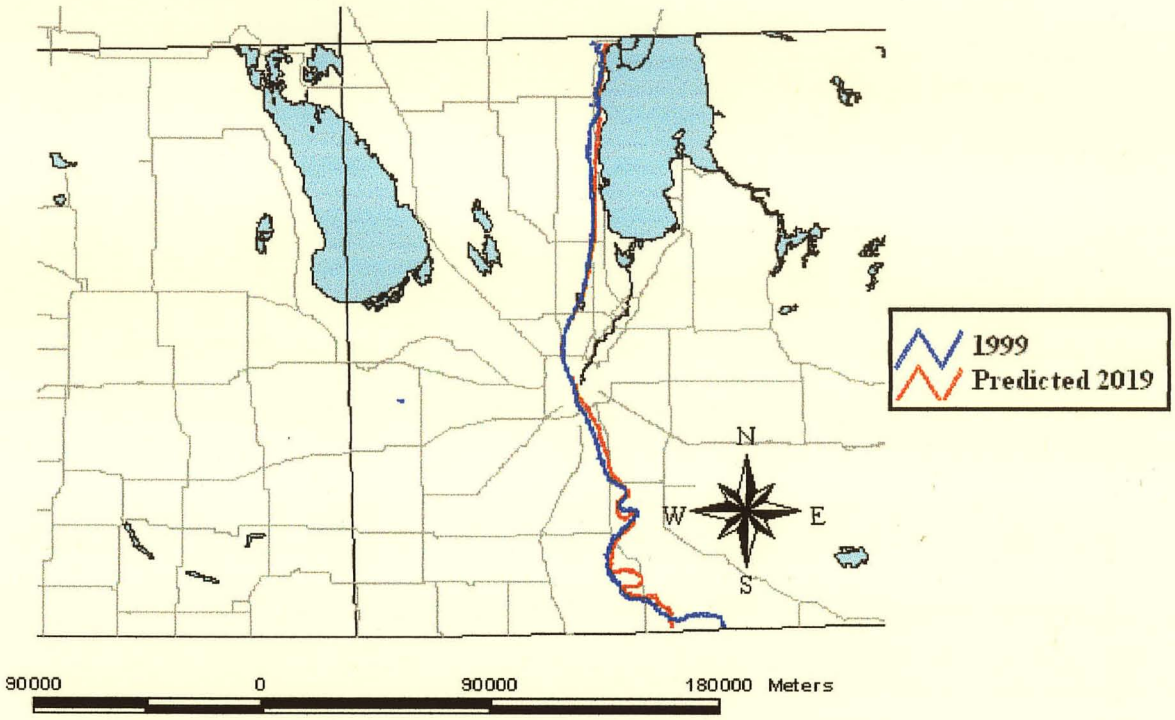

(A)

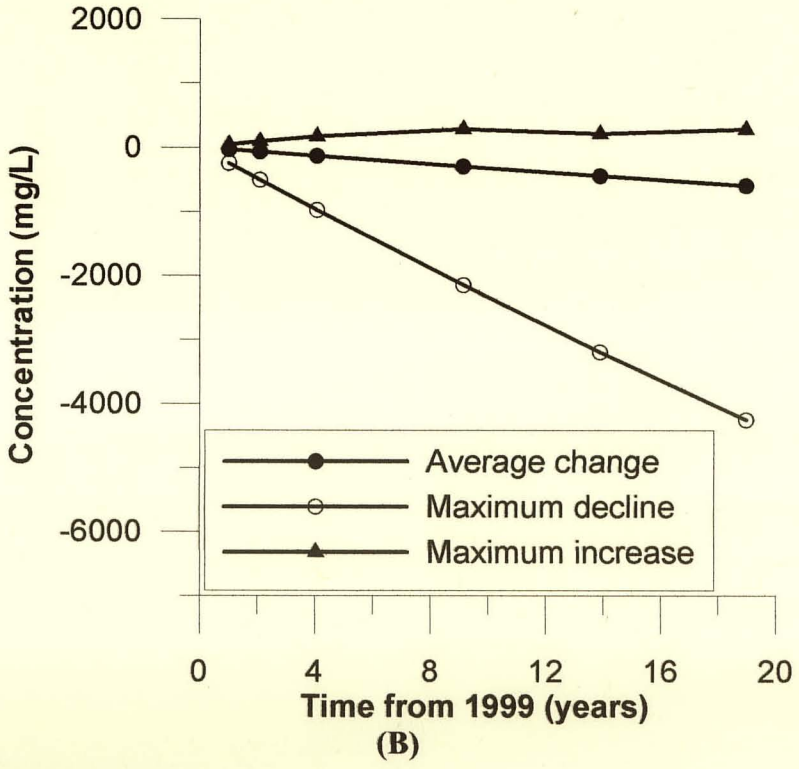

(B)

Figure 8.5 – Change in concentration in Sandstone Aquifer, maintaining pumping rates at 1999 levels: (A) C = 1 g/L contours; and (B) Plot of change in concentration versus time.

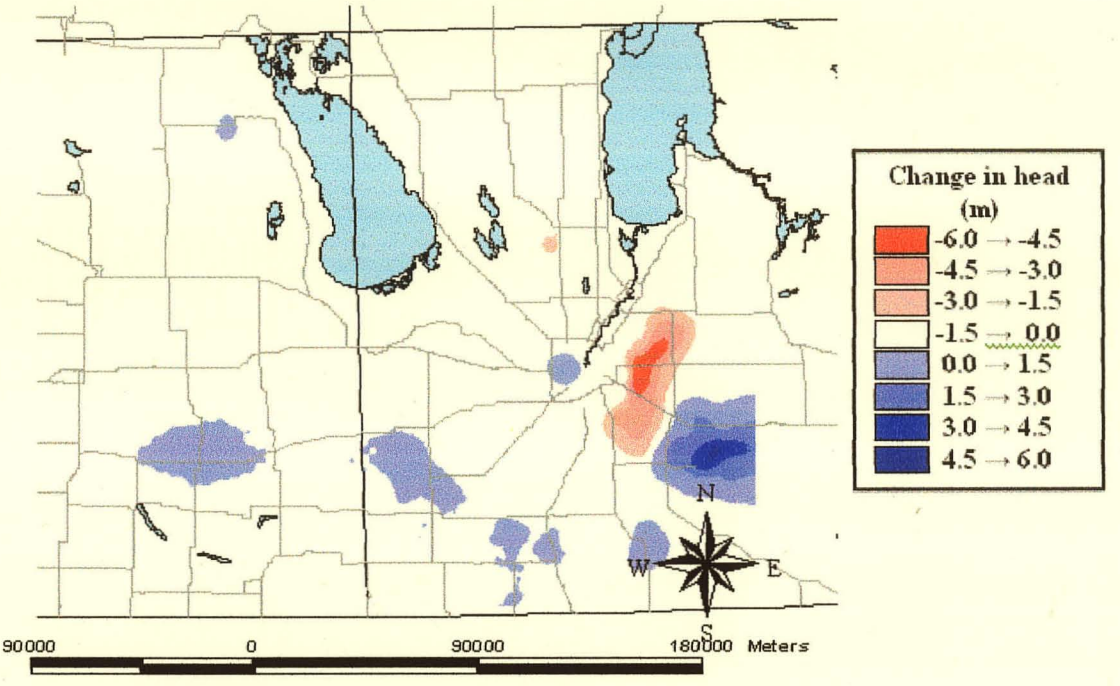

(A)

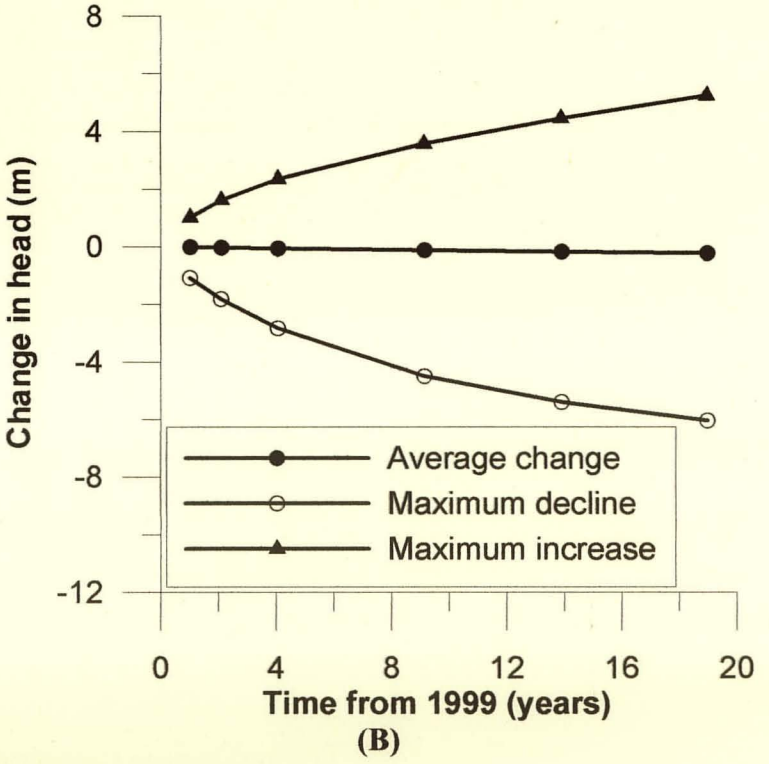

(B)

Figure 8.6 – Change in head in Carbonate Aquifer with time, while increasing pumping rates: (A) After 20 years; and (B) Plot of change in head versus time.

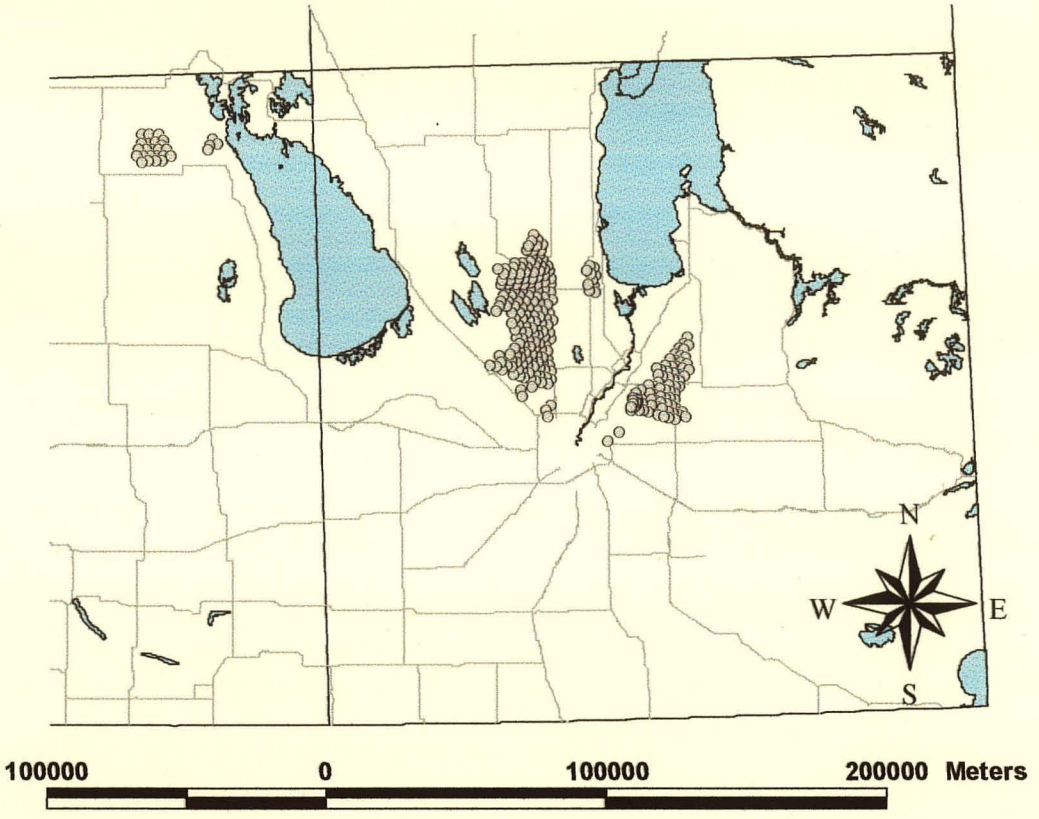

Figure 8.7 - Nodes in which the head dropped below the top of the Carbonate Aquifer after twenty years under the future sustainability conditions.

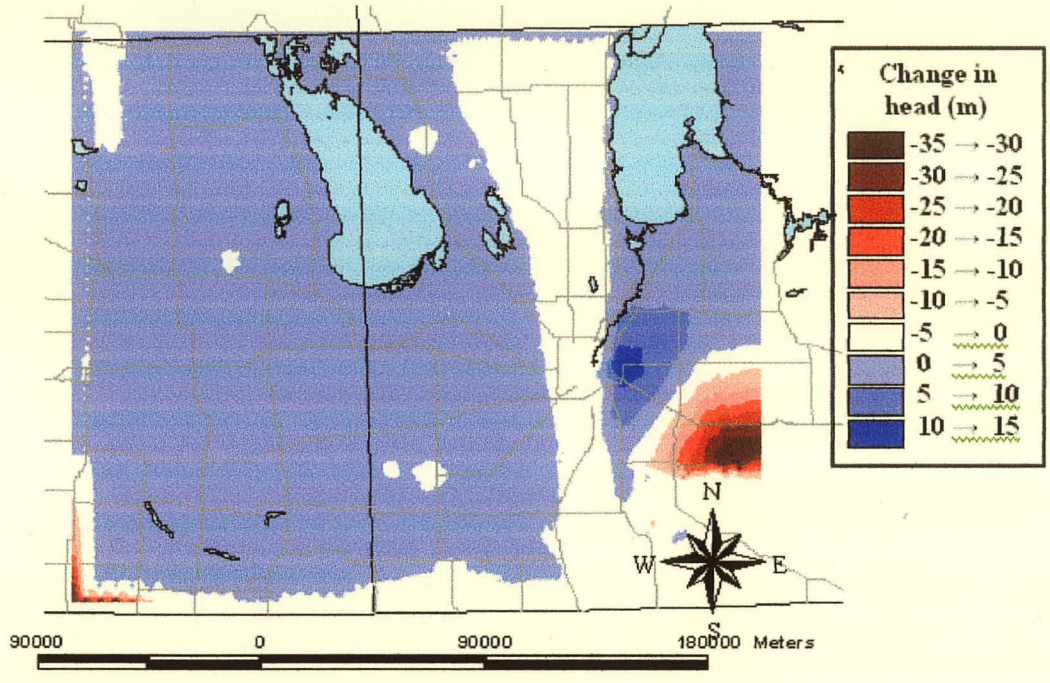

(A)

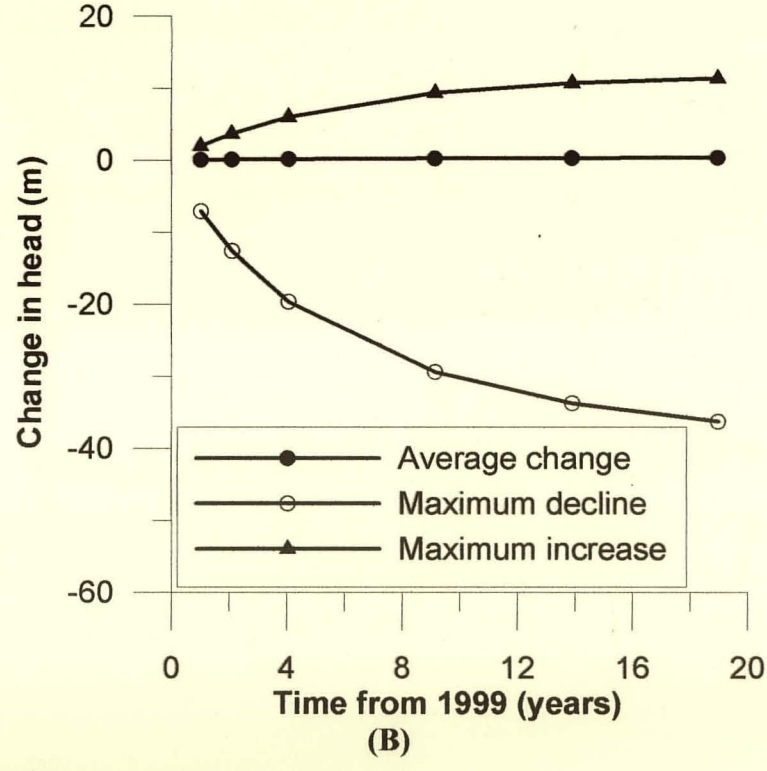

(B)

Figure 8.8 – Change in head in Sandstone Aquifer with time, while increasing pumping rates: (A) After 20 years; and (B) Plot of change in head versus time.

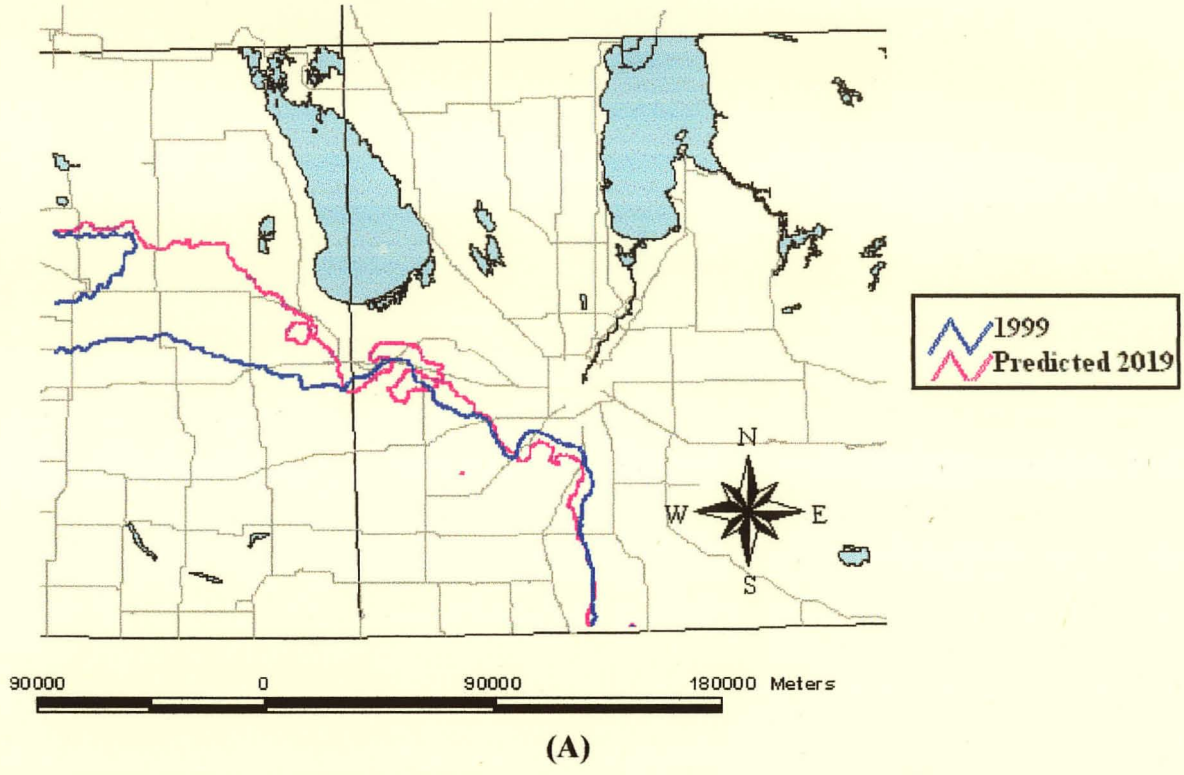

(A)

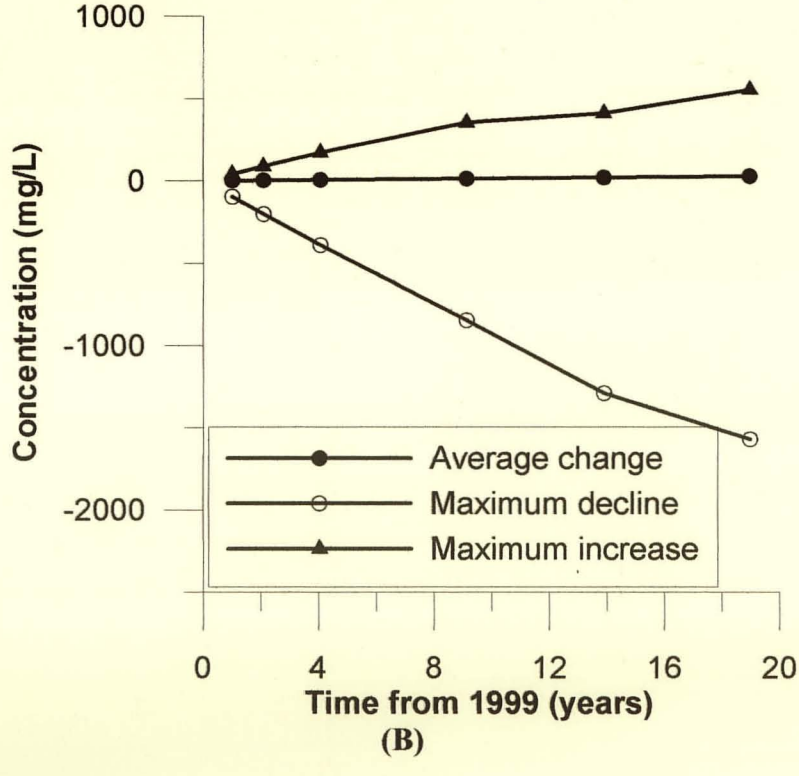

(B)

Figure 8.9 – Change in concentration in Carbonate Aquifer for future sustainability (A) C = 1 g/L; and (B) change in concentration versus time from 1999.

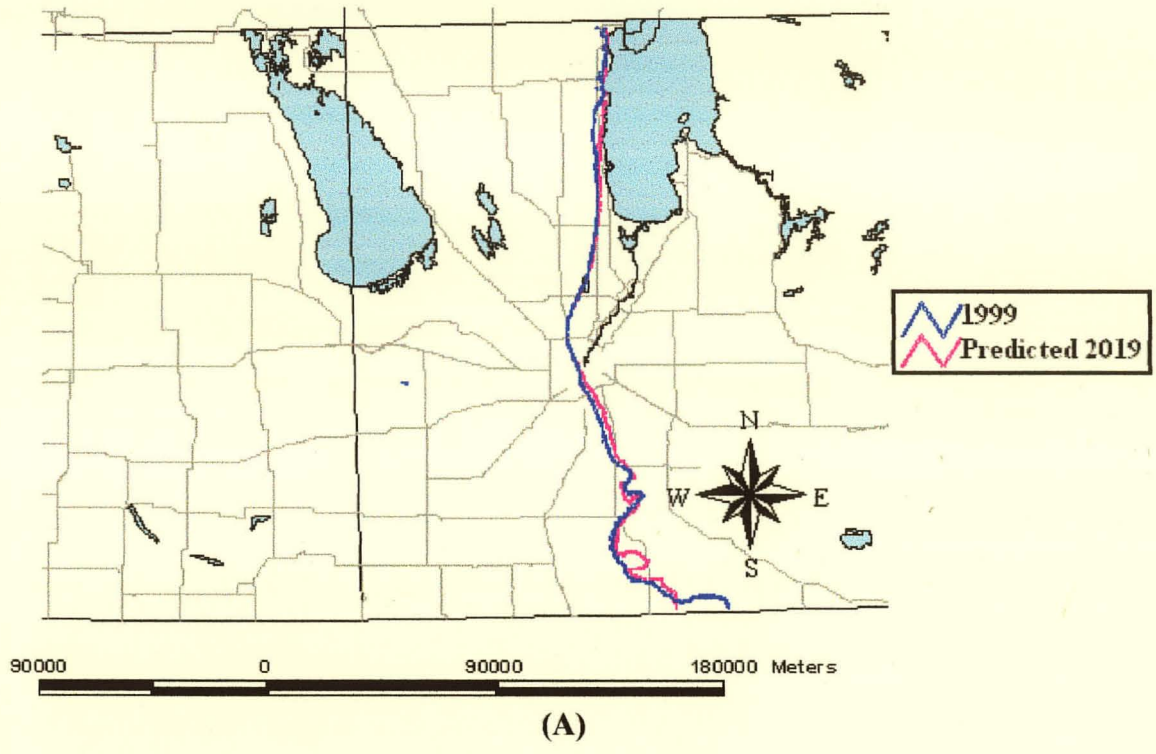

(A)

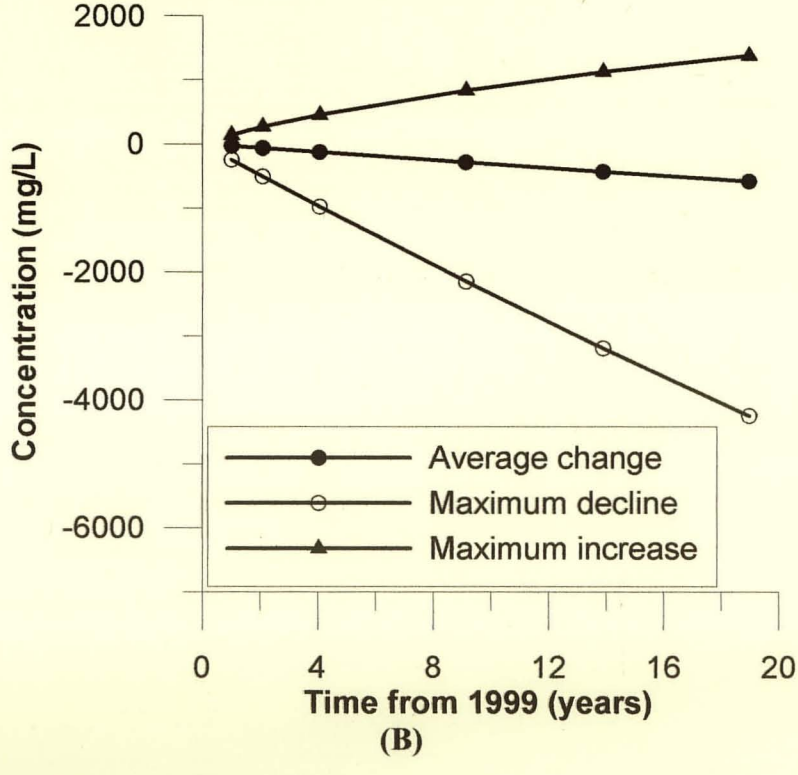

(B)

Figure 8.10 - Change in concentration in Sandstone Aquifer for future sustainability (A) C = 1 g/L; and (B) change in concentration versus time from 1999.

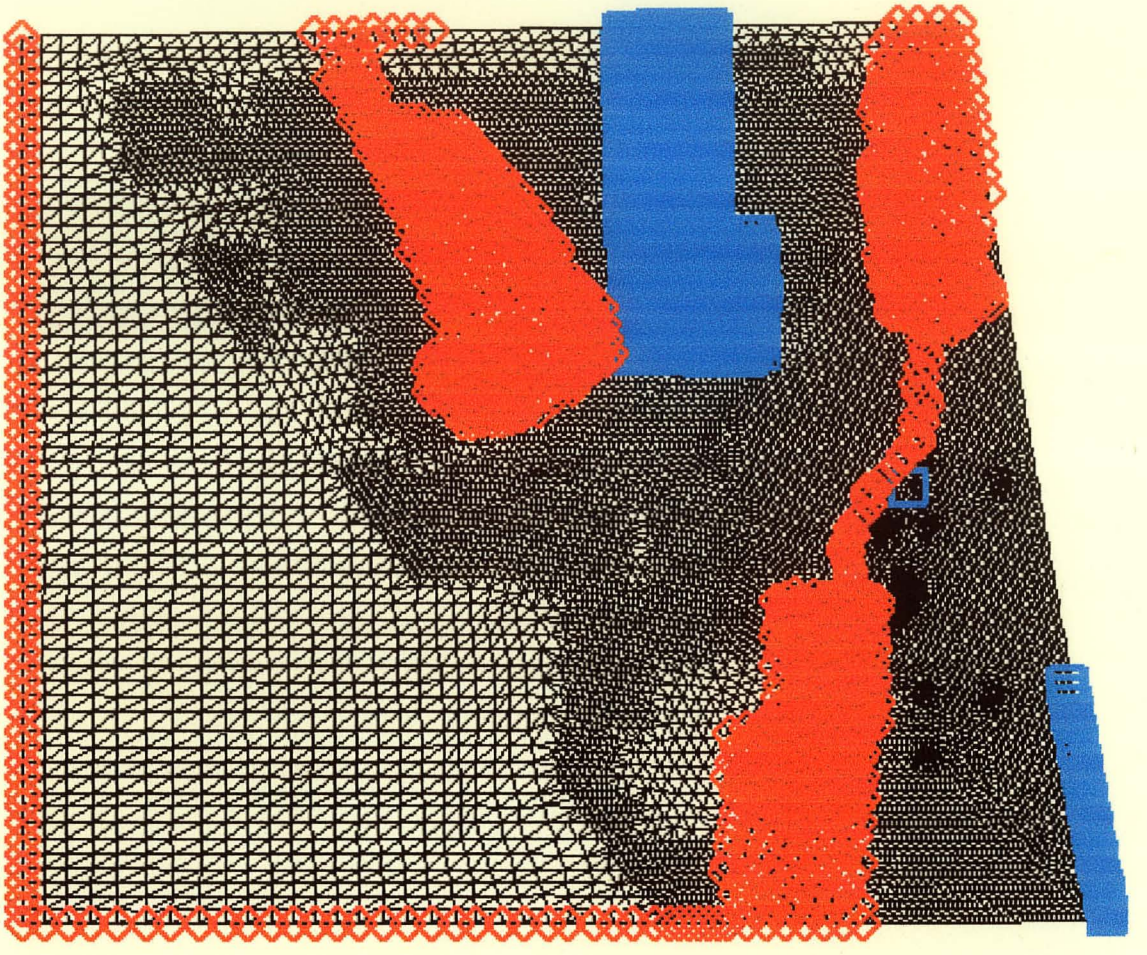

Figure 8.11 – Boundary conditions used during flooding phase of flood simulation.

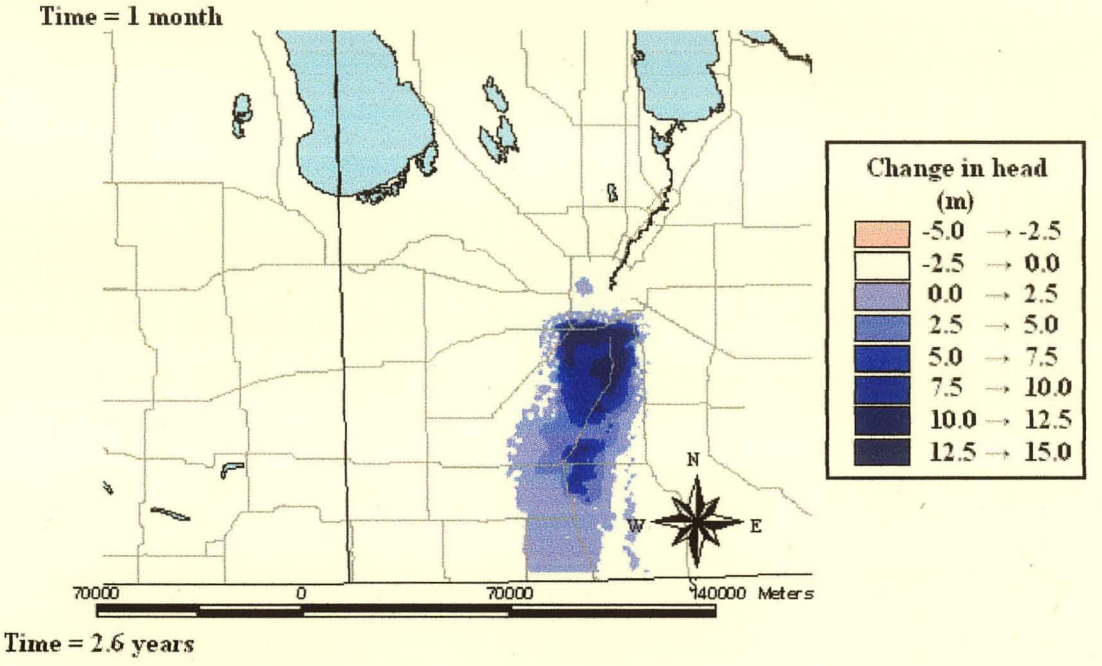

Figure 8.12 – Change in heads within Carbonate Aquifer as a result of a flood. (A) Plan view and (B) Plot of change in head versus time and (C) Average change in head with time.

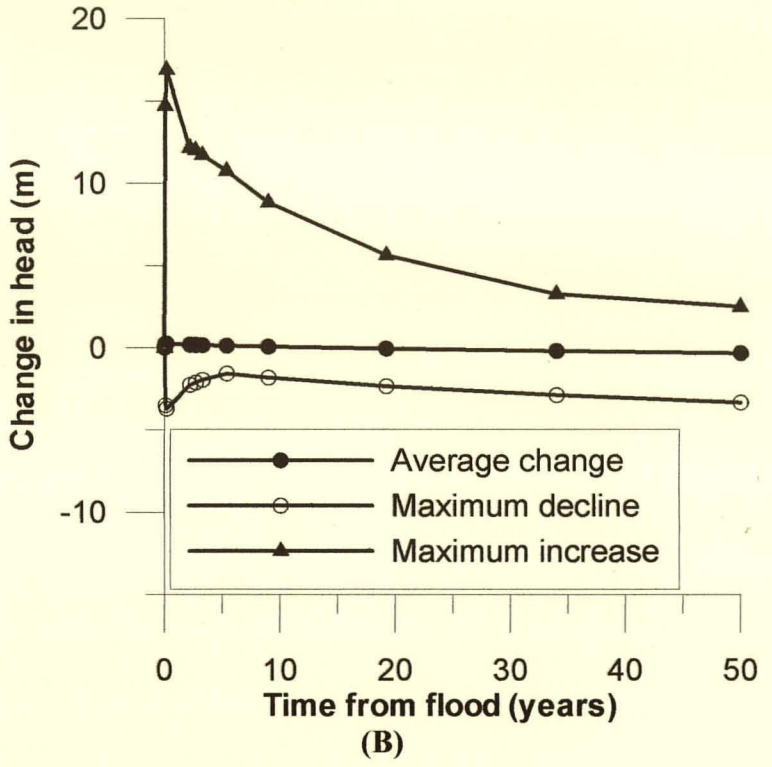

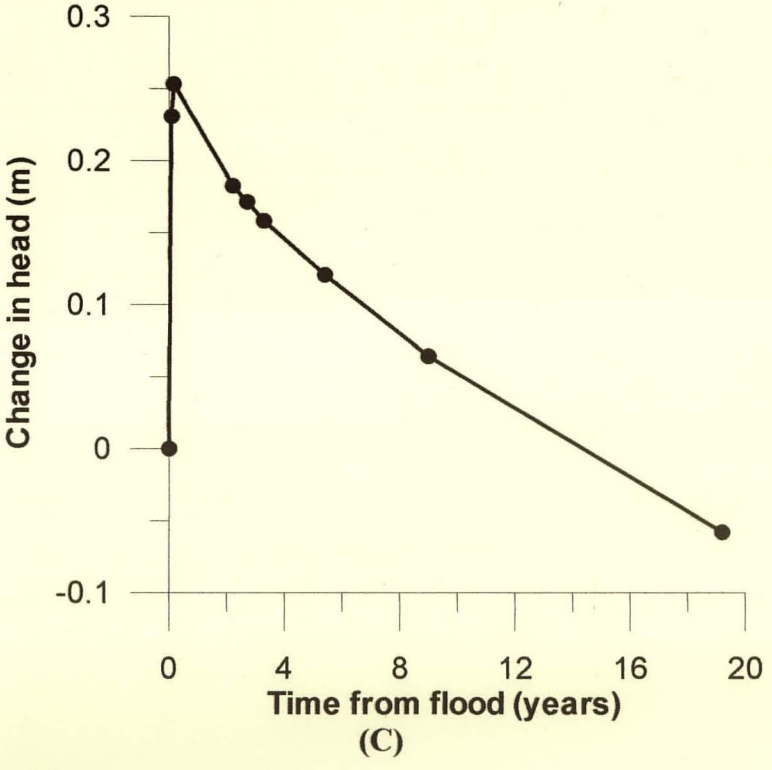

Figure 8.12 (continued) – Change in heads within Carbonate Aquifer as a result of a flood. (A) Plan view and (B) Plot of change in head versus time and (C) Average change in head with time.

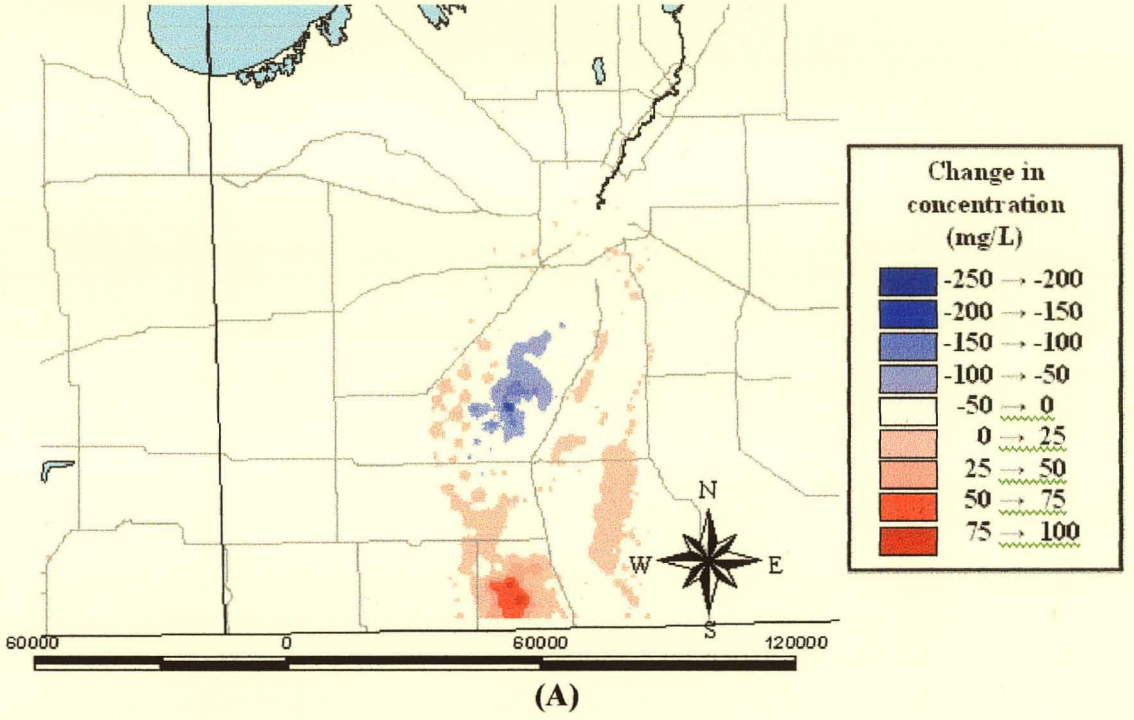

(A)

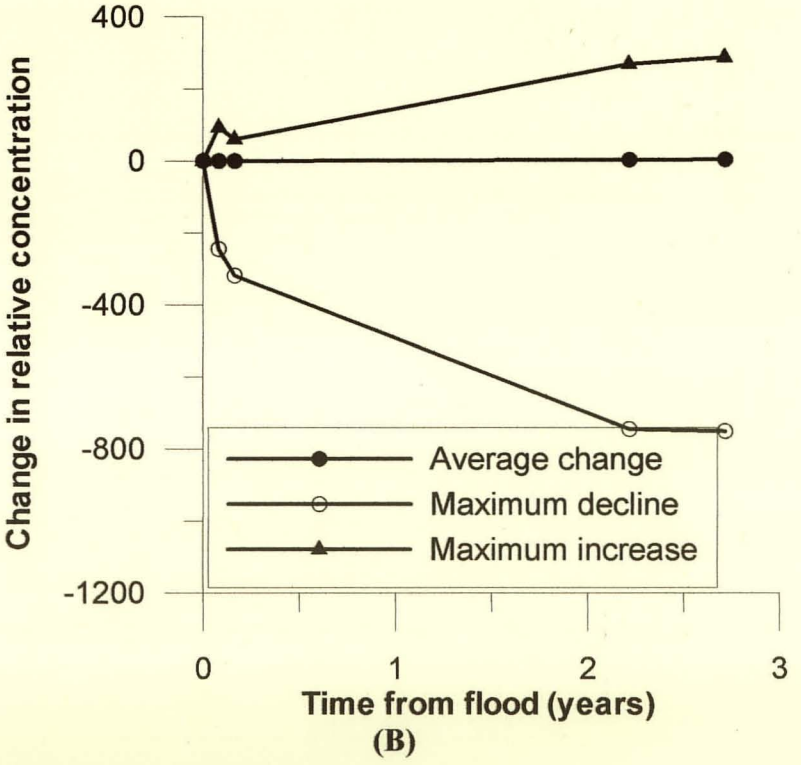

(B)

Figure 8.13 – Change in concentration in the Carbonate Aquifer as a result of a flood. (A) Plan view after one month and (B) Plot of change in concentration versus time.

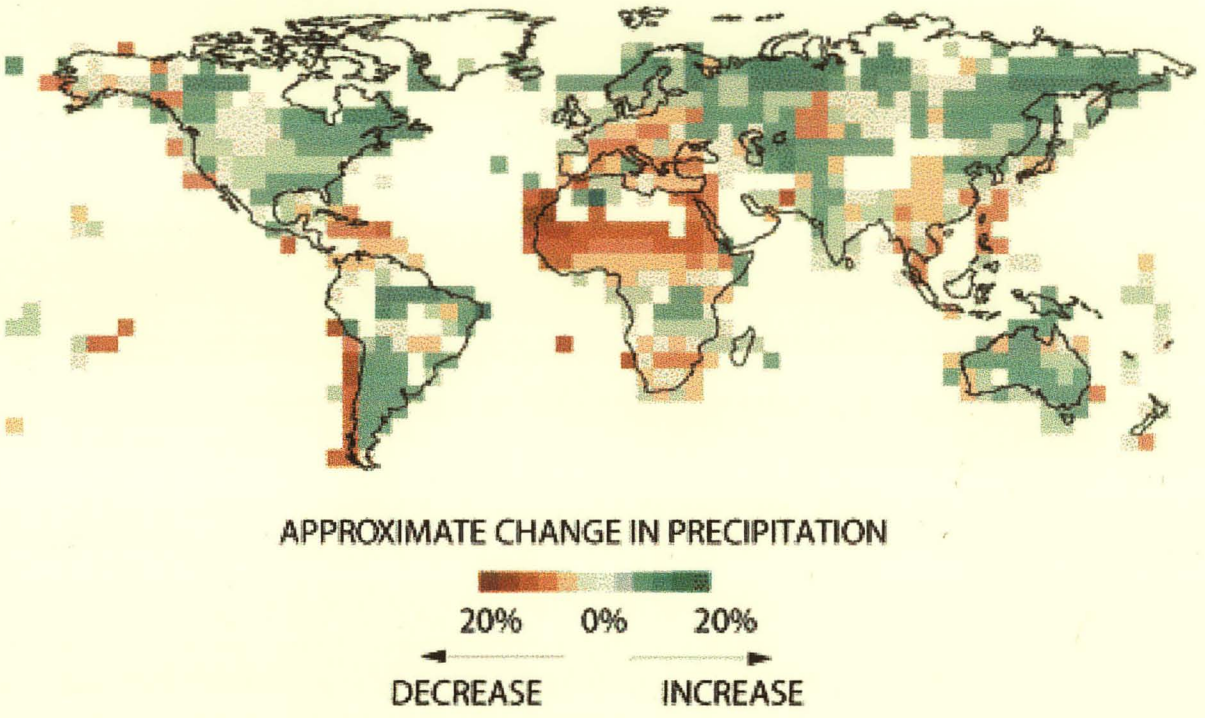

Figure 8.14 – Precipitation trends observed between 1900 and 1994 (taken from Scientific American website).

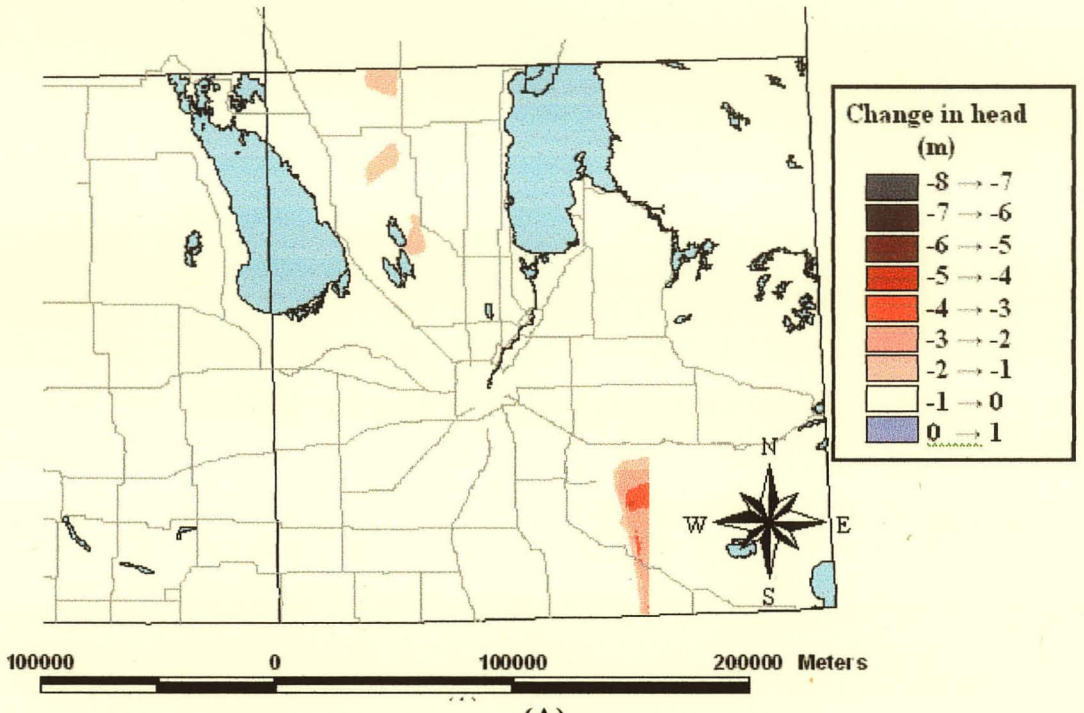

(A)

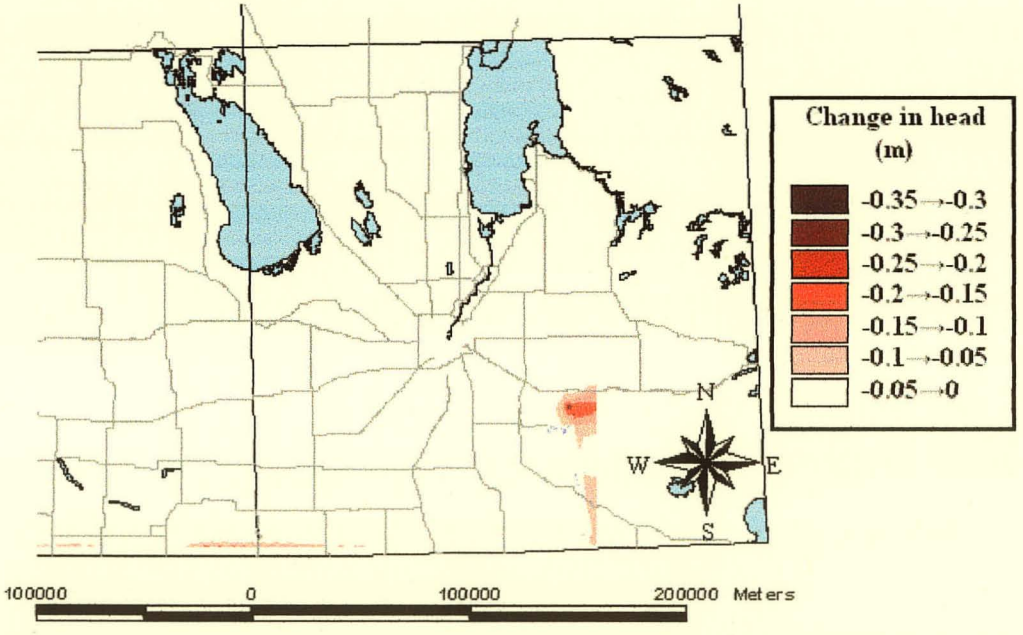

(B)

Figure 8.15 – Change in head after three years due to a drought causing a 50% reduction in recharge in (A) Carbonate Aquifer and (B) Sandstone Aquifer.

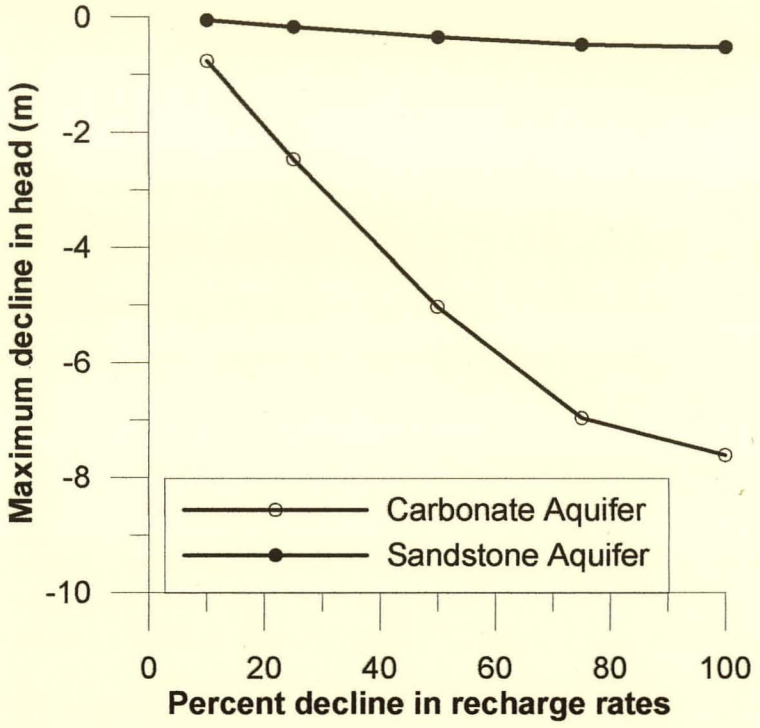

Figure 8.16 – Plot of maximum decline in head after three years of drought as a function of reduction in recharge.

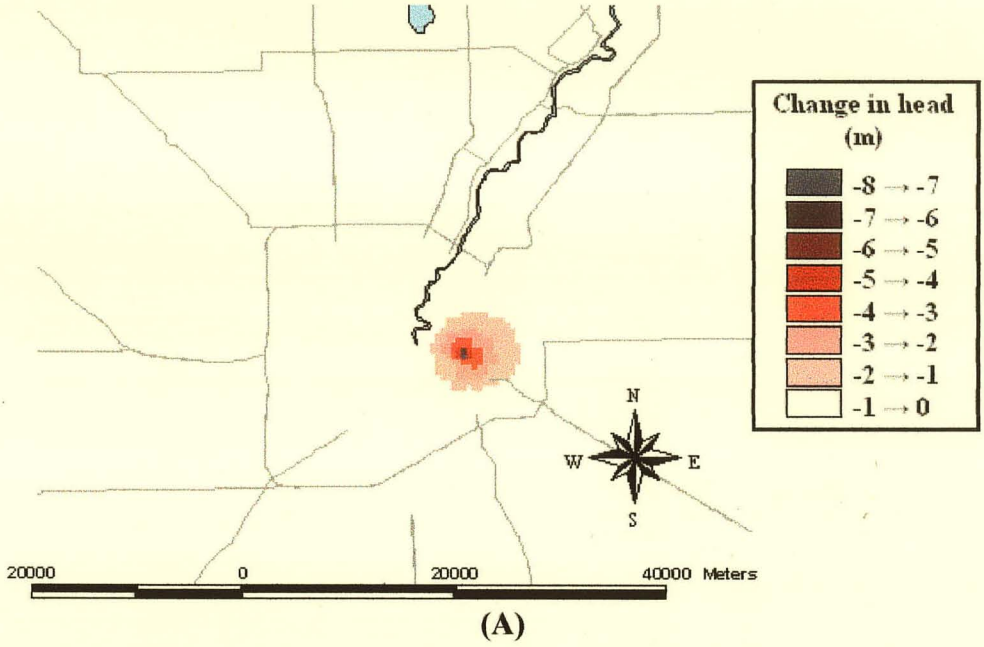

(A)

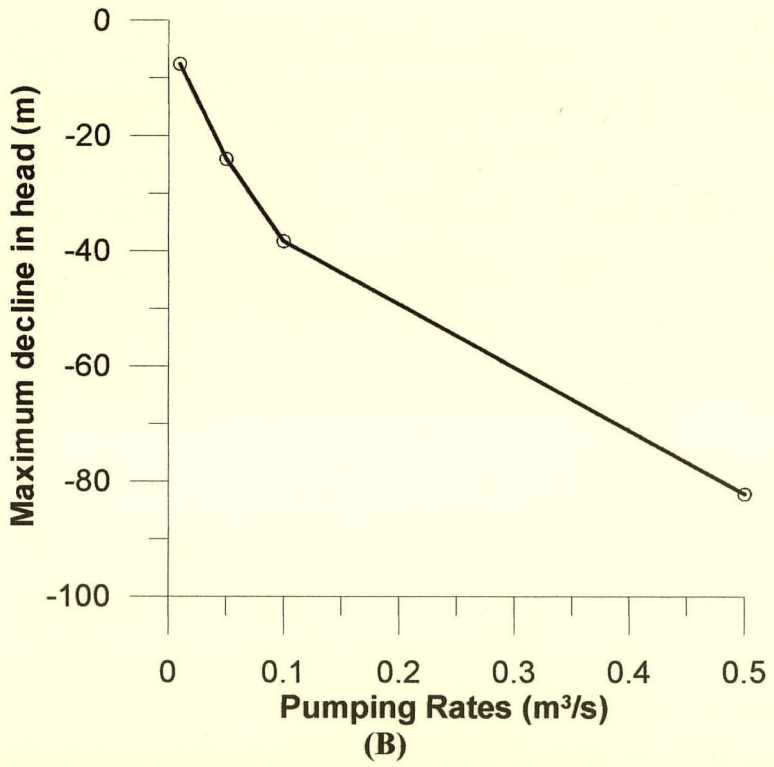

(B)

Figure 8.17 – Change in head in Carbonate Aquifer due to a pumping centre located in City of Winnipeg, screened over the Carbonate Aquifer for (A) a pumping rate of 0.05 m^3/s and (B) maximum decline in head as a function of pumping.

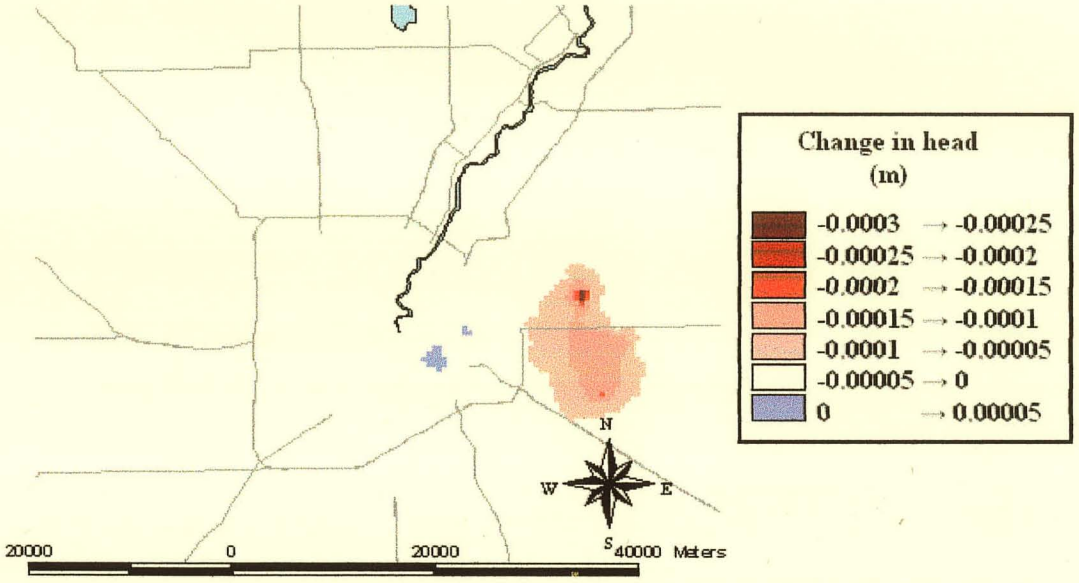

Figure 8.18 – Change in head within the Sandstone Aquifer due to a pumping centre located in City of Winnipeg, screened over the Carbonate Aquifer and pumping at 0.05 m^3/s.

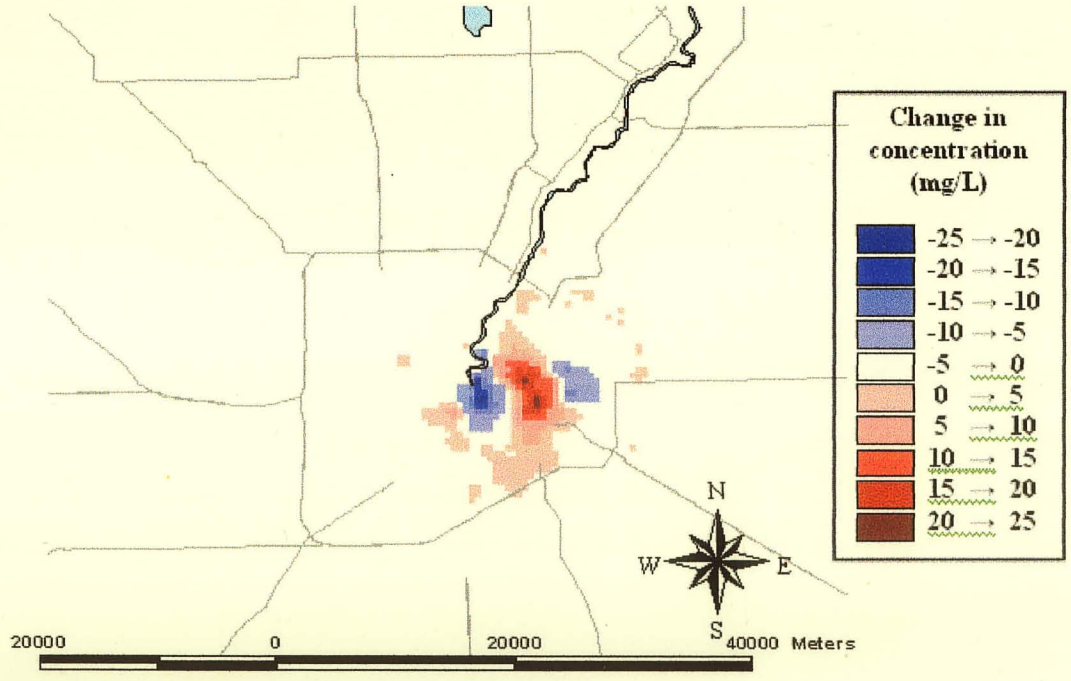

Figure 8.19 – Change in concentration in Carbonate Aquifer due to a pumping centre located within the City of Winnipeg, screened over the Carbonate Aquifer and pumping at a rate of 0.05 m^3/s.

CHAPTER 9 – SUMMARY AND CONCLUSIONS

The research conducted for this thesis consisted of developing a groundwater and solute transport model of a large three-dimensional system of aquifers in Southern Manitoba. The resulting model was used to evaluate sustainability under current and increased development. The model was also used to analyze several water resource applications such as the effect on the aquifers due to a drought, flood or new pumping centre. Several hypotheses were made during the construction of this model. To develop the hydrostratigraphic model (Chapter 3), it was hypothesized that the geology from various geologic databases would be adequate in defining these units. To perform geostatistical analysis (Chapter 5) it was postulated that data collected from mixed sources and test types would give satisfactory results. The heterogeneous hydraulic conductivity fields generated from Bayesian Updating (Chapter 6) were postulated to be useful in developing the model of flow and transport. To develop the model (Chapter 7) it was assumed that an equivalent porous media approach could be taken to simulate the fractured media of the Carbonate Aquifer. It was hypothesized that three dimensions were required to model the solute transport and that wells screened over both aquifers had to be considered. For transport parameters it was hypothesized that conditioned values of dispersivity would be lower than unconditioned values due to knowledge of the heterogeneous hydraulic conductivity. It was also postulated that the saltwater/freshwater transition zones were at equilibrium or moving very slowly. The incorporation of variable density effects was also hypothesized as being necessary. It was also postulated that the Red River

Floodway had to be incorporated to calibrate the model. This chapter summarizes the findings of this thesis as well as discusses each of the aforementioned hypotheses.

The construction of the flow and transport model for southeastern Manitoba followed the protocol summarized by Anderson and Woessner (1992). As part of this research, the suitability of this protocol is evaluated qualitatively. The first step in the protocol was to establish a purpose, which for this case was to examine sustainability of water supply and quality in the bedrock aquifers of Southern Manitoba. A conceptual model was constructed as covered in Chapters 3 and 4. The hydrostratigraphic model (Chapter 3) was developed by transferring lithostratigraphic units to hydrostratigraphic units. For this research, the bedrock geology and surficial unit geological information was fairly well defined for most units. However, where information was lacking assumptions were made. The Carbonate Aquifer is located within the more permeable fractured region of subcropping carbonate rocks. However, the exact thickness of the fractured zone was variable and not noted in any database. An aquifer of a thickness of 15 m was therefore assumed.

Data collection was also conducted as part of the conceptual model development and resulted in the most extensive collection of transmissivity data to date in Southern Manitoba. The data was collected from a variety of sources, and no physical testing was actually conducted as part of this thesis. The resulting database of transmissivity was quite extensive for a modeling project of this nature. In many cases, spatial locations of wells or measurement locations were estimated to obtain the UTM coordinates. Ground

elevations were determined from a digital elevation model. For the hydrogeological properties, the assumptions used to determine the x, y and z coordinates did not have an adverse effect on subsequent geostatistical analysis and Bayesian Updating interpolation.

A large quantity of transmissivity data (2708 points) for the Carbonate Aquifer was determined from pump and specific capacity tests. The database for the Sandstone Aquifer (78 points) was not as substantial given the large areal extent of this aquifer, and measurement locations were generally in the eastern portion of the region. In terms of other required hydrogeological properties, measurements were scarce. For storativity values, only two wells were analyzed within the Carbonate Aquifer and none within the Sandstone Aquifer. Therefore, ranges of storativity had to be estimated from first principles and were assumed homogeneous within each unit. The final value of storativity used in the model was determined through history matching and were assumed homogeneous within each unit. Porosity values for all units were also assumed homogeneous within each unit.

Parameters required by the solute model included the longitudinal, transverse and vertical dispersivities for each unit. However, no values of any of these parameters were available from physical measurements. Unconditional longitudinal dispersivity values were estimated from the transmissivity statistics and were determined to be 78 km for the Carbonate Aquifer and 35 km for the Sandstone Aquifer. However, through calibration of the numerical model, it was found that the conditional longitudinal dispersivity values were 50 km for the Carbonate Aquifer and 15 km for the Sandstone Aquifer. In both

cases, the conditional value of the longitudinal dispersivity is less than the unconditional value. This observation agrees with Neuman (1990), in that the value of dispersivity decreases with increasing knowledge of the heterogeneous hydraulic conductivity. Both aquifers were modeled with heterogeneous hydraulic conductivity assigned. For the Carbonate Aquifer, a fully heterogeneous hydraulic conductivity field was applied from interpolation using the Bayesian Updating method. For the Sandstone Aquifer, heterogeneities were incorporated through zonation.

The resulting database was fairly typical, if not better, than most databases for regional scale problems. However, there were still gaps in the dataset requiring many assumptions and estimations. This requirement of the protocol for such extensive amounts of data is very difficult to achieve in practicality.

Geostatistical analysis was conducted on the transmissivity datasets to determine the general properties, the distribution type and the correlation structure for each unit. Even though large quantities of specific capacity were used to estimate transmissivity, very good results from statistical analysis were achieved. For all units, the transmissivity was found to follow a log normal distribution by the Chi Square and normal scores plot tests. This distribution type agrees with that found in the literature (Freeze and Cherry, 1979). The Carbonate Aquifer had a log transmissivity that ranged between –12.5 (3.7×10^{-6} m^2/s) and –0.9 (0.4 m^2/s), with a mean of –7.2 (7.5×10^{-4} m^2/s) and variance of 2.7. The Sandstone Aquifer had a log transmissivity ranging between –12.4 (4.1×10^{-6} m^2/s) and –2.0 (0.14 m^2/s), with a mean of –8.0 (3.4×10^{-4} m^2/s) and variance of 2.2. The variogram

was determined using two semi-variance estimators: the Classical Estimator of Matheron (1960); and the Moving Window Estimator of Li and Lake (1994). The Moving Window Estimator was found to give much more stable results than the Classical Estimator. The results of the Moving Window Estimator were such an improvement that very representative models of the variograms could be constructed. Whereas, if the Classical Estimator had been used it would have been difficult to generate reliable variogram models. For all units, the semi-variance was found to increase and level off to a sill value equal to the variance of the data. In most cases, the exponential model was found to have the best fit according to the Akaike Information Criterion (AIC), which optimizes between goodness of fit and the number of parameters. The exponential model is in agreement with what has been cited in the literature previously (e.g. Sudicky, 1986; Gelhar, 1993; Woodbury and Sudicky, 1991; Hoeksema and Kitanidis, 1985). For the Carbonate Aquifer, it was found that a nested structure of a nugget, exponential model and spherical model (Equation 5.1), modeled the variogram at intermediate lag distances better than the exponential model. The parameters of the exponential model were a sill of 2.65, nugget of 2.0 and integral scale of 29,780 m. For the Sandstone Aquifer, the exponential model gave the best fit with sill of 2.9, nugget of 0.56 and integral scale of 16,828 m. Neither variogram of the Carbonate or Sandstone Aquifers were found to exhibit fractal nature, in the sense of showing self-similarity at different scales, agreeing with the results of Hoeksema and Kitanidis (1985).

Bayesian Updating was subsequently used to interpolate the log transmissivity observations to each node within the finite element mesh. This methodology uses the

general statistics, the correlation structure and uncertainty within the measurements themselves. For the Carbonate Aquifer, as the data was present throughout the entire study area, the resulting transmissivity field showed variability throughout. The transmissivity field generated from certain data compared well against that generated from kriging using the same statistics and measurements. The Bayesian Updated field had smaller standard deviation values and therefore lower uncertainty at each node than the kriging field. The Bayesian Updated field assuming uncertain measurements was found to give smoother results than the Bayesian Updated field from certain measurements. The smoother result was attributed to reduced impact from extreme values. The hydraulic conductivity was calculated by dividing the transmissivity by the assumed saturated thickness of 15 m. The elemental hydraulic conductivity of the Carbonate Aquifer in the model was assigned from nodal values using the geometric mean.

The heterogeneous log transmissivity field was also generated for the Sandstone Aquifer using Bayesian Updating. However, the database of transmissivity measurements for the Sandstone Aquifer was limited and clustered in the east. Therefore, the transmissivity field from Bayesian Updating shows variability in the east, but is very smooth and essentially equal to the mean in the west. This observed result in the west is a result of a lack of "new" information to alter the initial state. The hydraulic conductivity was calculated by dividing by the thickness of the Winnipeg Formation as determined from the geology. This heterogeneous hydraulic conductivity field was initially used in the modeling phase; however, the flow results did not match those observed in the field. For

this case, Bayesian Updating was not successful in assigning heterogeneous hydraulic conductivity. Therefore, the hydraulic conductivity for the Sandstone Aquifer was assigned by dividing the region into thirty-two zones assuming homogeneous hydraulic conductivity within each zone.

FRAC3DVS is a finite element, saturated/unsaturated, flow and transport code that was used for the modeling exercise. A finite element mesh was constructed from the hydrostratigraphic model units. The hydraulic conductivity for the Carbonate Aquifer was assigned from the heterogeneous log transmissivity field generated using Bayesian Updating. The hydraulic conductivity for the Sandstone Aquifer was assigned using zones and values determined through calibration. The remaining units were assigned a homogenous hydraulic conductivity. For all units it was assumed that $K_x = K_y$ and $K_z = 0.1 \cdot K_x$. All other properties were assumed homogeneous within each unit. The model simulated both flow and transport, solving for equivalent freshwater head for flow and relative chloride ion concentration for transport.

The boundary conditions for the flow model were assigned from observations. The water levels in both Lake Manitoba and Lake Winnipeg were assigned Type I BCs based on the measurements from the early 1920's. The western boundary was assigned a Type I BC from the observed potentiometric surface in this region. The recharge boundaries in the Interlake region, the Sandilands and Birds Hill were assigned Type II BCs. The values of the flux were not well defined and values were determined through the calibration and history match of the model. For the three-dimensional solute transport model, Type III

boundary conditions were incorporated on the western boundary. This boundary condition provided the source of solute entering the system. Initially Type I boundary conditions were used, but were found to cause irregularities on western boundary.

The flow model was calibrated by comparing the steady state model results with historical water levels. The set of historical water levels was collected from water levels at time of drilling for those wells constructed prior to 1920. Problems with this dataset were that the measurements themselves were taken over several years, resulting in a piezeometric surface that was not instantaneous. However, this dataset was the best source available for the model calibration. The other issue was that no historical data was acquired for the Sandstone Aquifer. A successful calibration of the Carbonate Aquifer flow model was determined and therefore this dataset of pre 1920 water levels was adequate. For the Sandstone Aquifer a steady state model was qualitatively assessed and then a history match was conducted. The history matching was conducted by stepping the model through time with variable density aspects incorporated, from 1920 to 1999, and comparing the model results against current water levels. These current water levels were collected from observation wells that were implemented by the Water Branch of the Manitoba government. This dataset was satisfactory to obtain instantaneous piezeometric surfaces and is present throughout much of the region for the Carbonate Aquifer. For the Sandstone Aquifer, however, there are only five observation wells. Therefore, the Sandstone Aquifer aspect of the flow model was constructed based only on the history match with five observations. The flow model results of the overall model satisfied the

calibration target, however, the lack of observations in the Sandstone Aquifer required by the protocol imposes limitations on the flow model.

In the end, the RMS error of the steady state flow model was 7.49 m and of the history match was 10.4 m. For the transport model, the RMS error was 0.039, which corresponds to an absolute value of chloride ion concentration of 2,925 mg/L. Plots of computed versus observed values were generated for all calibration and history match exercises. Linear regression was conducted and the slope and intercept compared against the desired values of 1.0 and 0.0, respectively, using the t-test. The R^2 value was compared against a value of 0.0 and if found significantly different then correlation was said to exist. For the three-dimensional flow model, the RMS values were below the calibration target of 13 m, the slope was significantly close to 1.0, the intercept was significantly close to 0.0 and correlation between computed and observed heads was found to exist. Therefore, the flow model satisfied all of the pre-defined calibration targets. The three-dimensional model satisfied all targets and was judged reasonable. Therefore, data collected from water well measurement and compared against water levels from wells was adequate in constructing a regional scale flow model.

The chloride ion concentration was used to model the brine movement in the solute transport model. FRAC3DVS does not directly determine the steady state transport solution. Therefore, as steady state is the limiting case of the transient solution, the "steady state" solution was generated by running the model over a significantly long time. There was no historical dataset of chloride ion concentrations for either aquifer.

Therefore, the concentrations used as an initial condition at 1920 could not be assessed quantitatively but simply estimated on a qualitative basis. This initial condition of concentrations was then used to step the transport model forward from 1920 to 1999. Datasets of chloride ion concentrations from 1999 sampling were used to evaluate the model through history match.

For the transport model, the RMS was 2.9 g/L, which is less than calibration target of 7.5 g/L. The linear regression of computed versus observed did not have as successful results. Correlation was found to exist; however, the slope was significantly different from 1.0. No changes in parameters were found to improve this result. It was judged that the transport model would be suitable to simulate large scale brine movement. However, small scale concentration changes could not be adequately predicted.

Two problems associated with the calibration procedure of the protocol were found in this research. The first was that a historic dataset of water level measurements was available for the Carbonate Aquifer but there was no similar dataset for the Sandstone Aquifer. For the transport model, no historic dataset of measurements of chloride ion concentration was available for either aquifer. Therefore, only a calibration according to the protocol could be conducted for the Carbonate Aquifer flow. For a history match there was an adequate dataset for the Carbonate Aquifer but limited for the Sandstone Aquifer. Therefore, it is difficult to find measurements taken under two different stress conditions. The second problem associated with this calibration procedure is that the model results are compared against a set of measurements that are uncertain. Many

errors are associated with these measurements, such as: measurement error, location error, interpolation error and scaling effects. The fact that a model is said to be calibrated if a good fit is achieved between model results and the uncertain measurements cause even the best models to be questionable. Errors between measurement and model results are allowed within defined targets. However, different combinations of hydrogeological properties and boundary conditions could easily satisfy the targets. Therefore, solution uniqueness comes into question. A history match is used to increase probability of having reliable results. A post audit after significant development of the groundwater system would again increase confidence in the model. However, the model results are still compared against uncertain measurements. Another method of model evaluation would be a good research area to be investigated in the future.

To determine whether the three-dimensional transport model was a significant improvement over the individual two-dimensional models, the means and variances of the residuals were compared. To test whether there is a significant difference between residual means the t-test was used. The absolute mean of residuals for the three-dimensional transport model was significantly lower than that of the two-dimensional models. This test shows that there was less error in the three-dimensional transport model. The variances were compared using a variance ratio test. This test proved that the variance of the three-dimensional model is significantly lower than that of the two-dimensional models. These statistical tests prove that the region requires modeling in three-dimensions.

The model was used to evaluate several problems encountered in water resources engineering. The first two issues related to sustainability of the system. A base case was examined by running the model over twenty years while maintaining pumping rates constant. The maximum head decline in the Carbonate and Sandstone Aquifers are -1.5 m and -2.2 m, respectively. The head drop in the Carbonate Aquifer over an area of 5 square kilometers continued to decline past twenty years simulation, and could signify potential problems in this region. In the Carbonate Aquifer, the transport model showed movement towards the northeast of the 1.0 g/L chloride concentration contour. For the Sandstone Aquifer the 1.0 g/L chloride concentration contour moved only slightly. The model predicted flow through wells screened over both aquifers to be 0.03 m^3/s.

A second sustainability case was examined, in which pumping rates were increased to simulate continued development. The model was again for run for twenty years simulation time. For the Carbonate Aquifer, the maximum decline in head was -6.0 m after twenty years. This is an increase of -4.5 m between the base and increased development cases of sustainability at twenty years. Within the Sandstone Aquifer, the maximum decline in head is -36 m, which is a -33.8 m decrease in head between the current and future sustainability cases at twenty years. For the Carbonate Aquifer, the 1.0 g/L chloride ion concentration contour line shows similar movement to the northeast as the base case. For the Sandstone Aquifer, the movement of the 1.0 g/L chloride ion concentration contour appears to be the same as that of the base case.

The model was also used to observe the effects of a flood on the aquifers. The flood scenario showed noticeable increase in head in the Carbonate Aquifer during the flooding phase and then slowly declined towards pre-flood conditions. In terms of concentrations, the Carbonate Aquifer displayed an increase in concentration in the flood region. However, the changes in concentration were slight and it is judged that the model could not accurately simulate such small changes. After the Flood of 97, increases in concentration were observed (Betcher, personal communication 2002). However, it was not known if these changes were due to groundwater movement or injection of contaminated water through wells. The effects on both head and concentration within the Sandstone Aquifer were found to be negligible.

A drought scenario was examined, even though it appears that precipitation trends are not predicted to change in the future. The drought simulation showed declines in head in the recharge zones of both aquifers. The effect on concentration was found to be negligible.

The final scenario examined was the effect of a pumping centre in the City of Winnipeg. This pumping centre was simulated by setting a well screened over the Carbonate Aquifer just east of the saltwater/freshwater zone. The model results showed a drawdown cone in the Carbonate Aquifer and a slight decline in head in the Sandstone Aquifer. The effect on the concentration within the Carbonate Aquifer shows a slight increase within the City of Winnipeg. Again it was though that the model could not simulate such small changes in concentration.

The model is successful in simulating different scenarios that could arise throughout the water resources development in the region. The results of the flow model are thought to be very good. Both the calibration and history match had RMS error within the target and good regression results. However, it must be remembered when using the model that for the Sandstone Aquifer, no calibration was conducted and the heads were only history matched against five measurements. For the Carbonate Aquifer flow model, the results were both calibrated and history matched against numerous observations and should give representative results.

In terms of solute transport, the model results were not as good as that of the flow model, limiting its usage. The model could not be calibrated for either aquifer due to lack of historical concentration data. Also, the history match for the Carbonate Aquifer was difficult due to high variability in the observations. For the Sandstone Aquifer, difficulties arose as all of the sampling was conducted in the freshwater zone. Therefore, no information on the plume was available. It was thought that the model would be capable of simulating large brine movement but not slight changes in concentration.

As stated at the beginning of this chapter, several hypotheses were formed as part of this research. It was hypothesized that the fractured carbonate rock of the Carbonate Aquifer could be modeled using the equivalent porous media approach. For the flow model, the successful calibration and history match proved the hypothesis. However, the transport model calibration was not as successful and therefore this hypothesis was not proved for this case. It was hypothesized that the hydrostratigraphy could be developed from

geology. The bedrock geology was from mineral and oil exploration wells and from WCSB Atlas wells. The overburden units were from a surficial model developed by ITM. The geology along with some assumptions was proved satisfactory in constructing the hydrostratigraphic model. The collection of transmissivity and hydraulic conductivity was from different sources and types of tests. It was hypothesized that the mixed data could be used for geostatistical analysis. The hypothesis was proved through successful analysis determining distribution type, general statistics and variograms. It was postulated that Bayesian Updating method would provide heterogeneous hydraulic conductivity fields for flow and transport model. This methodology proved successful for the Carbonate Aquifer, however lack of measurements in the Sandstone Aquifer resulted in this method being unsatisfactory. For the transport model, it was hypothesized that three-dimensions were required. Comparisons between two and three dimensional transport models proved that a significant improvement was gained when modeled in three dimensions. It was postulated that wells screened over both aquifers were necessary for calibration. It was found that improvements in calibration were obtained when cross contamination was considered. It has been postulated that brine movement is at equilibrium or moving extremely slowly. Predictions from the transport model confirm this hypothesis. The incorporation of the Red River Floodway to the flow model was found to improve the calibration however it was not required to reach the calibration target. Incorporation of variable density into the transport model improved the calibration.

In terms of future research, several aspects could be considered to improve the current model. The first would be to take further measurements of hydrogeological parameters, water levels and chloride ion concentrations. In terms of hydrogeological parameters, transmissivity measurements in the Sandstone Aquifer in the western portion of the region would make it possible to assign hydraulic conductivity based on Bayesian Updating. Also, field or laboratory measurements of all other parameters within both aquifers would be an asset. Increased water level measurements, especially within the Sandstone Aquifer in regions where no measurements are currently taken. For both aquifers more measurements of concentration are required. The measurements need to be taken across the entire region and strictly within each aquifer alone.

Another area of research that would aid the model is the determination of recharge rates. Spatial variation of the recharge rates across the recharge zones would be an asset. Information regarding discharge rates would also provide further verification of the model.

Further incorporations into the model itself can also be conducted. One example would be to attach the flow and transport model onto a climate control model. Therefore, changes in climate could be investigated to determine the effect on the water levels and concentrations within the aquifers. Also, thermal pollution, especially within the City of Winnipeg, could be incorporated. In many locations, water is withdrawn from the aquifers, for cooling purposes and the water of elevated temperature is returned to the aquifer.

In terms of modeling methodology, the protocol that was used for this research as stated previously requires large quantities of data, but also the model is compared against uncertain measurements. Research into methodologies for assessing whether models are depicting what is actually occurring would be beneficial for future regional models.

REFERENCES

Anderson, M.P. and Woessner, W.W. 1992. Applied Groundwater Modeling – Simulation of Flow and Advective Transport, Academic Press: 381pp.

Bear, J. 1972. Dynamics of Fluids in Porous Media, Dover Publications, Inc. 764pp.

Behie, G.A. and Forsyth, P.A. 1984. Incomplete Factorization Methods for Fully Implicit Simulation of Enhanced Oil Recovery. SIAM (Soc. Ind. Appl. Math.) J. Sci. Stat. Comput., **5**(3): 543-561.

Betcher, R.N. 1986. Regional Hydrogeology of the Winnipeg Formation in Manitoba. Presented at: Third Canadian Hydrogeology Conference, Saskatoon, Saskatchewan.

Betcher, R.N., Grove, G. and Pupp, C. 1995. Groundwater in Manitoba: Hydrogeology, Quality Concerns, Management, March 1995.

Bezys, R.K. and Conley, G.G. 1998. Manitoba Stratigraphic Database and the Manitoba Stratigraphic Map Series. Open File Report OF98-7. Manitoba Energy and Mines.

Bezys, R.K. and McCabe, H.R. 1996. Lower to Middle Paleozoic Stratigraphy of Southwestern Manitoba – Field Trip Guidebook B4; Geological Association of Canada/Mineralogical Association of Canada Annual Meeting, Winnipeg, Manitoba, May 27-29, 1996.

Bretthorst, G.L. 1988. Bayesian Spectrum Analysis and Parameter Estimation. Lecture Notes in Statistics, 48. Springer-Verlag.

Bryson, A.E. and Ho, Y. 1969. Applied Optimal Control, Hemisphere Publishing.

Conkling, H. 1946. Utilization of groundwater storage in stream system development. Trans. Am. Soc. Civil Engrs., **111:** 275-305.

Banks, H.O. 1953. Utilization of underground storage reservoirs. Trans. Am. Soc. Civil Engrs., **118**: 220-234.

Domenico, P.A. and Schwartz, F.W. 1990. Physical and Chemical Hydrogeology. John Wiley & Sons, Inc. 528pp.

Elder, J.W. 1967. Transient convection in a porous medium. Journal of Fluid Mechanics, **27**(3): 609-623.

Ferguson, G.A., Matile, G.L. and Woodbury, A.D. 2001. Estimating recharge rates in the Sandilands Area, Southeastern Manitoba, Canada using temperature logs, EOS Trans. AGU, **82**(47), Fall Meet. Suppl., Abstract H32D-0348, 2001.

Fetter, C.W. 1993. Contaminant Hydrogeology. Macmillan Publishing Co. New York, 458 pp.

Forsyth, P.A. and Sammon, P.H. 1986. Practical considerations for adaptive implicit methods in reservoir simulation. Journal of Computational Physics, **62**: 265-281.

Freeze, R.A. and Cherry, J.A. 1979. Groundwater. Prentice-Hall, Inc. 604pp.

Frind, E.O. 1982. Simulation of Long-Term Transient Density-Dependent Transport in Groundwater. Advances in Water Resources, **5**: 73-88.

Gelhar, L.W. 1993. Stochastic Subsurface Hydrology, Prentice-Hall Inc., 390pp.

Gelhar, L.W. and Axness, C.L. 1983. Three-dimensional stochastic analysis of macrodispersion in aquifers. Water Resources Research, **19**(1): 161-180.

Gelhar, L.W., Welty, C. and Rehfeldt, K.R. 1992. A Critical Review of Data on Field-Scale Dispersion in Aquifers. Water Resources Research, **28**(7): 1955-1974.

Grasby, S., Betcher, R. and McDougall, W. 1999. Water quality of the Carbonate Rock aquifer, southern Manitoba, Geological Survey of Canada Open File no. 3725.

Haverkamp, R. and Vauclin, M. 1979. A Note on Estimating Finite Difference Interblock Hydraulic Conductivity Values for Transient Unsaturated Flow Problems. Water Resources Research, **15**(1): 181-187.

Henry, H.R. 1964. Effects of dispersion on salt encroachment in coastal aquifers, U.S. Geological Survey Water Supply Paper, 1613-C: C71-C84.

Hoeksema, R.J. and Kitanidis, P.K. 1985. Analysis of the Spatial Structure of Properties of Selected Aquifers. Water Resources Research, **21**(4): 563-572.

Hsin-Chi, J.L., Richards, D.R. and C.A. Talbot, C.A. 1997. FEMWATER: A Three-Dimensional Finite Element Computer Model for Simulating Density-Dependent Flow and Transport in Variably Saturated Media. Technical Report CHL-97-12.

Huyakorn, P.S. and Pinder, G.F. 1983. Computational Methods in Subsurface Flow. Academic Press, New York, NY.

Journel, A.G. and Huijbregts, Ch.J. 1978. Mining Geostatistics. Academic Press Inc. 600pp.

Kapur, J.N., 1989. Maximum Entropy Models in Science and Engineering, John Wiley, New York, 635pp.

Kennedy, J.B. and Neville, A.M. 1976. Basic Statistical Methods for Engineers and Scientists, 2nd edition. Dun-Donnelley Publisher, 490pp.

Kennedy, P.L., Woodbury, A.D. and Wang, K. 2000. Minimum Relative Entropy: Theory and application to surface temperature reconstruction from borehole temperature measurements. Geophysical Research Letters, **27**(19): 3081-3084.

Kitanidis, P.K. 1996. Introduction to Geostatistics – Applications in Hydrogeology, Cambridge University Press: 249pp.

Kolditz, O., Ratke, R., Diersch, H-J.G. and Zielke, W. 1998. Coupled groundwater flow and transport: 1. Verification of variable density flow and transport model. Advances in Water Resources, **21**(1): 27-46.

Konikow, L.F. and Bredehoeft, J.D. 1992. Ground-water models cannot be validated. Advances in Water Resources, **15**: 75-83.

Kropinski, M.C.A. 1990. Numerical techniques for saturate-unsaturated groundwater flow. M.Sc. Thesis, University of Waterloo, Waterloo, Ont.

Li, D and Lake, L.W. 1994. A moving window semivariance estimator. Water Resources Research, **20**(5): 1479-1489.

Linsley, R.K., Franzini, Freyberg and Tchobanoglous. 1992. Water Resources Engineering, 4th edition. McGraw-Hill, New York. 841 pp.

Manitoba Natural Resources, Water Resources, Hydrotechnical Services. 1986. Carbonate Aquifer Capacity as Related to the town of Selkirk Water Supply. Report.

Manitoba Natural Resources, Water Branch. 1988. The Water Rights Act, c. W80. 21pp.

Matheron, G. 1962. Traite do geostatistique appliquée, vol. I, Mem. BRGM, 14.

Matile, G.L.D. and Keller, G. 1999. Digital Elevation Model of Southern Manitoba (version 1.0). Open File Report OF99-15 Manitoba Industry, Trade and Mines.

Maxey, G.B. 1964. Hydrostratigraphic Units. Journal of Hydrology **2**: 124-129.

McCabe, H.R. 1971. Stratigraphy of Manitoba, An Introduction and Review. The Geological Association of Canada, Special Paper Number 9: 167-187.

McCabe, H.R. 1978. Reservoir Potential of the Deadwood and Winnipeg Formations Southwestern Manitoba. Manitoba, Department of Mines, Resources and Environmental Management Mineral Resources Division. Geological Paper 78-3, 54pp.

McCabe, H.R., Betcher, R.N. and Render, F.W. 1993. The Fort Garry Aquifer in Manitoba. Geological Report GR93-1: 15pp.

McKay, M.D., Beckman, R.J. and Conover, W.J. 1979. A Comparison of Three Methods for Selecting Values of Input Variables in the Analysis of Output from a Computer Code. Technometrics, **21**(2): 239-245.

Meinzer, O.E. 1923. Outline of groundwater in hydrology with definitions. U.S. Geol. Surv. Water Supply Papers, v. 577.

Mualem, Y. 1976. A new model to predict the hydraulic conductivity of unsaturated porous media. Water Resources Research, **12**: 513-522.

Neuman, S.P. 1990. Universal Scaling of Hydraulic Conductivities and Dispersivities in Geologic Media. Water Resources Research, **26**(8): 1749-1758.

Pach, J.A. 1994. Hydraulic and Solute Transport Characteristics of a Fractured Glacio-Lacustrine Clay Winnipeg, Manitoba. Master of Science Thesis, University of Waterloo, Ontario.

Press, S.J. 1989. Bayesian Statistics: Principles, Models and Applications: John Wiley, 237pp.

Render, F.W. 1970. Geohydrology of the Metropolitan Winnipeg Area as Related to Groundwater Supply and Construction. Canadian Geotechnical Journal, **7**: 243.

Sampat, P. 2000. Groundwater Shock. World Watch: 10-22.

Scheafer, R.L. and McClave, J.T. 1995. Probability and Statistics for Engineers, Duxbury Press, 745pp.

Shore, J.E. 1981. Minimum cross-entropy spectral analysis, IEEE Trans. Acoustics Speech and Signal Processing, ASSP-29: 230-237.

Sivia, D.S. 1996. Data Analysis: A Bayesian Tutorial. Oxford Science Publications: 189pp.

Sudicky, E.A. 1986. A Natural Gradient Experiment on Solute Transport in a Sand Aquifer: Spatial Variability of Hydraulic Conductivity and its role in the Dispersion Process. Water Resources Research, **22**(13): 2069-2082.

Tarantola, A. 1987. Inverse Problem Theory Methods for Data Fitting and Model Parameter Estimation. Elsevier Science Publishing B.V. 613pp.

Therrien, R., and Sudicky, E.A. 1996. Three-Dimensional Analysis of Variably-Saturated Flow and Solute Transport in Discretely-Fractured Porous Media. Journal of Contaminant Hydrology, **23**: 1-44.

Ulrych, T.D., Sacchi, M.D. and Woodbury, A.D. 2001. A Bayes tour of inversion: a tutorial. Geophysics, **66**(1): 55-69.

UMA Engineering Ltd. 1987. The City of Winnipeg Hydrogeological Study Brady Road Landfill. Report.

UMA Engineering Ltd. 1991a. Meadow Material, A Branch of Dow Corning Silicon Energy System Including Production Well Installation – Silicon Pilot Plan, East Selkirk, Manitoba. Report.

UMA Engineering Ltd. 1991b. Montcalm Site Evaluation. Report.

UMA Engineering Ltd. 1993. Bristol Aerospace Limited Rockwood Propelland Plant. Report.

UMA Engineering Ltd. 1997. Town of Selkirk Summary Report on the Test Well Installation and Test Pumping Program. Report.

van Genuchten, M.Th. 1980. A closed-form equation for predicting the hydraulic conductivity of unsaturated soils. Soil Sci. Soc. Am. J., **44**: 892-898.

Villarroya, F. and Aldwell, C.R. 1998. Sustainable development and groundwater resources exploitation. Environmental Geology, **34**(2/3): 111-115.

Voss, C.I. and Souza, W.R. 1987. Variable Density Flow and Solute Transport Simulation of Regional Aquifers Containing a Narrow Freshwater-Saltwater Transition Zone. Water Resources Research, **23**(10): 1851-1866.

Viljoen, D., Chackowsky, L., Lenton, P. and Broome, H.J. 1999. Geology, Magnetic and Gravity Maps of Manitoba: A Digital Perspective, Manitoba Energy and Mines Geological Servies MEM OF99-12 Geological Survey of Canada GSC OF D3695, CD.

Wardrop Engineering Inc. 1995. Rural Municipality of Rosser Hydrogeological Assessment of Proposed Landfill Site.

WCED (World Commission on Environment and Development. 1987. Our Common Future (The Brundtland Report), Oxford University Press.

Woodbury, A.D. 1987. Inverse Theory and Model Identifiability: An Overview. *In* Proceedings of the CSCE Centennial Conference, 119-142.

Woodbury, A.D. 1989. Bayesian Updating Revisited. Mathematical Geology, **21**(3): 285-308.

Woodbury, A.D. and Sudicky, E.A. 1991. The Geostatistical Characteristics of the Borden Aquifer. Water Resources Research, **27**(4): 533-546.

Woodbury, A.D. and Ulrych, T.J. 1993. Minimum Relative Entropy: Forward Probabilistic Modeling. Water Resources Research, **29**(8): 2847-2860.

Woodbury, A.D. and Ulrych, T.J. 1996. Minimum Relative Entropy Inversion: Theory and Application to Recovering the Release History of a Groundwater Contaminant. Water Resources Research, **32**(9): 2671-2681.

Woodbury, A.D. and Ulrych, T.J. 1998. Minimum Relative Entropy and Probabilistic Inversion in Groundwater Hydrology. Stochastic Hydrology and Hydraulics, 12: 317-358.

Woodbury, A.D. and Ulrych, T.J. 2000. A Full-Bayesian Approach to the Groundwater Inverse Problem for Steady State Flow, Water Resources Research, **36**(8): 2081-2093.

Woodbury, A.D., Sudicky, E., Ulrych, T.J. and Ludwig, R. 1998. Three-Dimensional Plume Source Reconstruction Using Minimum Relative Entropy Inversion. Journal of Contaminant Hydrology, **32**: 141-158.